UNCLASSIFIED

[redacted]

WT-1119

[redacted]

685

Operation TEAPOT

NEVADA TEST SITE

February – May 1955

VERIFIED UNCLASSIFIED
3-11-80 [signature]

Project 2.5.1

FALLOUT STUDIES

Issuance Date: July 23, 1958

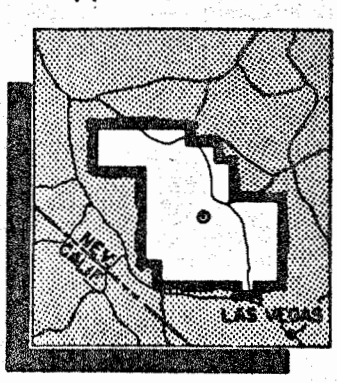

FORMERLY RESTRICTED DATA

Handling Restricted Data in formerly [illegible] dissemination [illegible] section 144b, Atomic Energy Act of 1954.

This material contains information affecting the national defense of the United States within the meaning of the espionage laws, Title 18, U.S.C., Secs. 793 and 794, the transmission or revelation of which in any manner to an unauthorized person is prohibited by law.

HEADQUARTERS FIELD COMMAND, ARMED FORCES SPECIAL WEAPONS PROJECT
SANDIA BASE, ALBUQUERQUE, NEW MEXICO

UNCLASSIFIED

[redacted]

LASL

Dick Smalley Office
Rad Safety Group

[redacted]

UNCLASSIFIED

WT-1119

OPERATION TEAPOT—PROJECT 2.5.1

Report to the Test Director

FALLOUT STUDIES

M. J. Schumchyk
E. H. Bouton

U. S. Army Chemical Corps
Chemical Warfare Laboratories
Army Chemical Center
Maryland

[redacted]

[redacted]

SUMMARY OF SHOT DATA, OPERATION TEAPOT

Shot	Code Name	Date	Time*	Area	Type	Latitude and Longitude of Zero Point
1	Wasp	18 February	1200	T-7-4†	762-ft Air	37° 05' 11.6856" 116° 01' 18.7368"
2	Moth	22 February	0545	T-3	300-ft Tower	37° 02' 52.2654" 116° 01' 15.6967"
3	Tesla	1 March	0530	T-9b	300-ft Tower	37° 07' 31.5737" 116° 02' 51.0077"
4	Turk	7 March	0520	T-2	500-ft Tower	37° 08' 18.4944" 116° 07' 03.1879"
5	Hornet	12 March	0520	T-3a	300-ft Tower	37° 02' 25.4043" 116° 01' 31.3674"
6	Bee	22 March	0505	T-7-1a	500-ft Tower	37° 05' 41.3880" 116° 01' 25.5474"
7	ESS	23 March	1230	T-10a	67-ft Underground	37° 10' 06.1283" 116° 02' 37.7010"
8	Apple	29 March	0455	T-4	500-ft Tower	37° 05' 43.9200" 116° 06' 09.9040"
9	Wasp'	29 March	1000	T-7-4‡	740-ft Air	37° 05' 11.6856" 116° 01' 18.7368"
10	HA	6 April	1000	T-5§	36,620-ft MSL Air	37° 01' 43.3642" 116° 03' 28.2624"
11	Post	9 April	0430	T-9c	300-ft Tower	37° 07' 19.8965" 116° 02' 03.8860"
12	MET	15 April	1115	FF	400-ft Tower	36° 47' 52.6887" 115° 55' 44.1086"
13	Apple 2	5 May	0510	T-1	500-ft Tower	36° 03' 11.1095" 116° 06' 09.4937"
14	Zucchini	15 May	0500	T-7-1a	500-ft Tower	37° 05' 41.3880" 116° 01' 25.5474"

* Approximate local time, PST prior to 24 April, PDT after 24 April.
† Actual zero point 36 feet north, 426 feet west of T-7-4.
‡ Actual zero point 94 feet north, 62 feet west of T-7-4.
§ Actual zero point 36 feet south, 397 feet west of T-5.

ABSTRACT

The purpose of Project 2.5.1 "Fallout Studies" was to obtain data required to construct closed contours for dose rate levels down to and including 1-r/hr at H + 1 hour and in so doing obtain information concerning: (1) the role of the base surge as a primary carrier of activity; (2) radiation intensities in areas contaminated by fallout, base surge, and in the crater-lip region; (3) time of arrival of activity at various distances from ground zero; (4) depth of burial of activity in the crater and on the lip, and (5) air-to-ground radiation intensity correlation factors calculated from data obtained during aerial surveys of the contaminated areas. This information then could be applied to the problem of: verifying and extending existing scaling relationships for the determination of contamination patterns resulting from the underground detonation of nuclear weapons at different scaled depths; developing countermeasures for reducing the radiation hazard in the contaminated areas; estimating the magnitude of the effort required to reclaim the crater-lip area; and improving instrumentation and techniques for rapid aerial survey of contaminated areas.

Ground and aerial radiation-intensity measurements made by this project and others have been used to construct closed contours for the 100-mr/hr at H + 1-hour dose rate line and nearly closed contours for a dose rate of 10-mr/hr at H + 1 hour. The areas enclosed by the different dose rate contours of Teapot Shot 7 are generally greater than the preshot predictions.

The fallout pattern extended a shorter distance downwind than had been predicted by current scaling methods, even though the cloud rose to a greater height than had been used in the prediction technique. Most of the total activity (80 percent) was accounted for within the 0.1-r/hr to 3,000-r/hr at H + 1 hour dose rate contour.

Analysis of time-of-arrival-of-activity data, radiochemistry, photography, and dose rate contours indicates that the base surge was the primary carrier of activity in the upwind and crosswind direction. Time-of-arrival data at seven locations from 300 to 4,500 yards from ground zero indicated that fallout traveled downwind at less than 2 mph (ground speed), although the surface wind was 12 mph.

At D + 8 days, about 90 percent of the radioactive contamination in the crater lip was contained in the first 12 inches of soil. Readings taken at that time, 3 feet above the crater lip, indicated a radiation intensity of 6,000 to 12,000 mr/hr. Three months after the shot the lip intensity was 200 to 500 mr/hr but was still located in the first 12 inches of soil. However, 80 to 90 percent of the activity within the crater was covered by cave-ins and land slides to a depth of at least 3 feet. Readings taken 3 feet above the crater lip, approximately six months after the shot, gave a radiation intensity of 100 to 200 mr/hr.

Gamma-intensity measurements made in the fallout area showed the average dose-rate decay exponent for the period H+ 2 hours to D + 4 days was −1.2. The beta decay was similar to that found at other tests. Data were obtained which will furnish information concerning the effect of scaled depth upon such properties as specific activity, activity versus particle size distribution, and total activity associated with fallout.

The aerial survey studies were complicated by the steepness of the radiation contours which existed. It was found that the rate at which radiation intensity decreased with increasing altitude of measurement is dependent upon the position within the fallout pattern

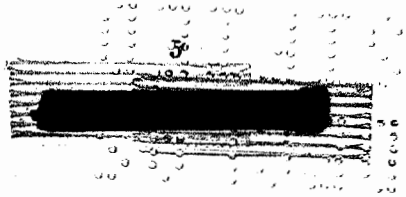

above which the measurements are made. For example, air-to-ground correlation factors (intensity at altitude/intensity on ground), determined at different positions in the fallout pattern, were found to vary from 0.12 to 0.46 for an altitude of 500 feet. The gamma radiation intensities decreased approximately logarithmically with increasing altitude above any specific point. However, the rate of change varied widely from position to position within the fallout pattern.

FOREWORD

This report presents the final results of one of the 56 projects comprising the Military Effects Program of Operation Teapot, which included 14 test detonations at the Nevada Test Site in 1955.

For overall Teapot military-effects information, the reader is referred to the "Summary Report of the Technical Director, Military Effects Program," WT-1153, which includes the following: (1) a description of each detonation including yield, zero-point location and environment, type of device, ambient atmospheric conditions, etc.; (2) a discussion of project results; (3) a summary of the objectives and results of each project; (4) a listing of project reports for the Military Effects Program.

PREFACE

The authors wish to acknowledge the fine work of the personnel and organizations which participated in the field work, assisted in gathering the voluminous data and contributed support essential toward the preparation of this report.

Particular appreciation is expressed to William Van Horn, Engineer Research and Development Laboratories, Fort Belvoir, Virginia, for his valuable assistance and recommendations on the core sampling and field surveying phases of this project.

Organizations which assisted in gathering the data for this report are as follows: 50th Chemical Platoon, Camp Desert Rock, US Naval Radiological Defense Laboratory (Project 2.5.2), Rad-Safe (Test Site), Engineer Research and Development Laboratories, Fort Belvoir, Virginia, Project 37.2 (University of California, Los Angeles), ARMA Corporation Pathfinder Equipment, and Raydist Navigation Group.

CONTENTS

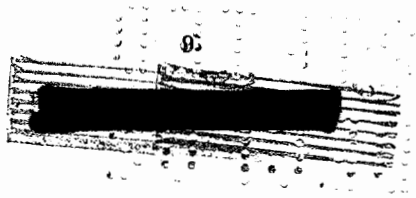

TABLES

FIGURES

[redacted]

Chapter 1

INTRODUCTION

1.1 OBJECTIVES

The work performed at Operation Teapot under Project 2.5.1 was a logical extension of fallout studies conducted at previous nuclear tests. This project participated in Shot 7, an underground shot detonated at a depth of 67 feet with a yield of 1.2 kt. As far as scaling parameters are concerned, the shot differed from the one previous underground shot only in the depth of detonation, which made the study of fallout extremely important for correlation and extrapolation. Project 2.5.1 documented the radioactivity associated with the base surge fallout, cloud fallout, and crater-lip areas.

The general objectives of this project were: (1) to determine the radiation intensities in areas contaminated by the cloud fallout, base surge fallout, and crater-lip resulting from a deep underground nuclear explosion; (2) to provide additional information relative to the role of base surge as a primary carrier of activity and thus to extend present knowledge regarding the mechanism of formation and the importance of the base surge; (3) to obtain information which can be applied to the problem of verifying and extending the usefulness of existing scaling relationships for the determination of contamination patterns resulting from the underground detonation of nuclear weapons at different scaled depths; and (4) to determine the dependence of properties such as specific activity, active particle size distribution, and total activity associated with fallout upon the scaled depth of burst.

To accomplish these general objectives, this project concentrated its activities on: (1) residual gamma radiation fallout patterns (at least to 1 r/hr at H + 1 hour); (2) time and rate of arrival of the base surge and fallout; (3) amount and distributions of radioactive materials associated with the base surge and fallout; (4) correlation of air and ground surveys to determine air to ground extrapolation data; (5) variation of radioactive contamination in the crater and lip as a function of depth at varying distances from ground zero; (6) gross beta decay rates of radioactive fallout materials; and (7) particle characteristics of the fallout material, such as activity versus particle size, gross particle size distribution, radioactive particle size distribution, and distribution of activity within particles.

1.2 BACKGROUND

1.2.1 Base Surge. A base surge forms following a subsurface detonation when the material in the column falls back to the surface and the smaller particles roll out radially along the surface to form a low cloud which appears following the subsidence of the initial throwout.

The base surge phenomenon was first observed at the Bikini Baker test of Operation Crossroads (Reference 1). Since it was a relatively unexpected occurrence, very little

base surge data were obtained and conflicting data resulted concerning the role of the base surge in carrying activity. As a result of the observation and the subsequent concern over the possibility that the surge was a dangerous carrier of radioactivity, extensive studies of the base surge phenomenon have been conducted at both nuclear and high-explosive tests.

Documentation of the base surge was first carried on at Jangle, the first underground nuclear burst, but only a limited amount of basic physical effects data were obtained. The question of base surge activity was not resolved. The base surge from the Jangle underground shot had a definite maximum radius, but no correlation was observed between the extent of the base surge and the level of the activity remaining on the surface of the ground. The upwind and crosswind extent of the upper cloud and base surge were about equal for the Jangle underground shot, making it impossible to establish the separate contributions of the cloud and base surge to the fallout. In addition, observations made at Jangle took place after a time interval sufficiently long to allow a redistribution of active material by the winds. As a result, definite conclusions regarding the significance of the base surge for Jangle scaled depth could not be reached. It has been postulated that, for a greater scaled depth, the base surge would carry and distribute a larger proportion of the radioactivity (Reference 2).

Some basic information on the mechanism and physical formation of the base surge from subsurface high-explosive (HE) detonations has been obtained since Jangle (References 3 and 4).

In Reference 3 it is concluded that the column and cloud from an underground detonation with a 0.5 $ft/lb^{1/3}$ scaled depth will collapse producing solely base surge. This conclusion stems mainly from experimentation with HE shots. In an underground nuclear detonation the gaseous products of the explosion form a jet which should be at a much higher temperature than the similar jet from an HE shot. In addition, the jet from a nuclear shot should rise more quickly and to a greater altitude than the jet from a comparable HE burst. For this reason, the Teapot underground shot, which was at a 0.5 $ft/lb^{1/3}$ scaled depth, was not expected to collapse as predicted.

It was shown at the underground shot of Operation Jangle and confirmed at Operation Castle (Reference 5) that early fallout is deficient in fission products with long-lived gaseous precursors such as Sr^{89} and Ba^{140}. It is believed that the rare gas precursors of these nuclides cannot be incorporated into the early remnants of the fireball until after these rare gas precursors have decayed into their daughter nuclides. The base surge is produced by the column falling back to earth. If the falling column is contaminated the contamination must be produced by mixing with the early remnants of the fireball. Therefore, from these considerations, the column and the subsequent base surge should be deficient in Sr^{89} and Ba^{140}.

1.2.2 Fallout. Documentation of fallout from surface and subsurface nuclear detonations has been conducted at previous test programs. The phenomenon was first observed at Operation Trinity (Reference 8). Since that time, through Operations Jangle, Ivy, and Castle, it has become well established that the residual gamma radiation hazard resulting from fallout must be considered seriously as a problem of military significance for all types of detonations, except the air burst where the fireball at no time touches the surface of the earth. Scaling methods have been developed for the prediction of contamination patterns, but no verification of the reliability of these methods has been possible.

Fallout was first fully documented at Jangle. Limited data were obtained at Crossroads and Greenhouse. The first residual gamma radiation dose-rate contours from a nuclear detonation were recorded at Crossroads (Reference 9). The first comprehensive

study of fallout forecasting was made at Greenhouse (Reference 10). The latter study revealed significant residual contamination from the Dog and Easy tower shots.

In the Jangle fallout studies, fallout data were obtained to a distance of several miles from ground zero (Reference 11). Contamination patterns for both the surface and subsurface detonations were recorded as dose-rate contours (Reference 12). The 100-hr/hr contour line at H + 1 hour after the Jangle detonations extended 4,000 yards downwind for the surface burst, 5,000 yards downwind for the underground burst, and covered crosswind distances of 500 and 1,500 yards, respectively.

The radioactive fallout from tower shots of Tumbler-Snapper and Upshot-Knothole have been plotted as dose rate contours by utilizing the data from the radiological monitoring logs of the Rad-Safe ground and air monitors (Reference 13).

The early rate of fallout was measured at Ivy (References 14 and 15) and Castle (References 16 and 17). The physical and chemical properties of the particulate matter, together with its distribution in time and areas were investigated during both of these operations.

The residual radiation hazard resulting from the fallout of radioactive particles generated in the surface detonation of very high yield nuclear weapons has been demonstrated at Castle (Reference 18). The fallout contaminated vast areas extending well beyond those areas affected by blast and thermal effects. Radiation levels of 250 r/hr were found to exist at downwind distances greater than 180 miles.

These previous surface and underground shots formed the basis of estimating probable fallout patterns at Shot 7, Teapot. This scaling study is presented in Chapter 2 and was used to establish station locations.

1.2.3 Crater and Lip. Knowledge to date concerning the crater and lip formed by a subsurface detonation is based on the one shallow-depth atomic detonation at Jangle (Reference 19) and extensive high explosive underground test shots (Reference 20). Uncertainties exist in extrapolating this high explosive information to underground detonations at greater depths, especially in the cratering equivalents of nuclear weapons (Reference 21).

Attempts were made to obtain early core samples from the lip of the Jangle underground crater using remotely controlled weasels and straight pipe samplers (Reference 22). However, the soil was so loose and friable that the samples fell out of the pipe upon withdrawal from the ground.

Several months after the underground shot at Operation Jangle, the crater and lip were sampled (Reference 23) by digging 2-by-2-foot holes to a depth of 2 feet and removing 50-in^3 samples at depths of 0, 3, 6, 12, and 24 inches. Seven samples were taken on each of four radii at 30-foot intervals from the center of the crater. The radioactive contamination was found to be distributed between the surface and a depth of 6 inches. It was tentatively concluded that the contamination of the crater and lip is a near-surface phenomenon, but there is a possibility that leaching from rain and snow had caused the contaminant to be at a greater depth than it was just after the detonation.

Chapter 2
PROCEDURE

2.1 INITIAL PLANNING

To determine the procedures required to accomplish the stated objectives, it was necessary to estimate the magnitude of the physical effects expected. Table 2.1 shows estimated dimensions and overpressures associated with the crater, column, and base surge. These estimates are based upon data given in pertinent reports of previous nuclear tests and in Reference 24.

The value of 1,940 yards for the maximum extent of base surge was estimated from high explosive test data using an energy yield for Shot 7 equivalent to two-thirds mechanical efficiency. Mechanical yield is expressed as kilotons of TNT, assumed to be two-thirds of the total yield (Reference 6). The predicted maximum extent of base surge, calculated from data in Reference 24, is only 1,216 yards.

For high explosive tests, the scaled depth of 0.5 $ft/lb^{1/3}$ appears to be near the point at which the cloud has a high probability of falling quickly to the surface. It was predicted, however, that the cloud would rise to an altitude in the neighborhood of 3,500 feet. This estimate appeared reasonable, since the maximum height of the cloud resulting from the 320,000-pound HE test at a scaled depth of 0.5 $ft/lb^{1/3}$ was 2,300 feet (Reference 3) and for the Jangle underground shot was 5,000 feet. For a nuclear explosion a smaller portion of the upper cloud should fall along with the material in the column than would be the case for an HE shot at the same scaled depth. This is due to the larger proportion of energy emitted as heat at the time of the nuclear explosion and the consequent greater buoyancy of the upper cloud. In the case for the proposed Teapot underground shot, the radius of the base surge would be smaller than 1,900 yards.

Extrapolation of the Jangle dose-rate contours to the scaled depth of Teapot Shot 7 was not expected to give reasonably accurate results because of the uncertainties regarding the height to be attained by the cloud. However, estimated maximum downwind distances for several dose-rate contours at H + 1 hour are given in Table 2.2, assuming a cloud height of 3,500 feet and an average wind speed of 5 mph. These estimates are scaled from the Jangle contours and are based upon a method of correcting for depth of detonation first suggested in Reference 44. In this method, if μ denotes the ratio of cloud heights and dimensions for two detonations at different depths, it can be inferred that the dose rate will vary as $1/\mu^2$ at distances scaled as μ.

In the event of a partial collapse of the upper cloud, the typical downwind fallout area associated with nuclear detonations will be smaller than indicated but the activities will be higher.

For complete data in the base surge region, stations distributed over 360 degrees to a distance of 1,900 yards from ground zero are desirable. A more limited coverage of the area was found to be necessary, however, because of the required restrictions on funds available to this project. Since meteorological conditions strongly influence the direction of base surge and fallout travel, it was stipulated that no firing should

occur unless the wind was in such a direction that fallout would occur in the sector where the sampling apparatus was located.

The wind direction at the time of firing was expected to be from the west or northwest. Based on the above prognostications, the station layout (Figure A.1) was designed to include five instrumentation lines (legs) four extending downwind and one in a crosswind direction. Using north as the zero degree reference line and going around in a clockwise direction, legs E, F, G, H, and L were located on the 80-, 100-, 120-, 140-, and 220-degree azimuths. Intermittent fallout collectors were placed on legs E, G, and L at 300, 700, 1,650, 3,400, and 4,500 yards from ground zero; on legs F and H at 3,400

TABLE 2.1 ESTIMATED PHYSICAL EFFECTS, SHOT 7, 1.2 KT AT 65 FEET UNDERGROUND

Location	Radius	Overpressure at Outer Edge	Comments
	yd	psi	
Crater	82	24	Depth, 93 ft; volume, 328,000 yd^3
Crater plus lip	164	10	Thermal radiation negligible beyond lip
Column	200	7	—
Base Surge	1,940 (max)	1	Time to maximum radius 200 sec

and 4,500 yards; and on leg F at 11,000 yards from ground zero. Air samplers designed to sample isokinetically were placed on legs G and L at 700 yards from ground zero. Leg G was downwind, while leg L was crosswind.

2.2 INSTRUMENTATION

2.2.1 Intermittent Fallout Collectors. The intermittent fallout collector (IFC) (References 14 and 16) consisted of a circular disk (or spider) divided into 24 sectors, a driving and timing mechanism, a housing, and power supply. Each sector contained a triangular tray $3\frac{3}{8}$ inches by 10 inches and $\frac{3}{4}$ inch deep. One tray at a time was exposed to base surge and cloud fallout through an opening of similar dimensions in the top cover. The glass counting cups and jars which were used on previous tests were eliminated and the holes in the trays were sealed with rubber stoppers. A door covered the sampling opening both before and after the sampling time.

The instrument was started by an external timing signal. At 3,400 and 4,500 yards, after a delay of 1 minute, the IFC cover door opened and the first tray moved into sampling position. At the 300-, 700-, and 1,650-yard stations, a −1 minute signal actuated an interval clock timer which controlled the movement of the trays into sampling position.

Succeeding trays moved into position under the cover, opening at set intervals of 30 seconds for 300-yard stations, 1 minute for others in the expected base surge (including 1,650-yard stations), and 5 minutes for stations out of the expected base surge area until the cycle was completed. The door then closed and the machine shut itself off.

Two views of the intermittent fallout collector are shown in Figures 2.1 and 2.2. For further detailed description of the IFC, see References 14 and 16.

2.2.2 Aerosol Sampler. The aerosol sampler (Reference 25) was designed to take intermittent samples of the air at preset time intervals of approximately 1 to 30 minutes

per sample and for total maximum sampling time up to 12 hours. For this test, 50-second time intervals were used. Particulate samples were collected on millipore filter paper over the size range of 0.1 to 100 microns, but particles over 30 to 40 microns in size were retained loosely on the filter.

The major units which make up the aerosol sampler, Figure 2.3, include an isokinetic and wind-directional sampling head, a filter-changing and storage apparatus, two thermocouple-type velocity-sensing heads, amplifier and flow control valve, a converter to change the battery output to 110-volt 60-cycle current, and a vacuum pump and motor. A close-up of the aerosol sampling unit in Figure 2.4 shows the cage-like cover around the ambient velocity-sensing head, sampling inlet with wind vane, and the solenoid-

TABLE 2.2 ESTIMATED DOWNWIND EXTENT OF CONTAMINATION RESULTING FROM A 1.2 KT YIELD AT A DEPTH OF 65 FEET

Dose Rate Contours at H + 1 Hour	Downwind Distance
r/hr	yd
1,000	1,100
500	2,000
200	3,500
100	5,000
10	10,000

controlled stop for the rotary-disk type feeder mechanism. Figure 2.5 is a line diagram showing the internal components and flow-control system of the aerosol sampler.

The sampling head consists of a cone with an included angle of 90 degrees. A sealed bearing at the top of this cone permits the sampling nozzle, a 90-degree elbow 0.58 inch in diameter, to rotate freely about its central axis into the prevailing winds.

A rotary type feeder mechanism alternately moves a filter and a spacer (each $4\frac{3}{4}$ inches in diameter) from the unexposed filter magazine to the exposed filter sampling port. The filter and backing are held vertically in a specially designed filter holder which provides rigidity and protection to the filtering surface (4 inches in diameter). The filter magazines, or canisters, hold 24 filters and 24 spacers. Two holes are provided in the rotating table; the purging port and carrying port. The purging port is smaller in diameter than either the filter holder or spacer and hence passes underneath. The motion of the mechanism is stopped when the carrying port reaches a point between the two magazines, and the purging port is directly under the sampling nozzle.

When the signal from the control timer energizes the system, the blower operates at full capacity for a brief period to purge the sampling nozzle. The carrier plate then rotates the carrying port under the unexposed-filter magazine and a filter, in its holder, is pushed into position and held by a clamping cam. It is then moved to the sampling position where the rotary motion stops for the predetermined sampling period. When the sampling period is over, the carrier plate again rotates, carrying the exposed filter to a position directly beneath the exposed-filter magazine. The filter is then stopped by a lug which prevents any lateral motion of the filter. The clamping cam moves out of position at this time and allows an inclined ramp on the carrier plate, which continues to rotate, to push the filter into the magazine. The carrier port then picks up a spacer and moves it over to the exposed-filter magazine where it is also forced into the canister by the same action. The plate stops rotating when the carrying port is midway between the two magazines.

The complete cycle for purging, loading, and depositing requires two revolutions of the carrier plate. This complete cycle is accomplished in a 12-second period; 3 seconds

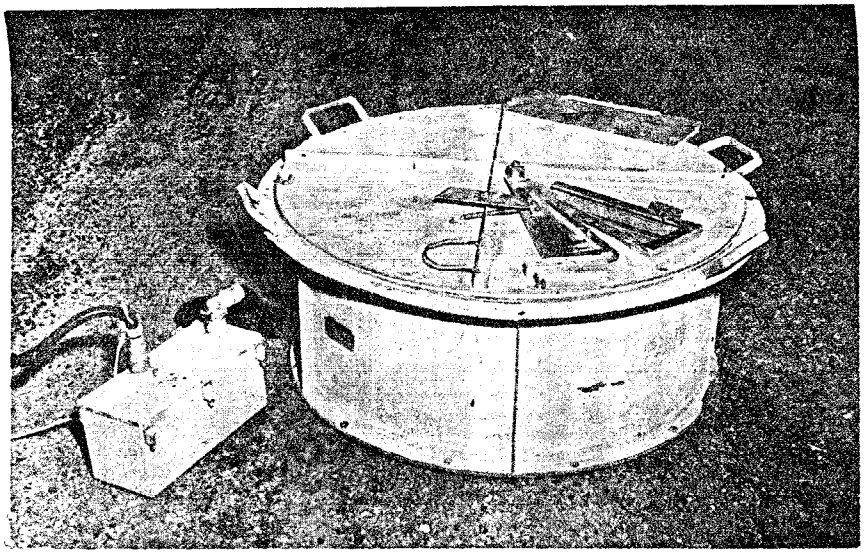

Figure 2.1 Intermittent fallout collector (IFC) with cover closed and sampling door open.

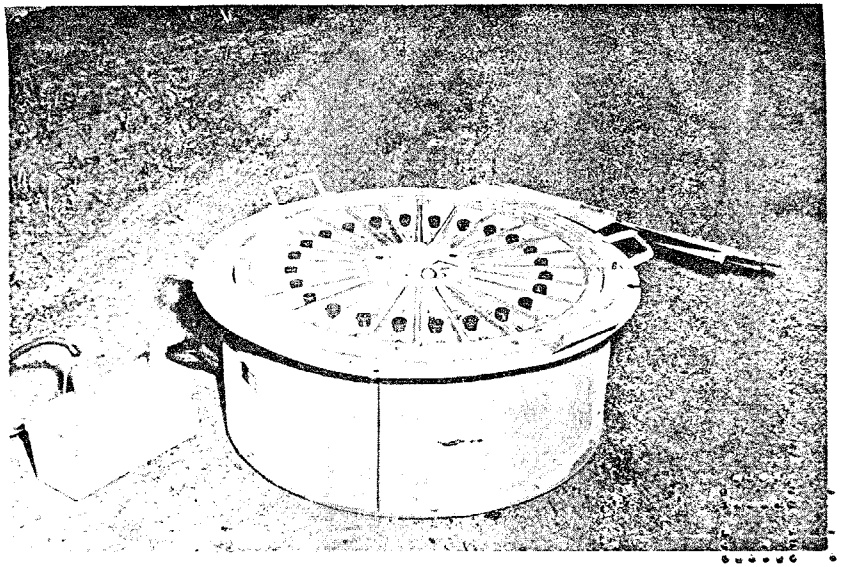

Figure 2.2 IFC with cover open showing spider and sampling trays.

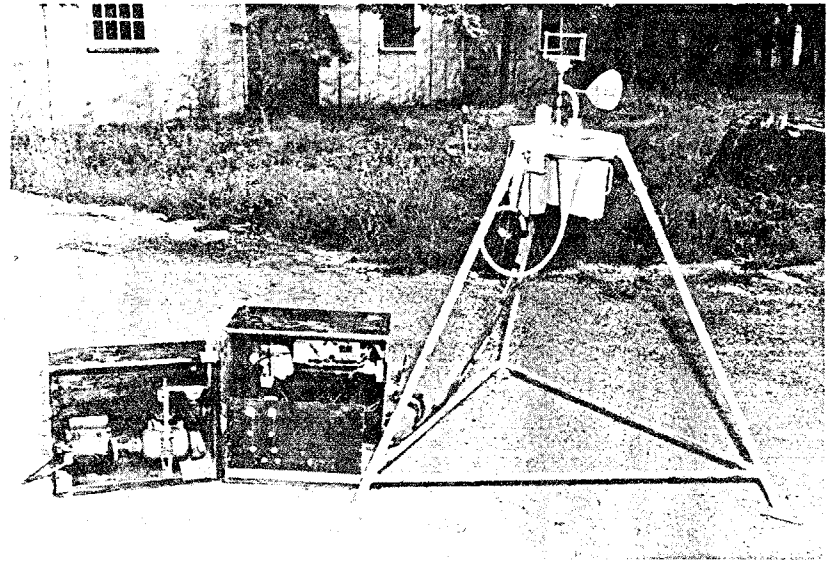

Figure 2.3 Aerosol sampler equipment showing (left to right) vacuum pump, amplifier with flow control and sampling unit on tripod stand.

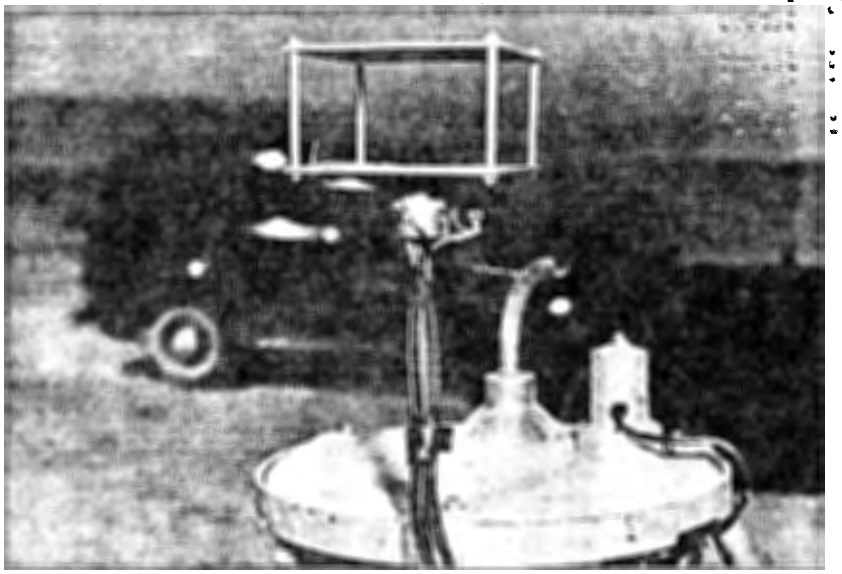

Figure 2.4 Closeup of aerosol sampling unit.

are required to move the filter from the unexposed filter chamber to the sampling position and 9 seconds to move the filter and spacer into the exposed filter magazine and stop in the purge position.

The flow-control system, Figure 2.3, is based on velocity sensing heads which consist of hot-wire thermocouples. These thermocouples are heated by a constant-voltage alternating current. The direct-current voltage of the thermocouples is a function of the air velocity past the junctions since this determines the amount of cooling and thus the junction temperature.

Two velocity-sensing heads are used, one a nondirectional head located in the ambient air, and the other located behind the filter in a tube having the same inside diameter as the sampling-head inlet. These thermocouples are connected in opposition. The same air velocity past both will, therefore, result in no output signal, and a difference in velocity will result in an output signal which is proportional to the difference in velocity and which also indicates the direction of the unbalance. The output signal is then amplified and used to drive a motorized valve in such a direction as to make the sampling velocity identical to the ambient-air velocity.

The sampling air is induced by a constant-speed, vane-type vacuum pump. Since the characteristic of this pump is such that it provides an almost constant volume flow over a range of pressures, a bypass flow-control valve is used in parallel with the filter to control the flow through the filter.

A theoretical study (Reference 25) was made to determine the degree to which isokinetic sampling would be achieved so that the sample would be representative of the air sampled at that point. This study is summarized in Appendix J.

2.2.3 Aerial Survey Instrument. Initially, the aerial survey instrument (Reference 26) consisted of an external probe operated at the end of a special 500-foot cable. The cable was wound on a reel mounted in an H-19 helicopter. A meter and control panel were mounted inside the helicopter and indicated the radiation intensity in roentgens per hour. An ionization chamber detector was located within the probe at a distance of 3 feet from the lower end. After several trial surveys on shots preceding the underground shot, the ionization chamber and meter described in the above reference were found to be unsatisfactory. Subsequent experiments resulted in the use of Jordan survey meters, Models AG-500 and AGB-10K-SR, with 500- and 1,200-foot conductor cables, respectively. The cable was wound on a hand-operated reel mounted on an aluminum frame carried inside the helicopter. A microswitch on the lower end of the probe activated a light on the control panel and thus indicated to the operator when the probe was in contact with the surface of the earth.

In use, the survey probe was lowered through the side door of the helicopter until the probe touched the ground with the detector 3 feet above the surface and the activity measurement was then recorded. In moving from point to point the operator reeled in a few feet of cable and then relowered the probe to take a reading at the next point. A second gamma survey meter (T1B) was used to monitor the inside of the helicopter.

The method of locating dose-rate contours on the ground by use of an aerial survey instrument was attempted in order to find a technique for covering large areas in a minimum time and reducing the radiation exposure to personnel. In addition, measurements were taken at different altitudes to obtain data on gamma air attenuation factors versus height above terrain (air-to-ground correlation factors).

The aerial survey instrument with Jordan Survey Meter Model AGB-10K-SR and 1,200-foot cable reel is shown in Figure 2.6. The ionization chamber is the Neher-White type, consisting of a metal shell with a subminature tube sealed in pure argon at 10 atmospheres. A relatively high output current from the chamber flows directly to the indicating

meter, eliminating the need for complex circuitry required in other types of radiation monitors. The response is logarithmic, which makes possible the wide range of 0.01 mr/hr to 10,000 r/hr in three scales. Accuracy is quoted at ± 10 percent of applied dose rate anywhere on scale. The spectral response of the instrument is made essentially flat between 300 kev and 1.3 Mev by using a lead absorber on the outside of the steel chamber shell and an aluminum secondary absorber on the inside. A built-in Sr^{90} source is supposed to insure a convenient and rapid field calibration check (see Figure 2.7). However, it was found that this source is not strong enough for accurate calibration and can only be used to ascertain that the instrument is operational.

Further information on the aerial survey instrument may be found in Reference 27.

A gamma survey meter (T1B) was used to monitor the inside of the helicopter and to determine the shielding effects of its fuselage.

2.2.4 Land Survey Instrument. The land survey instrument (Reference 28) consisted of a mobile ionization chamber, complete with preamplifier, mounted on a light trailer towed behind a $2\frac{1}{2}$-ton truck which carried a cabinet unit containing a Brown recorder and associated circuitry, and a gasoline driven generator supplying 300 watts at 115 volts, 60 cycles. The instrument was so arranged that the drive of the Brown recorder chart was moved from a tachometer attached to the trailer wheel. This yielded a direct plot of intensity versus distance.

The 3-cycle, logarithmic, recorder-chart scale was set by means of a selector switch to respond to any of the following ranges: 0.02 to 20 mr/hr, 0.2 to 200 mr/hr, and 20 to 20,000 mr/hr. A source designed to fit into a special calibrating-source holder on top of the ion chamber was used to check the calibration from day to day. An internal electronic signal allowed the instrument to be checked at any time for short-term drifts, even in the presence of high radiation fields. Other electronic controls permitted the checking and adjusting of the logarithmic recorder for response at any time.

Continuous use over rough terrain of the $2\frac{1}{2}$-ton truck carrying the recorder for the land survey meter caused failure of the instrument on D−1 day. Repair efforts were futile, so the Pathfinder, a vehicle position indicating system was substituted for the land survey meter. Gamma survey meters were used to take readings at various locations in the field. The Pathfinder is described in Section 2.4.5.

2.2.5 Core Sampler. The core sampler (Figure 2.8) consisted of two pieces of telescoping steel tubing 4 feet long, one piece $1\frac{1}{16}$ inch outside diameter with a 0.165-inch wall thickness and the other piece $1\frac{3}{16}$ inch outside diameter with a 0.060-inch wall thickness. The wall thickness of the inside piece of tubing (heavy wall) was decreased slightly to make a slip fit into the other tubing. Starting at the top, two matching slots 2 inches long by 1 inch wide were cut on 3-inch centers, followed by five matching slots 4 inches long and 1 inch wide, but on 6-inch centers, to form seven sampling cups. A sharp steel point was attached to the bottom of the outside tubing to facilitate ground penetration and a solid steel driving block was attached to the top of the inside and outside tubes to facilitate driving the sampler into the ground. Two stops 180 degrees apart were provided, one stop to position slots in closed position (180 degrees apart) when driving and recovering the sampler and the other stop to position the slots in open (0 degrees), as when taking samples.

The core sampler described above was tested at Jangle underground crater to insure that adequate representative samples would be obtained. The many experiments leading to the final instrument and sampling technique are described in Appendix G.

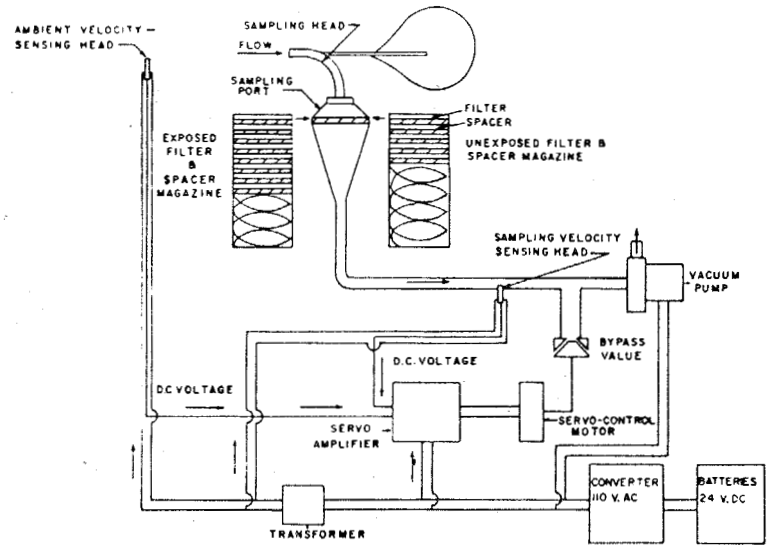

Figure 2.5 Functional diagram of the aerosol sampler control system.

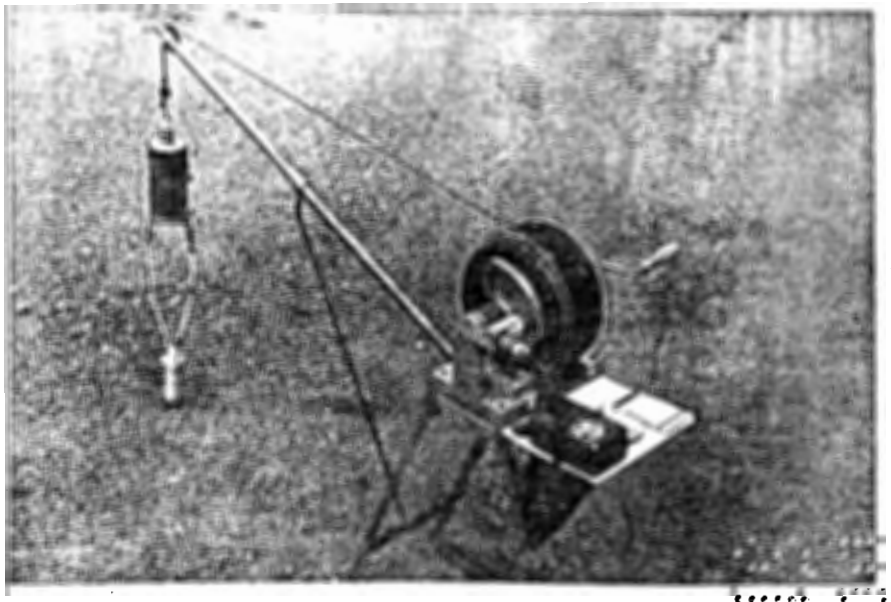

Figure 2.6 Aerial survey instrument.

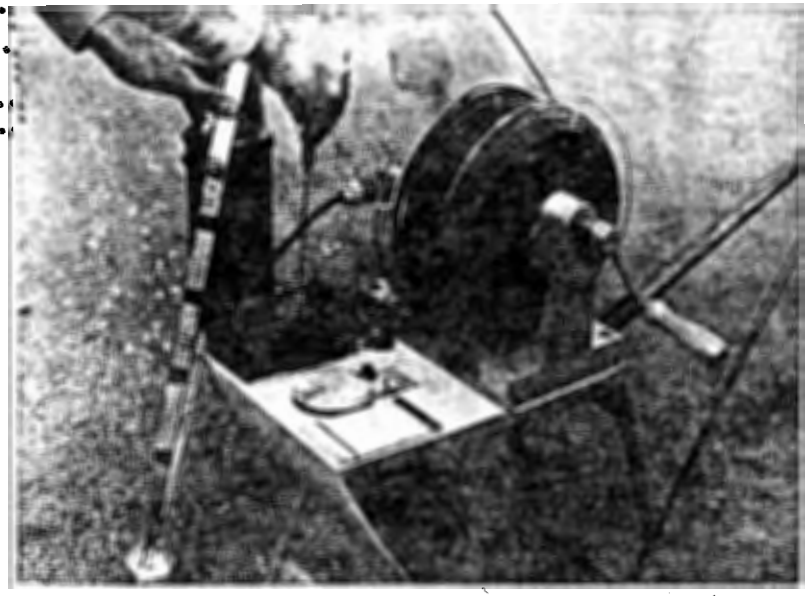

Figure 2.7 Calibration check of aerial survey instruments.

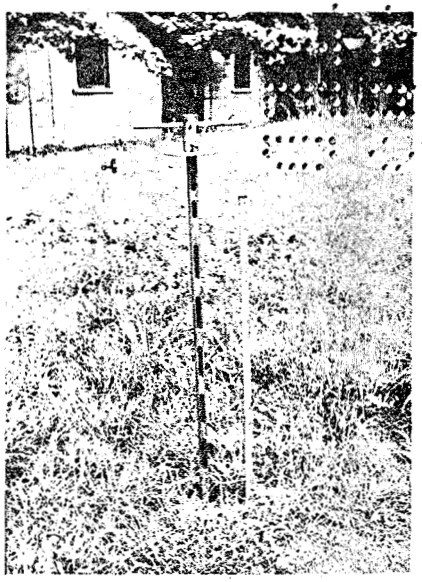

Figure 2.8 Core samplers; closed (left) and opened (right).

2.3 BASE SURGE AND FALLOUT SAMPLING

2.3.1 Field Operations. Project personnel arrived at the Nevada Test Site (NTS) at approximately D−50 days and remained until approximately D + 30 days. Following orientation, equipment was received, unpacked, and checked.

Twenty intermittent fallout collectors and two isokinetic differential aerosol samplers were installed at the predetermined locations described in Section 2.2 and illustrated in Figure A.1. The aerosol samplers and the fallout collectors which were located at distances of less than 1,650 yards from ground zero (the expected base-surge radius) were set for approximately 1-minute sampling intervals, except that 300-yard stations sampled on a 30-second cycle; the collectors at more distant stations used sampling intervals of approximately 5 minutes.

All collectors used in the expected base-surge area were mounted on modified Chemical Corps trailers (see Figures 2.9 and 2.10) to which long cables were attached to facilitate early sample recovery in highly contaminated areas. The length of the cables ($\frac{1}{4}$-inch diameter) used successfully to pull out instrumented trailers located at 300 and 700 yards from ground zero were 4,000 and 3,000 feet, respectively. Figure 2.9 also shows (center foreground) a gamma detector of Project 2.4.

Outside the base surge area, the collectors were mounted on 3-foot high wooden platforms (see Figure 2.11). This picture also shows the Naval Radiological Defense Laboratory (NRDL) bucket type fallout collector and adhesive paper sampling station.

The sampling instruments at each station were actuated by a radio timing signal at H−1 minute. Installation of instruments was completed in time for participation in timing signal dry runs and to check operation of instruments. However, a complete timing signal dry run was not furnished until late on D−1; too late for couple instrument check.

Samples were recovered at an early time after the test in order to meet the requirement for early decay measurements. In high-activity areas, vehicles were used to pull out trailers holding sampling instruments. Recovery parties drove to the end of the trailer cable lines located away from ground zero, attached the cable to the vehicle, and pulled the trailer to a lower activity area. Figure 2.12 shows an intermittent fallout collector on Trailer Station L-1 after it had been towed 4,000 feet by a $2\frac{1}{2}$-ton truck and cable. The amount of fallout on the trailer bed at the base of the collector is visible. The trailer and cable system definitely proved to be a successful method of recovering sampling instruments at early times and reducing the radiation exposure of recovery personnel. In low-activity areas, recovery parties drove up in vehicles to the station and recovered samples.

Fifteen sampling stations were recovered prior to H + 6 hours and the remaining five stations on D + 1 day. Samples were monitored, packaged and shipped by air to the Army Chemical Corps (ACC) at H + 12 and H + 24 hours.

2.3.2 Analytical Procedures. Samples obtained from the fallout collectors were used for determining decay rates, activity versus particle-size distribution, distribution of activity within particles, and weight and activity of fallout as a function of arrival time. The airborne activity within the base-surge area was determined from the filter samples collected by the aerosol sampler. These results will be correlated with the aerial and ground survey data.

Selected samples from the fallout collectors were analyzed at the test site for early beta activity and decay. The remainder were shipped to ACC for detailed analyses.

Upon arrival at ACC, each tray was monitored for gamma activity with an ionization-chamber-type survey meter and for beta-gamma activity with a Geiger-Muller (GM)

Figure 2.7 Calibration check of aerial survey instruments.

[redacted]

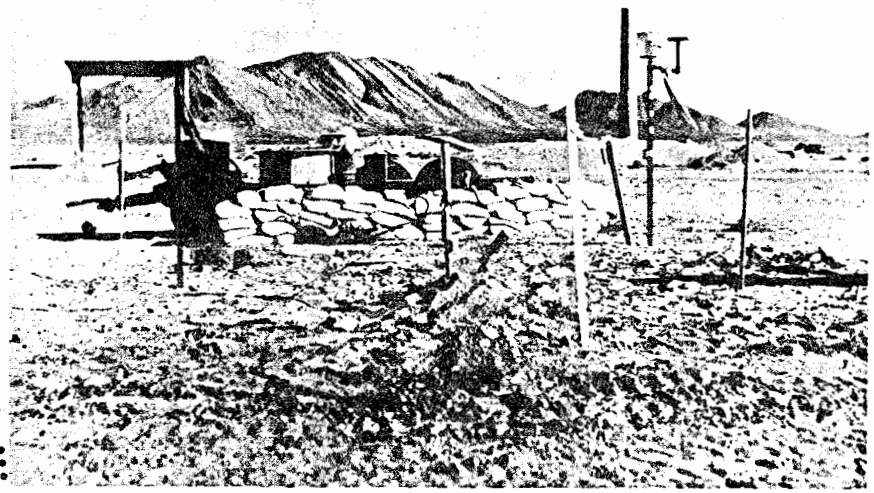

Figure 2.9 IFC on trailer; Station E-1.

Figure 2.10 IFC on platform; Station H-7.

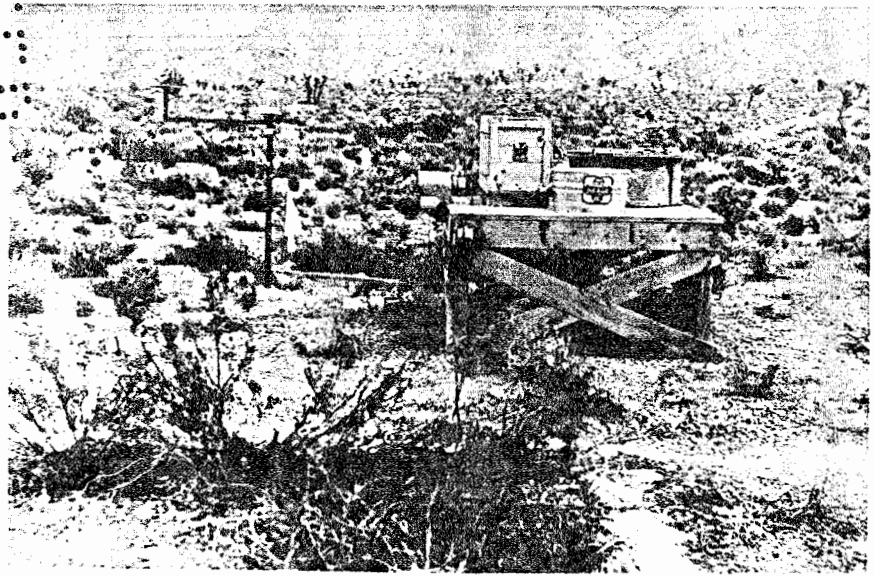

Figure 2.11 IFC on trailer; Station H-7.

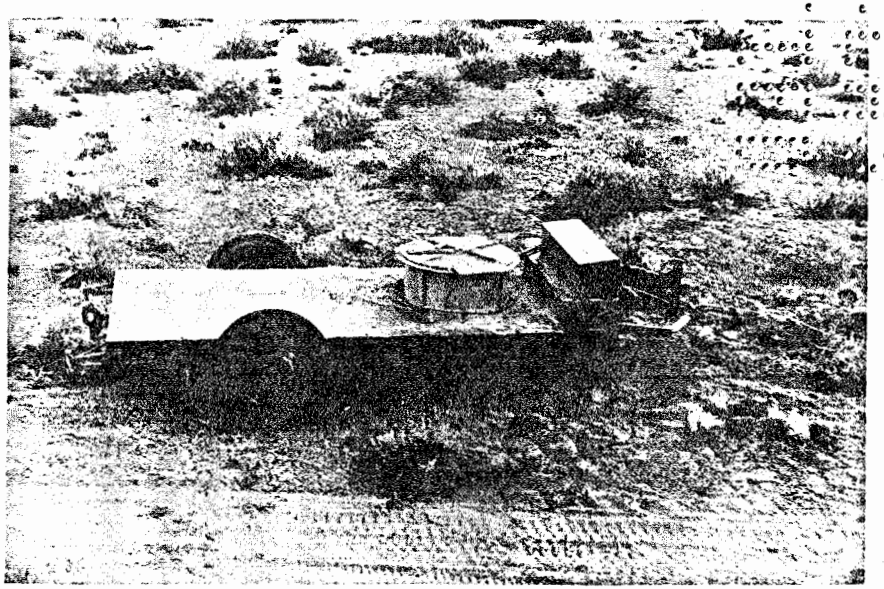

Figure 2.12 Recovery of IFC on trailer; Station L-1. Note fallout on trailer bed.

type survey meter. The total weight of the samples collected by each tray was measured. An accurately weighed portion of the total sample was saved for beta measurements.

Beta activities of the sample were determined by using GM tubes with window thicknesses of less than 2 mg/cm^2. The GM tubes were mounted in vertical lead shields, Technical Associates Model AL 14A, having a wall thickness of 2-inches lead, 0.25-inches brass, and 0.25-inches aluminum. A geometry-defining brass plate was inserted between the GM tube and the sample (Reference 29). The output of the tubes was fed into Model 1060 Atomic Scalers having a characteristic resolving time of 5 μsec. Samples with activities greater than 1,000 cpm were counted for 10,000 counts and samples with activities less than 1,000 cpm were counted for 10 minutes. Each sample was counted twice. In cases where the two counts did not agree within one standard deviation, a third count was taken and the three counts averaged.

It was necessary to apply several corrections in order to determine the disintegration rate of the samples. The various correction factors were evaluated in terms of the sample itself in order to avoid the errors associated with a direct comparison with a single isotope standard. The procedure is as follows:

1. The raw counts per minute were corrected for coincidence loss (Reference 30).

2. The count was corrected for geometry (G), defined as the fraction of solid angle subtended by the sensitive volume of the GM tube. This factor was determined by using the first three terms of the Blachman series (Reference 31). Succeeding terms of this series are insignificant and were not used for this correction.

3. Backscattering determinations (F_b) were made by mounting a GM tube in a hollow support of lead bricks approximately three feet from the floor and counting samples in this setup. This arrangement provided negligible backscattering from the floor of the support. A brass aperture was placed below the tube to minimize scattering from the walls of the support. Equal aliquots of dissolved fallout from the sample under analysis were pipetted into counting cups. One cup with a bottom of very thin rubber hydrochloride film (0.003 inches) was measured in the above arrangement which provided negligible backscattering. A glass-bottom cup was measured in the regular counting apparatus. The backscattering correction factor, obtained by dividing the count obtained in the regular apparatus by the count obtained in the arrangement with negligible backscattering, was used to correct all samples from that shot. Since the energy distribution of mixed fission products is known to be time dependent, this correction was made for various times. However, it was found that the variation was insignificant during the time the measurements were made on the samples concerned. The average backscattering was approximately 15 percent for the time interval of counting.

4. A correction (F_a) was made for absorption by the air between the sample and the tube window, and the tube window itself (Reference 32). To obtain this correction, precise absorption curves were determined on a sample from each shot. A correction factor was calculated from the following equation:

$$F_a = \frac{n_t}{N_o} = e^{-ut} \qquad (2.1)$$

Where: n_t = corrected counting rate observed with thickness t between the sample and the sensitive volume

N_o = true sensitive volume

t = thickness of material between the source and sensitive volume

u = mass absorption coefficient expressed in mg/cm^2

$$= \frac{1}{\Delta t} \ln \frac{n_t}{n_t + \Delta t}$$

$n_t + \Delta t$ = counting rate at thickness $t + \Delta t$

This method is applicable as long as the spectrum of beta ranges extends to zero energy with the same exponential relation observed by adding absorbers. This is characteristic of fission product beta energy spectra.

5. Self-absorption corrections for the samples in question were considered negligible, since the weight per unit area was kept to less than 10 mg/cm^2. According to Reference 33 a radioactive sample which consists of less than 10 mg/cm^2 and has an energy greater than 0.4 Mev requires no self-absorption correction. Furthermore, according to Reference 34, the nuclides with maximum energies below this value which contribute more than 1 percent of the gross fission activity constitute approximately 10 percent of the activity of the sample at the time the measurements for this report were made; i.e., approximately at H + 100 hours. Therefore, the error entailed by the assumption of a negligible correction should be 10 percent or less. The practice of ignoring this correction has been further justified by comparison of the defined geometry method with four-pi counting techniques (Appendix H). In these comparisons the experimental error ranged from 3 to 7 percent. The value of 0.4 Mev is the minimum beta energy measured. A part of the spectrum below this value is measured, but corrections for self-absorption below this range are probably high and are not considered.

6. The average beta activity (A_b) was treated by the above corrections to obtain the sample activity (A_d) in disintegrations per minute.

$$A_d = \frac{A_b}{F_a F_b G} \tag{2.2}$$

The above method has been used to determine the disintegration rate of known mixtures of nuclides with excellent results (Reference 35).

Decay data were taken for each collection interval, because the extrapolation of the beta activity from counting time to sampling time required the use of this data. For study of early decay at the test site one sample per six collection intervals for each IFC was used. These samples were processed in the same manner as the samples counted at ACC. The early-decay work commenced as soon as possible after the shot (H + 1 hour). Samples used for decay measurements at the test site, as well as all remaining usable samples were returned to ACC to provide a cross-calibration of the two counting systems.

A limited amount of particle size measurements were made on the IFC samples to cover the entire range of sizes for samples collected inside and outside the base surge. A number of standard sieve screens, as adopted by the National Bureau of Standards (NBS), were used to size the large particles down to 44 microns. Below 44 microns, the Roller Analyzer (Reference 36) was used to obtain smaller size fractions. This is an instrument used for particle size analysis and fractionation in the sub-sieve range (1 to 40 microns) employing air elutriation.

The distribution of activity within individual particles was studied. Selected IFC fallout samples were mixed together and sieved through 420, 297, 210, 149, 105, 88, 62, and 44 micron sieves. Each of the resulting fractions was split into two aliquots. The particles from one aliquot were radioautographed and the physical characteristics of the radioactive particles determined. The particles from the second aliquot were placed in the bottom of a cylindrical mold. Lucite was put in the mold and the contents of the mold were heated to the melting point of lucite. After cooling, enough of a layer was shaved off the lucite mounts to cut the embedded particles of each fraction in half. Radioautographs of the particles were made using Kodak Metallographic plates. The plates were exposed for varying lengths of time, depending on the activity of the particles

on the mounts. The exposure was only long enough to obtain a sharply defined radioautograph showing the distribution of the activity within the particles. After the development of the radioautograph, they were matched with the particles on the mounts and examined under the binocular microscope. Note was made of the distribution of activity on the particles and the physical characteristics of the particles.

Radiochemical analysis was made on IFC fallout and crater-lip core samples as required. Radiochemical data to support documentation of the base surge and fallout formation and contamination was obtained by the following method: (1) samples were selected from intermittent fallout collectors; one in the crosswind direction (southwest leg) in the base-surge area where little cloud fallout was expected and the other in the downwind direction where both base-surge fallout and cloud fallout could occur; (2) the Sr^{89}, Ba^{140}, Ce^{144}, and Mo^{99} concentrations (Mo is considered as ideally representative of fission products without long-lived gaseous precursors) were determined on similar time-interval samples from each collector (approximately ten intervals from each collector); and (3) a comparison of the analyses of these two collectors was made in order to offer data to differentiate between cloud fallout and base-surge fallout and to permit an estimate of the time when significant cloud fallout arrived at the station.

The premise of the experimental plan was that less cloud fallout would occur at the crosswind station than at the downwind station, and consequently, that the crosswind samples are most representative of the base-surge contamination. On the basis of this premise and the rare gas precursor effect discussed in Section 1.3.1, radiochemical analyses for Sr^{89}, Ba^{140}, Ce^{144}, and Mo^{99} in time incremental samples collected in the downwind area will indicate the time of arrival and contribution of significant fallout in this area. The Sr^{89} and Ba^{140} represent fission products with rare gaseous precursors while Ce^{144} and Mo^{99} represent the fission product without rare gaseous precursors. The data are presented as R values which are the ratios of the counting rates of two nuclides analyzed in the shot samples divided by the counting rates of these same two nuclides analyzed in the thermal neutron irradiation of U^{235}. These counting rates are measured under identical conditions and are corrected for radioactive decay to zero time, for the chemical yield of the separation and for self-absorption and self-scattering. The Sr^{89}/Mo^{99} R values, for example, are:

$$\text{R value} = \frac{\dfrac{(\text{counts/min } Sr^{89})}{(\text{counts/min } Mo^{99})\ \text{shot sample}}}{\dfrac{(\text{counts/min } Sr^{89})}{(\text{counts/min } Mo^{99})\ U^{235}}}$$

2.4 AERIAL AND GROUND SURVEY

2.4.1 Field Operations. Station locations for the various projects of Program 2 were laid out on an extensive circular grid system of approximately 150 points, as shown in Figure A.2. These points were marked by Project 2.5.1 with colored flags, painted signs, and lime in order to facilitate identification of the different sampling points by aerial and ground survey parties. Downwind stations were laid out on six sectors around ground zero starting on the 60-degree azimuth and spaced 20 degrees apart to the 160-degree azimuth. On each radius, thirteen stations were established at various intervals from 300 to 18,000 yards from ground zero. Upwind and crosswind stations were laid out on twelve 20-degree sectors starting on the 180-degree azimuth

and ending on the 40-degree azimuth. On each of these radial lines, six stations were marked at from 300 to 2,500 yards from ground zero. A crosswind line was extended to 4,500 yards on the 220-degree azimuth.

2.4.2 Aerial Survey of Crater and Lip. The radiation intensity in the crater and lip was surveyed from helicopters with the instruments described in Section 2.2.3. At H + 2 and H + 3 hours, two helicopters began a survey of the crater, lip, and other fallout areas. Surveys were conducted from an altitude of 500 to 800 feet, depending upon radiation intensity within the aircraft and ability to hover. In general, aerial surveys were planned for those areas where the ground intensity was greater than 10r/hr

2.4.3 Aerial Surveys Utilizing Raydist. In addition to the aerial survey data obtained on the initial Rad-Safe aerial surveys, arrangements were made with Project 5.2 to install Raydist equipment in one helicopter for the purpose of surveying areas beyond the extent of the close-in established grid system. A test run indicated that the area of expected fallout was within the range of this equipment extending from the immediate shot area out to approximately 11 miles downwind from ground zero. With the aerial survey instrument probe extended, the pilot was directed to change course so as to continually cross and recross a particular radiation-intensity line. At each crossing the Raydist operator was given a signal and the position of the helicopter was recorded. Thus, a continuous plot of a particular isodose line was possible.

2.4.4 Ground Survey by 50th Chemical Platoon. Measurement of the radiation intensity was made by several ground survey parties who had been assigned separate portions of the expected fallout area. Following orientation by Project 2.5.1 personnel, seven survey crews from the 50th Chemical Platoon at Camp Desert Rock were assigned sections of the Program 2 station array shown in Figure A.2. One crew was directed to begin the survey at the most distant station on the 160-degree true azimuth of I-line and proceed toward ground zero until a dosage of 300 mr had been accumulated, then to return. In like manner, crews were assigned to the 60-, 80-, 100-, 120-, and 140-degree azimuths (the D, E, F, G, and H lines). The seventh crew was assigned all upwind and crosswind station locations, beginning on those stations at 2,500 yards and moving in toward ground zero.

In order to establish the background radiation in the area and to become familiar with the terrain, the survey parties began the survey on D−6 days and made three surveys prior to the shot. Each party consisted of from two to four men in a jeep and two calibrated gamma survey instruments (T1B). The crew stopped at each station location, left their vehicle, and made two radiation intensity readings at a height of three feet above the ground. Extra personnel were assigned to each crew to insure that replacements would be available who were familiar with the route. Prior to beginning the surveys, each station was marked with a system of two colored flags to identify the locations to be surveyed. In addition, a sign was painted, numbered, and installed at each location to insure that the correct station would be recorded on data sheets prepared especially for the survey crews. The routes to be used through the rough terrain were marked on contour maps showing the station grid systems and given to each survey party at the start of the operation.

2.4.5 Ground Survey Utilizing Pathfinder Positioning. Ground survey data was obtained with a calibrated T1B and Victoreen gamma survey meter by the Corps of Engineers, Fort Belvoir, Virginia, utilizing the Pathfinder as a vehicle position indicator.

Close-in surveys around ground zero and extended surveys out to 11 miles downwind were conducted with two readings taken at each located position. The Pathfinder, composed of a miniature gyroscope direction indicator and a computer for determining grid coordinates, was substituted for the land-survey meter which failed to operate prior to shot time.

2.4.6 Ground Survey by Recovery Parties. Additional ground-survey data were obtained by project recovery parties who entered the area at H + 2 and H + 24 hours to recover samples and instrumentation records. Gamma intensity measurements were made with a T1B survey meter at station locations visited by the recovery parties. Data were obtained for several days after the shot.

2.4.7 Instrument Calibration. All survey instruments, both aerial and ground, were calibrated daily at the Rad-Safe building. In addition, the aerial survey instrument was

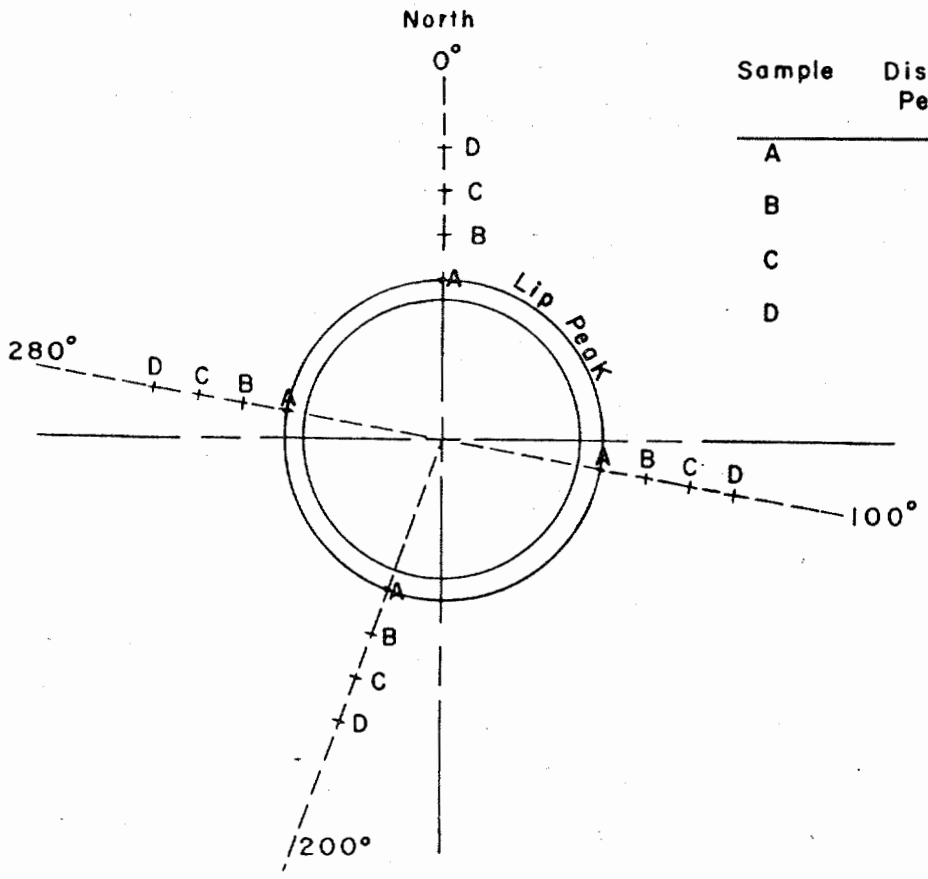

Sample	Distance From Peak Of Lip (ft)
A	0
B	30
C	60
D	90

Figure 2.13 Location of core samples from the crater lip area taken on D + 8 and D + 9 days.

calibrated at the Evans Signal Laboratory (ESL) facilities at Camp Mercury where a stronger source was available. The two sources were cross-calibrated by ESL personnel.

2.4.8 Analytical Procedures. Radioactivity readings (r/hr) obtained by aerial and land surveys were plotted on scaled maps of the test site and adjacent areas. Additional data from Projects 2.1, 2.4, 2.5.2, 37.2, and Rad-Safe were utilized in establishing the

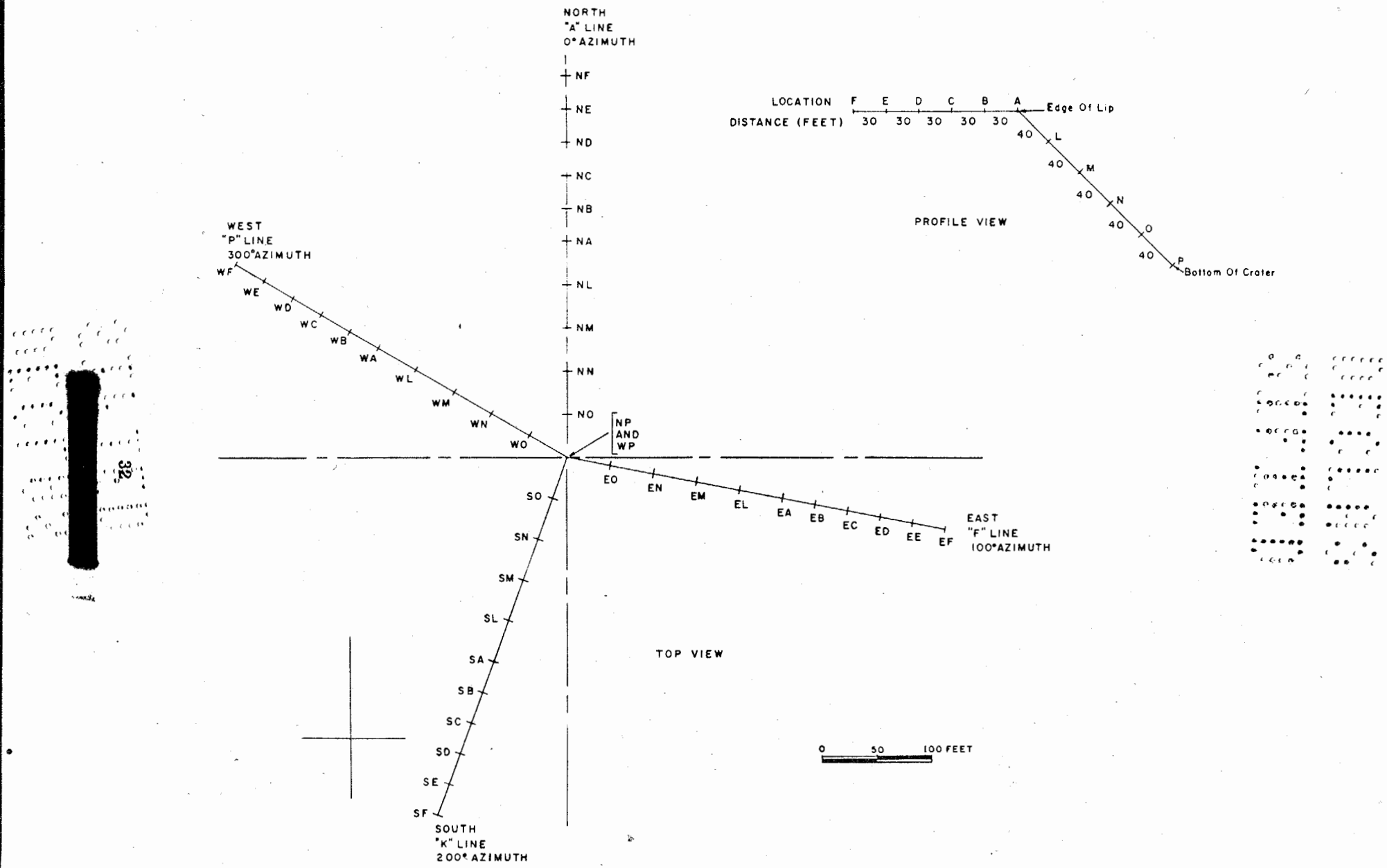

Figure 2.14 Location of core samples from the crater lip area taken on D + 97, D + 98, and D + 99 days.

residual gamma radiation fallout pattern. Dose-rate contours were drawn to the 1-r/hr line at H + 1 hour by correcting according to $T^{-1.2}$ decay. Aerial-survey data were plotted as gamma air attenuation factors versus height above terrain. Data resulting from the photographic analysis of the growth of the cloud and the extent of the base surge were used in conjunction with the survey data to determine the relation between the residual contamination and the extent of the base surge.

The dose-rate contours obtained from this shot were compared with those resulting from the surface and underground Jangle shots in an attempt to arrive at criteria useful in developing scaling relationships which take into account differences in scaled depth of burst.

2.5 CRATER AND LIP SAMPLING

2.5.1 Field Operations. Project personnel remained at the test site after D-day to recover crater-lip surface and core samples from the Shot 7 area. Samples were taken on D + 8 and D + 9 days. Surface samples at each core sampling position were taken in a small jar. The ground was very soft and the core samplers could be pushed in part way or all the way by hand. The locations of the core samples are shown in Figure 2.13. Technique in obtained core samples is presented in Appendix G.

Three project personnel returned to the test site on 27 June 1955 to obtain additional samples from the Shot 7 crater-lip area. Core and surface samples were taken in the same manner as mentioned above. The location of the core samples is shown in Figure 2.14. In addition, a ground survey of project stations was made close-in to ground zero.

2.5.2 Analytical Procedures. Beta activity was measured for all core samples in the same manner as described in the IFC analysis, Section 2.3.2. Decay data were obtained in the same manner as described in the IFC analysis, Section 2.3.2. The activities obtained were extrapolated to sampling time along the sample decay curves as experimentally and theoretically determined.

The gamma spectra of selected crater and lip samples were determined approximately forty days after shot time. Samples were selected to show any variation with depth below the surface and at varying distances from ground zero at one particular depth. The analyses present a semiquantitative estimation of the significant long-lived radionuclides present in the sample. Such information is valuable for interpreting the decay characteristics of these samples.

Chapter 3

RESULTS AND OBSERVATIONS

3.1 DOSE RATE CONTOURS

Aerial and ground-survey data obtained from several surveys of the contaminated area are presented in Appendixes C and D, respectively. Assuming that decay of the radioactive material followed $T^{-1.2}$, all survey data were corrected to H + 1 hour and dose-rate contours were constructed on scaled maps of the test site and surrounding areas. Data to support the $T^{-1.2}$ decay assumption are presented in Section 3.3.1 and in the following conclusion from Reference 37 which states, "It does appear, however, that for the underground event the decay follows generally a $T^{-1.2}$ type of decay except at times where there is obvious build-up, probably attributable to local redistribution of the activity by wind action." Dose rate contours for Shot 7 are shown in Figures 3.1 through 3.3. A planimeter was used to determine the areas in square miles enclosed by the various dose-rate contours. These areas are presented in Table 3.3. Idealized Teapot and Jangle dose-rate contours were determined and presented and discussed in Chapter 4.

An array of film badges in NBS holders was located in a grid network as shown for stations in Figure A.2. The film badges were recovered on D + 2 and D + 3 days and turned over to ESL for processing. Total dose contours, Figure 3.4, were determined by plotting the ESL gamma film badge data (Reference 38). The film badge data includes the radiation from the cloud as well as from the residual contamination. The total dose was measured from zero time to recovery time (D + 2 and D + 3 days). Since the film badges were recovered on two different days and the exact time of recovery is not known, no correction to a common time could be made. Therefore, the readings plotted represent a time period of D + 2 and D + 3 days. Total gamma-dose areas are summarized in Table 3.2.

Figure 3.5 shows the 10-mr/hr and 100-mr/hr dose-rate contours which were determined from survey data (Table D.7) obtained on D + 97 to D + 99 days. The areas enclosed by these contours are 0.825 sq mi for the 10-mr/hr line and 0.122 sq mi for the 100-mr/hr line.

3.2 BASE SURGE AND FALLOUT SAMPLING

Of the twenty intermittent fallout collectors installed to sample the base surge fallout and cloud fallout (Figure A.1), seven instruments collected samples. Three instruments, although they operated, were not within the fallout area. The remaining ten collectors failed to operate. Of the ten failures, six were caused by radio timing signal failures and four by instrument failures.

The two isokinetic aerosol samplers operated satisfactorily. In addition, samples of gross fallout were collected in total collectors (buckets) for the purpose of obtaining larger volumes of material for studies of the radioactive debris.

3.2.1 Time of Arrival of Activity at Station Locations. Time of arrival of activity at Project 2.5.1 stations was determined by measuring the beta disintegration rates of

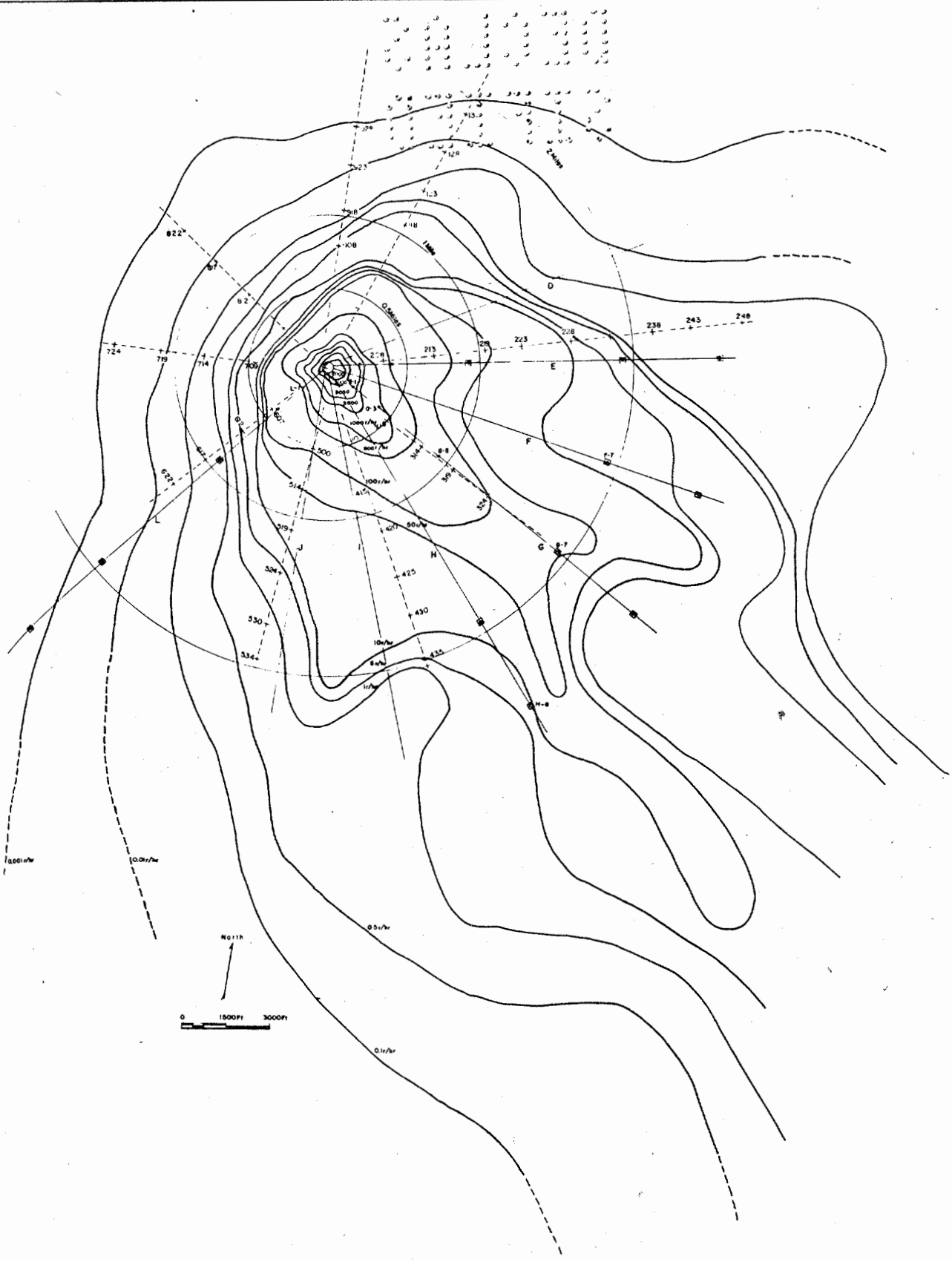

Figure 3.1 Dose-rate contours at H + 1 hour, 10 r/hr line closed.

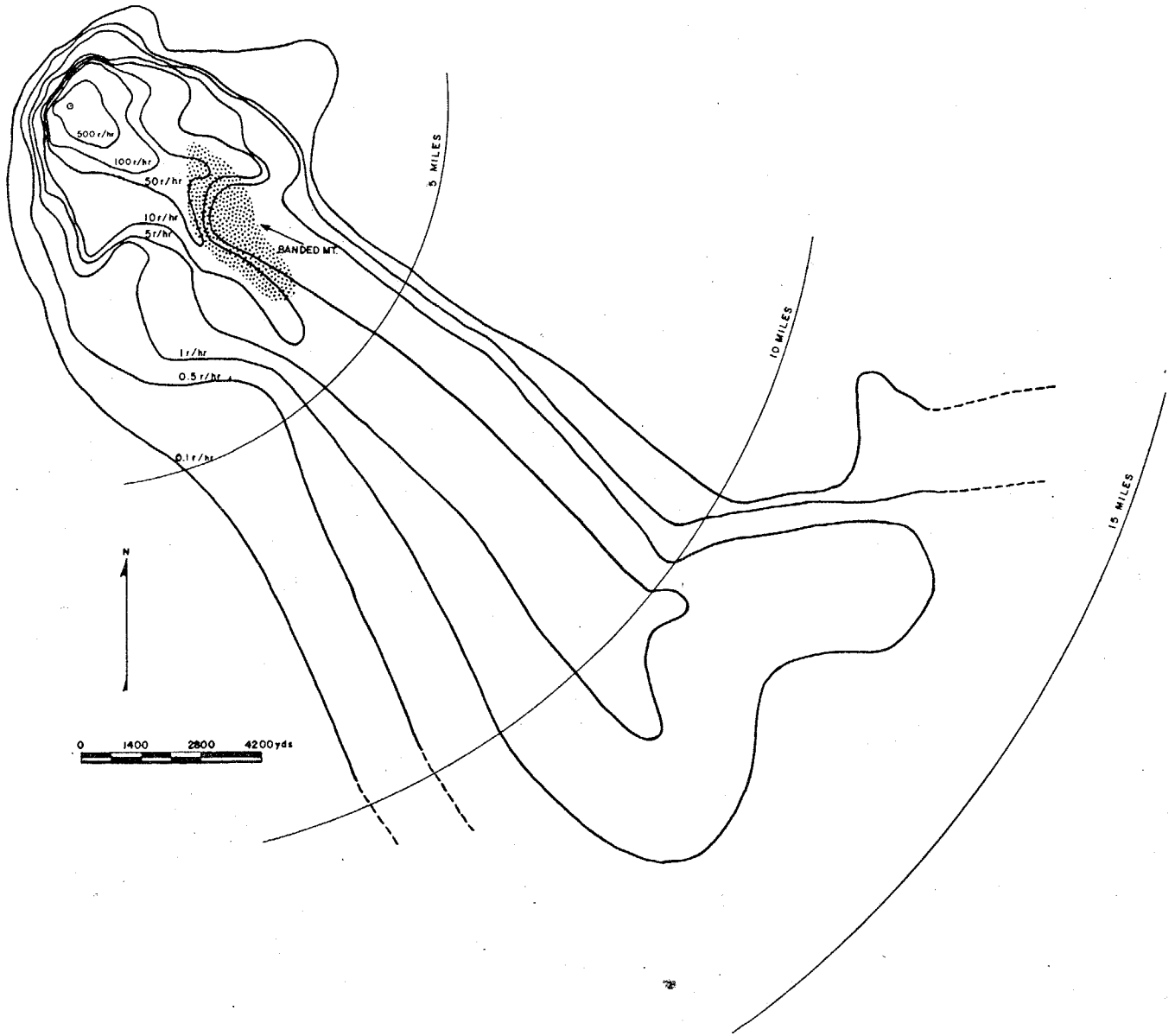

Figure 3.2 Dose-rate contours at H + 1 hour, 1 r/hr line closed.

Figure 3.2 Dose-rate contours at H + 1 hour, 1 r/hr line closed.

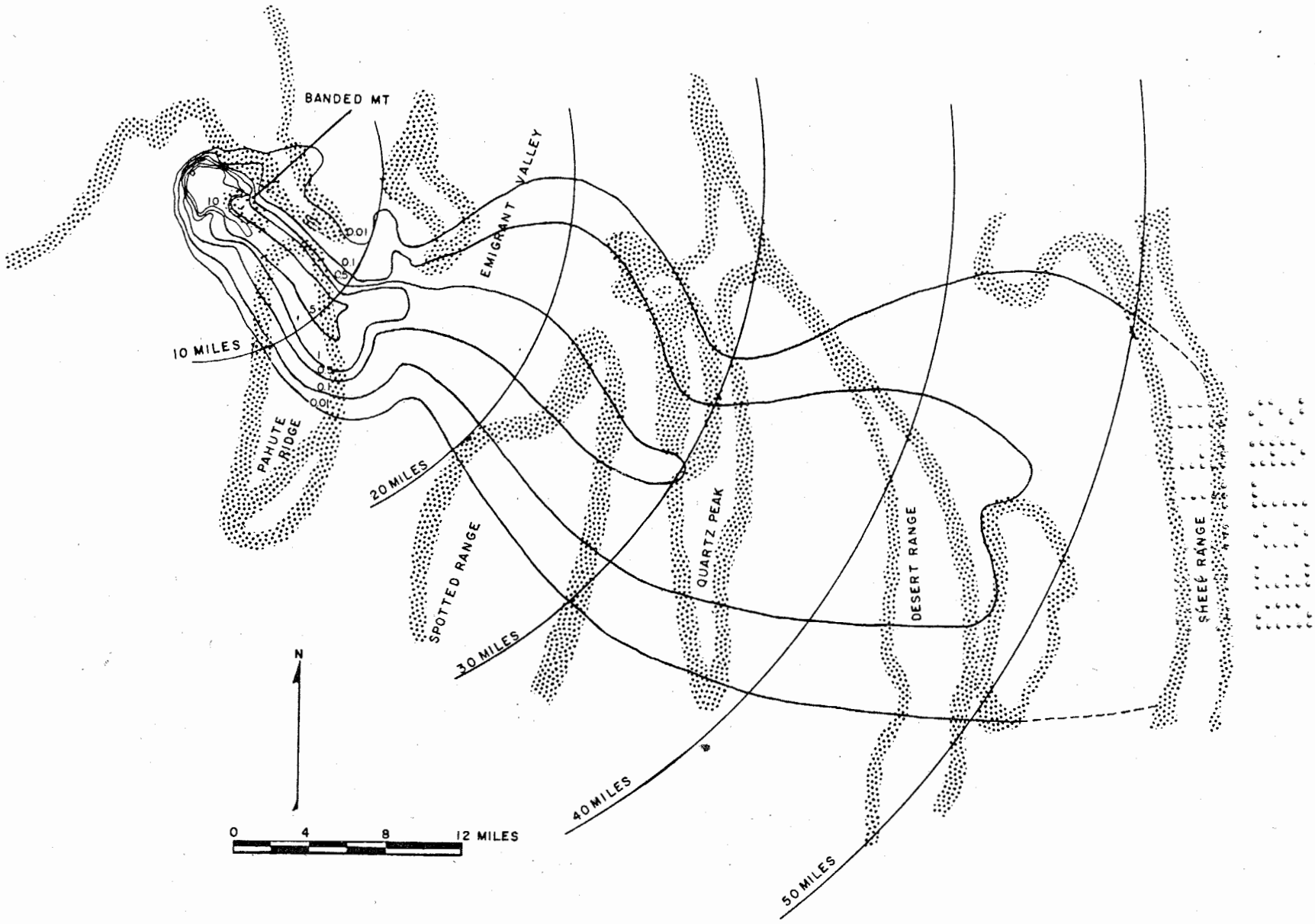

Figure 3.3 Dose-rate contours at H + 1 hour, 0.1 r/hr line closed.

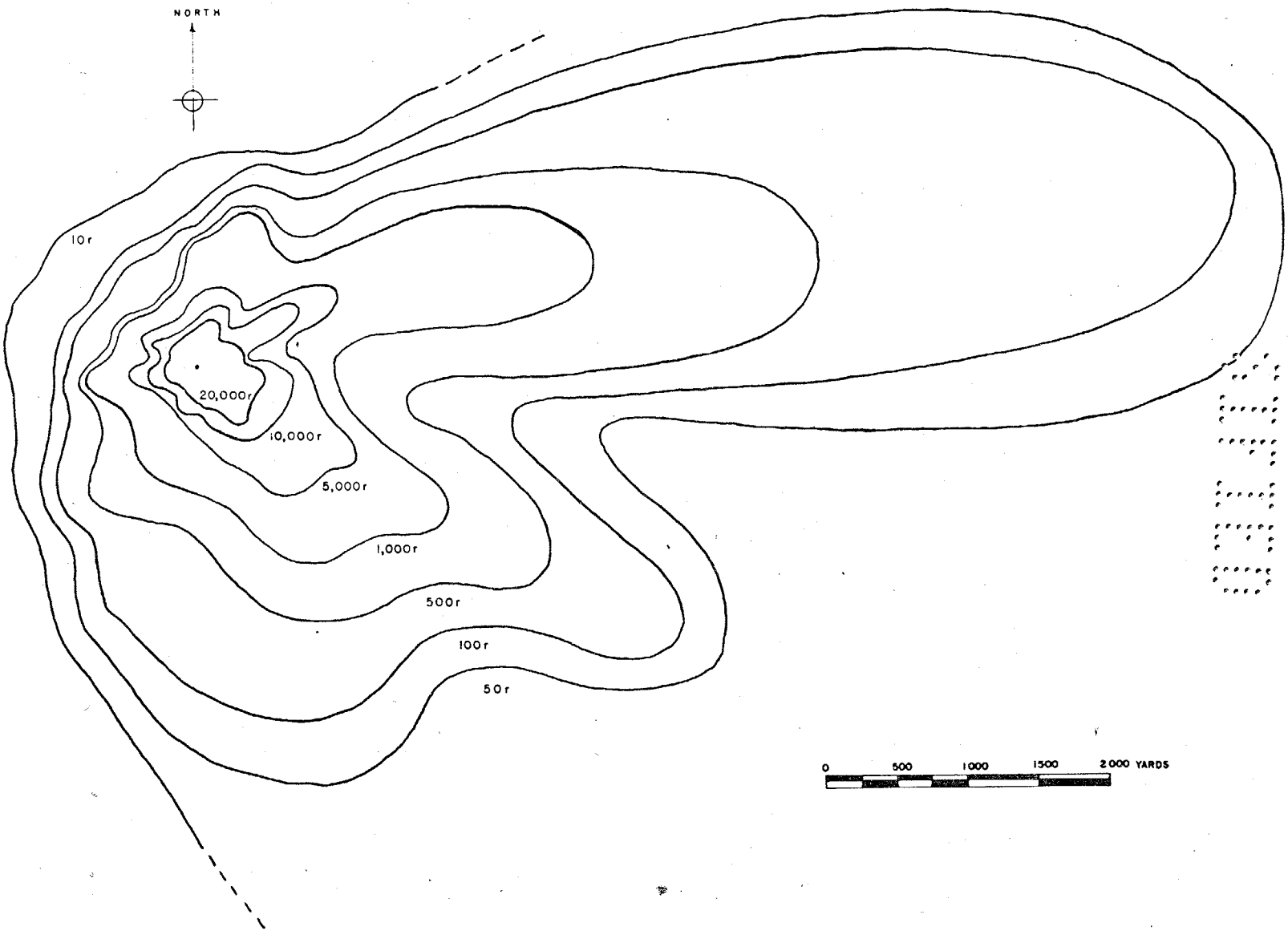

Figure 3.4 Total gamma dose contours from zero time to recovery time (D + 2 to D + 3 days).

TABLE 3.1 AREAS IN SQUARE MILES ENCLOSED BY

TABLE 3.1 AREAS IN SQUARE MILES ENCLOSED BY DOSE RATE CONTOURS AT H + 1 HOUR

Dose Rate	Idealized Station Locator 1 inch = 500 yards	Army Map Service 1 inch = 1,400 yards	Civil Defense Map 1 inch = 4 miles
r/hr	mi^2	mi^2	mi^2
6,000	0.013	—	—
5,000	0.029	—	—
3,000	0.070	—	—
2,000	0.121	—	—
1,000	0.261	—	—
500	0.518	0.46	—
100	1.41	1.23	—
50	2.42	2.15	—
10	5.55	5.00	5.12
5	—	14.96	15.20
1	—	37.79	39.20
0.5	—	—	102.9
0.1	—	—	450.9
0.01	—	—	992 *
0.01	—	—	809 †

* Area was determined from approximate extension and closure of the 0.01 r/hr dose-rate contour.

† Area was determined by closing the 0.01 r/hr dose-rate contour at the 50-mile radius arc from ground zero.

TABLE 3.2 TOTAL DOSE AREAS (D + 2 TO 3 DAYS)

Gamma Dose	Area
r	mi^2
20,000	0.094
10,000	0.207
5,000	0.452
1,000	1.49
500	3.19
100	7.03
50	9.34
10	—

TABLE 3.3 SAMPLING TIMES AFTER H-HOUR FOR EACH INTERMITTENT FALLOUT COLLECTOR INTERVAL

Station location and interval time; setting-times in minutes and seconds.

Tray	F-7	G-1	G-3	G-5	G-7	H-8	L-1
1	5:15	0:11	1:26	1:06	5:07	4:51	− 0:06
2	10:30	0:38	2:39	2:09	10:14	9:42	+ 0:21
3	15:45	1:05	3:52	3:12	15:21	14:33	0:48
4	21:00	1:32	5:05	4:15	20:28	19:24	1:15
5	26:15	1:59	6:18	5:18	25:35	24:15	1:42
6	31:30	2:26	7:31	6:21	30:42	29:06	2:09
7	36:45	2:53	8:44	7:24	35:49	33:57	2:36
8	42:00	3:20	9:47	8:27	40:56	38:48	3:03
9	47:15	3:47	11:10	9:30	46:03	43:39	3:30
10	52:30	4:14	12:13	10:33	51:10	48:30	3:57
11	57:45	4:41	13:36	11:36	56:17	53:21	4:24
12	63:00	5:08	14:49	12:39	61:24	58:12	4:51
13	68:15	5:35	16:02	13:42	66:31	63:03	5:18
14	73:30	6:02	17:15	14:45	71:38	67:54	5:45
15	78:45	6:29	18:28	15:48	76:45	72:45	6:12
16	84:00	6:56	19:41	16:51	81:52	77:36	6:39
17	89:15	7:23	20:54	17:54	86:59	82:27	7:06
18	94:30	7:50	22:07	18:57	92:06	87:18	7:33
19	99:45	8:17	23:20	20:00	97:13	92:09	8:00
20	105:00	8:44	24:33	21:03	102:20	97:00	8:27
21	110:15	9:11	25:46	22:06	107:27	101:51	8:54
22	115:30	9:38	26:59	23:09	112:34	106:42	9:21
23	120:45	10:05	28:12	24:12	117:41	111:33	9:48
24	126:00	10:32	29:25	25:15	122:48	116:24	10:15

representative samples which were collected by different portions of the IFC instruments. These total beta activity data for each sampling interval were corrected to H + 1 hour. Then, activity per sampling interval (dis/min) was plotted against collection time for each IFC as shown in Figures 3.6 through 3.12. The counting rate data shown in these figures are related to total activity in Tables B.1 through B.7. At stations G-1, G-3, G-5, H-8, and L-1, the IFC door was found open on recovery, indicating that the tray under the opening was exposed to fallout beyond its normal

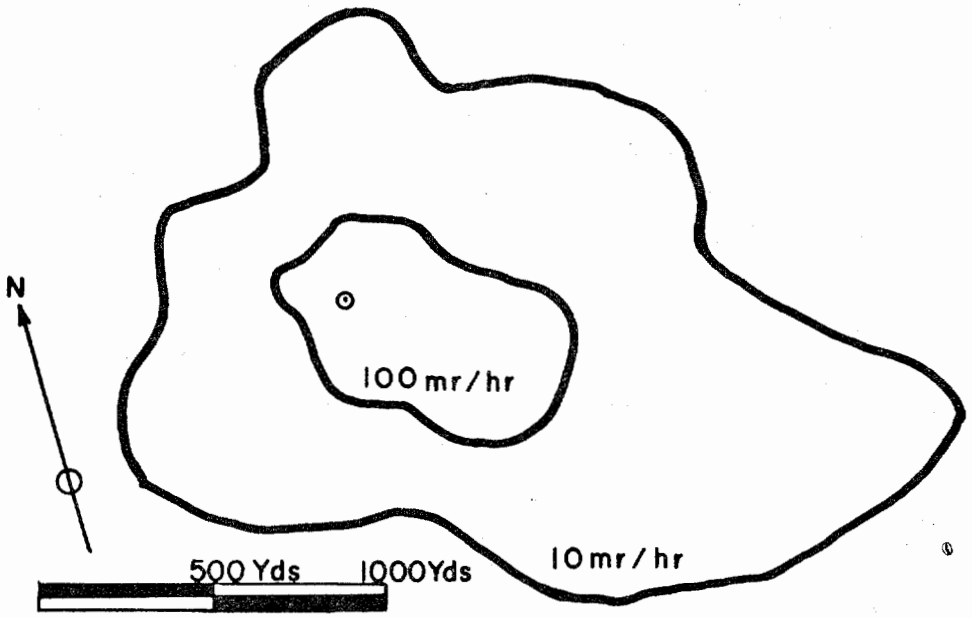

Figure 3.5 Dose-rate contours at D + 97, D + 98, and D + 99 days.

sampling time. Therefore, the data from these trays (usually No. 1) were not considered as valid. In the case of the collector at station L-1, tray No. 2 was under the opening; therefore, both 1 and 2 were considered not valid.

The end of the sampling time after H-hour for each IFC interval is listed in Table 3.3. Timing intervals for instruments located at stations G-1 and L-1 were set for approximately 30 seconds, at G-3 and G-5 for approximately 1 minute and at F-7, G-7, and H-8 for approximately 5 minutes.

3.2.2 Base-Surge Analysis: The final base-surge analysis was made after all of the documentary photographs were received, reviewed, and a detailed comparison made of photography, intermittent fallout collector data, isokinetic air sampler data, and visual observations to resolve the role of the base surge in carrying activity. Eyewitness accounts and technical photography of Shot 7 reveal that the sequence of events following the detonation were not the expected ones as indicated in Section 2.1. It appeared that some part of the fireball broke the surface of the ground. This may be seen in Lookout Mountain Laboratory (LML) aerial film, RKC-113. Several jets, or spears of earth, emerged through the top of the apparent fireball and soared to about 700 feet above the floor of the desert, Figure 3.13. There was a central jet which came up through the middle of the apparent fireball at tremendous velocity. Several other jets surrounding the central one traveled upward and outward at slower velocities than the central one but eventually reached the same maximum altitude. The throwout arched at much lower al-

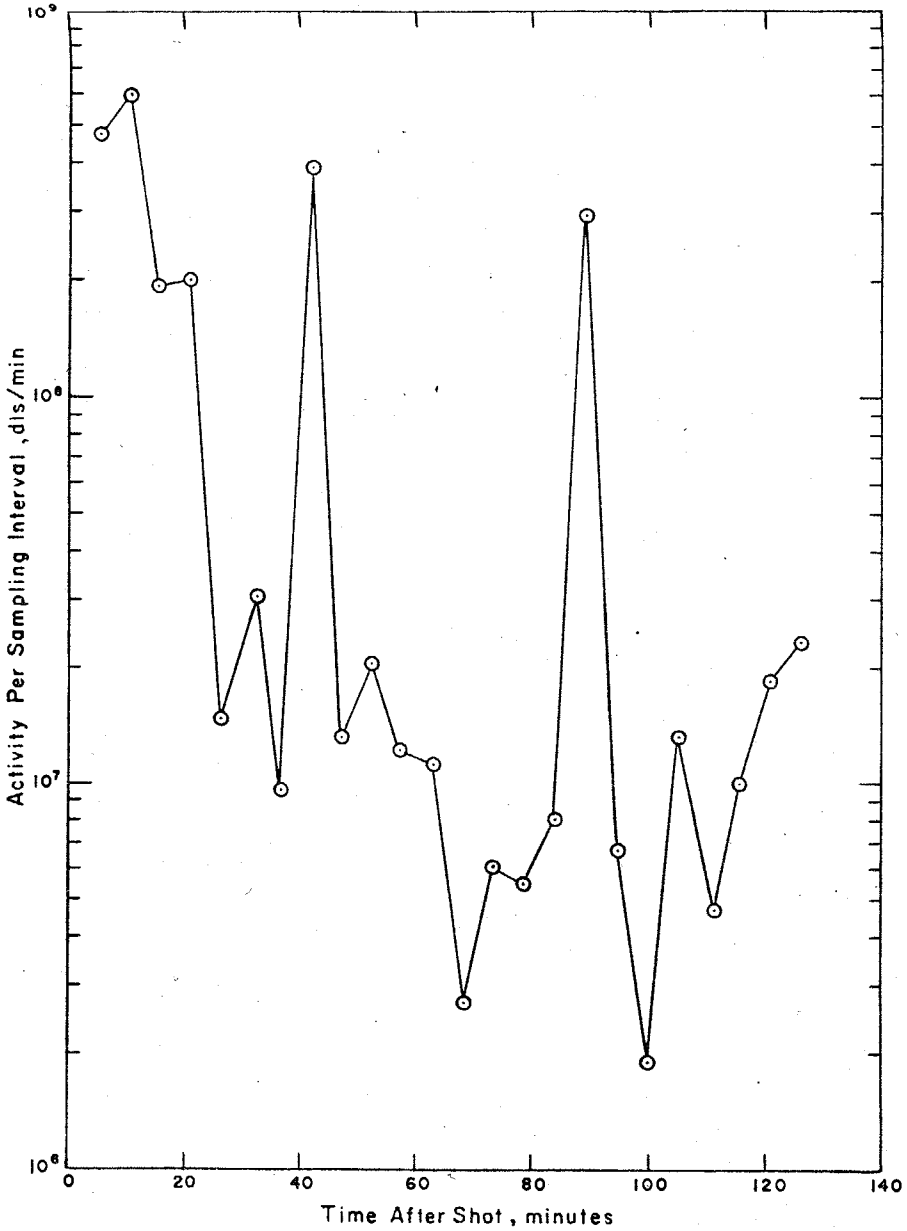

Figure 3.6 Time of arrival of activity corrected to H + 1 hour at Station F-7, 3,400 yards from ground zero, 100-degree azimuth. Sampling interval was set at 5 minutes 15 seconds.

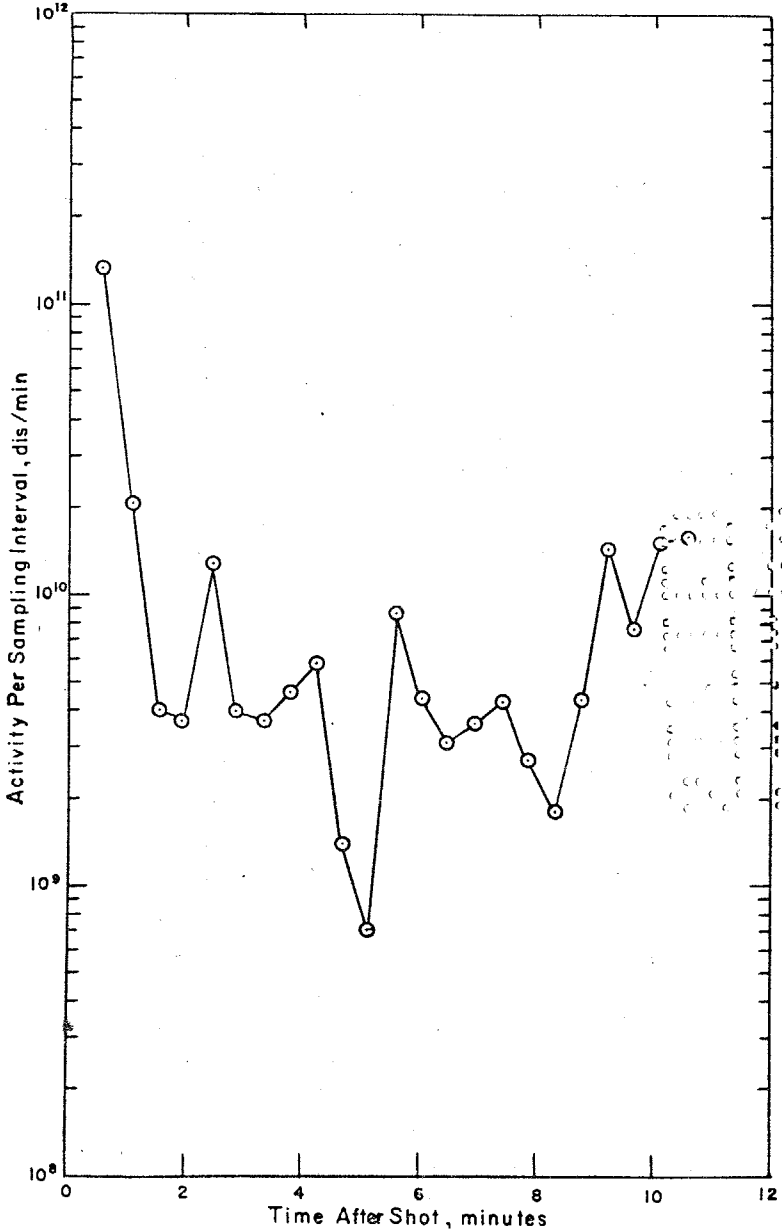

Figure 3.7 Time of arrival of activity corrected to H + 1 hour at Station G-1, 300 yards from ground zero on the 120-degree azimuth. Sampling interval was set at 27 seconds.

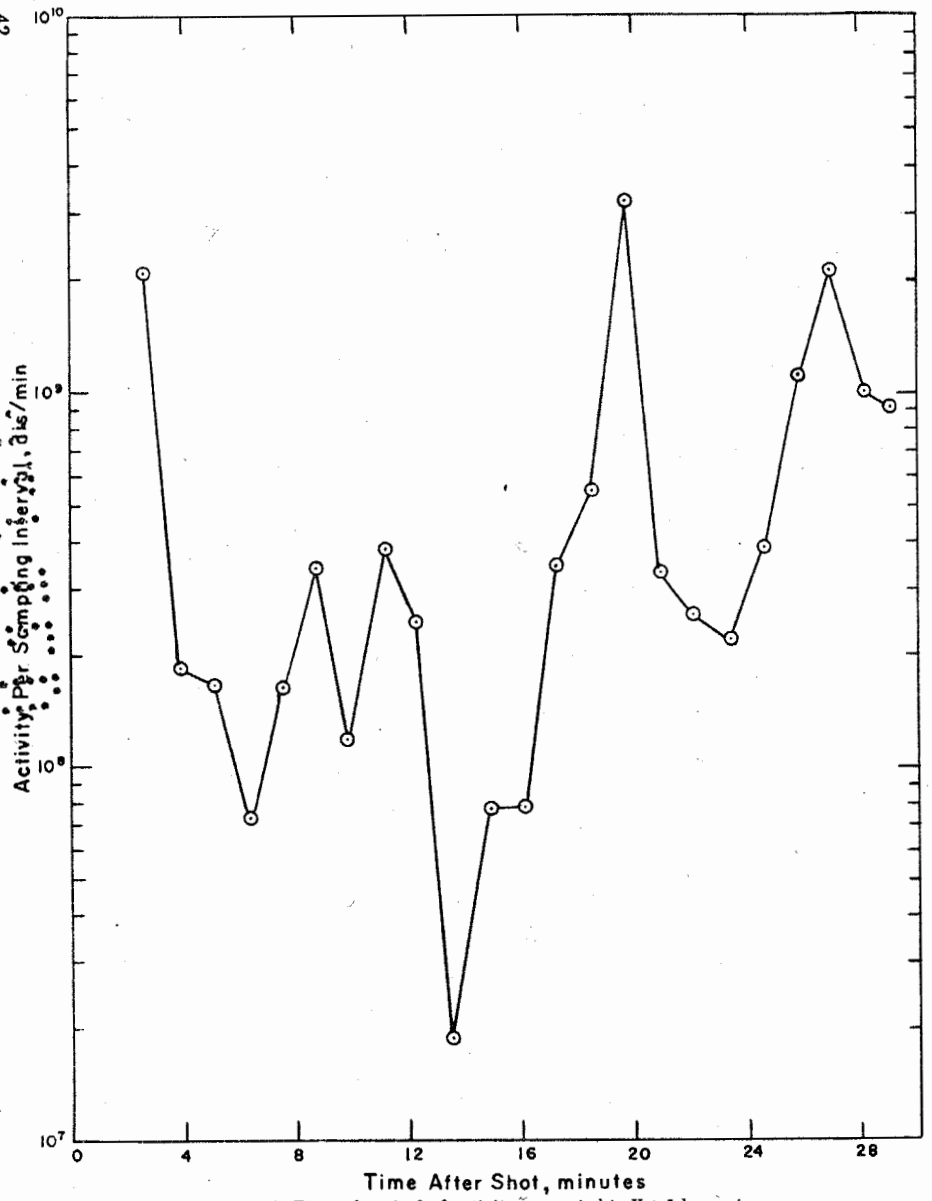

Figure 3.8 Time of arrival of activity corrected to H + 1 hour at Station G-3, 700 yards from ground zero on the 120-degree azimuth. Sampling interval was set at 73 seconds.

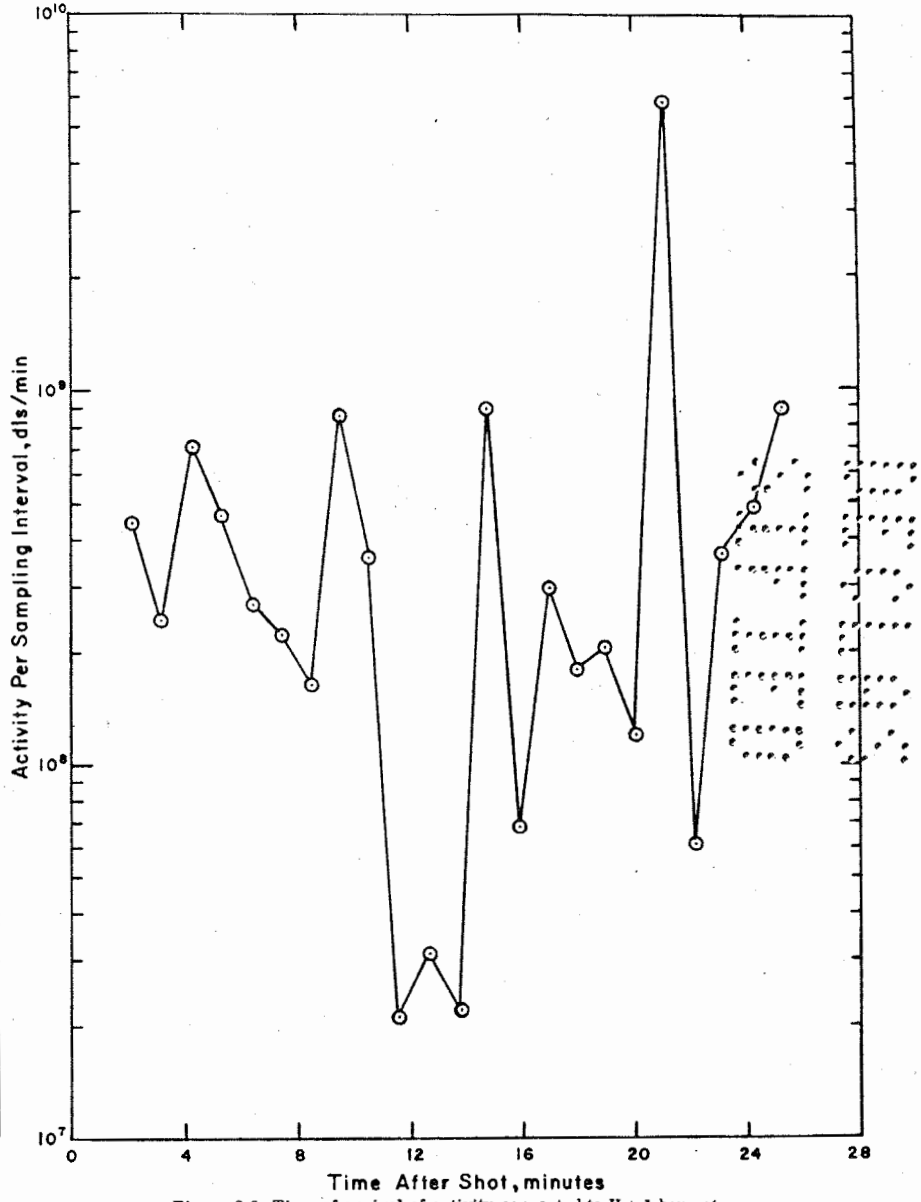

Figure 3.9 Time of arrival of activity corrected to H + 1 hour at Station G-5, 1,650 yards from ground zero on the 120-degree azimuth. Sampling interval was set at 63 seconds.

Figure 3.8 Time of arrival of activity corrected to H + 1 hour at Station G-3, 700 yards from ground zero on the 120-degree azimuth. Sampling interval was set at 73 seconds.

Station G-5, 1,000 yards [illegible]
Sampling interval was set at 63 seconds.

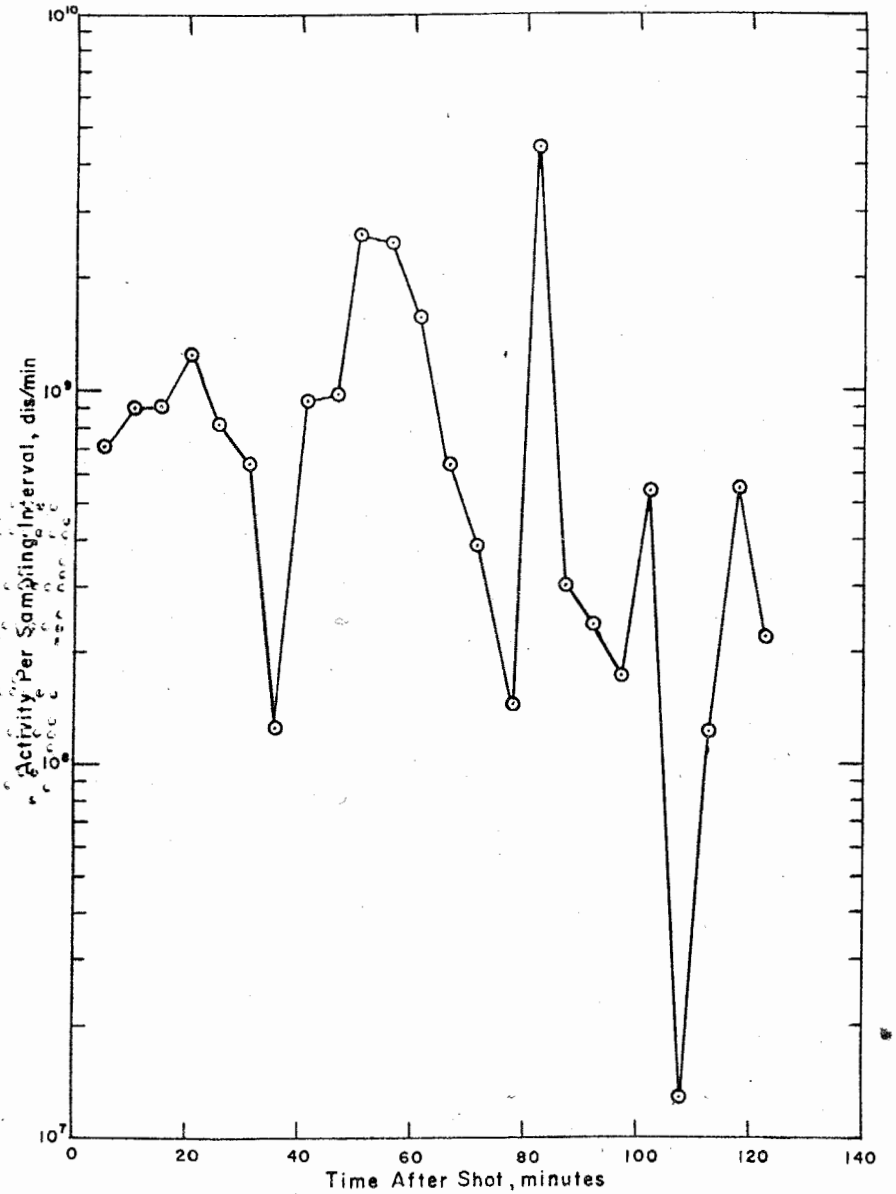

Figure 3.10 Time of arrival of activity corrected to H + 1 hour at Station G-7, 3,400 yards from ground zero on the 120-degree azimuth. Sampling interval was set at 5 minutes 7 seconds.

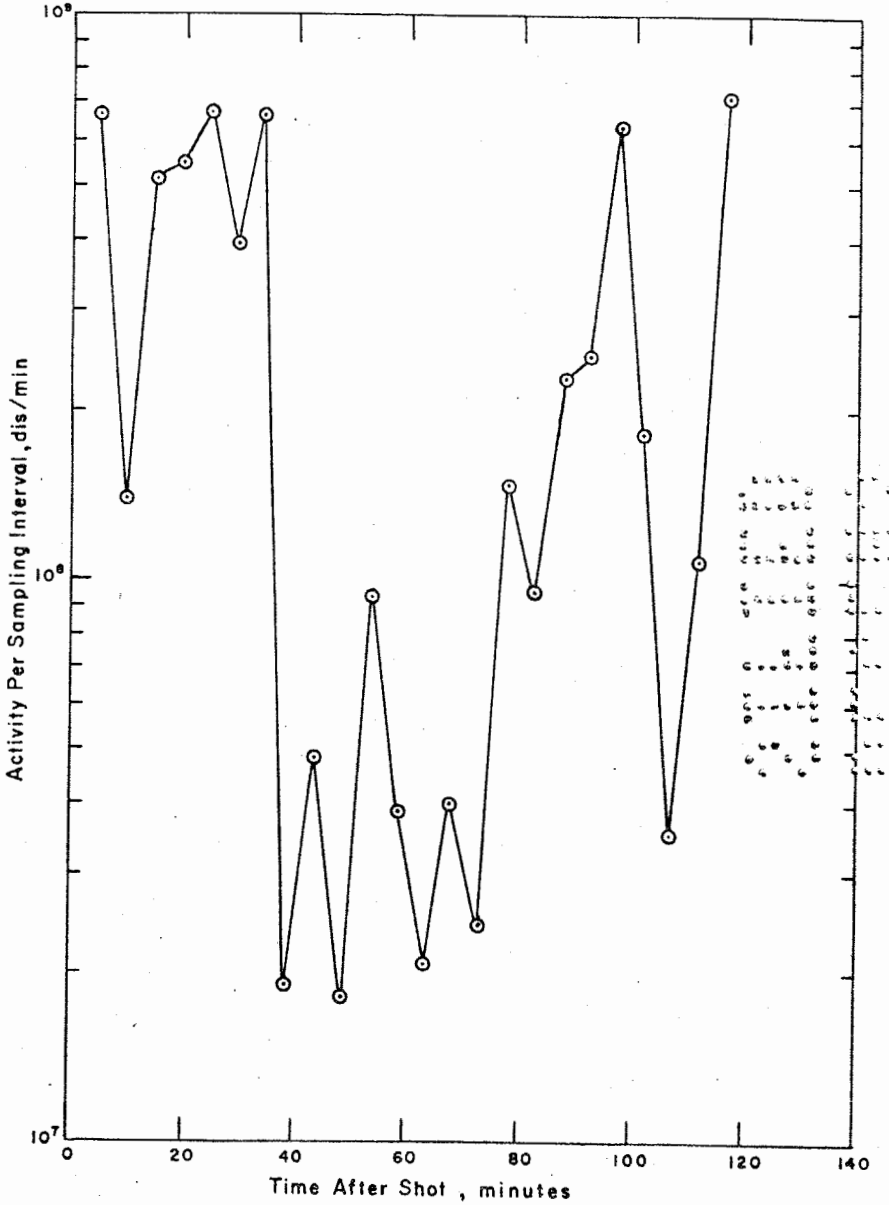

Figure 3.11 Time of arrival of activity corrected to H – 1 hour at Station H-8, 4,500 yards from ground zero on the 140-degree azimuth. Sampling interval was set at 4 minutes 51 seconds.

titudes and fell back to earth as hundreds of streamers (Figure 3.14). The throwout reached the ground at about 7 seconds after shot and this phase was complete at about 17 seconds.

The base surge first became visible at about 22 seconds (Figure 3.15). As the jets settled back to the desert floor, a massive base surge developed. When the jets began to fall, a typical mushroom cloud emerged from the center of the jets. The suspended material was transported downwind by the prevailing 10-knot wind so that this cloud became visible on the downwind side of the original detonation point. As the base surge

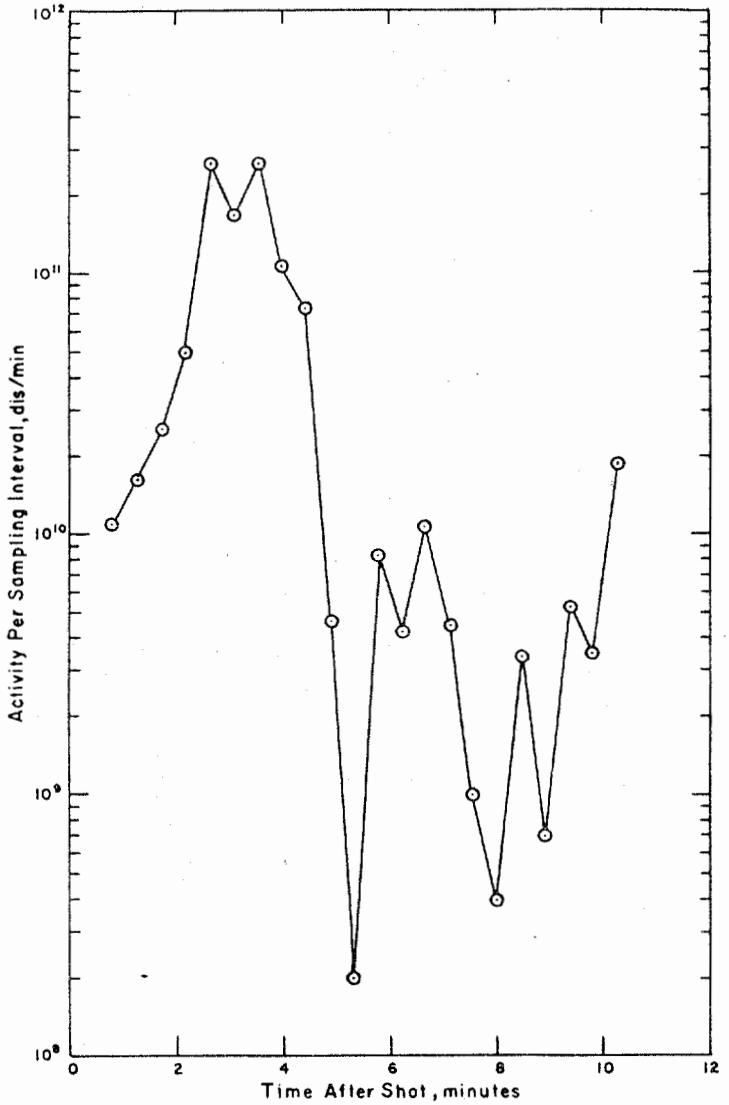

Figure 3.12 Time of arrival of activity corrected to H + 1 hour at Station L-1, 300 yards from ground zero on the 220-degree azimuth. Sampling interval was set at 27 seconds.

cloud traveled downwind it continued to rise. The last of the jets reached the ground at approximately 140 seconds. Initially, the surge height was about 340 feet on the upwind and 1,000 feet on the downwind sides respectively. The base surge reached a diameter of about 1,800 yards at about 53 seconds and a maximum upwind distance of about 600

yards at 112 seconds. The height of the base surge and the distance of travel downwind are shown in Figures 3.16 and 3.17. The first photograph shows the base surge as it reaches the 1-mile-radius circle and the second photograph shows the base surge as it passes the 1-mile radius. The times reported above are the averages of all the films studied, Edgerton, Germeshausen & Grier (EG&G) films, reel Numbers L-52, L-54, L-55, and L-56, and LML Films RKC 109 through 113, 118, and RKF 78, 79, and 101. Visual observations from the control point and from sample stations during recovering operations summarize that the base surge proceeded about 1,200 yards in a crosswind

TABLE 3.4 WEIGHT AND ACTIVITY CONCENTRATION OF TOTAL FALLOUT

Station Location	Weight Collected	Surface Area of Total Collector	Total Sample Activity Corrected to H+1 Hr	Activity Concentration Corrected to H+1 Hr	
	gram	ft^2	dis/min × 10^{10}	$\frac{\text{dis/min} \times 10^{10}}{\text{gm}}$	mc/gm
G-1	251.1	0.60	430.99	1.72	7.7
G-3	159.6	0.60	359.34	2.25	10.1
G-5	42.6	0.60	296.17	6.95	31.3
G-7	24.1	2.64	48.40 *	8.80 *	39.7
G-8	negative	0.60	—	—	—
L-3	30.0	0.60	94.86	3.17	14.2
L-5	negative	0.60	—	—	—
L-7	negative	2.64	—	—	—
E-5	3.3	0.60	†	—	25.8
E-7	negative	2.64	—	—	—
E-8	negative	0.60	—	—	—
F-7	1.0	2.64	†	—	27.5
F-8	negative	0.60	—	—	—
F-11	negative	0.60	—	—	—
H-7	0.7	2.64	†	—	14.9

* G-7 activity concentration has been corrected for collector surface area to put the activity concentration on a comparative basis with other stations, i.e., total collector activity was multiplied by the ratio 0.60/2.64.

† Only a portion of the total sample collected was recovered; therefore, total sample activity could not be determined.

direction, 600 yards upwind, and about 1,800 yards downwind. Aerial photographs of the area taken on D + 1 day indicate that the region of heavy material fallout extended about 1,800 yards in a southeast direction, as shown in Figures 3.18 and 3.19. Estimates of the extent of material deposition were made from aerial photographs illustrated in Chapter 4 and support these values for the distances of base surge travel and downwind deposition of the fallout.

The cloud reached heights (MSL) of 6,700 feet at 0.5 minutes, 7,500 feet at 1 minute, 9,800 feet at 3 minutes, and 11,560 feet (maximum) at 5.5 minutes. Details may be found in Reference 39. Figure 3.20 illustrates the cloud height as it drifts downwind (to the right in the photograph). Also shown in Figure 3.20 is the extent of the base surge in the upwind direction and the action of the surface winds on moving the airborne debris downwind.

3.2.3 Weight of Fallout and Beta Activity Concentrations. The weight and activity concentration (mc/gm) of fallout material collected by gross collectors at various times

Figure 3.13 Jets, or spears of earth, emerging through the top of the fireball shortly after detonation.

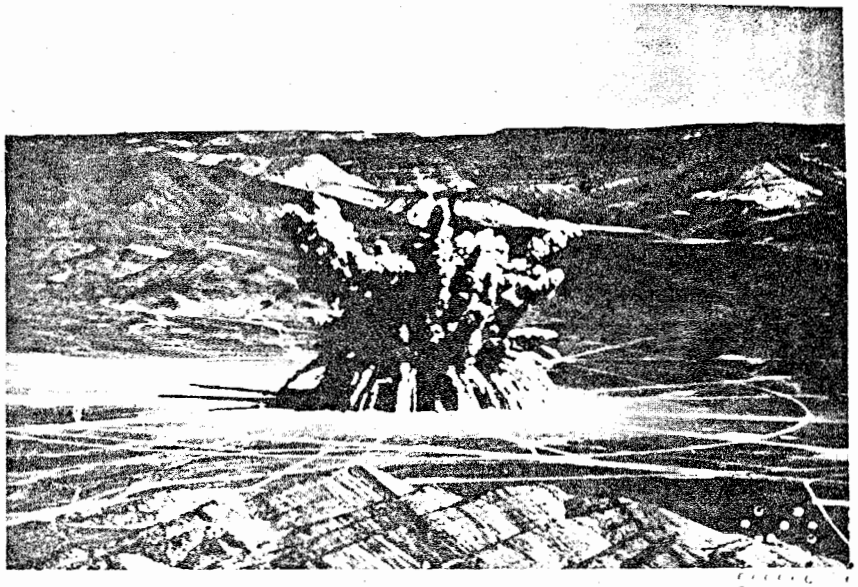

Figure 3.14 Throwout of debris when it reached the ground at H + 7 seconds. The 1 mile radius line can be seen encircling ground zero.

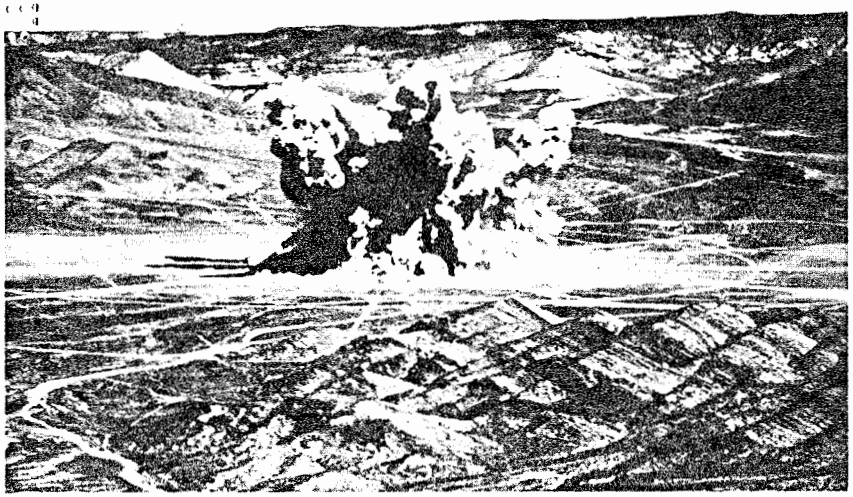

Figure 3.15 First visible base surge at H + 33 seconds.

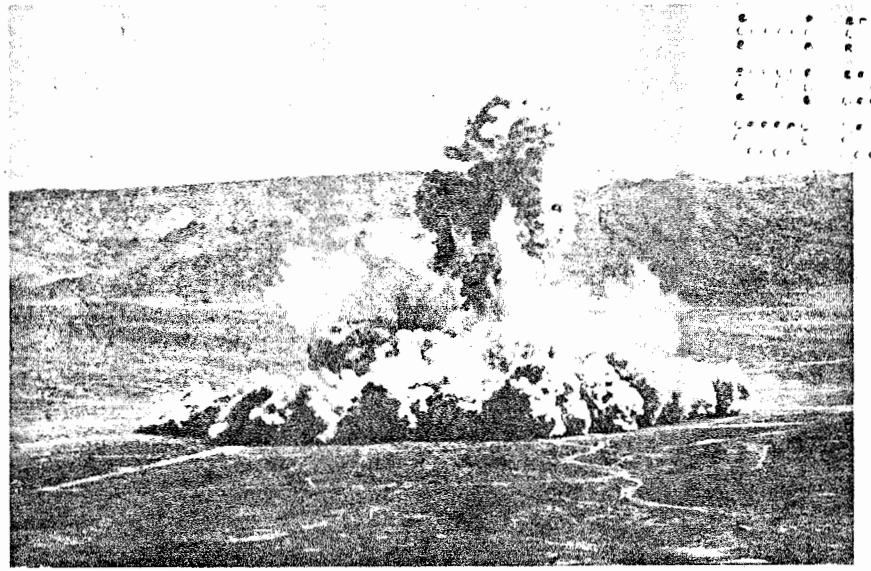

Figure 3.16 Base surge reaching 1 mile radius at H + 53 seconds. *Coming out of the picture the surge is traveling downwind in a southeasterly direction.*

Figure 3.17 Base surge rolling out and passing 1 mile radius. The reader is looking from the southeast or downwind direction.

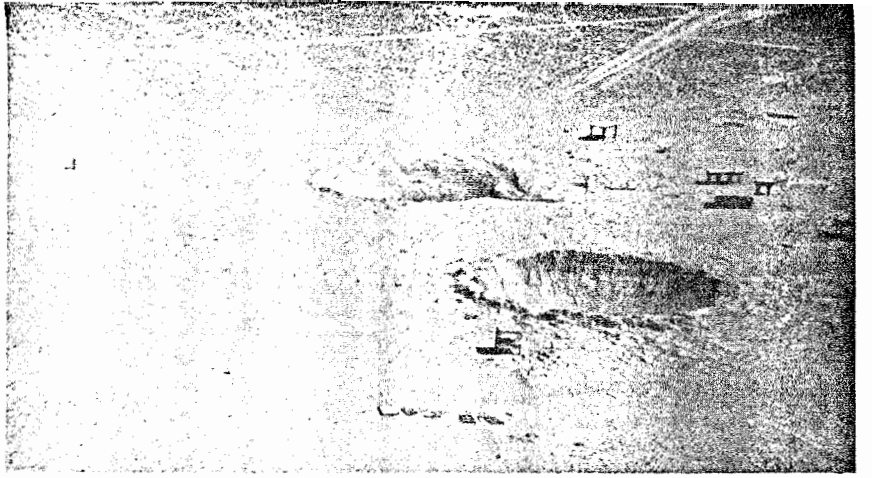

Figure 3.18 Upwind and crosswind deposition of fallout debris as seen in aerial photograph taken on D + 1 day. Upwind is the upper left hand corner and crosswind is the bottom of the picture. The bottom crater is from Operation Teapot Shot 7 and the top one is from Operation Jangle underground detonation.

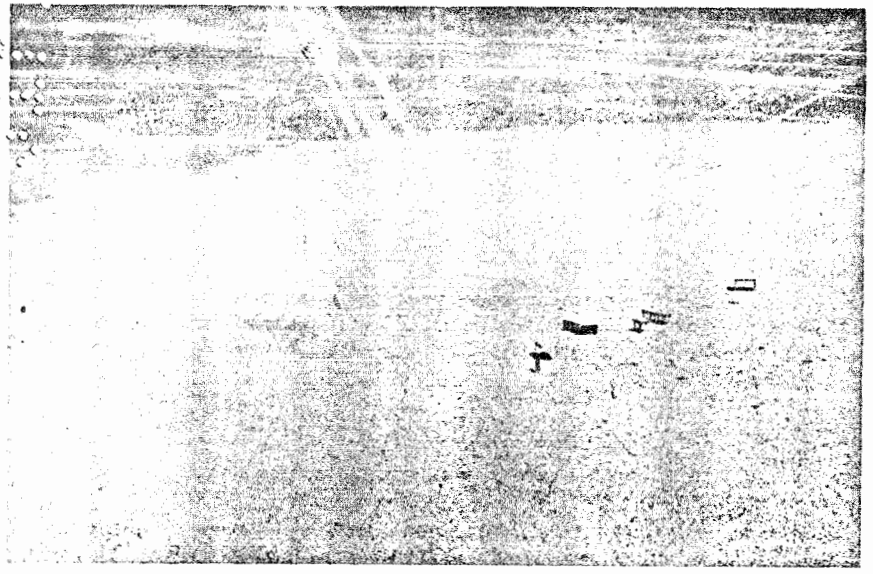

Figure 3.19 Downwind deposition of fallout debris as seen in aerial photograph taken on D + 1 day. Downwind is at the bottom of the picture.

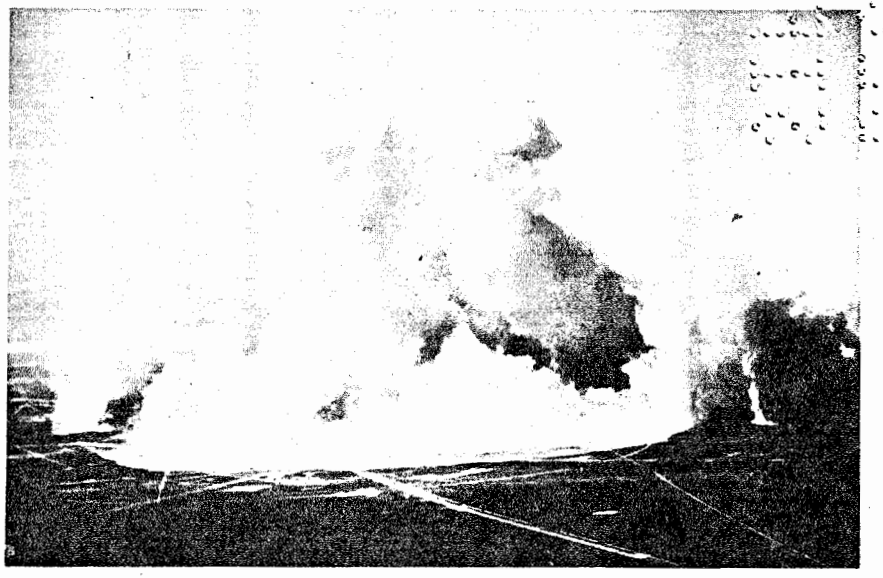

Figure 3.20 Cloud height reaching 8,000 feet (MSL) at H + 2 minutes. The cloud drifts downwind, to the right in the picture.

at Project 2.5.1 stations are presented in Table 3.4. Total activity was determined for the collectors from which a complete sample was recovered. The activity was corrected to H + 1 hour by means of a sample decay curve. Only a portion of each total sample was recovered at Stations L-3, E-5, and H-7. Therefore, total activity could not be determined for these locations.

Activity concentration data determined from the intermittent fallout collector samples are shown in Table 3.5.

3.2.4 Particle Size Studies. Particle size studies were made on total fallout samples collected from downwind and crosswind stations. The relationship between particle size, beta activity, weight, and distance is shown in the graphs in Figures 3.21 through 3.24. The original data are shown in Tables B.8 and B.9.

The particle size distribution data for radioactive (hot) and nonradioactive (cold) particles of the total fallout collector samples analyzed were determined by plotting the percent-less-than-stated-size versus diameter (microns) on logarithmic probability paper (Figures 3.25 through 3.28). No probability plot is shown for stations G-7 and L-1 because there were not enough hot particles from the G-7 sample to make a good statistical plot and a laboratory mishap caused a loss of the auto-radioautographs of the hot particles from the L-1 sample. The results of these plots, including the number median diameter (NMD), geometric standard deviation (σ), and average diameter (Davg) of the samples analyzed are presented in Table 3.6. For further detailed description of the particle size analysis and symbol definitions, see Reference 16.

3.2.5 Distribution of Activity within Individual Particles. Particles of fallout from IFC samples were seived and classified as follows:

Fraction	Size, Microns
AA	> 840
A	840 - 420
B	420 - 210
C	210 - 105
D	105 - 74
E	74 - 44
F	> 44

It was found in previous tests that the radioautographic and photomicrographic techniques did not lend themselves to obtaining data from particles below 150 microns in size; therefore, only the B, A, and AA fractions were used in this study. After mounting particles, radioautographs were made using Kodak Metallographic plates. The plates were exposed for varying lengths of time, depending on the activity of the particles. The exposure was only long enough to obtain a sharpely defined radioautograph showing the distribution of the activity within the particles. Photomicrographs were made through a Baush and Lomb binocular microscope, objectives ×0.66, ×3, ×6, using a Leica 35-mm camera with a Leitz Wetzler adapter, eyepiece ×⅓. The combination of objective and ocular pieces gave magnifications of 2, 9, and 18.

In comparing the activity distribution in the particles, two different types of particles were encountered: (1) surface active—those in which the activity was found only on the surface of the particles; and (2) fully active—those in which the activity was found generally throughout the particles. A count and comparison of the particles with their respective radioautographs are found in Table 3.7. These values were obtained from an actual

TABLE 3.5 INTERMITTENT FALLOUT COLLECTOR ACTIVITY CONCENTRATIONS AT H + 1 HOUR

Sampling times for each collector interval are presented in Table 3.3. Activities in mc/gm.

Tray	F-7	G-1	G-3	G-5	G-7	H-8	L-1
1	1.30	†	18.92	32.25	*	*	†
2	1.32	6.98	16.13	31.08	*	34.64	†
3	5.98	22.30	5.00	24.64	*	59.05	6.17
4	14.41	10.86	8.24	16.71	1,108.19	128.96	14.50
5	2.18	23.42	10.36	33.47	608.46	233.24	10.32
6	4.70	34.73	19.73	23.83	*	160.63	9.64
7	1.73	69.86	8.65	34.55	*	*	13.02
8	77.25	46.22	19.01	13.38	*	5.36	8.42
9	3.50	35.45	15.36	9.59	484.54	15.59	21.98
10	3.13	64.68	10.00	47.73	831.66	3.92	6.04
11	54.41	35.77	2.52	10.54	941.75	24.73	14.28
12	1.93	18.29	12.79	5.09	*	2.43	10.41
13	*	88.15	2.61	5.81	*	*	0.54
14	0.82	50.05	5.50	18.42	191.44	12.88	12.52
15	0.77	22.39	9.32	9.28	320.72	7.25	6.35
16	1.04	15.09	30.63	4.46	1,651.62	38.83	3.92
17	65.97	18.51	27.07	18.51	174.01	38.51	1.40
18	1.19	10.86	18.24	41.67	107.61	50.72	4.68
19	0.56	28.02	8.02	14.95	*	*	1.04
20	2.25	16.26	10.77	24.73	199.64	150.41	5.09
21	1.33	52.25	19.37	18.15	4.41	43.20	6.40
22	1.55	17.07	16.49	42.39	14.05	6.58	11.71
23	2.10	32.79	8.69	14.86	26.58	18.15	7.79
24	34.85	18.42	2.25	9.73	24.73	77.12	1.04

* No measurable weight of sample collected on this tray.

† Collector door was found open on recovery which exposed tray beyond its normal sampling time; therefore, the data was considered not valid.

TABLE 3.6 PARTICLE SIZE DISTRIBUTION DATA (TOTAL FALLOUT SAMPLES)

Station	NMD		σ		Davg (microns)	
	Hot	Cold	Hot	Cold	Hot	Cold
G-1	7.4	3.5	2.64	2.64	13.6	6.3
G-3	10.2	3.75	3.04	2.66	16.4	6.7
G-5	12.0	4.3	2.50	2.86	19.1	8.01
L-3	14.0	4.1	2.25	2.80	20.4	7.55

TABLE 3.7 PARTICLE DATA FROM IFC SAMPLES

Station	G-1			G-3			G-5			Total per Station			
Distance from Ground Zero	300 yards			750 yards			1,650 yards						
Size Fraction	B	A	AA	B	A	AA	B	A	AA	G-1	G-3	G-5	Total
Total Number Mounted	76	51	20	59	40	17	83	47	16	147	116	146	409
Fully Active	12	None	3	9	4	6	4	6	7	15	19	17	51
Surface Active	33	46	11	19	None	11	28	4	8	90	30	40	160
Radioactive Particles	45	46	14	28	4	17	32	10	15	105	49	57	210
Pct Fully Active of Total	16	None	15	15	10	35	5	13	47	10	16	12	12
Pct Surface Active of Total	43	90	55	30	None	65	33	8	50	61	26	27	39
Pct Radioactive of those Mounted	59	90	70	47	10	100	39	21	94	71	38	39	51
Pct Fully Active of those Radioactive	37	—	21	47	100	35	13	60	47	14	38	30	24

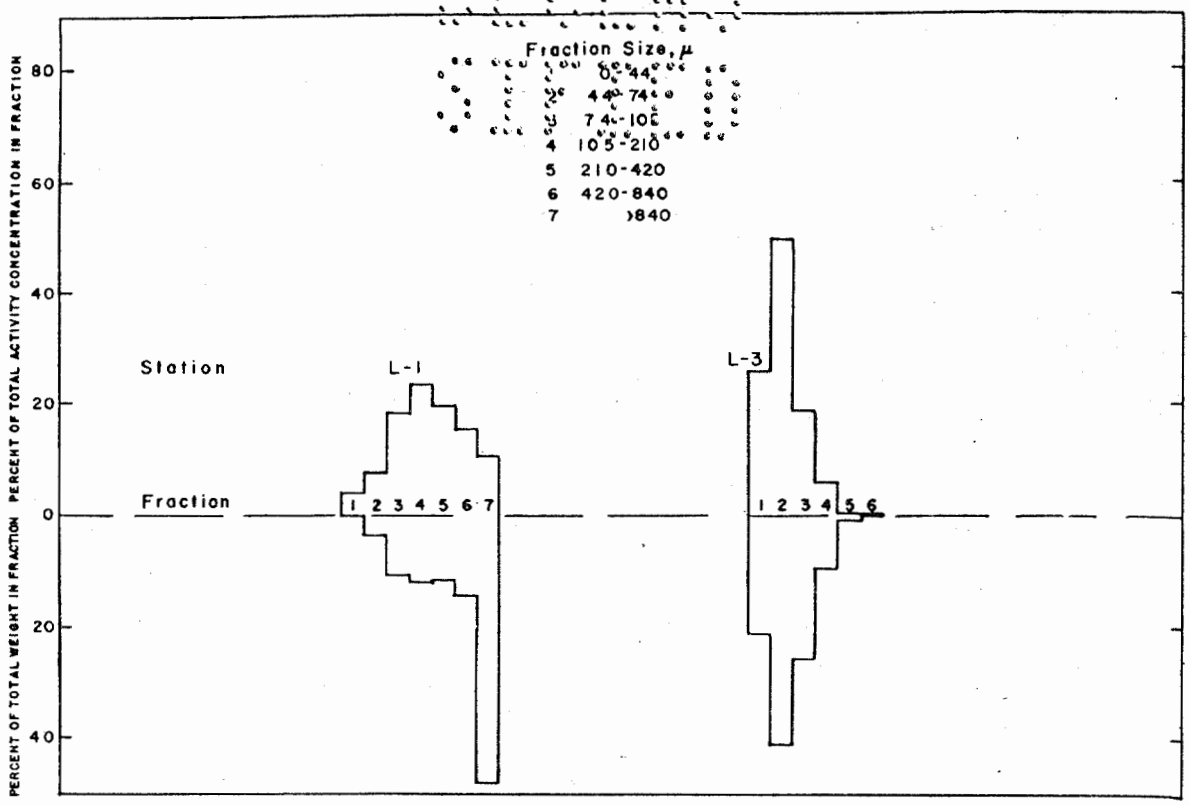

Figure 3.21 Particle size versus weight and activity, downwind (G-Leg).

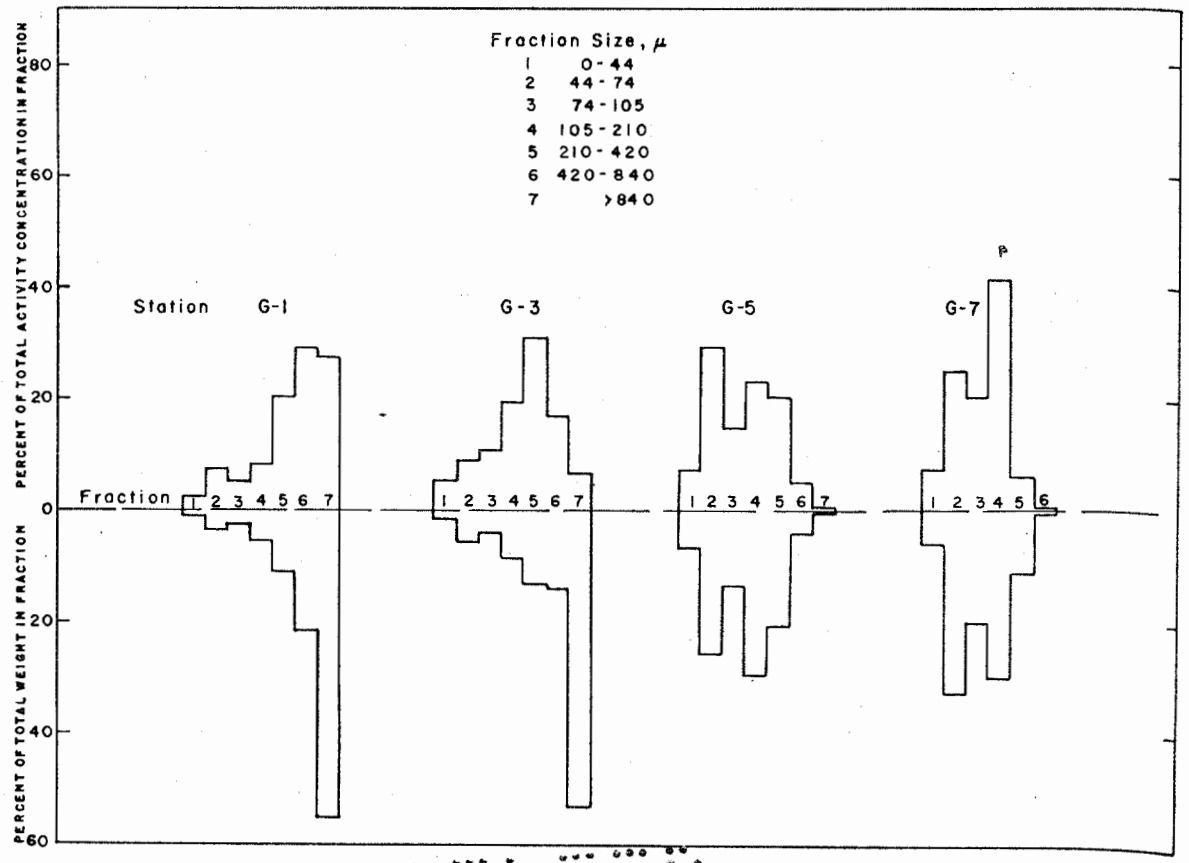

Figure 3.23 Particle size versus weight and activity, crosswind (L-Leg).

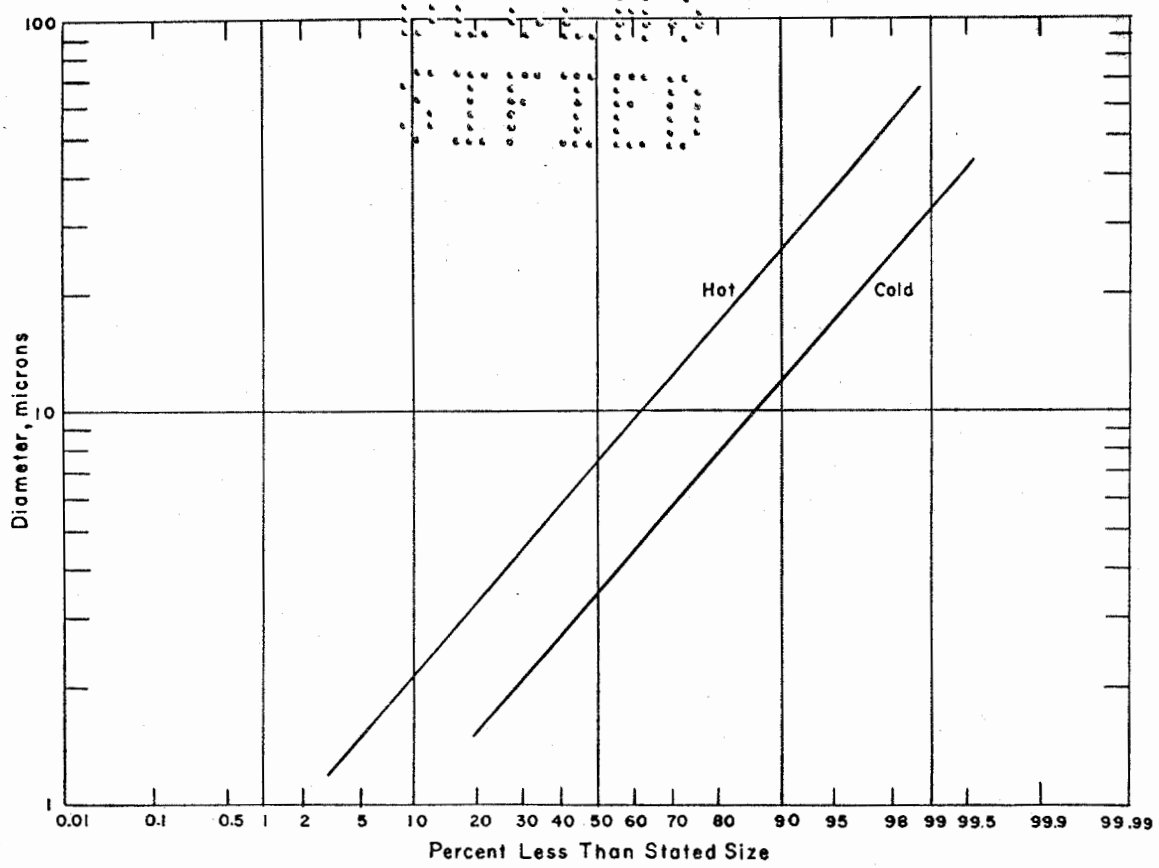

Figure 3.25 Probability plot for hot and cold particles of the total fallout collector sample from Station G-1.

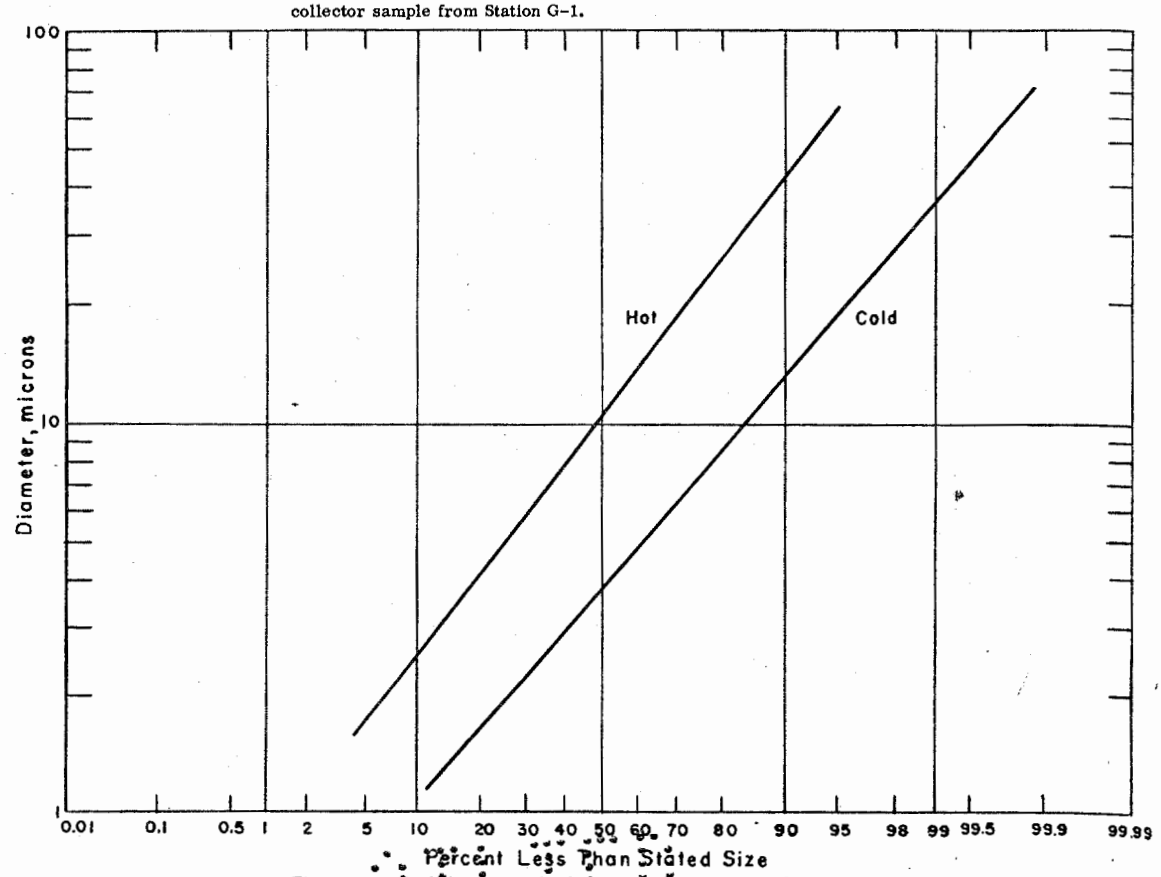

Figure 3.26 Probability plot for hot and cold particles of the total fallout collector sample from Station G-3.

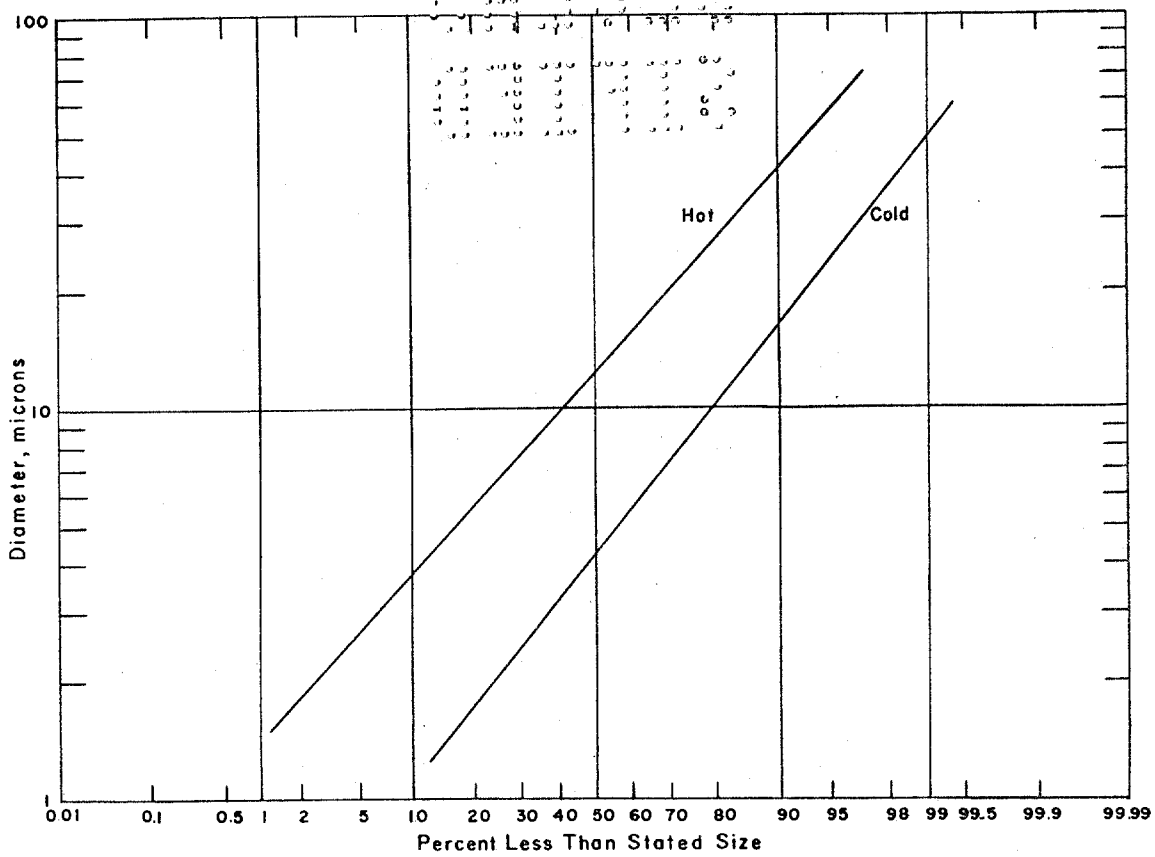

Figure 3.27 Probability plot for hot and cold particles of the total fallout collector sample from Station G-5.

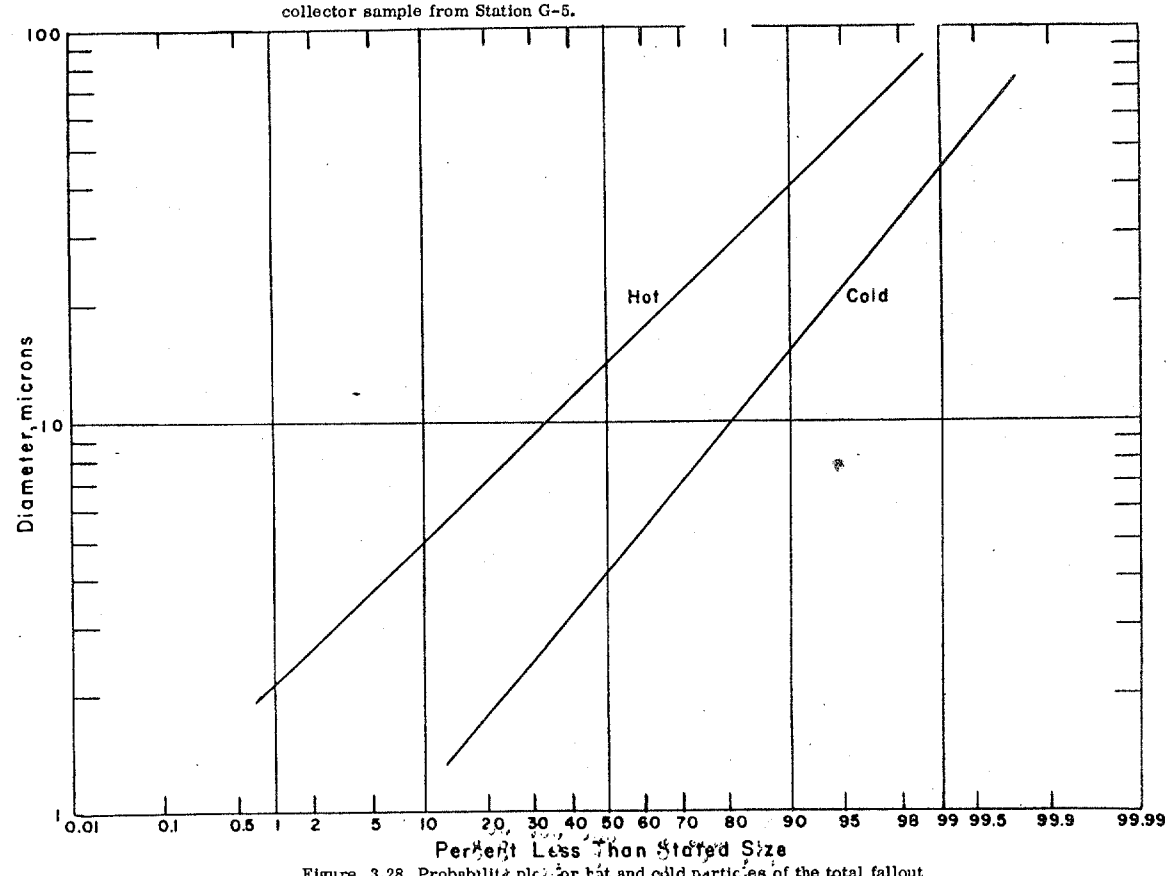

Figure 3.28 Probability plot for hot and cold particles of the total fallout collector sample from Station L-3.

count of particles on the microscope mounts and of the spots on the radioautographs. The types of particles collected and analyzed are illustrated and discussed in Chapter 4.

3.2.6 Radiochemistry. No radiochemistry analysis was planned as a part of this project. However, a small number of samples were studied to test theories of particle formation, the variations in decay rates, and times of arrival of activity.

The R-values of Sr^{89}/Mo^{99}, Sr^{89}/Ce^{144}, Ba^{140}/Mo^{99}, and Ba^{140}/Ce^{144} along with the specific activities of the nuclides (microcuries per gram of fallout) are given in Table 3.8 for the intermittent fallout collector samples of the crosswind station. The midpoint of the collection interval for each sample was used as the collection time. The R-values of Sr^{89}/Mo^{99} and Sr^{89}/Ce^{144} are plotted as a function of time of collection in Figure 3.29. Also included in Figure 3.29 is a plot of the R-values of Sr^{90}/Ce^{144}. The R-values of Ba^{140}/Ce^{144} and Ba^{140}/Mo^{99} are plotted as a function of time of collection in Figure 3.30. Similar data are given for the downwind intermittent fallout samples in Table 3.9 and are plotted in Figures 3.31 and 3.32. Apparently the crosswind sample R-values for Sr^{89} and Ba^{140} are greater than those for downwind sample. This is discussed in Section 4.6. A definition of R-values is presented in Section 2.3.2.

In the case of three of the samples at 547 seconds (Table 3.7) and at 241 and 376 seconds (Table 3.8) the reported values came from a combination of two successive samples. These

TABLE 3.8 R-VALUES AND MICROCURIES PER GRAM OF CROSSWIND SAMPLES AS A FUNCTION OF TIME

Crosswind station (L-1) was located 300 yards from ground zero on the 220-degree azimuth.

Time After Shot	R-Values					Microcuries per Gram			
	$\frac{Sr^{89}}{Mo^{99}}$	$\frac{Ba^{140}}{Mo^{99}}$	$\frac{Sr^{89}}{Ce^{144}}$	$\frac{Ba^{140}}{Ce^{144}}$	$\frac{Mo^{99}}{Ce^{144}}$	Sr^{89}	Mo^{99}	Ba^{140}	Ce^{144}
sec	$\times 10^{-1}$		$\times 10^{-1}$			$\times 10^{-2}$			$\times 10^{-2}$
10	7.72	1.68	7.04	1.53	0.912	9.08	2.93	1.10	2.66
34	2.45	0.718	2.78	0.813	1.13	16.3	16.5	2.66	12.1
61	2.06	0.596	2.33	0.676	1.13	13.2	16.0	2.13	11.7
88	—	—	0.704 *	—	—	3.50 *	—	—	10.3
115	—	—	0.42 *	—	—	5.23 *	—	—	25.7
142	0.609	0.328	0.764	0.412	1.26	5.97	24.4	1.79	16.1
169	—	—	0.825 *	—	—	6.34 *	—	—	15.8
196	—	—	0.779 *	—	—	5.06 *	—	—	13.4
223	0.730	0.384	0.882	0.464	1.21	6.00	20.4	1.75	14.1
250	—	—	1.13 *	—	—	6.22 *	—	—	11.4
304	5.30	1.24	5.70	1.34	1.08	14.9	7.01	1.95	5.42
331	—	—	4.56 *	—	—	12.1 *	—	—	5.48
358	—	—	4.36 *	—	—	1.92 *	—	—	0.911
385	1.10	0.419	1.45	0.550	1.31	1.42	3.19	0.299	2.02
547	4.53	1.04	4.26	0.979	0.942	10.3	5.68	1.32	5.01

* These values contain an estimated 30 percent contribution of Sr^{90}.

combinations were made because the samples were so small that individual analyses might have been too unreliable. The times reported for the combined samples were those of the intervals which contributed the most samples.

The total activities (disintegration per minute per gram and disintegrations per minute per collection interval) for the crosswind and downwind intermittent fallout collector samples are given in Table 3.10 and are plotted in Figures 3.33 and 3.34. It can be seen that the crosswind station collected more total activity than the downwind station. The opposite behavior was expected from visual observations of the shot and from the dose-rate readings

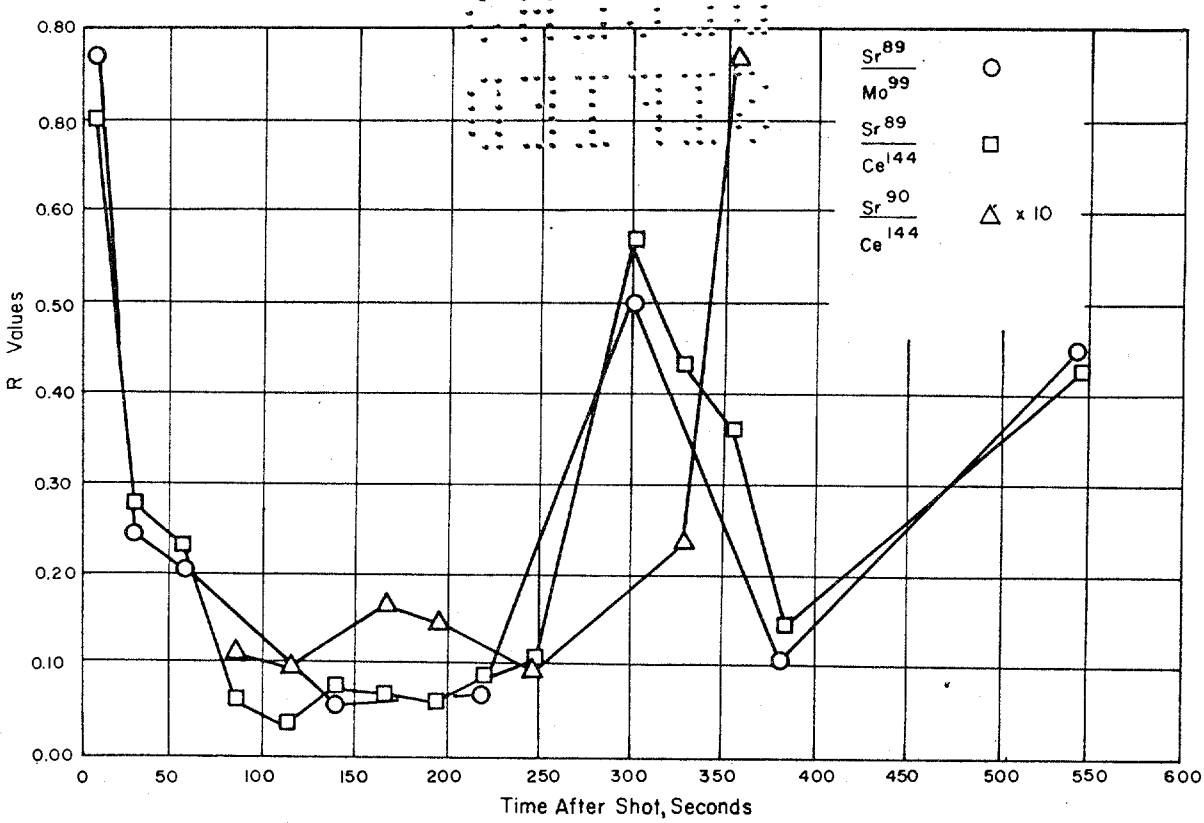

Figure 3.29 Strontium R-values as a function of time after shot for the crosswind station.

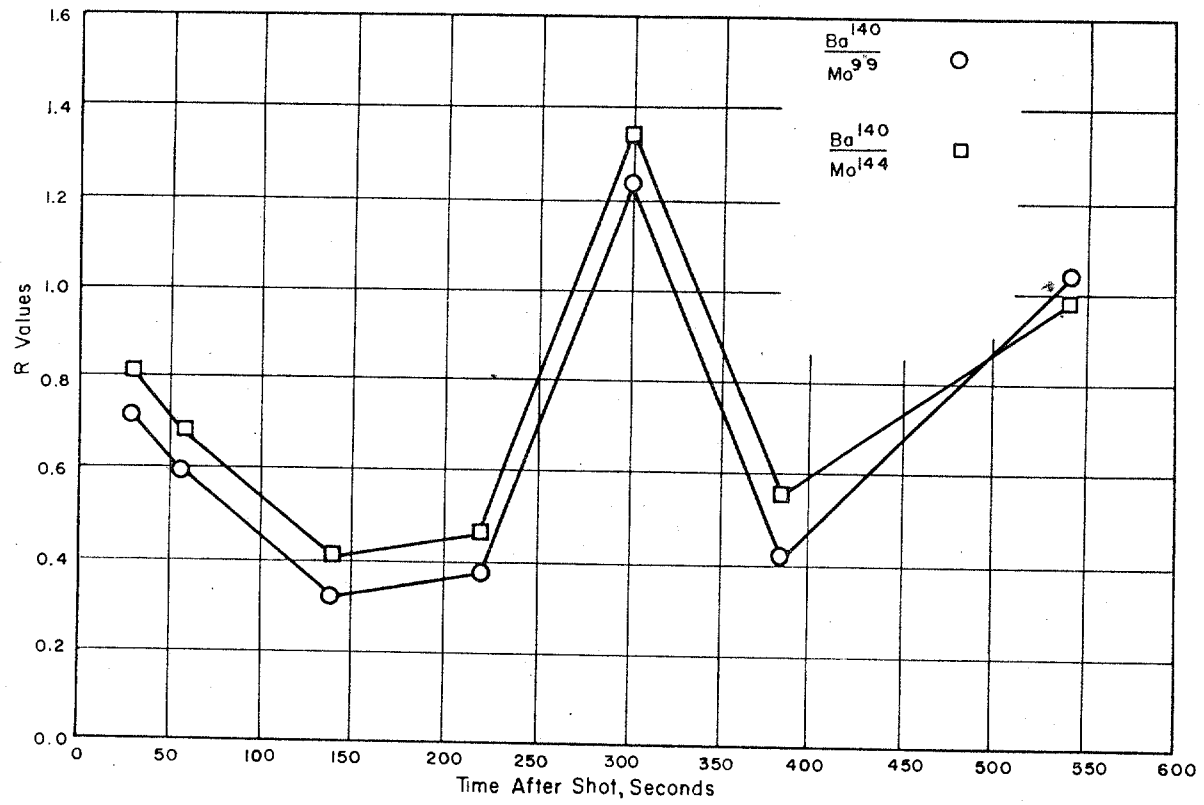

Figure 3.30 Barium R-values as a function of time after shot for the crosswind station.

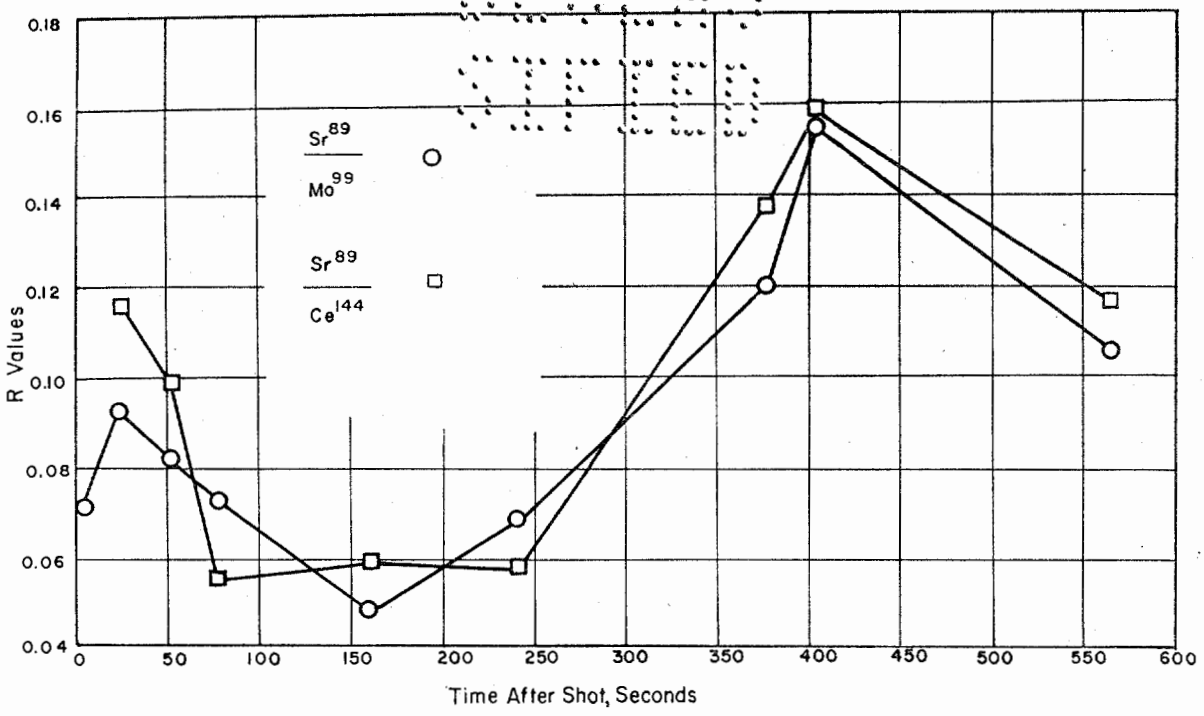

Figure 3.31 Strontium R-values as a function of time after shot for the downwind station.

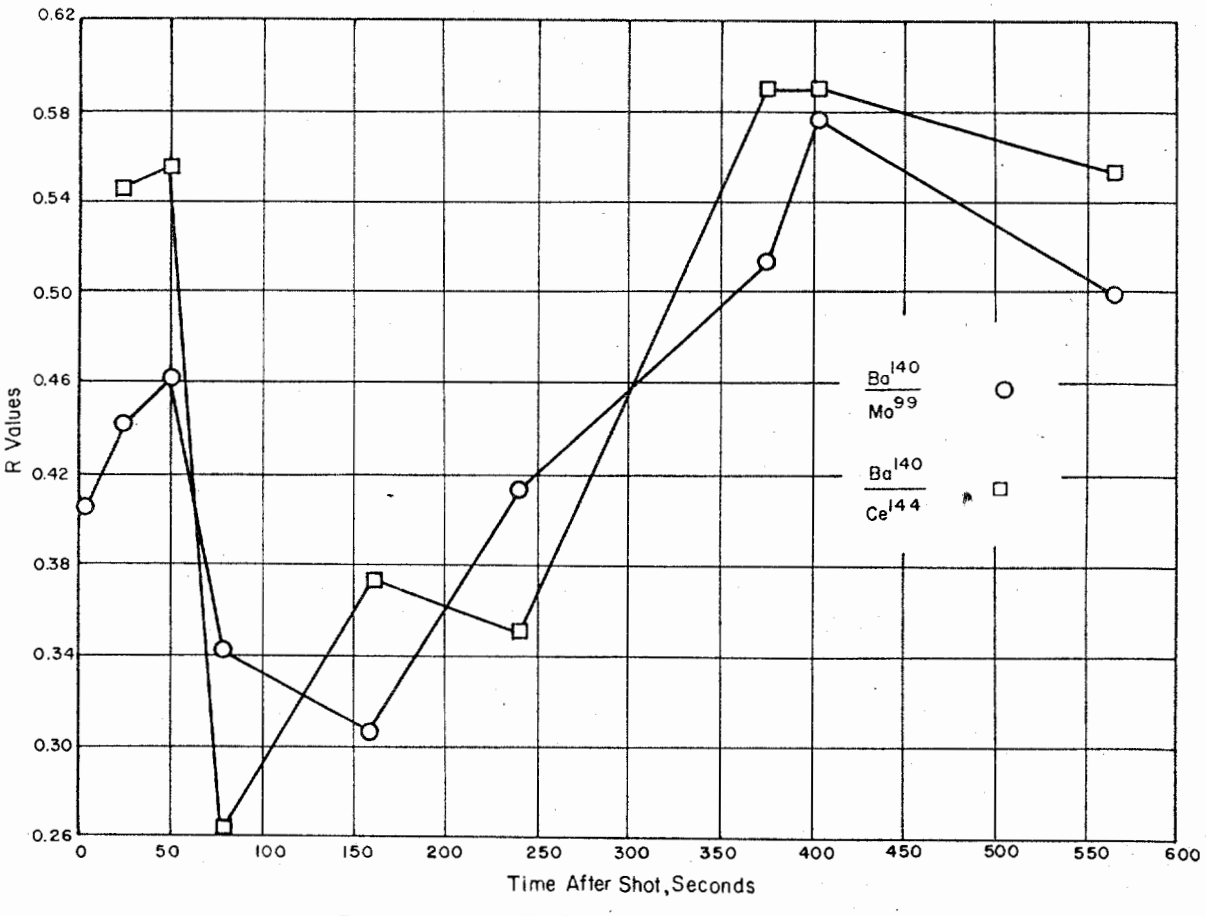

Figure 3.32 Barium R-values as a function of time after shot for the downwind station.

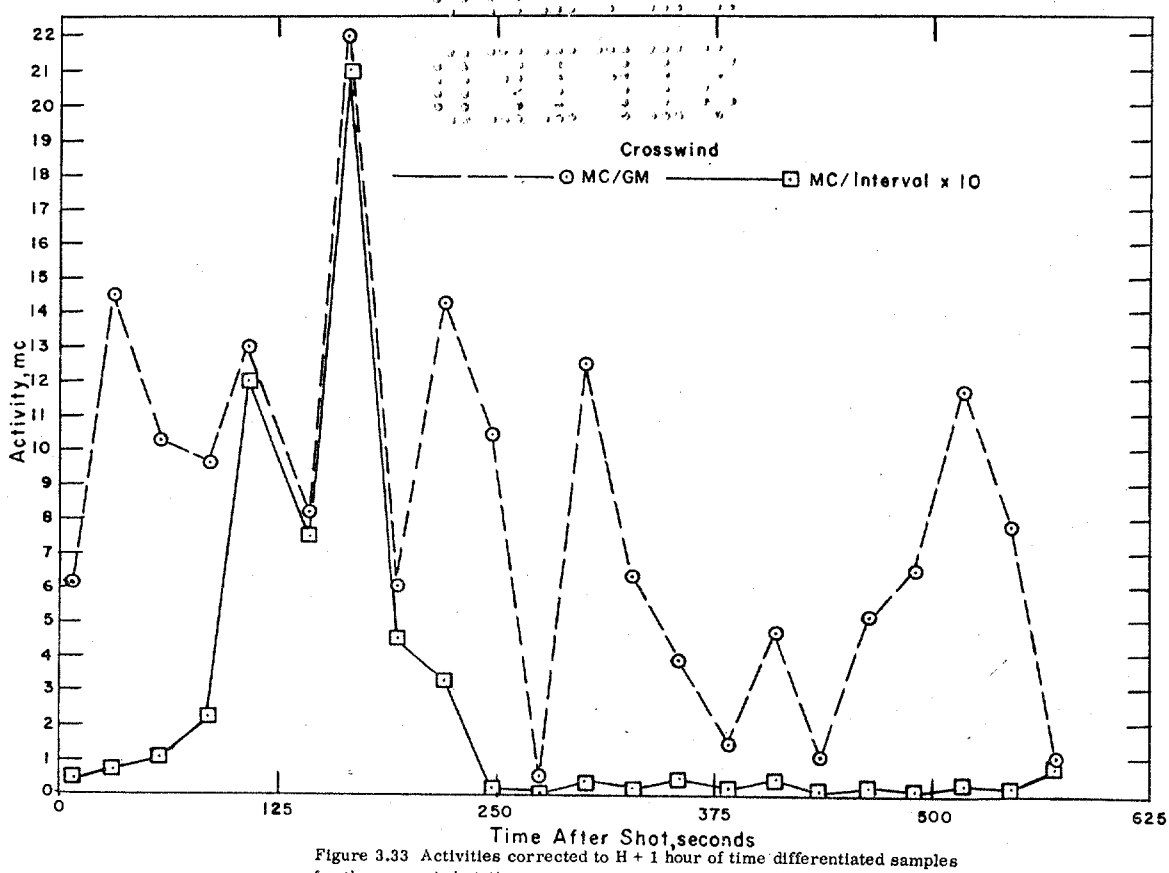

Figure 3.33 Activities corrected to H + 1 hour of time differentiated samples for the crosswind station.

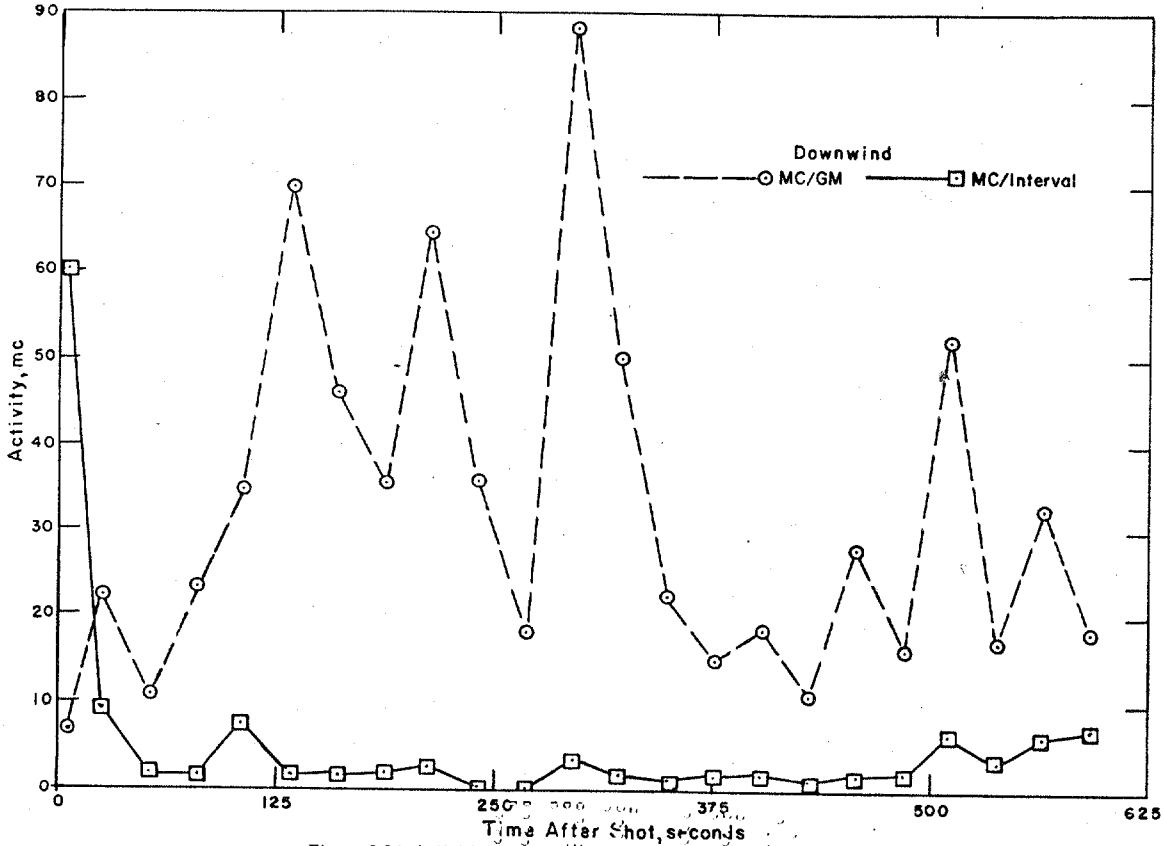

Figure 3.34 Activities corrected to H + 1 hour of time differentiated samples for the downwind station.

of these areas. The opening of the downwind collector was partially blocked by falling debris. This invalidated the total interval activity as compared with the crosswind station since less than the total 20 in^2 opening was exposed for collecting. However, the R-values, the microcuries per gram for the particular nuclides reported, and the total disintegration per minute per gram for each interval would not be affected by such a mishap.

The millicuries per gram in the crater lip for all the significantly contributing gamma activities at 44 days after shot are given in Table 3.11 as a function of depth underground and distance from ground zero. These same data, represented as percent of the total activity contributed by each nuclide, are listed in Table 3.12. The analyses were performed with a gamma scintillation spectrometer and are estimated to be approximately ± 10 percent accurate.

The accuracy of the R-values is estimated to be within 15 percent except for those values marked with an asterisk in Table 3.7. These designated analyses were made at a later date than the others in this table to further define the curve of Figure 3.25 and as a result contain larger percentages of Sr^{90}, because of the more rapid decay of Sr^{89}. It has been estimated that these later values are about 30 percent high. No attempt was made to eliminate the contribution of Sr^{90} by an absorption study because the counting rates of the samples at these later times were low and an absorption study would only increase the error on the final results. The accuracy of the microcurie values is ± 10 percent, as is the crater-lip sample analysis.

Further details and discussion of the radiochemistry results may be found in Reference 40.

3.2.7 Isokinetic Aerosol Samplers. The activity (dis/min) collected at 50-second intervals by the aerosol samplers was corrected to H + 1 hour and calculated on a percent basis as presented in Tables B.10 and B.11. Average sampling velocity was determined for the instruments from tape recorded data obtained as described in Section 2.2.2. The total activity per interval was reduced to activity per cubic foot of air sampled and these data are plotted in dis/min/ft^3 as a function of time after shot in Figures 3.35 and 3.36. These curves show how the relative activity concentration varied with time at one downwind station (G-3) and one crosswind station (L-3), both located the same distance (700 yards) from ground zero.

3.3 DECAY DATA

3.3.1 Large Area Decay Rate. Where four or more gamma-intensity readings were available from station surveys, the readings and the time at which they were taken were plotted on 3 × 3 log-log graph paper. A straight line was fitted to these points by inspection and the slope of the line was roughly determined by measurement from the graph. The limits of the 42 slopes plotted were from −0.70 to −2.05 with an average of −1.18. These readings were taken as early as 2.8 hours and as late as 120 hours after shot. The above average of −1.18 is so close to the normal −1.2 fission decay exponent that it served as a basis for using the −1.2 decay for correcting all survey data in order to plot and draw the dose-rate contours at H + 1 hour. The survey data show the overall gamma decay (including weathering effects) and are presented in Table 3.13.

3.3.2 Beta Decay of all Samples. Decay curves, approximately two hundred, were determined for all samples which were sufficiently active. All activity measurements were corrected to H + 1 hour by the use of an experimentally determined decay curve (top curve, Figure 3.37). The bottom curve in Figure 3.37 is the decay curve as determined from the

TABLE 3.9 R-VALUES AND MICROCURIES PER GRAM OF DOWNWIND SAMPLES AS FUNCTION OF TIME

Downwind station (G-1) was located 300 yards from ground zero on the 120-degree azimuth.

Time After Shot	R-Value					Microcuries per Gram			
	Sr^{89}/Mo^{99}	Ba^{140}/Mo^{99}	Sr^{89}/Ce^{144}	Ba^{140}/Ce^{144}	Mo^{99}/Ce^{144}	Sr^{89}	Mo^{99}	Ba^{140}	Ce^{144}
sec	$\times 10^{-2}$	$\times 10^{-1}$	$\times 10^{-2}$	$\times 10^{-1}$		$\times 10^{-2}$			$\times 10^{-1}$
6	7.18	4.05	—	—	—	10.1	34.9	3.16	—
25	9.33	—	11.6	5.46	1.24	11.4	30.5	3.01	2.04
52	8.23	4.62	9.90	5.56	1.20	9.97	27.7	2.87	1.92
79	7.34	3.44	5.58	2.62	0.760	19.7	66.8	5.15	7.30
160	4.87	3.08	5.93	3.75	1.22	14.4	73.5	5.07	5.01
241	6.89	4.14	5.83	3.50	0.846	9.55	34.4	4.19	3.38
376	12.0	5.14	13.8	5.91	1.15	12.5	25.7	2.96	1.86
403	15.5	5.78	15.8	5.91	1.02	13.9	22.3	2.88	1.81
565	10.6	5.00	11.7	5.55	1.11	12.7	29.8	3.34	2.24

TABLE 3.10 GROSS ACTIVITY CONCENTRATION VERSUS TIME (INTERMITTENT SAMPLES)

Crosswind Station, 220-Degree Azimuth and 300 yards from Ground Zero			Downwind Station 120-Degree Azimuth and 300 yards from Ground Zero		
Time of Collection	Millicuries per Gram	Millicuries per Interval	Time of Collection	Millicuries per Gram	Millicuries per Interval
sec	H + 1 hour	H + 1 hour	sec	H + 1 hour	H + 1 hour
10	6.17	4.9	6	6.98	60.1
34	14.5	7.3	25	22.3	9.33
61	10.3	11	52	10.9	1.82
88	9.64	22	79	23.4	1.65
115	13.0	120	106	34.7	5.78
142	8.42	75	133	69.9	1.81
169	22.0	210	160	46.2	1.67
196	6.04	45	187	35.5	2.08
223	14.3	33	214	64.7	2.63
250	10.4	2.1	241	35.8	0.637
277	0.54	0.10	268	18.3	0.296
304	12.5	3.8	295	88.2	3.92
331	6.35	1.9	322	50.1	1.99
358	3.92	4.7	349	22.4	1.41
385	1.42	2.1	376	15.1	1.64
412	4.68	0.47	403	18.5	1.93
439	1.04	0.18	430	10.9	1.20
466	5.09	1.5	457	28.0	0.810
493	6.40	0.32	484	16.3	1.99
520	11.7	2.3	511	52.3	6.50
547	7.79	1.6	538	17.1	3.42
574	1.04	8.7	565	32.8	6.85
—	—	—	592	18.4	7.05

TABLE 3.11 ACTIVITY AT D + 44 DAYS VERSUS DEPTH AND DISTANCE FOR PRINCIPAL GAMMA EMITTING NUCLIDES IN THE CRATER LIP

Millicuries per gram versus depth.

	Samples Collected on a 100-Degree Azimuth and 90 feet from Crater Edge				Samples Collected on a 100-Degree Azimuth and 30 feet from Crater Edge
Nuclides	Surface	6 Inches	18 Inches	36 Inches	6 Inches
Zr^{95}	0.50	0.52	0.38	0.29	0.41
Nb^{95}	0.36	0.38	0.27	0.21	0.29
Ru^{103}	0.21	0.22	0.18	0.15	0.17
Ba^{140}	0.15	0.17	0.13	0.084	0.13
La^{140}	0.18	0.20	0.15	0.097	0.15
Ce^{141}	0.51	0.54	0.45	0.34	0.42
Ce^{144}	0.071	0.076	0.059	0.044	0.060
Pr^{144}	0.071	0.076	0.059	0.044	0.060

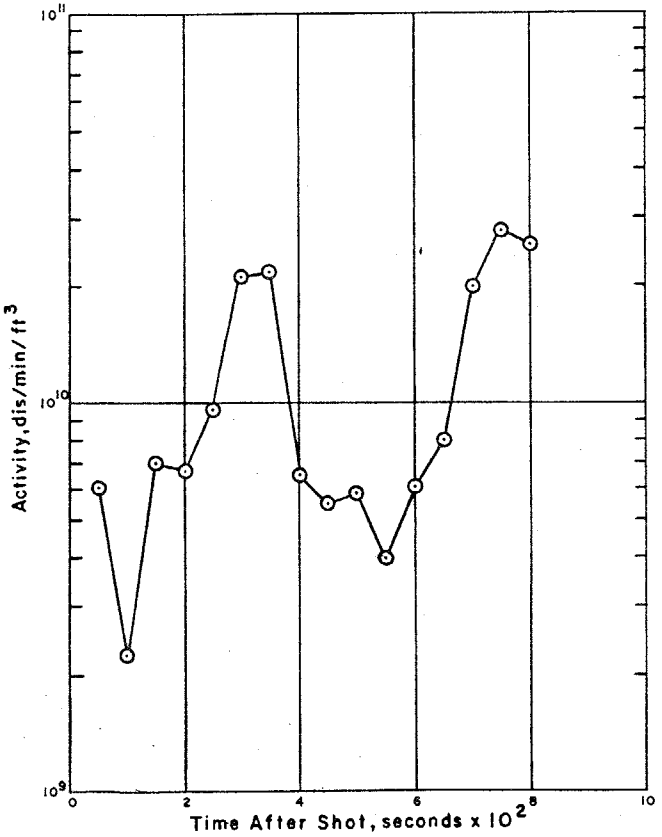

Figure 3.35 Activity concentration per cubic foot of air sampled for time intervals after shot at Station G-3.

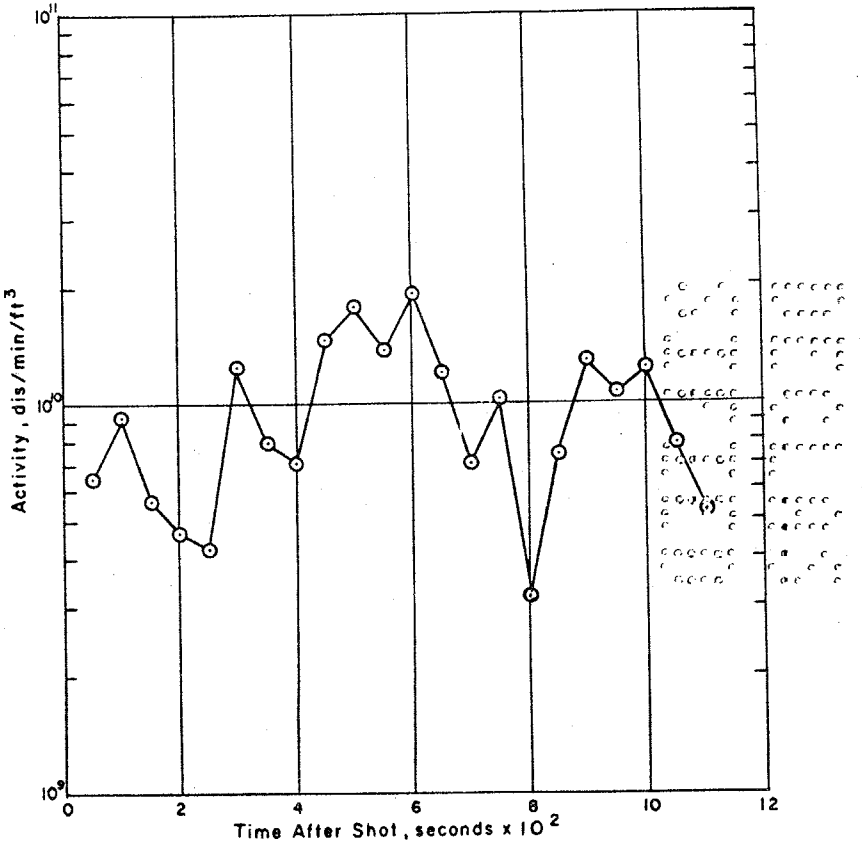

Figure 3.36 Activity concentration per cubic foot of air sampled for time intervals after shot at Station L-3.

TABLE 3.12 PERCENT ACTIVITY AT D+ 44 DAYS VERSUS DEPTH AND DISTANCE FOR PRINCIPAL GAMMA EMITTING NUCLIDES IN THE CRATER LIP

Percent contribution versus depth.

	Samples Collected on a 100-Degree Azimuth and 90 feet from Crater Edge				Samples Collected on a 100-Degree Azimuth and 30 feet from Crater Edge
Nuclides	Surface	6 Inches	18 Inches	36 Inches	6 Inches
Zr^{95}	24	24	23	23	24
Nb^{95}	18	17	16	17	17
Ru^{103}	10	10	11	12	10
Ba^{140}	7.3	7.8	7.7	6.7	7.7
La^{140}	8.8	9.2	8.9	7.7	8.9
Ce^{141}	25	25.	27	27	25
Ce^{144}	3.5	3.5	3.6	3.5	3.6
Pr^{144}	3.5	3.5	3.6	3.5	3.6

TABLE 3.13 GAMMA INTENSITY DECAY SLOPES

Station	Slope	Decay Period after Shot	
		From	To
		hours	hours
A-2	2.05	70	118
B-4	1.29	23.9	90.3
C-5	1.20	3.3	90.3
D-1	0.78	46.8	120.3
D-2	1.04	23.0	89.2
D-3	1.33	22.9	89.1
D-4	1.37	22.7	89.1
D-5	1.14	22.6	89.0
E-4	1.16	23.8	90.3
E-5	1.36	23.7	90.1
E-6	1.24	46.3	90.1
F-4	1.30	24.1	89.5
F-5	1.14	24.0	89.5
F-6	1.16	24.0	89.3
F-7	0.94	23.9	89.2
G-5	1.11	24.7	89.8
G-6	1.13	24.7	89.7
G-8	0.70	24.3	89.3
G-9	1.20	24.1	89.1
H-5	1.48	24.2	89.6
H-6	1.12	24.2	89.6
H-7	1.11	24.1	89.5
H-8	1.12	24.0	89.4
H-9	1.26	23.8	89.0
H-13	1.30	2.8	69.5
I-4	1.23	23.2	89.5
I-5	1.07	23.2	89.5
I-6	1.19	3.1	89.5
I-7	1.21	2.9	69.2
I-8	1.09	2.8	45.8
I-9	1.21	2.8	45.8
J-5	1.22	4.6	89.4
J-6	1.22	4.6	89.3
K-5	1.24	4.5	89.5
L-4	1.12	22.9	89.6
L-5	1.32	4.4	46.2
M-3	1.35	23.1	89.8
M-4	1.15	23.0	89.7
N-3	1.19	23.2	89.8
O-2	1.39	23.2	120.2
O-3	1.01	23.3	89.8
P-2	1.13	23.6	120.0
P-3	1.24	23.5	90.0
Q-2	1.04	46.8	120.0

uncorrected, raw counting data. A treatment of decay curves for the extrapolation of activities is presented in Appendix I.

3.4 CORE SAMPLING OF CRATER AND LIP

3.4.1 Activity Distribution in Crater and Lip. Gamma intensity measurements (Table 3.14) were taken at the lip area on D + 8 and D + 9 days. On D + 17 days an extensive survey of the crater was made and gamma intensity readings (Table 3.15) at various loca-

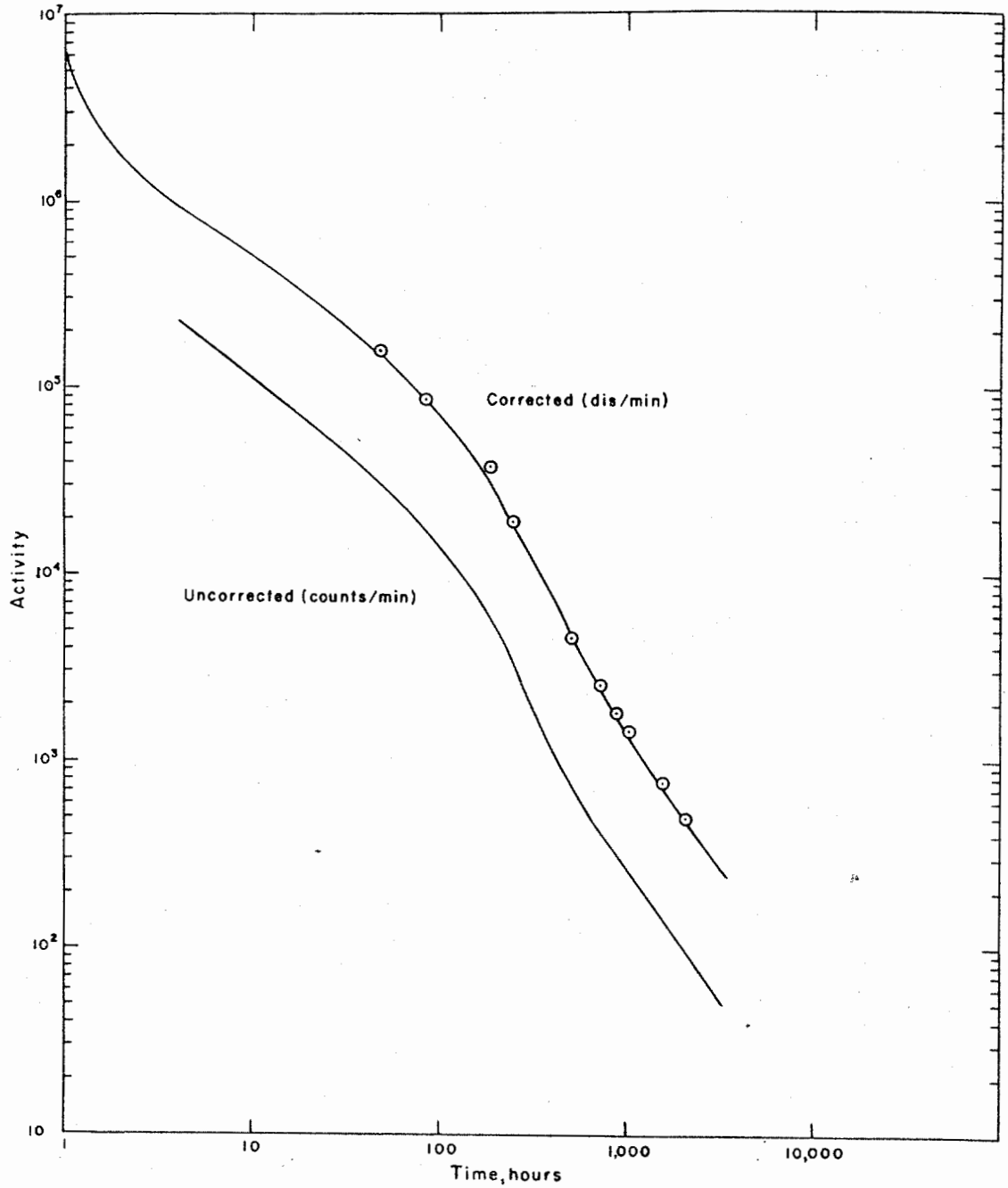

Figure 3.37 Experimental decay curves.

TABLE 3.14 GAMMA INTENSITY READINGS ON LIP AREA (D + 8 AND D + 9 DAYS)

Time		Distance from Edge of Lip	Direction and Gamma Intensity			
Date	Hour		North	East	South	West
		feet	r/hr	r/hr	r/hr	r/hr
31 March	1230	0	10	9	—	12
		30	10	6	—	12
		60	9	9	—	10
		90	6	10	—	8
		120	—	11	—	—
1 April	1230	0	—	8	6	—
		30	—	10	7	—
		60	—	10	8	—
		90	—	11	10	—
		120	—	11	—	—

TABLE 3.15 GAMMA INTENSITY READINGS IN THE CRATER (D+ 17 DAYS)

Time		Slant Depth in Crater from Lip Edge	Gamma Intensity
Date	Hour		
		feet	r/hr
9 April	1430	West Lip	1.9
		5	1.6
		30	1.0
		60	0.15
		80	0.13
		100	0.17
		120	0.20
		140	0.18
		160	0.21
		180 (bottom of crater)	0.33
		160	0.35
		140	0.16
		120	0.15
		100	0.18
		80	0.25
		60	0.21
		40	0.18
		20	0.95
		East Lip	2.1

TABLE 3.16 GAMMA INTENSITY READINGS ON LIP AREA (D + 17 DAYS)

Time		Distance from Edge of Lip	Direction and Gamma Intensity			
Date	Hour		North	East	South	West
		feet	r/hr	r/hr	r/hr	r/hr
9 April	1400	0	2.4	2.0	1.1	1.5
		30	2.5	2.8	1.3	2.1
		60	2.0	3.0	1.9	2.3
		90	2.7	3.3	2.0	2.2
		120	2.9	3.0	2.1	2.0
		150	2.6	2.8	2.2	1.9

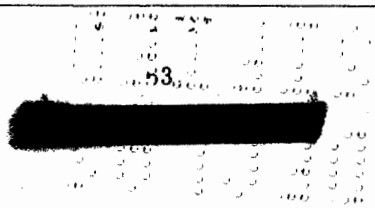

tions was determined. Readings were taken with a Jordan instrument probe (aerial survey) suspended on a cable stretched across the center of the crater. The survey probe was moved horizontally across the crater and lowered vertically into the crater at several points to obtain intensity readings at various distances along the slant depth of the crater. The survey probe was lowered as on the aerial survey procedure (see Section 2.2.3) until the ionization chamber was 3 feet above the survey point. On this particular survey with

TABLE 3.17 GAMMA INTENSITY READINGS IN THE CRATER-LIP AREA (D + 97 TO 99 DAYS)

Location from Edge of Lip	Distance from Edge of Lip	Direction and Gamma Intensity*				
		North	East	South		West
		30 June	29 June	28 June	29 June	28 June
	feet	r/hr	r/hr	r/hr	r/hr	r/hr
F	150	0.25	0.40	0.25	—	0.34
E	120	0.25	0.43	0.29	—	0.32
D	90	0.28	0.46	0.41	—	0.34
C	60	0.43	0.42	0.32	—	0.31
B	30	0.32	0.39	0.25	—	0.28
A	0	0.18	0.20	0.08	0.050	0.22
L	−40	0.013	0.019	—	0.022	0.023
M	−80	0.017	0.027	—	0.030	0.041
N	−120	0.018	0.027	—	0.024	0.039
O	−160	0.014	0.018	—	0.025	0.025
P	−200	0.20*	—	—	—	0.140

* All readings were taken in the afternoon of each day. Point of highest reading in bottom crater was not exact center.

the probe suspended from the cable at crater-lip level and over the approximate center of the crater, the reading was 270 mr/hr. When the probe was lowered to 30 feet above the bottom, the reading increased slowly to 300 mr/hr and then started to decrease from there to the bottom. Just outside the west lip edge of the crater the reading was 2,000 mr/hr. Gamma intensity readings taken on D + 17 days around the crater-lip area are shown in Table 3.16.

On D + 97 to D + 99 days, another extensive survey of the crater-lip area was made. Gamma intensity readings are reported in Table 3.17.

Core samples were taken on the lip area on D + 8 and D + 9 days (see Figure 2.12 for locations and Appendix G for sampling technique). From the measured activity (dis/min), of these samples, the percent of the total activity collected was calculated for each depth as illustrated by the lower curves in Figure 3.8 through Figure 3.41. The upper curves in these same figures are separated from the lower curves by the letter in the left-hand margin indicating distance from crater edge. The upper curves represent the cumulative percent activity for a respective sampling position. It can be seen from the upper curves that in all cases except Figure 3.39 over 90 percent of the activity collected is accounted for in the first depth in the lip area. Only two lines in Figure 3.39 fall below 90 percent. The lower curves in Figure 3.38 through Figure 3.41 further substantiate the location of the activity to be in the first 1-foot depth as the curves fall off rapidly to less than 10 percent activity at the 1½-foot depth.

On D + 97 to D + 99 days, core samples were obtained at the locations shown in Figure 2.13. The data obtained from these samples are presented in Appendix G, Table G.2, and show the distribution of activity as a function of depth and distance from the crater. The activity was determined by placing a 3-gram aliquot sample in a wide dish (4-inch

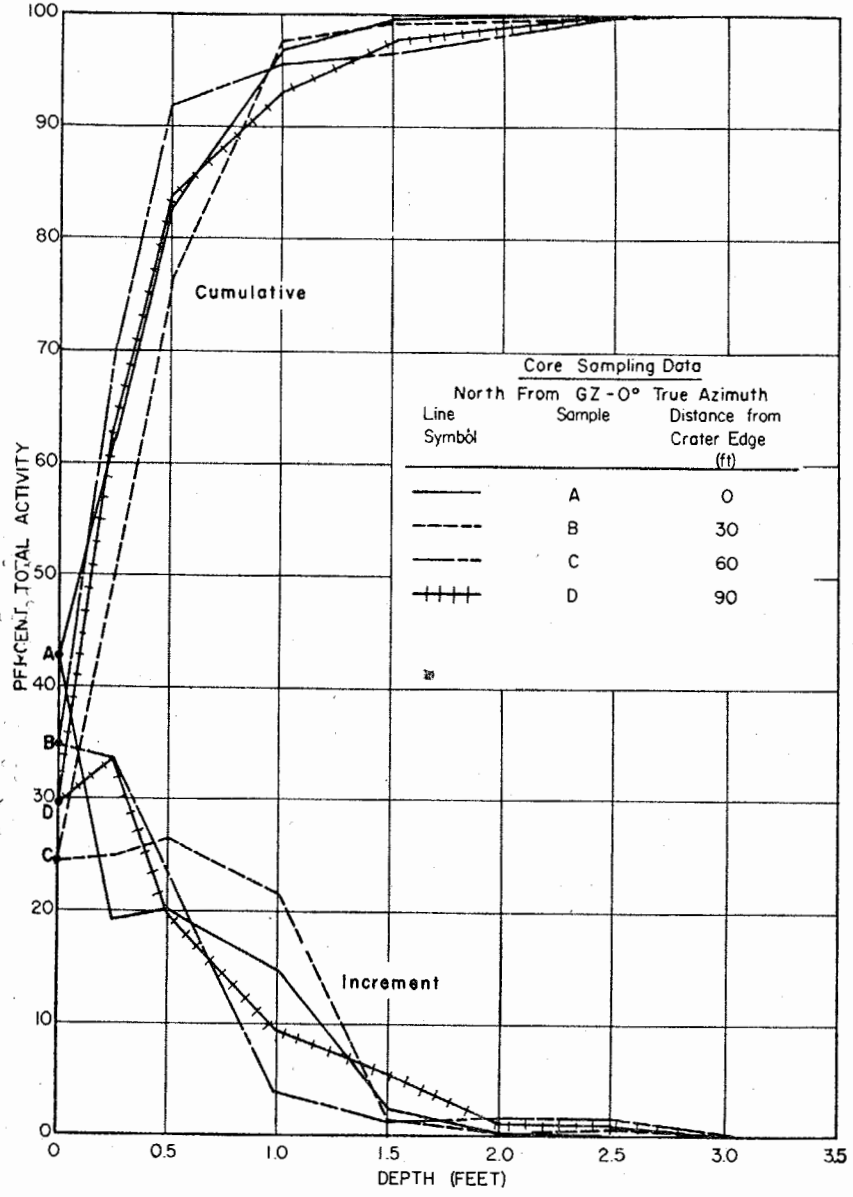

Figure 3.38 Crater lip activity distribution as a function of depth and distance (north).

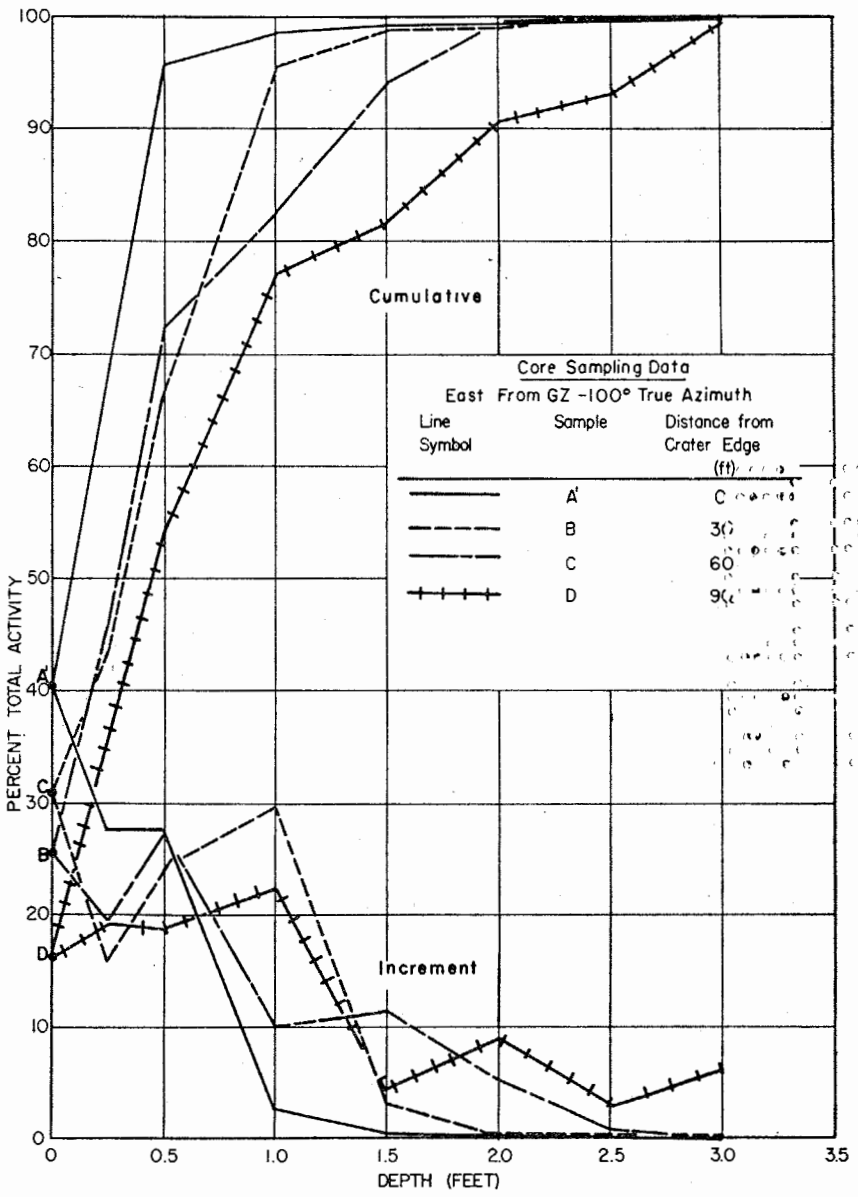

Figure 3.39 Crater lip activity distribution as a function of depth and distance (east).

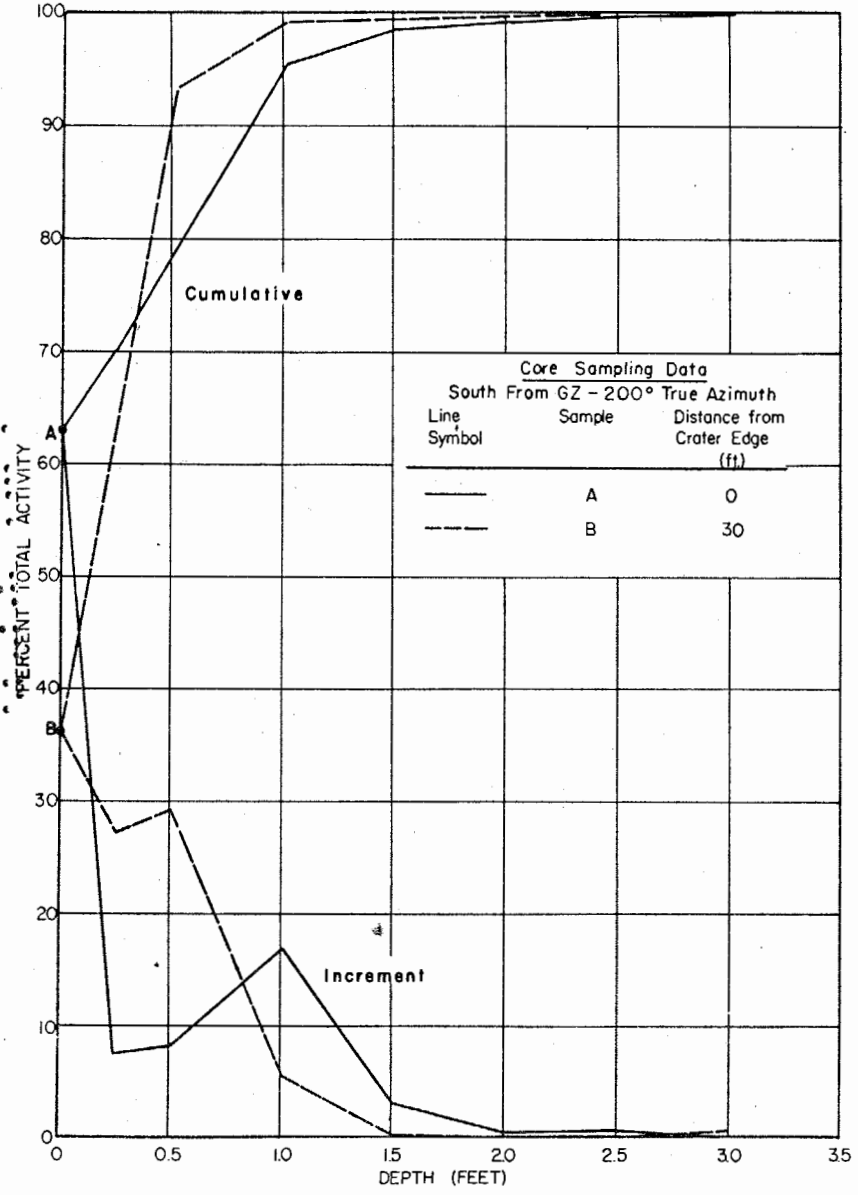

Figure 3.40 Crater lip activity distribution as a function of depth and distance (south).

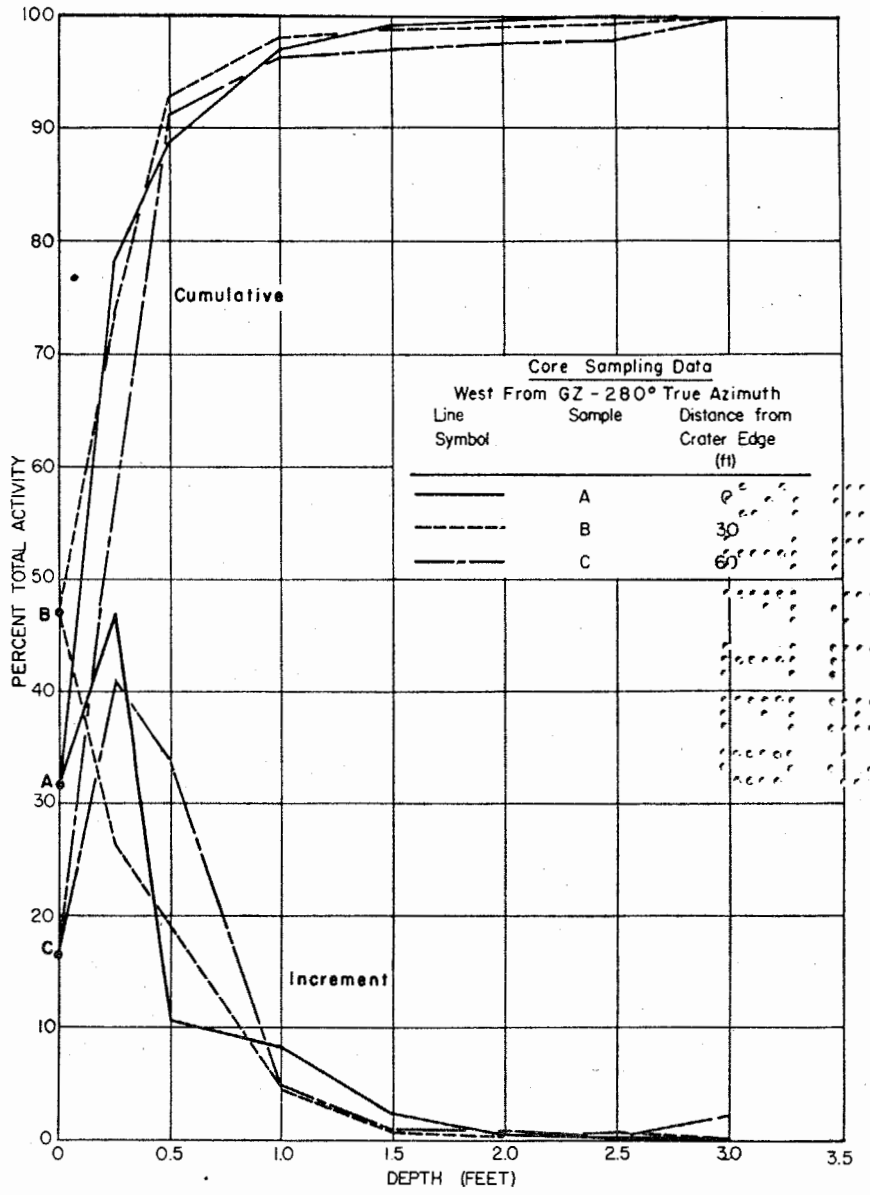

Figure 3.41 Crater lip activity distribution as a function of depth and distance (west).

diameter) and measuring the beta activity with a Nuclear Instrument Laboratory monitor employing a GM tube. All measurements were made at a constant distance from the sample and with the same geometry. A description of the sampling stations is presented in Appendix G, Section G.4.

A complete extensive survey of the Shot 7 crater-lip area was made on 1–2 October 1955. Data is presented in Reference 46. Activity ranged from 100 to 200 mr/hr within a distance of 300 feet from the crater edge.

3.4.2 Decay Rate within Crater and of Core Samples. Decay data from instruments placed in the crater by ESL at H + 2 hours and D + 8 days are not available. The instruments could not be recovered because of landslides and cave-ins.

Decay curves from several core samples were identical, and were similar to decay curves from other type samples; therefore, the corrected experimental decay curve pre-

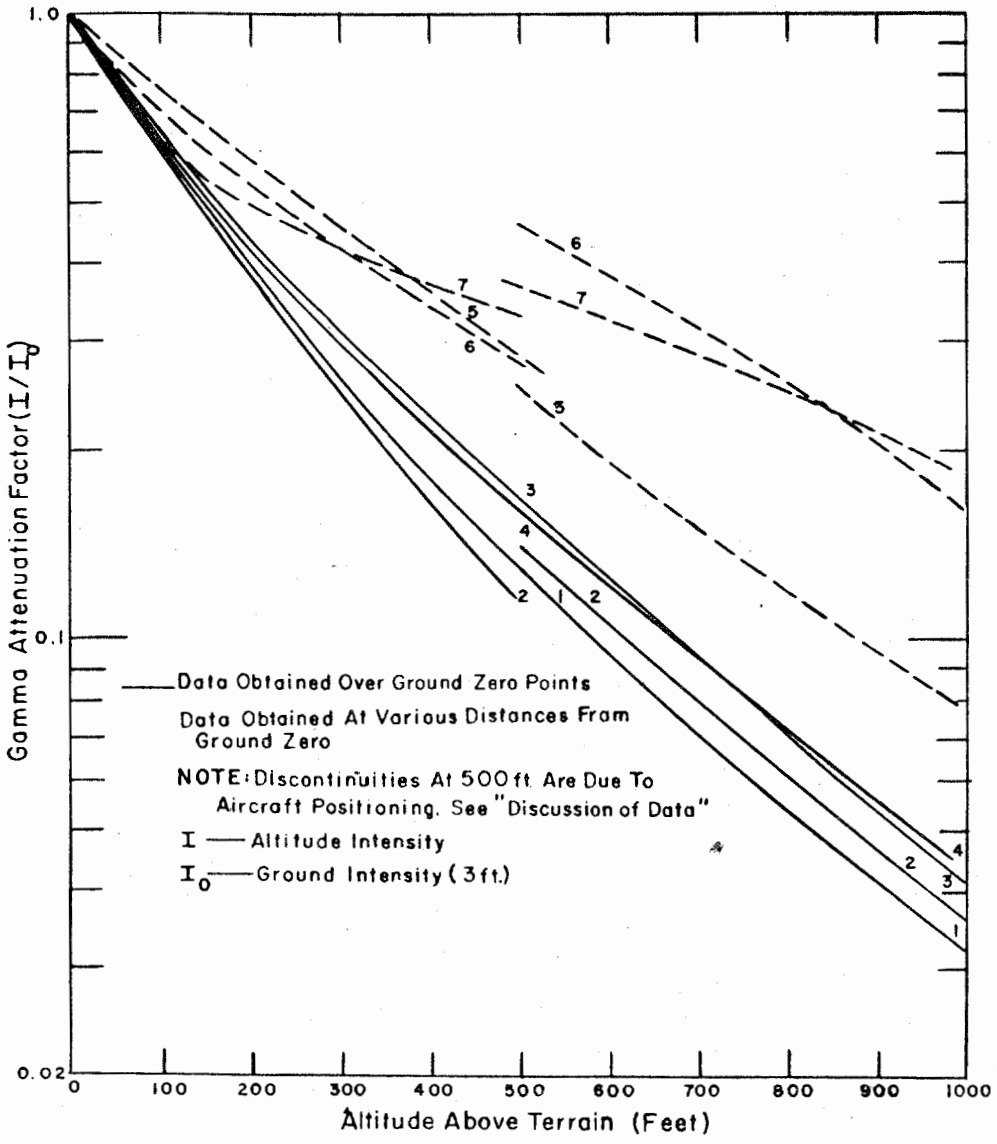

Figure 3.42 Gamma air attenuation factors versus altitude.

sented in Figure 3.37 is representative of the decay of samples from the crater-lip area.

3.5 AERIAL-SURVEY AIR-TO-GROUND INTENSITY CORRELATION

Aerial surveys were begun following Shot 1 of the test series to test the aerial-survey equipment and establish a technique for making the measurements at Shot 7. This early work resulted in the design and construction of a better instrument. However, an analysis of the data obtained prior to Shot 7 indicated the complexity of determining air-to-ground correlation factors. As a result, aerial surveys were continued for all shots remaining in the Teapot schedule after Shot 7. Intensities were measured at different heights from 3 to 1,000 feet above the ground. These readings were taken with the survey probe lowered to different levels starting first at 1,000 and then at 500 feet above the terrain. The data obtained were plotted on semi-log paper as gamma attenuation factors versus altitude (see Figure 3.42). The gamma attenuation factor is obtained by dividing the altitude intensity above a certain point on the ground by the ground intensity 3 feet above the same point.

The altitude of the helicopter was measured by an altimeter while the position of the probe below the helicopter was indicated by a footage meter on the cable-reel system. The accuracy of the helocopter altitude measurement is within the accuracy of the survey instrument which is quoted at ± 10 percent of applied dose rate anywhere on scale.

No corrections have been made for the variation in gamma ray spectra with position along the ground and with altitude. During Operation Teapot, the calibration data from the manufacturer indicated that the spectral response of the Jordan instrument was essentially flat between 75 kev and 1.3 Mev (see Section 2.2.3). Subsequent calibration of the Jordan instrument by the NBS (Reference 41) has shown that the energy response is essentially flat above 300 kev but reads higher by as much as 30 to 70 percent below 100 kev. However, these low-energy nuclides are not predominant at early times (D-day to D + 3 days and have little effect on the measurements made with the Jordan instrument when most of the aerial survey missions were conducted.

Reports are being written to discuss in detail aerial survey methods and air-to-ground intensity correlations (References 27 and 42).

The intensity readings in Appendix C were taken in cooperation with the Raydist project and were used to plot the 100 mr/hr dose-rate contour.

Chapter 4

DISCUSSION

4.1 FALLOUT CONTOURS

The dose-rate contour plots, shown in Figures 3.1, 3.2, and 3.3 were prepared from the survey data collected after Shot 7. In preparing these contours, the activity less than 5 mr/hr present south of ground zero due to a previous detonation in Area 7 was not subtracted from the plots. This fallout was not considered because it would modify only slightly the shape of the 100-mr/hr and the 10-mr/hr contours.

As discussed in Section 3.3.1 and presented in Table 3.13, the gamma radiation intensity measurements were found to have an average decay according to $T^{-1.2}$. Several of these measurements have been compared with Project 2.4 data obtained from continuous gamma intensity recorders. The data in Table 4.1 shows that, with one exception, the dose rate readings obtained by the two projects are in good agreement.

The areas enclosed by several of the dose-rate contours from Shot 7 as shown in Table 3.1 have been compared in Table 4.2 with the predictions given in the revised edition of Capabilities of Atomic Weapons (Reference 43). The areas enclosed by the 300- and 30-r/hr at H+ 1 hour dose-rate contours for Shot 7 were obtained by plotting the data from Table 3.1 as shown in Figure 4.1. The comparative data (Table 4.2) indicates that the areas enclosed by the Shot 7 contours are generally higher than the areas predicted by TM 23-200 (Reference 43).

The extent of the downwind and crosswind contours have been compared with the predictions of TM 23-200, the pretest predictions of this project, and the results from Operation Jangle. This comparison is presented in Table 4.3. The dose-rate contours of less than 10 r/hr are not shown because the mountainous terrain is known to have influenced these contours as fallout material traveled through mountain passes. The data in TM 23-200 were estimated for a 15 knot scaling wind, whereas, the meteorological data presented in Appendix E show that greater than a 10-knot wind existed at all altitudes. The predicted values of Project 2.5.1 were obtained as described in Section 2.1 and are shown in Table 2.2 for an effective wind speed of 5 mph. Since both the cloud height and wind speeds present at Shot 7 were greater than anticipated, the use of actual Shot 7 values for these two parameters would have increased the predicted extent of downwind contours. Therefore, the agreement indicated in the table is considered fortuitous.

Idealized Jangle dose-rate contours (Reference 44) for the underground shot have been reproduced in Figure 4.2. Idealized Teapot Shot 7 contours are included for purposes of comparison. These idealized dose rate contour distances are summarized in Table 4.4.

In general, above data show that the distance of downwind travel of the fallout was less than predicted in spite of the fact that the cloud rose to a greater altitude than expected; a condition which would maximize the extent of the downwind fallout. However, as mentioned previously, the travel of fallout from this test was markedly influenced beyond one mile from ground zero by the effects of mountainous terrain. It will be necessary to develop methods for relating depth of detonation, cloud height, and downwind fallout patterns before making a true comparison of Jangle and Teapot contamination

TABLE 4.1 COMPARISON OF GAMMA INTENSITY MEASUREMENTS

Except as noted, all Project 2.4 readings were obtained with a scintillation detector-type instrument.

Station Location	Gamma Intensity at H + 1 Hour		Project 2.4 Slope of Intensity Plot	Time Interval of Recording
	50th Cml Plt Project 2.5.1	Project 2.4 Recorder		
	r/hr	r/hr		min
E-1	3,200	3,300 *	1.2	25 to 130
E-3	443	330	1.2	9 to 700
E-5	70	62	1.3	33 to 230
G-1	4,150	1,400	1.48	20 to 330
G-3	1,060	950	1.3	25 to 200
G-7	43	30	1.3	9 to 350
O-3	7	10	1.28	2 to 25
O-5	0.03	0.55†	1.2	8 to 50

* Cadmium Sulfide Detector
† Ion Chamber

TABLE 4.2 AREAS ENCLOSED BY DOSE RATE CONTOURS OF SHOT 7 COMPARED WITH PREDICTED AREAS FROM TM 23-200 (REFERENCE 4)

Shot 7 contour areas

Dose-Rate Contour at H + 1 Hour	Field Measurements	TM 23-200 Predictions	Ratio: Actual to Predicted
r/hr	mi^2	mi^2	
3,000	0.070	0.052	1.3
1,000	0.261	0.135	1.9
300	0.78	0.49	1.6
100	1.41	1.21	1.2
30	3.2	3.38	0.95

TABLE 4.3 COMPARISON OF DOWNWIND DISTANCES OF DOSE RATE CONTOURS

Dose-Rate Contour at H + 1 Hour	Distance of Downwind Travel		
	2.5.1 Prediction	TM 23-200	Shot 7
r/hr	miles	miles	miles
3,000	—	0.42	0.27
1,000	0.62	0.96	0.62
500	1.1	1.32	0.75
200	2.0	2.78	1.3
100	2.8	3.75	1.4
10	5.7	—	4.5

TABLE 4.4 DOWNWIND DISTANCES OF IDEALIZED DOSE RATE CONTOURS FROM JANGLE UNDERGROUND AND TEAPOT SHOT 7

Dose Rate Contours	Distance of Downwind Travel	
	Operation Jangle Underground Shot	Operation Teapot Shot 7
r/hr	miles	miles
3,000	—	0.23
1,000	0.36	0.60
500	0.96	0.73
300	—	—
200	2.0	—
100	3.4	1.4
50	—	2.7
35	3.3	—

[redacted]

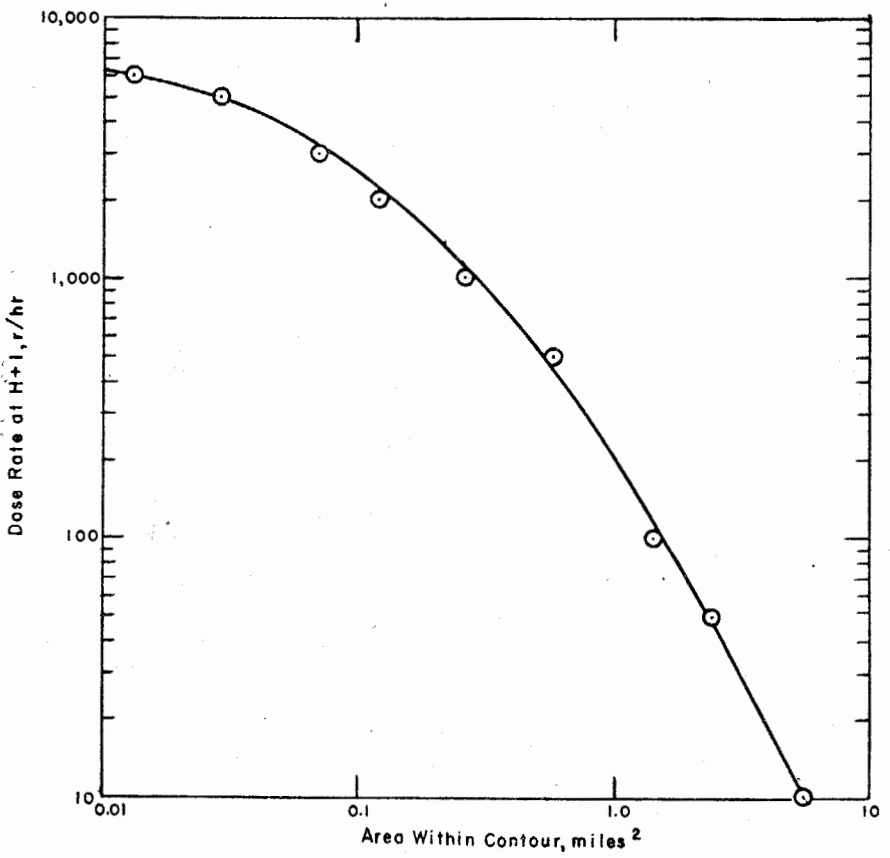

Figure 4.1 Area of dose rate contours 1.2 kt, at H + 1 hour.

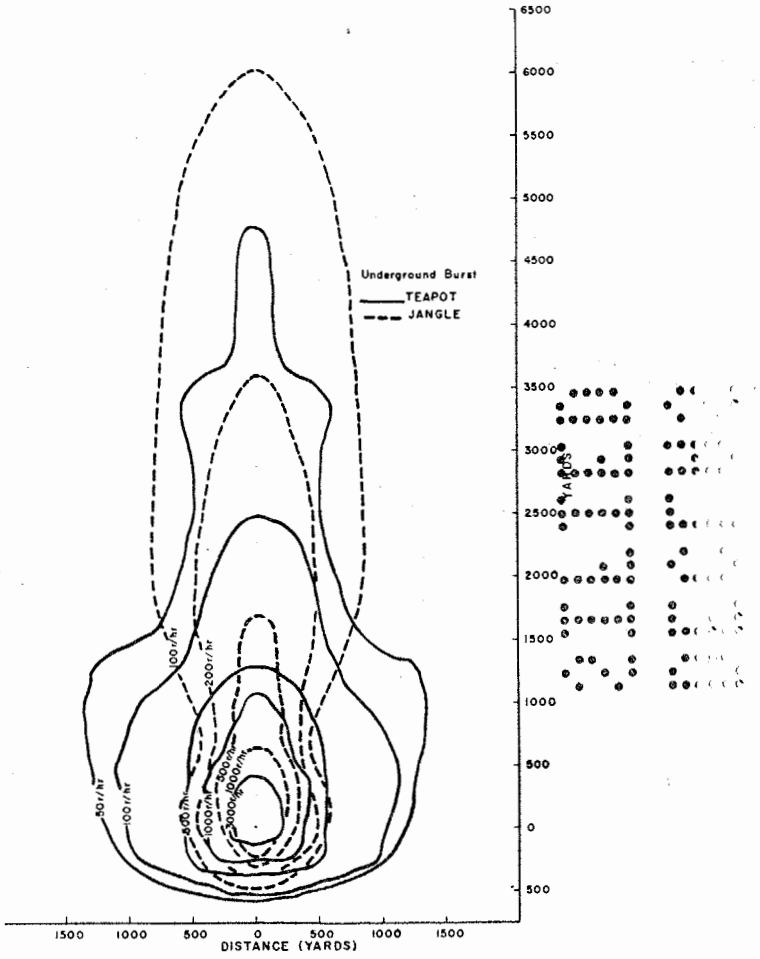

Figure 4.2 Idealized dose-rate contours, Operation Teapot and Operation Jangle underground shots.

patterns. Even contours which were not influenced by the mountainous terrain appear short in view of the cloud height and wind speed existing at Teapot.

Total gamma dose contours have been constructed from Project 2.1 data (Reference 38) and are presented in Figure 3.4. The gamma measurements were obtained with film badges recovered on D + 2 to 3 days. The data have not been corrected for differences in recovery time but if corrections were made the dosages would not be increased by more than 10–15 percent. In the exposure range from 1 to 50,000 r and in the energy range from 115 kev to 10 Mev, the accuracy of the film badge dosimeter is considered to be within ± 20 percent (References 38 and 45).

An attempt has been made to account for the fraction of the total fission product activity produced in the detonation which was deposited as fallout from Shot 7. For this purpose it was assumed that 360 megacuries of gamma-active fission products were available from a 1.2-kt device at a reference time of 1 hour after a detonation (Reference 43). Also, it was assumed that 1 megacurie of activity uniformly dispersed over an area of 1 square mile will produce a radiation intensity of 4 r/hr at H + 1 hour at a height of 3 feet above this area (References 18 and 43). An estimate of the megacuries of fission products which fell to the ground was made by determining the area enclosed by the various dose-rate contours. Because the contours shown in Figures 3.1, 3.2, and 3.3 are so irregular, it was difficult to estimate the average intensity and area between successive contours. In order to overcome this difficulty, it was necessary to measure the areas with a planimeter, and conduct a more detailed analysis. This analysis is presented in Appendix F and accounts for 80 percent of the activity produced by the detonation. The remainder of the activity was either carried downwind by the cloud beyond the area surveyed or buried in the crater-lip area. It is known that activity was buried to a depth of 12 inches on the crater-lip on D + 8. Additional measurements were made of the activity on the lip and in the crater on D + 97 to 99 days. These measurements taken at such a later time and presented in Appendix G indicate that an appreciable amount of activity still remained on the lip and that activity was buried to a depth of 3 feet in the crater.

A comparison of the aerial photographs, which are shown in Figures 4.3 and 4.4 with the dose-rate contours presented in Figure 3.1 shows a striking similarity between the amount of fallout on the ground and the intensity of the radiation.

4.2 BASE SURGE

The photographic results of Project 9.1 show that the maximum upwind extent of the base surge coincides with the visible fallout pattern upon the ground. As discussed above in Section 4.1, this visible fallout pattern and the high-intensity contours also coincide.

The Project 2.5.1 experiment was designed to compare crosswind and downwind fallout. As mentioned in Chapter 3, only a limited number of collectors were used. Only one crosswind station (L-1) operated. About 90 percent of the total activity collected at this station arrived within four minutes after the detonation (Figure 3.12). During this period of time, photographs show that the initial base surge rolled by this station and was not moved back past this station by the action of the wind until 1 minute later. The radiochemistry data of Figures 3.29 and 3.30, which show the second peak R-values at 5 minutes, verify this point. Therefore, as will be discussed in Section 4.6, the activity collected by this fallout collector may be attributed to the base surge. The station G-1, at an equivalent point downwind, collected its activity over the entire sampling time of 17 minutes (see Figure 3.7 and Table 3.10).

The transition from the Jangle underground shot pattern to the Teapot underground pattern is illustrated in Figure 4.2. This figure shows that at the greater scaled depth the surge

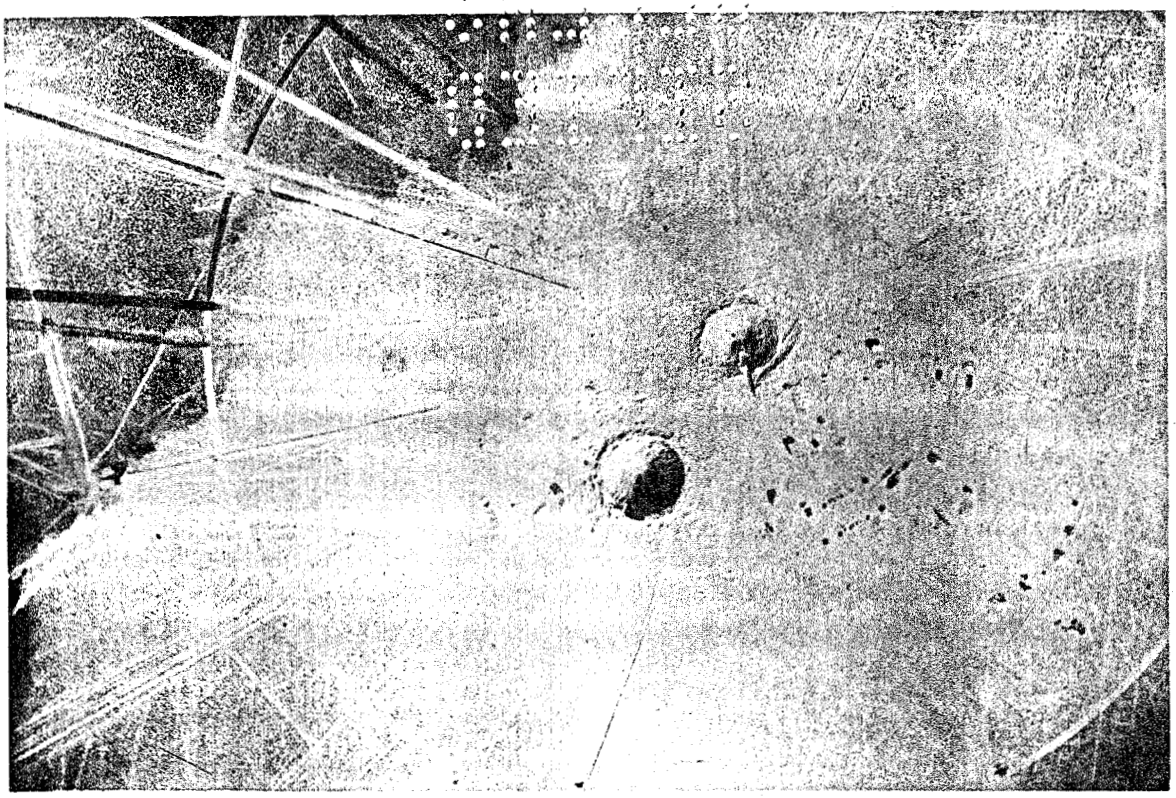

Figure 4.3 Aerial photograph of Shot 7, ground zero closeup.

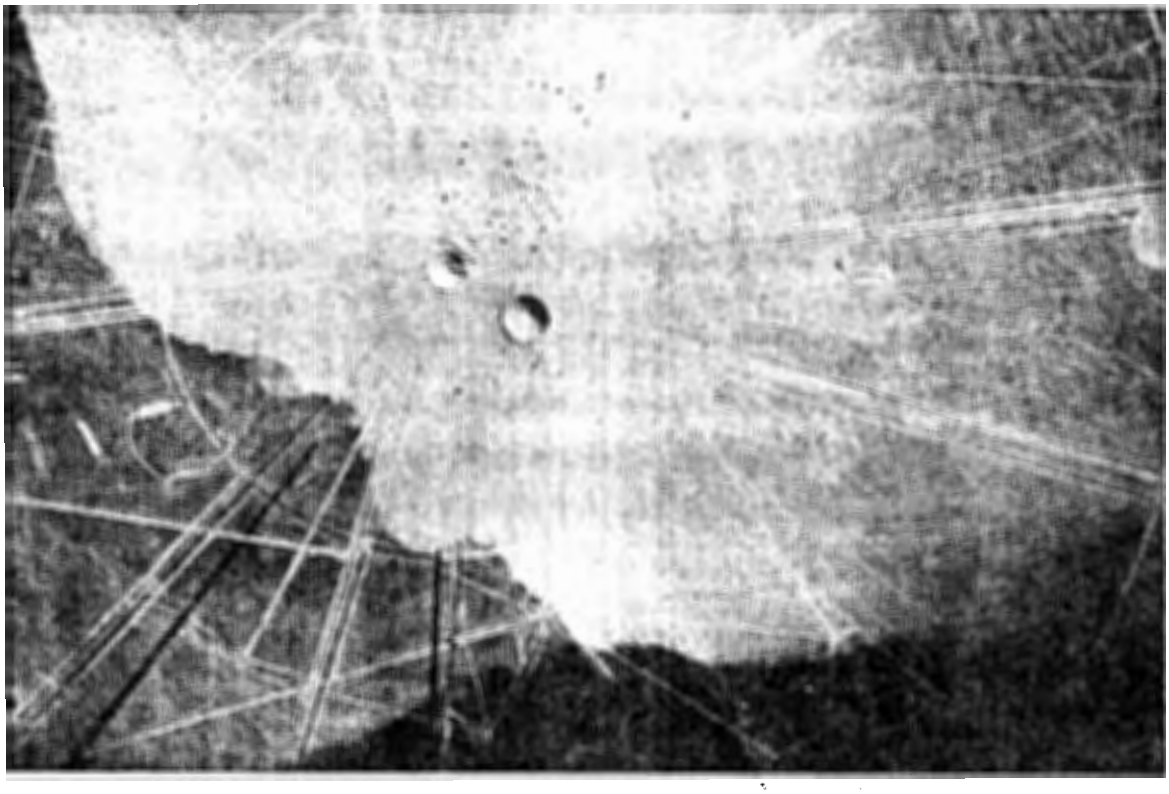

Figure 4.4 Aerial photograph of Shot 7, ground zero showing extent of fallout for comparison with project dose-rate contours.

must have been a predominant factor in the distribution of contamination because, as shown, dose-rate contours of greater intensity cover larger areas in the crosswind and upwind direction around ground zero for the Teapot shot than for the Jangle event. The Teapot contamination pattern is also shown in Figures 4.3 and 4.4 to be distributed extensively in the crosswind and upwind directions as well as downwind.

4.3 TIME OF ARRIVAL

The intermittent fallout collector data (plotted in Figures 3.6 through 3.12) show peaks which are believed to correspond to the arrival of maximum activity at the various stations. From tabulated data in Appendix B, the time and rate of arrival of fallout to 50 percent and

TABLE 4.5 TIME OF ARRIVAL OF ACTIVITY

Station Number	Distance from Ground Zero	Time to 50 pct Activity	Time to 95 pct Activity	Rate of Travel for 50 pct Activity	Rate of Travel for 95 pct Activity
	miles	hours	hours	mph	mph
F-7	1.93	0.22	1.5	8.9	1.3
G-1	0.17	0.02	0.28	7.3	0.6
G-3	0.40	0.32	0.47	1.2	0.8
G-5	0.94	0.34	0.41	2.8	2.3
G-7	1.93	0.88	1.7	2.2	1.2
H-8	2.56	0.55	1.9	4.7	1.3
L-1	0.17	0.05	0.09	3.4	1.8

95 percent of the activity was obtained. This information is summarized in Table 4.5 and shows 95 percent of the activity to have traveled to stations from 1.9 to 2.6 miles downwind at the rate of less than 2 mph ground speed. The rate of cloud travel as calculated from the time of arrival of 50 percent of the activity shows a wide variation for all stations while this variation is smaller for 95 percent of the activity.

4.4 SPECIFIC ACTIVITY

Specific activity or the beta activity measured with a known geometry (Section 2.3.2) converted to H + 1 by the experimental decay curves (Figure 3.37) and expressed as millicuries per gram of fallout was reported in Table 3.4 and Table 3.5 for total fallout and intermittent fallout samples, respectively. The average of the specific activities for the fallout samples is 21.4 mc/gm. At Operation Jangle, specific activities were found to average 75 mc/gm (Reference 6). Obviously, the average specific activity for Teapot Shot 7 is lower than that for Jangle underground shot.

4.5 ACTIVITY VERSUS PARTICLE SIZE

The activity versus particle size results are illustrated graphically in Figures 3.21 through 3.24. The analysis of samples collected at 300 yards downwind (Station G-1) shows that over 54 percent by weight of the total fallout was associated with particles larger than 840 microns. This size group contained, however, only 28 percent of the total activity. At the same location, 49 percent of the activity was associated with particles in the size range 210 to 420 microns. The equivalent crosswind location (Station L-1) likewise showed a large percentage (48 percent) of total fallout by weight to be associated with the larger particles (greater than 840 microns). At this crosswind location the large size group carried only 11 percent of

the total activity. The remaining activity was distributed quite uniformly in size groups from 74 to 420 microns.

At 700 yards downwind (Station G-3), over 50 percent of total fallout by weight was represented by particles greater than 840 microns, but most of the activity was generally associated with particles in the size groups from 0 to 420 microns. The equivalent crosswind station (L-3) was quite different. Over 40 percent by weight of the samples was in the 44 to 74 microns group. This group carried about 50 percent of the activity. At this crosswind location less than 1 percent of the weight and activity was associated with the large size groups.

Over 90 percent by weight of total fallout collected at 1,650- and 3,400-yard downwind stations (G-5 and G-7) were composed of 44 to 420 micron particles. At these stations, the same particle size groups, accounted for about 90 percent of the activity.

The distribution of activity within individual particles was determined by mounting the particles in plastic plugs, and then sectioning and photographing them as described in Sections 2.3.2 and 3.2.5. The two top illustrations in Figure 4.5 show a surface active particle on the left and its radioautograph on the right. The bottom illustrations show a particle with the radioactivity distributed throughout its volume. These studies showed two types of predominant radioactive particles. One observation that was consistent in this study of many samples of fallout was the presence of particles that were radioactive throughout. These particles, except in one instance, appeared in all size fractions from all stations. The number of such particles found was very small with respect to the total number of particles mounted (only 12 percent), but the contribution of these particles to the total activity of an aliquot of fallout was estimated to be about 90 percent. In appearance, all of these particles with radioactivity distributed throughout had the same general physical characteristics. They were black or dark gray in color, irregular in shape and looked very much like pieces of coke. The thin sections of the particles revealed pores or channels as one might find in coke. A large number of particles were active only on the surface. No chemical analysis was performed to determine what the chemical composition of these particles was; however, the particles appear to be the same glassy particles found by the NRDL at Operation Jangle (Reference 47) and further analyzed by the Stanford Research Institute (Reference 6).

4.6 RADIOCHEMISTRY

The R-values of Sr^{89}/Mo^{99}, Sr^{89}/Ce^{144}, Ba^{140}/Mo^{99}, Ba^{140}/Ce^{144}, for the crosswind samples presented in Table 3.8 and plotted in Figures 3.29 and 3.30 show excellent agreement among themselves in their variations with collection time. R-values for the downwind samples presented in Table 3.9 and plotted in Figures 3.31 and 3.32 illustrated similar trends among themselves although the agreement is not quite as good as in the crosswind samples. The R-values for the crosswind samples are generally higher than those for the downwind samples except that the major minima are essentially equal.

The Mo^{99}/Ce^{144} R-values are included in Tables 3.8 and 3.9 as a check of the rare gas precursor theory discussed in Reference 40. According to this theory the Mo^{99}/Ce^{144} R-values should not vary appreciably because neither nuclide has a rare gas precursor with a significantly long half-life. There is some variation in these R-values although the magnitude is not nearly as great as for the other R-values presented. These data indicate that the rare gas precursor effect is by far the most significant effect in this investigation, but that other phenomena are in operation. These other phenomena may depend upon the vapor pressure of the individual nuclides at the time of condensation, or on the scavengeability of the various nuclides by condensing soil. Whatever these phe-

nomena are, they are not considered in this investigation since they contribute only a small variation.

4.6.1 Origin of Minima on R-Value Curve. According to the rare gas precursor theory, low R-values indicate early sample removal from the fireball and consequently the presence of a radioactive base surge that had been contaminated in the column. The minima in Figures 3.29 through 3.32 correspond to contaminated samples that were first to depart from the fireball. According to the shot description in Section 3.2.2, the initial jets or spears of earth were the first to depart from the fireball as they rose up through the fireball shortly after it broke the surface of the ground. Consequently, the uppermost

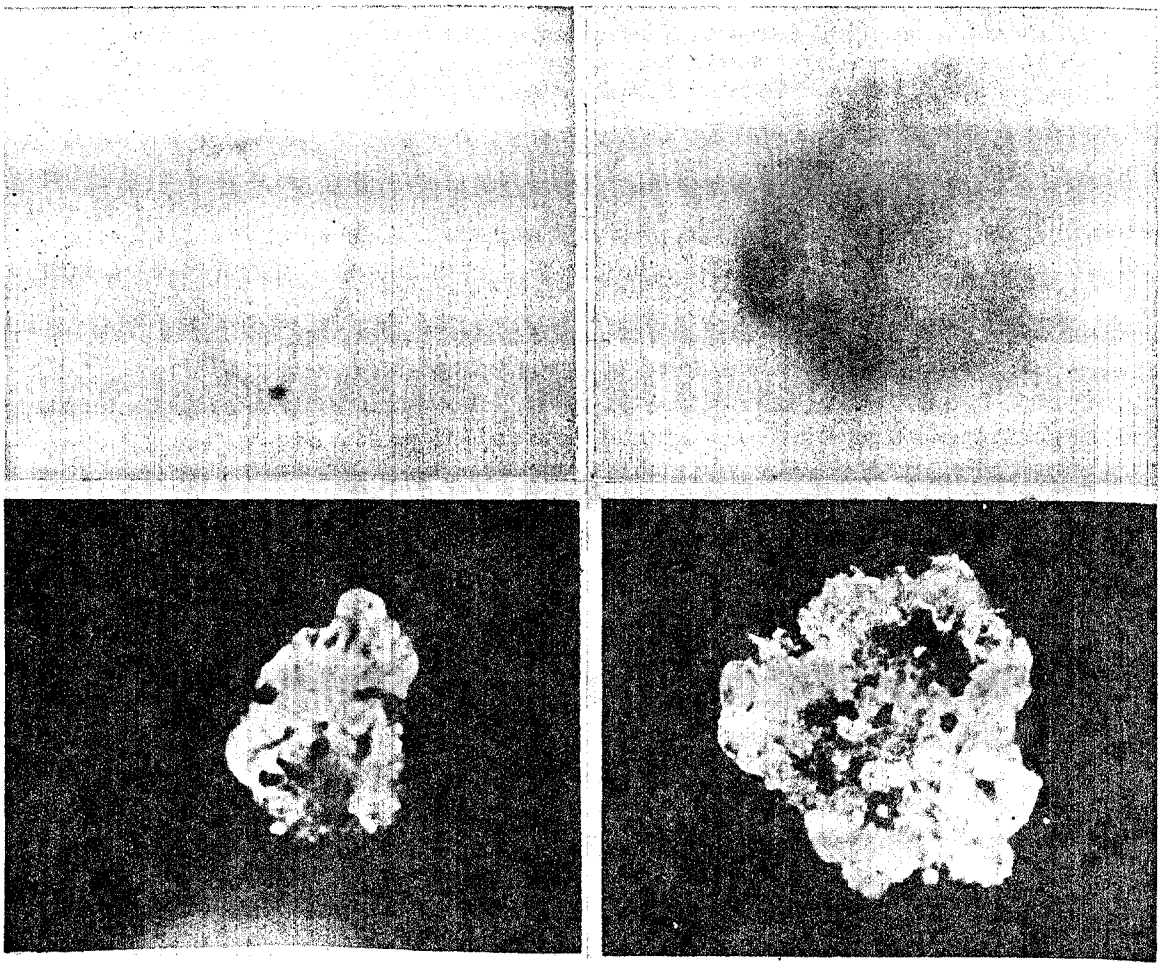

Figure 4.5 Surface active and fully active particles and their radioautographs.

edges of the jets should have the lowest R-values. The jets fell back to the ground producing the base surge. The last portion of the jets or the uppermost edges reached the ground at about 140 seconds. The minima for the crosswind samples occurred at 142 seconds which yields excellent correlation. There is also good agreement for the downwind samples.

4.6.2 Origin of the Two Maxima on R-Value Curve. The jets associated with this shot rose very rapidly to their maximum height. Having reached this maximum, these columns

of materials settled slowly to the earth. It is reasonable to assume that, in these vertical columns, the material which was last to be airborne would be the first to reach the ground. Effects which would result in the column not falling as a unit would be minimized due to the influence of mass subsidence.

The bottom parts of the jets were the last to pass through the fireball or early cloud, and consequently were the last parts to be contaminated. The R-values of these parts of the jets would be at a maximum. Since these parts were the first to reach the ground, the R-values of the time incremental samples should begin with a maximum and fall off to a minimum corresponding to the arrival of the uppermost parts of the jets. The base surge continued to roll out until it lost its momentum. Subsequently, the surface winds dissipated the base surge in the downwind direction. The leading edge of the base surge which rolled in the upwind direction was blown back across the sampling stations producing a second maximum in the R-value versus sampling time curves.

The explanations of the trends in the R-values in Figures 3.29 through 3.32 are partially supported by the total activity per interval measurements for the crosswind samples given in Table 3.10 and plotted in Figure 3.33. These data illustrate that all the significant activity at the crosswind station arrived during the initial passage of the base surge. As would be expected from the proposed origin of the second R-value peak, the total activity associated with this peak is insignificant when compared to the earlier collection. Similar downwind data do not follow this trend (Figure 3.34). It should be mentioned that there appears to be no significant correlation of total activity per gram in Figures 3.33 and 3.34 with either the R-values or the total interval activity except for the short period (88 to 196 seconds) during collection of the heavy samples in the crosswind area. The R-values go through a minimum while the total activity per sampling interval reaches a maximum during this period.

4.6.3 The Base Surge as the Primary Carrier of the Radioactivity. The fact that all the significant activity arrived at the crosswind collector during the time of the initial base surge rollout (Table 3.10 and Figure 3.33) has an important corollary. These data indicate that the base surge is the primary carrier of the activity in the crosswind area. The same conclusion cannot be drawn from similar data of the downwind station (Table 3.10 and Figure 3.34). However, the isodose contours developed in Section 3.1 suggest that the same is true in the downwind area because both crosswind and downwind stations were located inside extremely high dose-rate contours (Figure 3.1). In fact, all the intense isodose lines were within the extent of the base surge. This observation lends further support to the conclusion that the base surge is the primary carrier of the radioactivity within the area of its coverage.

On the basis of the above conclusion, one might expect the R-values to be similar in both the crosswind and downwind areas. Tables 3.8 and 3.9 show that the crosswind samples have higher R-values than the downwind samples except around the minima or during the initial rollout of the base surge. In an effort to explain this behavior, reference to the description of the shot must be made (Section 3.2.2). A central jet appeared to pass through the fireball and travel upward with extremely high velocities. It was surrounded by other jets that had slight angular trajectories and traveled at slower rates. The jets were the first material to break through the fireball and were bound to have the lowest R-values. Even as the central jet was still rising rapidly, the prevailing winds could have displaced some of the material in the central jet toward the more slowly rising downwind jets. This displaced material could have been mixed to some extent with the downwind jets as they grew. Consequently, when the downwind jets returned to the desert floor producing the base surge, the R-values were considerably lower than in the crosswind area because of this

contamination by the central jet. The equality of the R-values during the minimum at both stations supports this explanation since the minimum corresponds to the arrival of the uppermost edges of the jets which should have the same R-values regardless of the wind direction. This explanation ignores all possible abnormalities or unique characteristics of the weapon that would permit variation in the relative fission product concentration as a function of direction from the detonation.

4.6.4 Gamma Emitting Nuclides in the Crater Lip. The data of Table 3.12 shows that there are no significant changes in the relative concentrations of the principal gamma emitting nuclides at 44 days after the shot in the crater lip as a function of depth underground or distance from ground zero. These samples were taken 8 days after the shot. During the postshot period, no rain fell to produce any weathering.

4.7 BETA DECAY

The experimental beta decay curves presented in Figure 3.37 have been found to be representative of all samples analyzed. Sample decay measurements were started at the test site and covered the period from H + 4 to H + 3,000 hours. A treatment of decay curves for the extrapolation of activities and the determination of the experimental beta decay curves is presented in Appendix I. The decay rates of samples from the crater and the lip at various downwind and crosswind distances and from fallout collection at various times from 1 to 120 minutes after the shot are all similar.

4.8 CRATER AND LIP

Early core samples (D + 8 to 9 days) on the crater lip show activity to be concentrated near the surface. Even though there undoubtedly was drifting of loose dirt by the wind, all samples show at least 77 percent of the activity to be within the first foot of depth. At fourteen of the sixteen sampling locations, greater than 93 percent of the activity is within the first foot of depth.

Radiation intensity measurements taken with the aerial survey probe on the lip at H + 2 indicate the extrapolated dose rate was 6,000 r/hr at H + 1 hour. Measurements made at a later date also extrapolated to this same intensity. At D + 9, while taking core samples it was noted that the intensity increased as the distance down the lip away from the crater increased. On D + 17, a detailed survey of the lip area (Table 3.16) showed this to be true on all sides of the crater. It was noted that the high intensity region extended to at least 150 feet from the lip. The data of Table 3.15 were taken at this time and showed the crater itself to be reading less than the lip area by a factor of 10, indicating how the geometry influences the measurements.

Extensive intensity measurements which were made in the crater-lip area (D + 97 to 99 days) and are presented in Table 3.17 confirm the above results found at early times.

Later core sampling (D + 97 to 99 days) at numerous points on the crater lip still shows the activity to be concentrated near the surface (Table G.2). Core samples taken at the same time in the crater show the activity to be buried to a depth of about 3 feet, somewhat deeper than on the lip. The greater depth of burial of activity in the crater is probably due to the numerous cave-ins and land slides that occurred during the 3 months between the shot and sampling. This conclusion is verified by the change in

appearance of the crater bottom from a point to a flat bottom approximately 40 feet in diameter.

4.9 CORRELATION OF AIR AND GROUND RADIATION-INTENSITY MEASUREMENTS

Attenuation factors versus altitude (Figure 3.42) were plotted for readings over ground zero and at various distances from ground zero. The resulting curves show that the gamma-radiation intensity decreases approximately logarithmically with altitude above any specific point. The rate at which the intensity decreases with altitude is dependent upon the location over which the readings were taken. This is indicated by the fact that the curves have different slopes. There seems to be no simple relationship, however, between the slope of the curve and the position within the fallout pattern. It should be noted that, in every case, the steeper slopes were associated with the readings obtained over ground zero. Some of the curves are discontinuous at the 500-foot point. These discontinuities are due to positioning difficulties encountered in returning the helicopter to its exact original position at 500-foot elevation at the beginning of a new series of readings. The data are still valid, however, since the slope of the curve is the same on either side of the break. The discontinuity merely indicates that data for the second portion of the curve were taken over a point slightly to one side of the initial point on the ground.

Chapter 5

CONCLUSIONS and RECOMMENDATIONS

5.1 CONCLUSIONS

1. A very extensive area (450 square miles) was contaminated to an intensity level greater than 100 mr/hr at H + 1 hour by Shot 7.
2. The areas enclosed by the dose-rate contours were generally greater than predicted. However, they did not extend as far downwind as predicted.
3. Most of the activity (80 percent) was accounted for within the 0.1 r/hr to 3,000 r/hr at H + 1 hour dose-rate contours.
4. The base surge was the principal mechanism by which activity was carried in the upwind and crosswind direction.
5. Most of the activity (90 percent) in the crater-lip area was contained in the top 12 inches of soil.
6. During the first three months weathering had very little effect on the distribution of the crater-lip contamination.
7. Because of cave-ins and landslides a large percentage (80 to 90 percent) of the activity in the crater can be expected to be located in the top 3 feet of soil.
8. Gamma-intensity measurements in the fallout area showed that the dose rate from H + 2 to D + 4 days followed the -1.2 decay exponent.
9. The beta-decay was similar to that found at other tests.
10. Air-to-ground correlation factors varied considerably from position to position in the fallout area.
11. Although results from this study compare fairly well with those predicted from TM 23-200, it is not at all certain that results predicted from TM 23-200 would apply for other yields and/or other depths of burst.

5.2 RECOMMENDATIONS

A similar fallout study should be conducted for a contaminating event at a future weapons trial to confirm predictions in TM 23-200 for a different yield and/or depth of burst.

Appendix A

STATION LAYOUT

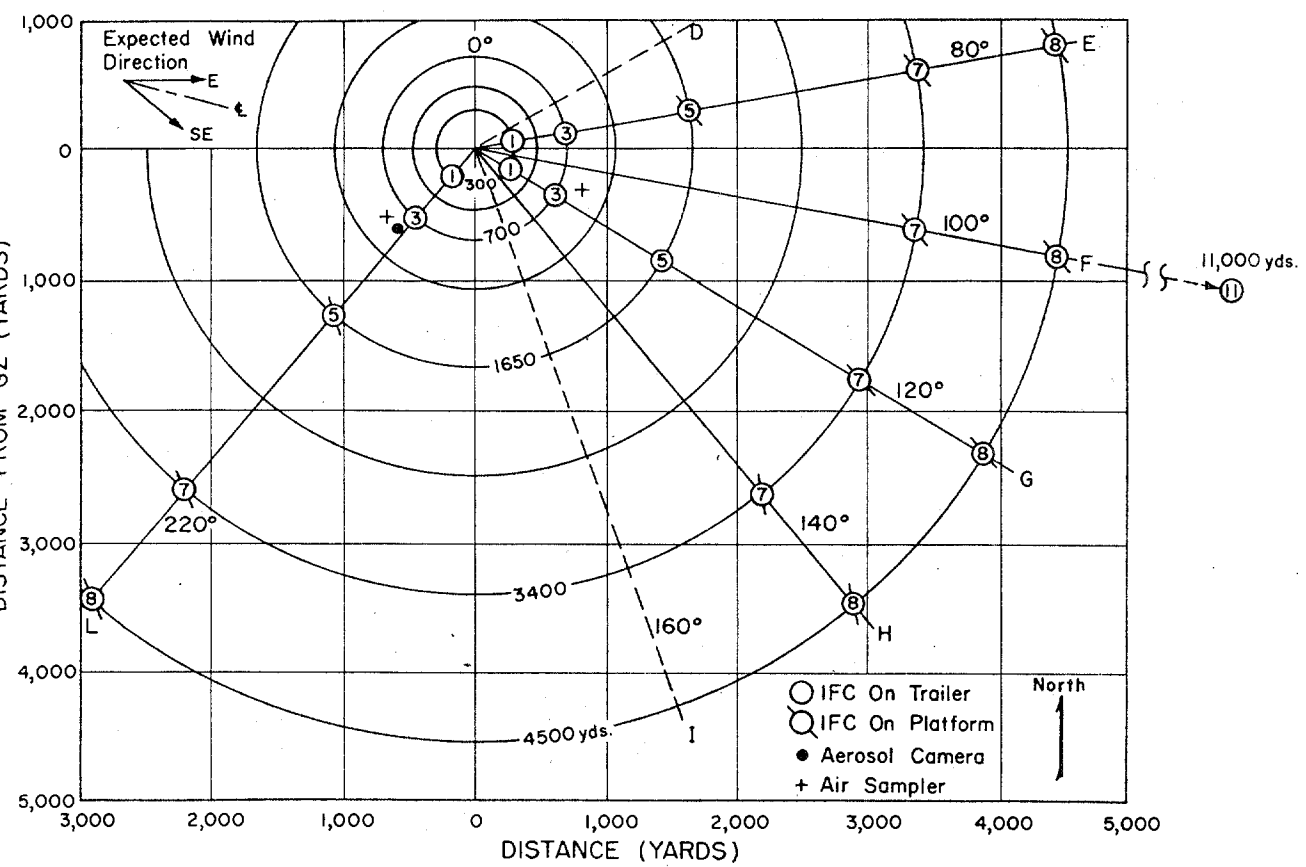

Figure A.1 Station layout, Project 2.5.1.

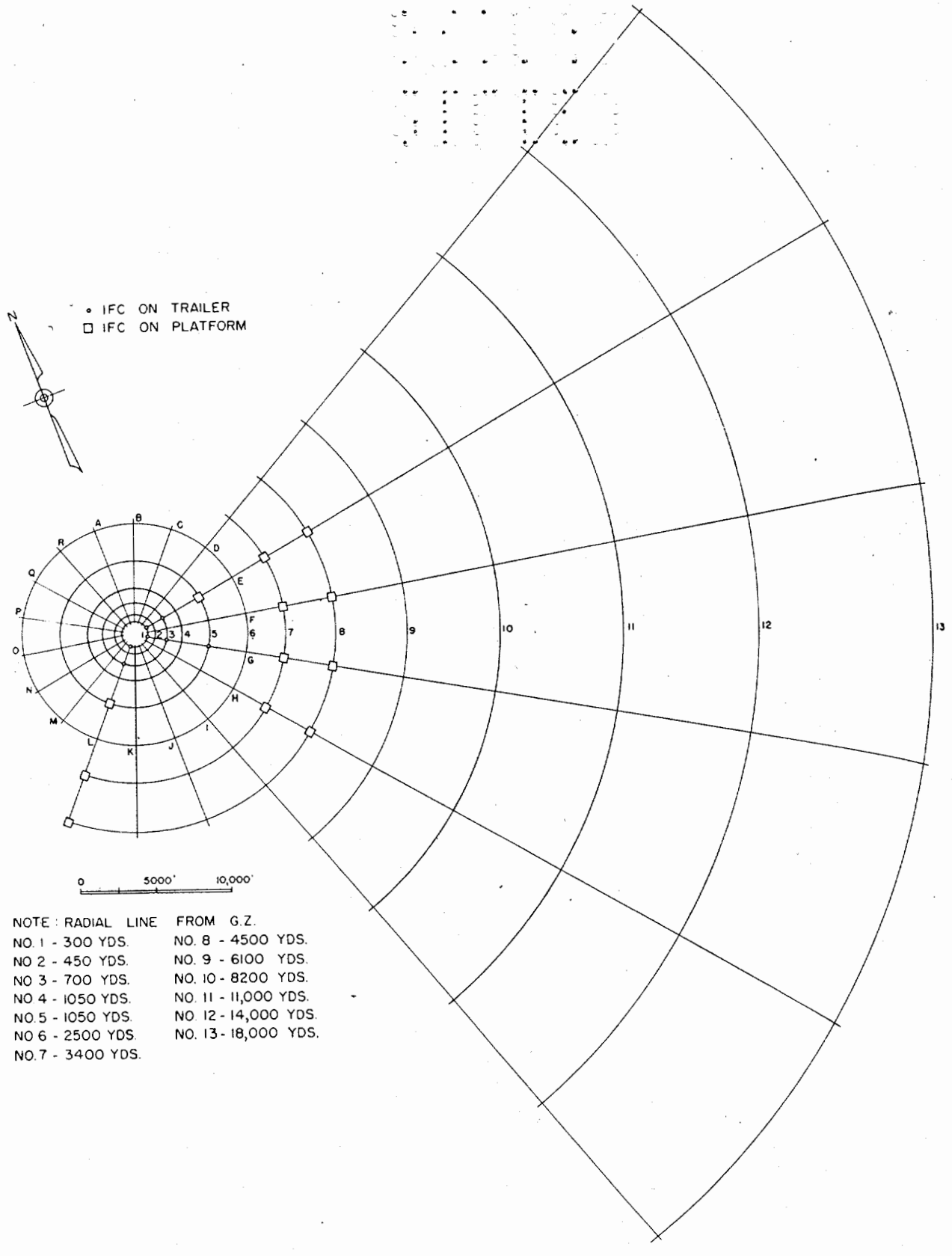

NOTE : RADIAL LINE FROM G.Z.

NO. 1 - 300 YDS.	NO. 8 - 4500 YDS.
NO 2 - 450 YDS.	NO. 9 - 6100 YDS.
NO 3 - 700 YDS.	NO. 10 - 8200 YDS.
NO 4 - 1050 YDS.	NO. 11 - 11,000 YDS.
NO.5 - 1050 YDS.	NO. 12 - 14,000 YDS.
NO 6 - 2500 YDS.	NO. 13 - 18,000 YDS.
NO.7 - 3400 YDS.	

Figure A.2 Master station locator.

Appendix B

COUNTING DATA

Tables B.1 through B.7 show the counting data of the intermittent fallout collector samples.

Tables B.8 and B.9 show the analysis data obtained from the total fallout samples collected on the downwind (G-leg) and crosswind (L-leg) directions.

Supporting data for the isokinetic aerosol samples are presented in Tables B.10 and B.11.

Note: Powers of 10 where indicated in tables are applicable to entire columns.

TABLE B.1 ORIGINAL COUNTING DATA OF THE INTERMITTENT FALLOUT COLLECTOR SAMPLES, STATION F-7

Collector Interval Number	Total Weight Collected	Weight of Sample Counted *	Activity of Sample Corrected to H + 1 Hour	Total Interval Activity †	Activity Concentration	Percent Activity
	gm	gm	d/m	d/m	d/m/gm	
1	0.1624		46.69×10^7		2.88×10^8	20.61
2	0.2047		59.95		2.93	26.47
3	0.0144		19.13		13.28	8.45
4	0.0062		19.84		32.00	8.76
5	0.0032		1.545		4.83	0.68
6	0.0029		3.028		10.44	1.34
7	0.0025		0.958		3.83	0.42
8	0.0018		30.87		171.50	13.63
9	0.0017		1.319		7.76	0.58
10	0.0022		1.526		6.936	0.67
11	0.0001		1.208		120.80	0.53
12	0.0026		1.112		4.28	0.49
13	NMW		0.270		—	0.12
14	0.0033		0.603		1.83	0.27
15	0.0032		0.547		1.71	0.24
16	0.0035		0.810		2.31	0.36
17	0.0020		29.29		146.45	12.93
18	0.0025		0.661		2.64	0.29
19	0.0015		0.188		1.25	0.08
20	0.0026		1.301		5.00	0.57
21	0.0016		0.473		2.96	0.21
22	0.0029		0.998		3.44	0.44
23	0.0040		1.866		4.67	0.82
24	0.0003		2.321		77.37	1.02

NMW, no measurable weight. Sampling interval 5m 5s.
* Same as total weight.
† Same as activity of sample.

TABLE B.2 ORIGINAL COUNTING DATA OF THE INTERMITTENT FALLOUT COLLECTOR SAMPLES, STATION G-1.

Collector Interval Number	Total Weight Collected	Weight of Sample Counted	Activity of Sample Corrected to H + 1 Hour	Total Interval Activity	Activity Concentration	Percent Activity
	gm	gm	d/m	d/m	d/m/gm	
1	70.4055	0.0055	26.68×10^7	—	—	*
2	8.6118	0.0118	18.29×10^7	13.35×10^{10}	1.55×10^{10}	47.54
3	0.4185	0.0059	29.18×10^7	2.07×10^{10}	4.95	7.37
4	0.1680	0.0052	12.53×10^7	0.40	2.41	1.42
5	0.0705	0.0038	19.75	0.37	5.20	1.32
6	0.1665	0.0053	40.86	1.28	7.71	4.56
7	0.0259	0.0048	74.47	0.40	15.51	1.42
8	0.0362	0.0065	66.70	0.37	10.26	1.32
9	0.0587	0.0084	66.15	0.46	7.87	1.64
10	0.0407	0.0065	93.37	0.58	14.36	2.07
11	0.0178	0.0048	38.11	0.14	7.94	0.50
12	0.0162	0.0025	10.14	0.07	4.06	0.25
13	0.0445	0.0050	97.84	0.87	19.57	3.10
14	0.0397	0.0052	57.77	0.44	11.11	1.57
15	0.0630	0.0054	26.81	0.31	4.97	1.10
16	0.1086	0.0061	20.44	0.36	3.35	1.28
17	0.1041	0.0056	23.01	0.43	4.11	1.53
18	0.1102	0.0066	15.90	0.27	2.41	0.96
19	0.0289	0.0090	55.97	0.18	6.22	0.64
20	0.1224	0.0041	14.80	0.44	3.61	1.57
21	0.1244	0.0086	99.80	1.44	11.60	5.13
22	0.2004	0.0082	31.05	0.76	3.79	2.71
23	0.2088	0.0067	48.73	1.52	7.28	5.41
24	0.3829	0.0172	70.83	1.57	4.09	5.59

* Door was open all the way on recovery. Sampling interval 44s.

[redacted]

TABLE B.3 ORIGINAL COUNTING DATA OF THE INTERMITTENT FALLOUT COLLECTOR SAMPLES, STATION G-3

Collector Interval Number	Total Weight Collected	Weight of Sample Counted	Activity of Sample Corrected to H + 1 Hour	Total Interval Activity	Activity Concentration	Percent Activity
	gm	gm	d/m	d/m	d/m/gm	
1	11.5	0.0517	217.08×10^7	—	4.20×10^{10}	*
2	0.0587	0.0092	32.89	210×10^7	3.58	14.66
3	0.0165	0.0165	18.30	18.30	1.11	1.28
4	0.0091	0.0091	16.63	16.63	1.83	1.16
5	0.0032	0.0032	7.36	7.36	2.30	0.51
6	0.0037	0.0037	16.19	16.19	4.38	1.13
7	0.0178	0.0178	34.20	34.20	1.92	2.39
8	0.0028	0.0028	11.81	11.81	4.22	0.82
9	0.0112	0.0112	38.21	38.21	3.41	2.67
10	0.0111	0.0111	24.65	24.65	2.22	1.72
11	0.0034	0.0034	1.90	1.90	0.56	0.13
12	0.0028	0.0028	7.948	7.95	2.84	0.56
13	0.0137	0.0137	7.88	7.88	0.58	0.55
14	0.0274	0.0274	33.40	33.40	1.22	2.33
15	0.0265	0.0256	54.76	54.76	2.07	3.82
16	0.0471	0.0034	23.12	320	6.80	22.34
17	0.0055	0.0055	33.03	33.03	6.01	2.31
18	0.0063	0.0063	25.52	25.52	4.05	1.78
19	0.0123	0.0123	21.95	21.95	1.78	1.53
20	0.0161	0.0161	38.43	38.43	2.39	2.68
21	0.0259	0.0038	16.33	110	4.30	7.68
22	0.0571	0.0047	17.21	210	3.66	14.66
23	0.0509	0.0079	15.24	100	1.93	6.98
24	0.1814	0.0250	12.47	90	0.50	6.28

* Door was open all the way on recovery. Sampling interval 73s.

TABLE B.4 ORIGINAL COUNTING DATA OF THE INTERMITTENT FALLOUT COLLECTOR SAMPLES, STATION G-5

Collector Interval Number	Total Weight Collected	Weight of Sample Counted	Activity of Sample Corrected to H + 1 Hour	Total Interval Activity	Activity Concentration	Percent Activity
	gm	gm	d/m	d/m	d/m/gm	
1	0.0858	0.0140	100.27×10^7	—	7.16×10^{10}	*
2	0.0064	0.0064	44.19	4.42×10^8	6.90×10^{10}	3.54
3	0.0044	0.0044	24.06	2.41	5.47	1.93
4	0.0191	0.0191	70.88	7.09	3.71	5.68
5	0.0063	0.0063	46.81	4.68	7.43	3.75
6	0.0043	0.0043	22.75	2.28	5.29	1.83
7	0.0029	0.0029	22.24	2.22	7.67	1.78
8	0.0055	0.0055	16.33	1.63	2.97	1.31
9	0.0040	0.0040	8.53	8.53	2.13	6.84
10	0.0034	0.0034	35.80	3.58	10.53	2.87
11	0.0009	0.0009	2.11	0.21	2.34	0.17
12	0.0027	0.0027	3.06	0.31	1.13	0.25
13	0.0017	0.0017	2.19	0.22	1.29	0.18
14	0.0217	0.0031	12.69	8.88	4.09	7.12
15	0.0028	0.0028	5.76	0.58	2.06	0.47
16	0.0297	0.0073	7.22	2.94	0.99	2.36
17	0.0044	0.0044	18.08	1.81	4.11	1.45
18	0.0022	0.0022	20.34	2.03	9.25	1.63
19	0.0036	0.0036	11.96	1.20	3.32	0.96
20	0.0944	0.0019	10.43	51.8	5.49	41.53
21	0.0015	0.0015	6.05	0.61	4.03	0.49
22	0.0039	0.0039	36.68	3.67	9.41	2.94
23	0.0146	0.0146	48.12	4.81	3.30	3.86
24	0.0408	0.0408	88.16	8.82	2.16	7.07

* Door was open ¼ inch on recovery. Sampling interval 63s.

[redacted]

TABLE B.5 ORIGINAL COUNTING DATA OF THE INTERMITTENT FALLOUT COLLECTOR SAMPLES, STATION G-7

Collector Interval Number	Total Weight Collected	Weight of Sample Counted *	Activity of Sample Corrected to H + 1 Hour	Total Interval Activity †	Activity Concentration	Percent Activity
	gm	gm	d/m	d/m	d/m/gm	
1	NMW		71.72×10^7		—	3.32
2	NMW		89.49		—	4.14
3	NMW		91.06		—	4.21
4	0.0005		123.01		246.02×10^{10}	5.69
5	0.0006		81.05		135.08	3.75
6	NMW		64.36		—	2.98
7	NMW		12.58		—	0.58
8	NMW		93.91		—	4.35
9	0.0009		96.81		107.57	4.48
10	0.0014		258.48		184.63	11.96
11	0.0012		250.88		209.07	11.61
12	NMW		155.61		—	7.20
13	NMW		63.91		—	2.96
14	0.0009		38.25		42.50	1.77
15	0.0002		14.24		71.20	0.66
16	0.0012		439.99		366.66	20.36
17	0.0008		30.90		38.63	1.43
18	0.0010		23.89		23.89	1.11
19	NMW		17.00		—	0.79
20	0.0012		53.18		44.32	2.46
21	0.0013		1.27		0.98	0.06
22	0.0039		12.17		3.12	0.56
23	0.0094		55.47		5.90	2.57
24	0.0040		21.97		5.49	1.02

NMW, no measurable weight. Sampling intervals 5m 07s.
* Same as total weight.
† Same as activity of sample corrected to H+ 1 hour.

TABLE B.6 ORIGINAL COUNTING DATA OF THE INTERMITTENT FALLOUT COLLECTOR SAMPLES, STATION H-8

Collector Interval Number	Total Weight Collected	Weight of Sample Counted *	Activity of Sample Corrected to H + 1 Hour	Total Interval Activity †	Activity Concentration	Percent Activity
	gm	gm	d/m	d/m	d/m/gm	
1	NMW		66.58×10^7		—	‡
2	0.0018		13.85		7.69×10^{10}	2.47
3	0.0039		51.12		13.11	9.13
4	0.0019		54.40		28.63	9.72
5	0.0013		67.31		51.78	12.02
6	0.0011		39.23		35.66	7.01
7	NMW		66.58		—	11.89
8	0.0016		1.90		1.19	0.34
9	0.0014		4.85		3.46	0.87
10	0.0021		1.82		0.87	0.33
11	0.0017		9.33		5.49	1.67
12	0.0072		3.87		0.54	0.69
13	NMW		2.07		—	0.37
14	0.0014		4.00		2.86	0.71
15	0.0015		2.41		1.61	0.43
16	0.0017		14.66		8.62	2.62
17	0.0011		9.41		8.55	1.68
18	0.0018		20.27		11.26	3.62
19	NMW		24.87		—	4.44
20	0.0019		63.44		33.39	11.33
21	0.0019		18.23		9.59	3.26
22	0.0024		3.51		1.46	0.63
23	0.0027		10.87		4.03	1.94
24	0.0042		71.90		17.12	12.84

NMW, no measurable weight. Sampling interval 4m 51s.
* Same as total weight.
† Same as activity of sample corrected to H + 1 hour.
‡ Door open 1/8-inch on recovery.

TABLE B.7 ORIGINAL COUNTING DATA OF THE INTERMITTENT FALLOUT COLLECTOR SAMPLES, STATION L-1

Collector Interval Number	Total Weight Collected	Weight of Sample Counted	Activity Sample Corrected to H + 1 hour	Total Interval Activity	Activity Concentration	Percent Activity
	gm	gm	d/m	d/m	d/m/gm	
1	71.4	0.0792	95.23×10^{10}	*	*	*
2	0.5	0.0115	17.30	*	*	*
3	0.8	0.0183	25.00	1.09×10^{10}	1.37×10^{10}	1.05
4	0.5	0.0061	19.65	1.61	3.22	1.56
5	1.1	0.0116	26.60	2.52	2.29	2.44
6	2.3	0.0095	20.30	4.91	2.14	4.75
7	9.1	0.0424	122.43	26.28	2.89	25.41
8	8.9	0.0082	15.36	16.68	1.87	16.13
9	9.7	0.0055	15.23	26.86	4.88	25.97
10	7.5	0.0067	8.99	10.06	1.34	9.77
11	2.3	0.0053	16.81	7.29	3.17	7.05
12	0.2	0.0034	7.85	0.46	2.31	0.44
13	0.1923	0.0473	5.53	0.02	0.12	0.02
14	0.3	0.0014	3.89	0.83	2.78	0.80
15	0.3	0.0041	5.78	0.42	1.41	0.41
16	1.2	0.0056	4.85	1.04	0.87	1.01
17	1.5	0.0141	4.14	0.44	0.29	0.42
18	0.1	0.0113	11.74	0.10	1.04	0.10
19	0.1708	0.0657	15.05	0.04	0.23	0.04
20	0.3	0.0167	18.85	0.34	1.13	0.33
21	0.05	0.0119	16.87	0.07	1.42	0.07
22	0.2	0.0085	22.09	0.52	2.60	0.50
23	0.2	0.0082	14.15	0.35	1.73	0.34
24	8.4	0.0269	6.06	1.89	0.23	1.83

* Door was open on recovery. Sampling interval 27s + 5s.

TABLE B.8 TOTAL FALLOUT DATA (G-Leg)

Fraction Size	Activity Corrected to H + 1 Hour	Total Activity Corrected to H + 1 Hour	Percent Total Weight	Percent Total Activity
microns	d/m/gm	d/m		
Station G-1				
0-44	4.61×10^{10}	11.03×10^{10}	0.95	2.6
44-74	3.59	29.57	3.28	6.9
74-105	3.20	21.63	2.70	5.0
105-210	2.62	36.43	5.54	8.4
210-420	3.14	87.77	11.15	20.4
420-840	2.29	125.84	21.87	29.2
> 840	0.87	118.72	54.51	27.5
Station G-3				
0-44	7.53×10^{10}	20.36×10^{10}	1.70	5.7
44-74	3.63	32.93	5.80	9.3
74-105	6.01	39.18	4.08	10.9
105-210	5.26	70.42	8.40	19.6
210-420	5.45	112.06	12.90	31.1
420-840	2.86	60.77	13.30	16.9
> 840	0.28	23.62	53.80	6.6
Station G-5				
0-44	8.37×10^{10}	22.46×10^{10}	6.3	7.6
44-74	7.83	86.19	25.8	29.1
74-105	7.57	43.16	13.4	14.6
105-210	5.39	67.80	29.5	22.9
210-420	6.90	60.20	20.5	20.3
420-840	8.26	14.82	4.2	5.0
> 840	14.28	1.54	0.25	0.5
Station G-7				
0-44	7.46×10^{10}	2.47×10^{10}	6.0	7.1
44-74	10.17	18.09	32.4	24.8
74-105	8.67	9.56	20.0	20.1
105-210	8.00	13.20	30.1	41.3
210-420	8.03	4.95	11.3	6.4
420-840	13.59	0.13	0.2	0.35

TABLE B.9 TOTAL FALLOUT DATA (L-LEG)

Fraction Size	Activity Corrected to H + 1 Hour	Total Activity Corrected to H + 1 Hour	Percent Total Weight	Percent Total Activity
microns	d/m/gm	d/m		
Station L-1				
0-44	3.18×10^{10}	*	0.24	4.7
44-74	3.29	*	3.56	7.5
74-105	2.75	*	10.4	18.3
105-210	3.09	*	11.9	23.6
210-420	2.68	*	11.3	19.4
420-840	1.69	*	14.4	15.7
> 840	0.35	*	48.2	10.7
Station L-3				
0-44	3.92×10^{10}	24.53×10^{10}	21.0	25.9
44-74	3.79	47.01	41.5	49.5
74-105	2.16	17.41	26.9	18.3
105-210	1.93	5.47	9.6	5.8
210-420	1.45	0.41	0.91	0.43
420-840	0.97	0.03	0.09	0.027
> 840	—	—	—	—

* Figures for total activity and total weight are not available due to the fact that the total fallout bag was not received; but in its stead, a bottle of sample which had been scraped off the trailer was used.

TABLE B.10 AIR SAMPLER DATA, (G-3)

Interval Number	Activity Corrected to H + 1 Hour	Percent of Total Activity	Average Sampling Velocity	Volume of Air through Sampler	Activity/ft^3	Percent of Total Activity/ft^3
	10^9 dpm		mph *	ft^3	10^9 dpm/ft^3	
1	9.31	2.52	11.5	1.55	6.01	3.28
2	3.69	1.00	12.2	1.65	2.24	1.22
3	12.57	3.41	13.3	1.80	6.98	3.81
4	13.50	3.66	14.9	2.01	6.72	3.67
5	21.22	5.75	16.4	2.21	9.60	5.24
6	41.52	11.25	14.6	1.97	21.08	11.50
7	44.40	12.03	15.2	2.05	21.66	11.82
8	12.67	3.43	14.5	1.96	6.46	3.52
9	10.19	2.76	13.6	1.84	5.54	3.02
10	14.22	3.85	18.1	2.44	5.83	3.18
11	7.80	2.11	14.5	1.96	3.98	2.17
12	11.33	3.07	13.9	1.88	6.03	3.29
13	14.53	3.94	13.5	1.82	7.98	4.35
14	35.95	9.74	13.3	1.80	19.97	10.89
15	61.19	16.58	16.3	2.20	27.81	15.17
16	54.91	14.88	16.0	2.16	25.42	13.87

* Average sampling velocity was determined from tape recorded data obtained by the isokinetic sampling system as described in Section 2.2.2.
Sampling intervals 50s.

TABLE B.11 AIR SAMPLER DATA (L-3)

Interval Number	Activity Corrected to H + 1 Hour	Percent of Total Activity	Average Sampling Velocity	Volume of Air through Sampler	Activity/ft^3	Percent of Total Activity/ft^3
	dpm		mph*	ft^3		
1	10.19×10^9	2.67	11.5	1.55	6.57×10^9	3.10
2	15.45	4.05	12.2	1.65	9.36	4.41
3	10.02	2.63	13.2	1.78	5.63	2.65
4	9.35	2.45	14.9	2.01	4.65	2.19
5	9.35	2.45	16.4	2.21	4.23	1.99
6	24.21	6.35	14.6	1.97	12.29	5.79
7	16.28	4.27	15.2	2.05	7.94	3.74
8	13.80	3.62	14.5	1.96	7.04	3.32
9	26.99	7.08	13.6	1.84	14.67	6.92
10	43.58	11.43	18.1	2.44	17.86	8.42
11	27.20	7.14	14.5	1.96	13.88	6.54
12	36.06	9.46	13.9	1.88	19.18	9.04
13	21.74	5.70	13.5	1.82	11.95	5.63
14	12.67	3.32	13.3	1.80	7.04	3.32
15	22.46	5.89	16.3	2.20	10.21	4.81
16	6.92	1.82	16.0	2.16	3.20	1.51
17	15.35	4.03	15.8	2.13	7.21	3.40
18	16.48	4.32	9.4	1.27	12.98	6.12
19	12.67	3.32	8.8	1.19	10.65	5.02
20	14.83	3.89	8.9	1.20	12.36	5.83
21	9.40	2.47	8.8	1.19	7.90	3.72
22	6.20	1.63	8.7	1.17	5.30	2.50

* Average sampling velocity was determined from tape recorded data obtained by the isokinetic sampling system as described in Section 2.2.2.
Sampling intervals 50s.

Appendix C
AERIAL SURVEY DATA

To assist in locating the helicopter on aerial survey missions followed the underground detonation, Raydist navigation was employed to determine the 100 mr/hr dose-rate contour.

Instructions for laying out a hyperbolic grid for Raydist baselines at Mercury, Nevada[1], from the data in Table C.1 are as follows.

Layout Raydist baselines on UTM grid with the coordinates of the sites given as follows:

Station	UTM Easting	UTM Northing
North	584,500	4,120,000
East	601,000	4,094,250
Master	584,150	4,087,800

(Station locations taken from AMS Series V796, 1:50,000, charts. Coordinates in Universal Transverse Mercator Grid.)

One baseline runs from the Master Station to the North Station; the other runs from the Master Station to the East Station. The baseline lengths in half-wave lengths at a frequency of 1,746 kc are as follows:

Master - North	372.23 $\lambda/2$
Master - East	209.75 $\lambda/2$

Where $\lambda/2$ = 281.553 feet

Working with one baseline at a time and with convenient equal increments of $\lambda/2$'s, start at the Master Station end of the baseline to inscribe concentric circles using the Master Station as the center. In order to cover the area in use, it will be necessary to draw arcs beyond the end station. Then, using the end station as the center, draw about it concentric circles that are tangent to the Master Station circles at the baseline intersections. These are all construction lines and should be removed before constructing hyperbolas for the second baseline, or drawn on separate tracing paper overlays so that the intersections for one baseline will not be confused with the intersections for the other. The hyperbolas may be faired in with suitable ship's curves by beginning at the baseline and connecting diagonally opposite intersections of the two set of circles.

Repeat the above procedure for the second baseline.

---

[1] At the outset, recognition should be made of the fact that this sort of layout cannot be made for an area in which the Mercator expansion factor makes a plottable difference unless proper adjustment is made in the radial lines.

TABLE C.1 RAYDIST DATA

All readings are 100 mr/hr. 23 March 1955

Point Number	Time, hr	Baseline Readings 1	2	Point Number	Time, hr	Baseline Readings 1	2
1	1513:45	277.25	103.75	32	1547:50	219.10	124.80
2	1515	289.00	104.25	33	1548:05	221.10	124.10
3	1515:30	292.25	104.35	34	1548:16	223.25	123.35
4	1516:18	299.10	105.00	35	1548:37	226.10	122.20
5	1517:15	306.75	106.75	36	1549:17	229.20	119.40
6	1518:30	315.75	110.90	37	1550:05	233.50	118.00
7	1521:50	306.10	121.10	38	1555:35	255.80	119.10
8	1523:20	293.20	124.30	39	1556:10	263.10	118.80
9	1524:40	282.20	127.40	40	1556:50	263.80	114.50
10	1525:35	276.50	139.50	41	1557:15	263.10	112.50
11	1529	259.75	124.60	42	1557:50	267.50	112.50
12	1529:30	255.00	124.90	43	1558:10	270.10	112.20
13	1530:15	248.10	129.30	44	1558:38	274.10	112.25
14	1530:45	247.90	132.50	45	1558:55	276.50	112.10
15	1531:50	238.90	135.50	46	1680:45	274.00	111.10
16	1532:48	227.25	138.25	47	1601:45	265.00	108.00
17	1533:16	216.80	142.50	48	1602:30	268.50	107.40
18	1533:35	211.50	144.50	49	1603:30	257.25	104.25
19	1534:05	200.90	148.50	50	1604:05	271.25	104.10
20	1534:25	194.80	151.25	51	1604:40	274.25	103.75
21	1534:40	190.75	154.00	52	1605:10	278.10	103.90
22	1535:15	182.80	159.25	53	1605:35	280.80	103.90
23	1535:35	178.50	161.50	54	1607:00	290.50	104.50
24	1540	186.10	137.25	55	1607:35	294.10	104.80
25	1540:20	183.25	136.00	56	1607:55	297.20	104.90
26	1543:15	186.25	135.80	57	1608:15	299.80	105.25
27	1543:25	185.50	134.80	58	1608:40	302.40	105.75
28	1544	190.50	132.30	—	—	—	—
29	1544:30	195.50	130.80	—	—	—	—
30	1547:15	213.50	127.25	—	—	—	—
31	1547:37	217.10	125.75	—	—	—	—

TABLE C.2 RAYDIST DATA

All readings are 100 mr/hr except No. 32, 150 mr; No. 52, 40 mr; and No. 53, 15 mr. 24 March 1955.

Point Number	Time hr	Baseline Readings 1	2	Point Number	Time, hr	Baseline Readings 1	2
1	1016:20	280.90	104.20	27	1026.13	299.95	122.55
2	1061:30	282.60	104.05	28	1026:35	297.15	123.25
3	1016:57	284.55	103.70	29	1027:15	288.90	123.50
4	1017:33	288.85	104.30	30	1028:00	278.50	122.80
5	1017:43	290.40	104.40	31	1028:36	281.55	120.65
6	1018:05	293.85	104.80	32	1029:27	270.95	117.35
7	1018:30	296.60	105.05	33	1031:12	263.65	114.85
8	1018:42	298.50	105.35	34	1031:42	266.70	113.30
9	1018:55	300.30	105.55	35	1032:00	267.50	112.35
10	1019:20	303.60	106.40	36	1032:59	277.65	112.80
11	1019:40	305.95	107.10	37	1033:06	278.25	112.45
12	1019:58	308.30	107.80	38	1033:20	279.50	111.95
13	1020:20	310.35	109.00	39	1035:37	271.50	105.40
14	1020:45	313.05	110.05	40	1035:54	273.75	105.55
15	1021:05	314.15	111.00	41	1036:07	275.95	105.55
16	1021:30	315.05	111.70	42	1036:58	279.65	103.95
17	1021:50	314.85	112.40	43	1037:23	283.25	104.00
18	1022:20	315.55	113.75	44	1038:05	287.30	104.10
19	1022:30	315.15	114.45	45	1038:10	288.35	104.15
20	1023:15	314.00	115.85	46	1038:30	291.60	104.65
21	1023:35	312.35	116.55	47	1038:38	293.05	104.65
22	1023:52	311.45	117.25	48	1038:57	295.35	105.00
23	1024:15	310.15	118.20	49	1043:45	280.95	120.25
24	1024:47	309.90	119.50	50	1044:00	278.75	118.95
25	1025:15	308.15	120.45	51	1046:55	246.15	115.60
26	1025:55	302.60	121.65	52	1049:00	241.15	118.80
				53	1059:10	234.05	114.30

[redacted]

Appendix D
GROUND SURVEY DATA

Appendix D contains radiation-intensity data obtained by various organizations performing ground surveys following the underground detonation at Operation Teapot. Calibrated gamma-intensity measuring instruments (T1B, Victoreen, Jordan) were used on these surveys. The experimental average gamma decay slope of -1.18 is so close to the normal -1.2 fission decay exponent that it served as a basis for using the -1.2 decay for correcting survey data in order to plot and draw the dose-rate contours at H + 1 hour. Details on the surveys conducted are presented in Section 2.4.

Data are presented in sections under the organizations who had performed the surveys.

Refer to Figure A.2 for ground location of station numbers as used in Tables D.1, D.2, D.3, and D.7.

Ground locations for station numbers in Table D.4 are shown in Figure 3.1. The first digit of these numbers indicates a stake line or direction from ground zero. The remaining digits indicate the approximate distance in hundreds of yards from ground zero. Reference North for these stake lines is the 900-series stake line.

TABLE D.1 PROJECT 2.5.1 SURVEY DATA

Station Location	Time of Survey		Time after Shot	Radiation Intensity	Corrected to H + 1 Hour
	hour	date	hour and minute	r/hr	r/hr
A-3	1145	4 April		0.1	92
A-2	1020	28 March		2.4	—
	1145	4 April		0.38	350
A-1	1020	28 March		4.5	—
	1250	28 March		7.0	—
	1145	4 April		0.8	730
B-3	1145	4 April		0.22	200
B-2	1020	28 March		2.9	—
	1145	4 April		0.385	340
B-1	1020	28 March		6.8	—
	1251	28 March		8.5	—
	1145	4 April		1.2	1060
C-3	1145	4 April		0.24	220
C-2	1020	28 March		2.6	—
	1145	4 April		0.6	550
C-1	1020	28 March		6.5	—
	1251	28 March		7.0	—
	1145	4 April		0.95	760
D-3	1155	4 April		0.22	200
D-2	1155	4 April		0.35	320
D-1	1252	28 March		9	—
	1155	4 April		0.1	920
E-8	1800	23 March	5:30	0.02	0.15

TABLE D.1 CONTINUED

Station Location	Time of Survey		Time after Shot	Radiation Intensity	Corrected to H + 1 Hour
	hour	date	hour and minute	r/hr	r/hr
E-7	1745	23 March	5:25	0.06	0.44
E-5	1300	24 March		1.05	—
E-3	1200	30 March		5	—
	1155	4 April		0.3	265
E-2	1155	4 April		0.7	620
E-1	1253	28 March		10	—
	1200	30 March		9	—
	1155	4 April		1.6	1450
F-11	1620	23 March	3:48	0.008	0.04
F-8	1650	23 March	4:30	0.7	4
F-7	1730	23 March		1.1	7.6
	1305	1 April		0.015	—
F-3	1155	4 April		0.51	465
F-2	1155	4 April		1.2	1080
F-1	1254	28 March		14.0	—
	1155	4 April		1.9	1550
G-8	1705	23 March	4:35	0.8	4.6
G-7	1720	23 March	4:48	1.1	7.2
	1250	1 April		0.94	—
G-3	1240	1 April		1.1	—
	1155	4 April		0.93	840
G-2	1155	4 April		2.1	1920
G-1	1254	28 March		13.0	—
	1200	30 March		8.0	—
	1155	4 April		2.3	2100
H-8	1345	24 March		0.36	—
H-7	1400	24 March		0.17	—
H-3	1155	4 April		1.3	1170
H-2	1155	4 April		2.65	2450
H-1	1255	28 March		13.0	—
	1155	4 April		3.2	2900
I-3	1155	4 April		0.6	550
I-2	1155	4 April		1.6	1450
I-1	1257	28 March		11.0	1730
	1155	4 April		1.9	—
J-3	1155	4 April		0.12	108
J-2	1155	4 April		0.47	430
J-1	1258	28 March		7.0	—
	1155	4 April		1.3	1160
K-3	1155	4 April		0.14	127
K-2	1155	4 April		0.35	230

[redacted]

TABLE D.1 CONTINUED

Station Location	Time of Survey		Time after Shot	Radiation Intensity	Corrected to H + 1 Hour
	hour	date	hour and minute	r/hr	r/hr
K-1	1259	28 March		6.5	—
	1155	4 April		1.1	1000
L-7	1220	1 April		0.007	—
L-5	1900	23 March	6:30	0.04	0.4
L-3	1715	23 March	4:45	10.0	65.0
	1020	28 March		0.39	—
	1230	1 April		0.12	—
	1100	4 April		0.03	—
L-2	1020	28 March		1.4	—
	1100	4 April		0.38	350
L-1	1020	28 March		3.4	—
	1300	28 March		3.4	—
	1100	4 April		0.8	700
M-3	1100	4 April		0.13	112
M-2	1020	28 March		1.5	—
	1100	4 April		0.29	250
M-1	1020	28 March		3.4	—
	1301	28 March		3.2	—
	1100	4 April		0.62	560
N-3	1100	4 April		0.13	113
N-2	1020	28 March		2.3	—
	1100	4 April		0.4	360
N-1	1020	28 March		4.2	—
	1302	28 March		4.2	—
	1100	4 April		0.85	760
O-3	1242	28 March		0.024	—
	1100	4 April		0.008	—
O-2	1020	28 March		1.0	—
	1243	28 March		0.9	—
	1100	4 April		0.16	150
O-1	1020	28 March		2.2	—
	1244	28 March		2.1	—
	1100	4 April		0.46	420
P-3	1100	4 April		0.006	—
P-2	1020	28 March		1.3	—
	1100	4 April		0.23	210
P-1	1020	28 March		2.9	—
	1100	4 April		0.42	390
Q-3	1100	4 April		0.006	—
Q-2	1020	28 March		0.4	—
	1100	4 April		0.06	55
Q-1	1020	28 March		2.4	—
	1247	28 March		2.1	—
	1100	4 April		0.35	325
R-3	1100	4 April		0.006	—
R-2	1020	28 March		0.5	—
	1100	4 April		0.08	74
R-1	1020	28 March		1.7	—
	1248	28 March		1.6	—
	1100	4 April		0.29	260

TABLE D.2 DESERT ROCK SURVEY DATA

Station Location	Time of Survey		Time after Shot	Radiation Intensity	Corrected to H + 1 Hour	Average of Good Points
	hour	date	hour and minute	r/hr	r/hr	r/hr
A-6	1609	23 March	3:39	0.005	0.024	0
A-5	1540	23 March	3:10	0.014	0.05	—
	1220	24 March	23:50	0.005	0.20	—
A-4	1216	24 March	23:46	0.04	1.75	—
	1120	25 March	46:50	0.015	1.47	1.6
A-3	1123	25 March	46:53	0.75	76.5	—
	1031	26 March	70:01	1.0	170	—
	0642	27 March	90:12	0.7	160	165
A-2	1030	26 March	70:00	4.5	760	—
	0644	27 March	90:14	2.9	660	—
	1030	28 March	118:00	2.4	760	723
A-1	1030	28 March	118:00	4.5	1,400	—
	1250	28 March	120:20	7.0	2,250	1,825
B-6	1602	23 March	3:32	0.001	0.004	—
B-5	1544	23 March	3:14	0.07	0.29	—
	1223	24 March	23:53	0.008	0.34	0.6
B-4	1226	24 March	23:56	3.15	142	—
	1125	25 March	46:55	1.200	123	—
	1035	26 March	70:05	0.900	152	—
	0648	27 March	90:18	0.65	146	141
B-3	1032	26 March	70:02	1.85	310	—
	0645	27 March	90:15	1.200	270	290
B-2	1030	28 March	118:00	2.85	900	900
B-1	1030	28 March	118:00	6.750	2,200	—
	1251	28 March	120:21	8.500	2,730	2,465
C-6	1556	23 March	3:26	0.046	205	—
	1236	24 March	24:06	0.005	230	0.22
C-5	1550	23 March	3:20	1.000	4.200	—
	1231	24 March	24:01	0.090	4.120	—
	1132	25 March	47:02	0.036	3.700	—
	1040	26 March	70:10	0.029	4.800	—
	0653	27 March	90:23	0.022	4.9000	4.3
C-4	1129	25 March	46:59	1.050	108	—
	1037	26 March	70:07	0.950	160	—
	0650	27 March	90:20	0.600	135	134
C-2	1030	28 March	118:	2.500	780	780
C-1	1030	28 March	118:	6.500	2,050	—
	1251	28 March	118:	7.000	2,200	2,125
D-13	1535	23 March	3:05	0.0001	0.0004	—
D-12	1545	23 March	3:15	0.0002	0.0008	—
D-11	1550	23 March	3:20	0.0004	0.002	—
D-10	1600	23 March	4:00	0.0012	0.007	—
D-9	1605	23 March	4:05	0.001	0.006	—

[redacted]

TABLE D.2 DESERT ROCK SURVEY DATA CONTINUED

Station Location	Time of Survey		Time after Shot	Radiation Intensity	Corrected to H + 1 Hour	Average of Good Points
	hour	date	hour and minute	r/hr	r/hr	r/hr
D-8	1610	23 March	4:10	0.001	0.006	—
D-7	1615	23 March	4:15	0.001	0.006	—
D-6	1622	23 March	4:22	0.020	0.117	—
D-6	1100	24 March	22:30	0.002	0.085	0.1
D-5	1105	24 March	22:35	0.455	19.2	—
	1000	25 March	46:30	0.200	20.3	—
	0945	26 March	68:15	0.130	21.2	—
	0535	27 March	89:05	0.095	21.2	20.5
D-4	1113	24 March	22:43	2.500	107	—
	1005	25 March	46:35	0.900	100	—
	0949	26 March	68:19	0.750	120	—
	0539	27 March	89:09	0.445	100	107
D-3	1120	24 March	22:50	6.000	260	—
	1009	25 March	46:39	2.350	240	—
	0952	26 March	68:22	1.800	295	—
	0542	27 March	89:12	1.450	325	280
D-2	1128	24 March	22:58	11.5	500	—
	1012	25 March	46:42	5.5	560	—
	0954	26 March	68:24	3.7	600	—
	0545	27 March	89:15	3.0	670	556
D-1	1015	25 March	46:45	17.0	1,750	—
	0958	26 March	68:28	13.5	2,150	—
	0547	27 March	89:17	9.5	2,100	—
	1252	28 March	120:22	9.0	2,900	2,225
E-13	1522	23 March	2:52	0.002	0.006	—
E-12	1603	23 March	3:33	0.0008	0.007	—
E-11	1635	23 March	4:05	0.003	0.014	—
E-10	1658	23 March	4:28	0.004	0.022	—
	1125	24 March	22:55	0.003	0.104	—
E-9	1140	24 March	23:10	0.003	0.122	—
E-8	1150	24 March	23:20	0.004	0.150	—
E-7	1200	24 March	23:30	0.037	1.650	—
	1039	25 March	46:09	0.003	0.240	—
E-6	1048	25 March	46:18	0.287	28.800	—
	1205	24 March	23:35	0.600	26.800	—
	1045	26 March	70:15	0.165	27.500	—
	0640	27 March	90:10	0.120	27.100	27.6
E-5	1215	24 March	23:45	1.300	58.	—
	1053	25 March	46:23	0.800	80.	—
	1047	26 March	70:17	0.395	67.	—
	0643	27 March	90:13	0.240	74.	70
E-4	1220	24 March	23:50	3.600	162	—
	1058	25 March	46:28	1.975	198.000	—
	1049	26 March	70:19	1.050	177.000	—
	0647	27 March	90:17	0.700	158.000	174

TABLE D.2 DESERT ROCK SURVEY DATA CONTINUED

Station Location	Time of Survey		Time after Shot	Radiation Intensity	Corrected to H + 1 Hour	Average of Good Points
	hour	date	hours and minute	r/hr	r/hr	r/hr
E-3	1102	25 March	46:32	4.250	430.	—
	1051	26 March	70:21	2.875	480.	—
	0650	27 March	90:20	1.850	420.	443
E-2	1105	25 March	46:35	12.100	1,230	—
	1053	26 March	70:23	8.500	1,420	—
	0650	27 March	90:20	5.500	1,240	1,263
E-1	1253	28 March	120:23	10	3,200	3,200
F-13	1545	23 March	3:15	0.0008	0.003	—
F-12	1620	23 March	3:50	0.0012	0.006	—
F-11	1640	23 March	4:10	0.0004	0.002	—
F-10	1150	24 March	23:20	0.0008	0.004	—
F-9	1210	24 March	23:40	0.0015	0.007	—
F-8	1215	24 March	23:45	0.040	1.800	—
	1040	25 March	46:10	0.026	2.600	—
	1145	26 March	71:15	0.015	2.600	2.3
F-7	1223	24 March	23:53	0.112	5.100	—
	1050	25 March	46:20	0.075	7.600	—
	1152	26 March	71:22	0.040	6.900	—
	0545	27 March	89:15	0.032	7.200	6.7
F-6	1227	24 March	23:57	0.180	8.200	—
	1055	25 March	46:25	0.100	10.00	—
	1154	26 March	71:24	0.060	10.200	—
	0550	27 March	89:20	0.040	9.100	9.4
F-5	1233	24 March	24:03	0.335	15.2	—
	1100	25 March	46:30	0.210	21.	—
	1158	26 March	71:28	0.100	16.8	—
	0555	27 March	89:25	0.087	19.6	17.9
F-4	1237	24 March	24:07	2.300	106.	—
	1102	25 March	46:32	1.300	132.	—
	1200	26 March	71:30	0.700	120.	—
	0557	27 March	89:27	0.495	112.	118
F-3	1242	24 March	24:12	5.5	252.	—
	1205	25 March	47:35	7.9	800.	—
	1202	26 March	71:32	4.0	690.	—
	0600	27 March	89:30	3.55	800.	636
F-2	1207	25 March	47:37	15.	1,570	—
	1205	26 March	71:35	12.	2,000	—
	0602	27 March	89:32	10.	2,250	1,940
F-1	1254	28 March	120:24	14.	4,500	4,500
G-13	1130	24 March	23:00	0.002	0.087	—
G-12	1150	24 March	23:20	0.008	0.355	—
G-11	1205	24 March	23:35	0.023	1.030	—
	1040	25 March	46:10	0.011	1.120	—
G-10	1220	24 March	23:50	0.036	1.620	—
	1055	25 March	46:25	0.016	1.620	—

[redacted]

TABLE D.2 DESERT ROCK SURVEY DATA CONTINUED

Station Location	Time of Survey		Time after Shot	Radiation Intensity	Corrected to H + 1 Hour	Average of Good Points
	hour	date	hour and minute	r/hr	r/hr	r/hr
G-9	1240	24 March	24:10	0.045	2.080	—
	1110	25 March	46:40	0.027	2.750	—
	1000	26 March	69:30	0.030	5.100	—
	0540	27 March	89:10	0.020	4.500	3.4
G-8	1250	24 March	24:20	0.060	2.800	—
	1120	25 March	46:50	0.042	4.280	—
	1010	26 March	69:40	0.070	11.600	—
	0550	27 March	89:20	0.026	5.800	6.2
G-7	1300	24 March	24:30	0.950	44.5	—
	1140	25 March	47:10	0.340	35.	—
	1020	26 March	69:50	0.215	36.5	—
	0605	27 March	89:35	0.240	54.5	42.6
G-6	1310	24 March	24:40	1.900	90.	—
	1145	25 March	47:15	0.900	90.	—
	1025	26 March	69:55	0.460	78.	—
	0615	27 March	89:45	0.420	93.	87.8
G-5	1315	24 March	24:45	3.600	170.	—
	1150	25 March	47:20	1.900	192.	—
	1030	26 March	70:00	1.050	178.	—
	0618	27 March	89:48	0.900	200.	185
G-4	1151	25 March	47:21	4.400	455.	—
	1034	26 March	70:04	3.450	575.	—
	0620	27 March	89:50	2.600	590.	540
G-3	1152	25 March	47:32	9.900	1,000	—
	1033	26 March	70:03	5.000	860	—
	0622	27 March	89:52	6.000	1,320	1,060
G-2	0624	27 March	89:54	9.000	2,000	2,000
G-1	1254	28 March	120:24	13.	4,150	4,150
H-13	1515	23 March	2:45	0.950	3.20	—
	1110	24 March	22:40	0.048	2.05	—
	1030	25 March	46:00	0.027	2.70	—
	1000	26 March	69:30	0.018	3.08	2.8
H-12	1120	24 March	22:50	0.042	1.8	—
	1040	25 March	46:10	0.025	2.5	—
	1035	26 March	70:05	0.010	1.7	2.0
H-11	1156	24 March	23:26	0.040	1.77	—
	1100	25 March	46:30	0.016	1.62	—
	1100	26 March	70:30	0.010	1.72	1.7
H-10	1210	24 March	23:40	0.080	3.55	—
	1100	25 March	46:40	0.033	3.35	—
	1120	26 March	70:50	0.019	3.28	3.4
H-9	1220	24 March	23:50	0.150	6.8	—
	1120	25 March	46:50	0.080	8.0	—
	1130	26 March	71:00	0.036	6.2	—
	0535	27 March	89:05	0.0395	8.8	7.5

TABLE D.2 DESERT ROCK SURVEY DATA CONTINUED

Station Location	Time of Survey		Time after Shot	Radiation Intensity	Corrected to H + 1 Hour	Average of Good Points
	hour	date	hour and minute	r/hr	r/hr	r/hr
H-8	1232	24 March	24:02	0.400	18.4	—
	1130	25 March	47:00	0.225	23.0	—
	1140	26 March	71:10	0.113	19.4	—
	0555	27 March	89:25	0.100	22.2	20.8
H-7	1240	24 March	24:10	0.260	11.8	—
	1137	25 March	47:07	0.135	14.0	—
	1155	26 March	71:25	0.068	11.7	—
	0600	27 March	89:30	0.070	15.6	13.3
H-6	1243	24 March	24:13	0.460	21.0	—
H-6	1140	25 March	47:10	0.220	23.0	—
H-6	1200	26 March	71:30	0.113	19.5	—
H-6	0605	27 March	89:35	0.110	24.2	21.9
H-5	1246	24 March	24:16	3.000	138	—
	1145	25 March	47:15	1.100	114	—
	1205	26 March	71:35	0.600	103	—
	0610	27 March	89:40	0.900	200	139
H-4	1147	25 March	47:17	11.500	1,200	—
	1209	26 March	71:39	3.200	550	—
	0612	27 March	89:42	3.050	680	810
H-3	1150	25 March	47:20	12.500	1,300	—
	1211	26 March	71:41	7.500	1,300	—
	0613	27 March	89:43	8.000	1,780	1,460
H-2	0615	27 March	89:45	12.	2,660	2,660
H-1	0616	27 March	89:46	20.	4,500	—
	1255	28 March	120:25	13.	4,150	4,325
I-13	1435	23 March	2:05	0.0002	0.0005	—
I-12	1450	23 March	2:20	0.004	0.012	—
I-11	1455	23 March	2:25	0.046	0.133	—
I-11	1055	24 March	22:25	0.003	0.135	—
I-10	1510	23 March	2:40	0.100	0.325	—
I-10	1110	24 March	22:40	0.008	0.345	—
I-9	1518	23 March	2:48	0.310	1.070	—
I-9	1120	24 March	22:50	0.023	0.980	—
I-9	1017	25 March	45:47	0.015	1.200	1.1
I-8	1523	23 March	2:53	0.315	1.120	—
I-8	1125	24 March	22:55	0.031	1.34	—
I-8	1021	25 March	45:51	0.015	1.480	1.3
I-7	1528	23 March	2:58	0.800	3.000	—
I-7	1130	24 March	23:00	0.090	3.900	—
I-7	1025	25 March	45:55	0.030	3.000	—
I-7	0945	26 March	69:15	0.019	3.250	3.3
I-6	1538	23 March	3:08	3.150	12.	—

TABLE D.2 DESERT ROCK SURVEY DATA - CONTINUED

Station Location	Time of Survey		Time after Shot	Radiation Intensity	Corrected to H + 1 Hour	Average of Good Points
	hour	date	hour after Shot	r/hr	r/hr	r/hr
I-6	1137	24 March	23:07	0.310	13.5	—
I-6	1027	25 March	45:57	0.100	10.0	—
I-6	0950	26 March	69:20	0.120	20.5	—
I-6	0555	27 March	89:25	0.0595	13.2	13.8
I-5	1143	24 March	23:13	0.800	35.	—
I-5	1030	25 March	46:00	0.370	37.	—
I-5	0955	26 March	69:25	0.300	51.	—
I-5	0600	27 March	89:30	0.201	45.	42.8
I-4	1145	24 March	23:15	3.300	143.	—
I-4	1032	25 March	46:02	1.700	170	—
I-4	1000	26 March	69:30	1.250	208.	—
I-4	0603	27 March	89:33	0.600	133	163.5
I-3	1033	25 March	46:03	8.000	800.	—
I-3	1005	26 March	69:35	4.200	700.	—
I-3	0607	27 March	89:37	2.750	620	707
I-2	1003	26 March	69:33	7.000	1,200	—
I-2	0609	27 March	89:39	8.000	1,750	1,475
I-1	1257	28 March	120:27	11.000	3,500	3,500
J-6	1710	23 March	4:40	1.800	11.7	—
	1100	24 March	22:30	0.240	10.0	—
	1027	25 March	45:57	0.085	8.5	—
	0940	26 March	69:10	0.085	14.5	—
	0550	27 March	89:20	0.048	10.7	11.1
J-5	1705	23 March	4:35	3.750	23.5	—
	1105	24 March	22:35	0.500	21.2	—
	1032	25 March	46:02	0.190	19.0	—
	0945	26 March	69:15	0.132	22.8	—
	0555	27 March	89:25	0.115	25.2	22.3
J-4	0948	26 March	69:18	0.430	74.0	—
	0558	27 March	89:28	0.300	67.	71
J-1	1258	28 March	120:28	7.000	2,220	2,200
K-6	1111	24 March	22:41	0.020	0.850	—
	1040	25 March	46:10	0.0075	0.760	0.8
K-5	1658	23 March	4:28	3.400	20.5	—
	1109	24 March	22:39	0.485	20.5	—
	1036	25 March	46:06	0.180	18.0	—
	0953	26 March	69:23	0.150	25.8	—
	0602	27 March	89:32	0.105	23.0	21.6
K-4	0950	26 March	69:20	0.455	78.	—
	0605	27 March	89:35	0.325	72.	75.0
K-3	0606	27 March	89:36	0.700	155.	155.0
L-6	1115	24 March	22:45	0.002	0.08	—

TABLE D.2 DESERT ROCK SURVEY DATA CONTINUED

Station Location	Time of Survey		Time After Shot	Radiation Intensity	Corrected to H + 1 Hour	Average of Good Points
	hour	date	hour and minute	r/hr	r/hr	r/hr
L-5	1653	23 March	4:23	0.060	0.360	—
	1120	24 March	22:50	0.007	0.280	—
	1043	25 March	46:13	0.003	0.310	0.3
L-4	1124	24 March	22:54	2.200	95.	—
	1048	25 March	46:18	0.800	80.	—
	0957	26 March	69:27	0.650	108	—
	0610	27 March	89:40	0.490	112.	98.8
L-3	1000	26 March	69:30	0.675	113.	—
	0609	27 March	89:39	0.405	92.	—
	1040	28 March	120:	0.390	124.	109.7
L-2	1030	28 March	120:	1.400	450	450.
L-1		28 March	120:	3.350	1,070	—
	1300	28 March	120:30	3.400	1,080	1,075
M-6	1513	23 March	2:43	0.0005	0.002	0.002
M-5	1518	23 March	2:48	0.025	0.086	—
	1129	24 March	22:59	0.004	0.173	0.13
M-4	1133	24 March	23:03	0.100	4.35	—
	1050	25 March	46:20	0.035	3.5	—
	1005	26 March	69:35	0.031	5.3	—
	0614	27 March	89:44	0.255	5.6	4.7
M-3	1136	24 March	23:06	4.050	176	—
	1052	25 March	46:22	1.200	120	—
	1003	26 March	69:33	1.425	245	—
	0616	27 March	89:46	0.800	177	180
M-2		28 March	120:	1.450	470	470
M-1		28 March	120:	3.200	1,050	—
	1301	28 March	120:31	3.200	1,060	1,055
N-6	1642	23 March	4:12	0.003	0.002	—
N-5	1522	23 March	2:51	0.012	0.040	0.04
N-4	1140	24 March	23:10	0.032	1.370	—
	1057	25 March	46:27	0.010	1.000	1.2
N-3	1146	24 March	23:16	3.775	162.	—
	1055	25 March	46:25	1.400	140.	—
	1008	26 March	69:38	1.050	180.	—
	0619	27 March	89:49	0.800	180.	166
N-2	1010	26 March	69:40	4.1	700.	—
	0620	27 March	89:50	2.7	620.	660
O-6	1637	23 March	4:07	0.0002	0.002	—
O-5	1524	23 March	2:54	0.009	0.033	0.03
O-4	1155	24 March	23:25	0.014	0.610	0.6
O-3	1149	24 March	23:19	0.175	7.5	—
	1242	28 March	120:12	0.024	7.5	—
	1100	25 March	46:30	0.057	5.8	—
	1015	26 March	69:45	0.038	6.5	—
	0623	27 March	89:55	0.0295	6.5	6.8

[redacted]

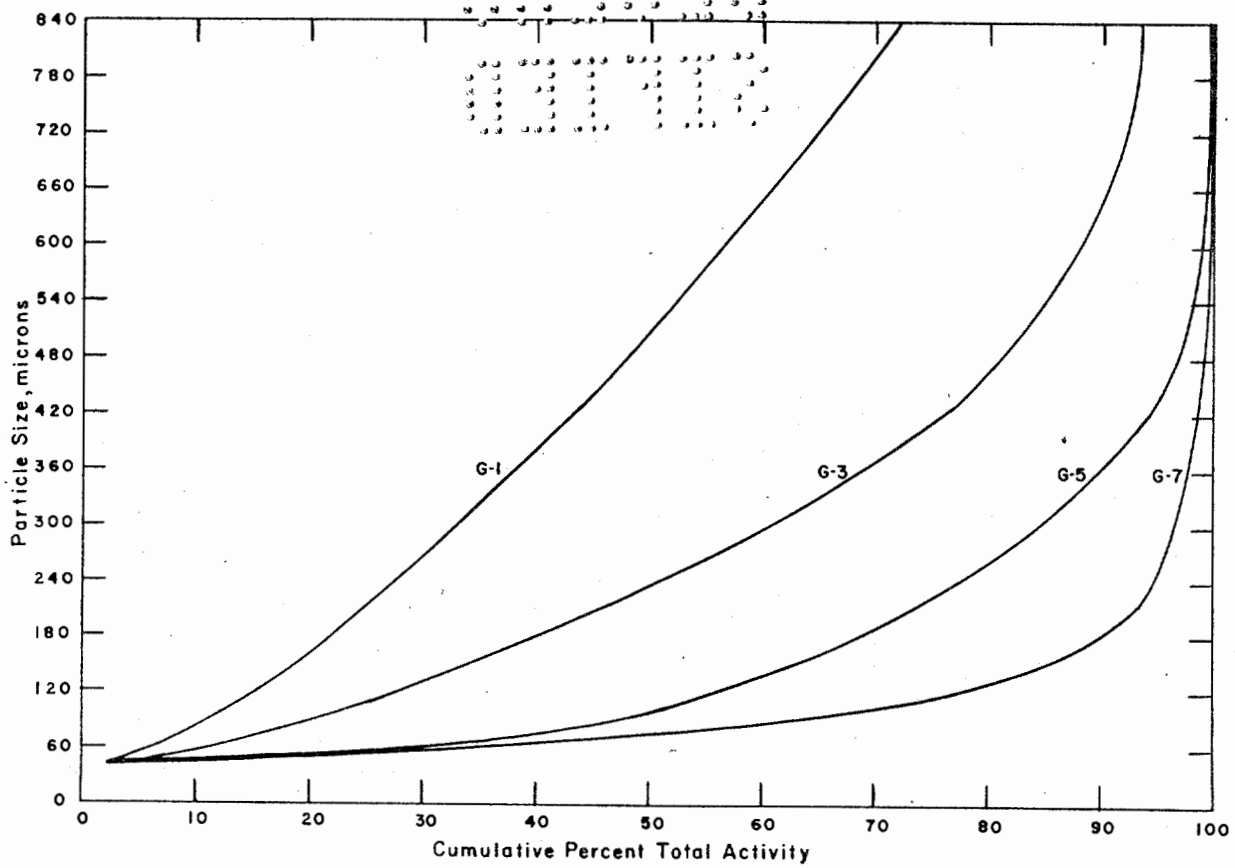

Figure 3.23 Particle size versus cumulative percent total activity downwind.

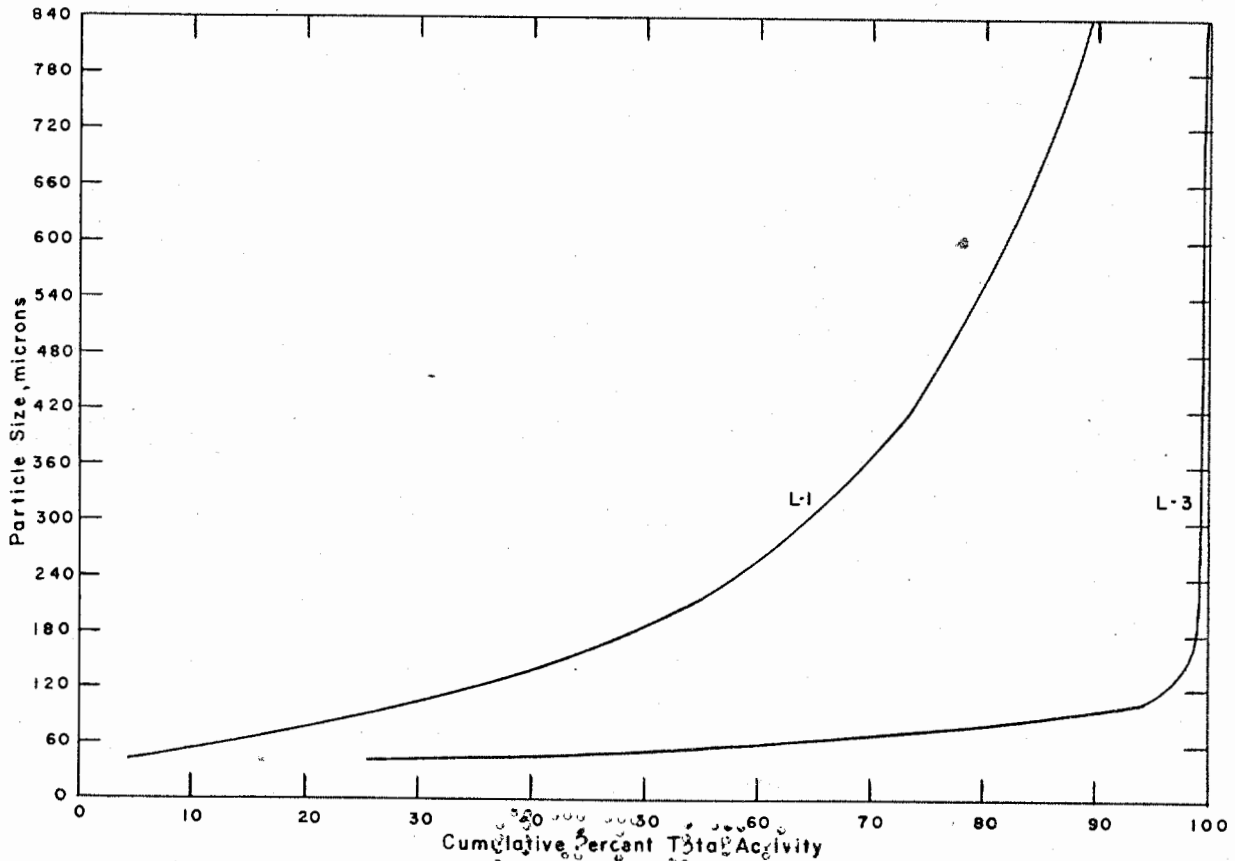

Figure 3.24 Particle size versus cumulative percent total activity crosswind.

TABLE D.2 DESERT ROCK SURVEY DATA CONTINUED

Station Location	Time of Survey		Time after Shot	Radiation Intensity	Corrected to H+ 1 Hour	Average of Good Points
	hour	date	hour and minute	r/hr	r/hr	r/hr
O-2	1150	24 March	23:20	+ 5.0	210	—
	1101	25 March	46:31	1.85	185.	—
	1012	26 March	69:32	1.55	265.	—
	0625	27 March	89:55	1.0	220	—
		28 March	120:	0.95	300	—
	1243	28 March	120:13	0.9	290	245
O-1		28 March	120:	2.2	700	—
	1244	28 March	120:14	2.1	670	695
P-6	1631	23 March	4:01	0.0002	0.001	—
P-5	1526	24 March	3:56	0.006	0.029	0.03
P-4	1159	24 March	23:29	0.009	0.400	0.4
P-3	1201	24 March	23:31	0.105	4.7	—
	1105	25 March	46:35	0.038	3.85	—
	1017	26 March	69:47	0.025	4.2	—
	0630	27 March	90:00	0.020	4.4	4.3
P-2	1204	24 March	23:34	8.0	350	—
	1107	25 March	46:37	2.7	275	—
	1018	26 March	69:48	2.15	370	—
	0629	27 March	89:59	1.45	320	—
		28 March	120:	1.25	400	343
P-1	0627	27 March	89:57	3.6	810	—
		28 March	120:	2.9	900	855
Q-6	1624	23 March	3:54	0.0004	0.0002	0.002
Q-5	1531	23 March	3:01	0.005	0.018	0.02
Q-4	1210	24 March	23:40	0.011	0.480	0.5
Q-5	1207	24 March	23:37	0.100	4.4	—
	1110	25 March	46:40	0.032	3.2	—
	1023	26 March	69:53	0.020	3.4	3.7
Q-2	1115	25 March	46:45	1.000	100	—
	1020	26 March	69:50	0.775	133	—
	0635	27 March	90:05	0.500	112	—
		28 March	120:	0.380	120	116.3
Q-1	0628	27 March	89:58	2.775	620	—
		28 March	120:	2.400	760	—
	1247	28 March	120:17	2.100	670	663
R-6	1614	23 March	3:44	0.0004	0.002	0.002
R-5	1536	23 March	3:06	0.006	0.023	0.02
R-4	1213	24 March	23:43	0.015	0.670	0.7
R-3	1118	25 March	46:48	0.046	4.6	—
	1025	26 March	69:55	0.030	5.1	—
	0639	27 March	90:09	0.023	5.1	4.9
R-2	1112	25 March	46:42	0.950	95.	—
	1028	26 March	69:58	1.000	170.	—
	0637	27 March	90:07	0.650	145.	—
		28 March	120:	0.500	157.	141
R-1		28 March	120:	1.65	520	—
	1248	28 March	120:18	1.6	510	515

TABLE D.3 NRDL SURVEY DATA

Station Location	Time of Survey		Radiation Intensity	Corrected to H + 1 Hour
	hour	date	r/hr	r/hr
A-1	1240	28 March	46	1,460
A-2	1224	26 March	4.1	700
A-3	1300	25 March	1.6	78
A-4	1427	24 March	0.032	1.6
A-5	1445	24 March	0.0004	0.21
A-6	1450	24 March	0	0
B-1	1245	28 March	8.2	2,600
B-2	1310	25 March	8.0	840
B-3	1231	26 March	1.75	300
B-4	1515	24 March	0.600	31.2
B-5	1510	24 March	0.003	0.16
B-6	1500	24 March	0	0
C-1	1327	28 March	4.5	1,430
C-2	1230	26 March	4.5	765
	1325	28 March	2.8	888
C-3	1320	25 March	2.8	300
C-4	1400	30 March	0.255	—
C-5	1525	24 March	0.06	6.7
C-6	1530	24 March	0.0004	0.021
D-1	1330	28 March	6.5	2,060
D-2	1255	26 March	2.95	508
D-3	1249	26 March	1.65	282
D-4	1244	26 March	0.600	103
D-5	1530	24 March	0.380	20.5
D-6	1530	24 March	0.0006	0.032
D-7	1500	24 March	0.0006	0.031
D-8	1500	24 March	0.0007	0.036
D-8	1400	24 March	0.0008	0.039
D-10	1345	24 March	0.0007	0.034
D-11	1520	30 March	0.003	—
D-12	1455	30 March	0.003	—
D-13	1440	30 March	0.002	—
E-1	1335	28 March	6.5	2,060
E-2	1258	26 March	6.0	1,030
E-3	1302	26 March	2.35	404
E-4	1314	26 March	0.8	138
E-5	1322	26 March	0.235	407
	1600	24 March	10.0	570
	1636	30 March	0.07	—
E-6	1300	24 March	0.600	28
E-7	1250	24 March	0.005	0.23
E-8	1618	30 March	0.007	—
	1315	24 March	0.001	0.056
E-9	1130	24 March	0.0008	0.023
E-10	1412	30 March	0.008	—
E-11	1405	30 March	0.007	—
E-12	1345	30 March	0.029	—
E-13	1320	30 March	0.030	—
F-1	1435	28 March	11.	3,490
F-2	1420	28 March	9.	2,850
F-3	1230	26 March	6.	1,020
F-4	1500	25 March	1.	110
F-5	1410	30 March	0.060	—
	1400	25 March	0.180	19.5
F-6	1330	25 March	0.085	9.3
F-7	1323	25 March	0.065	7.0
F-8	1130	25 March	0.030	3.0
F-9	1352	30 March	0.016	
F-10	—	—	—	—
F-11	1430	30 March	0.048	—
F-12	1248	30 March	0.018	—
F-13	1215	30 March	0.010	—
G-1	1417	28 March	14	4,440
G-2	1415	28 March	8	2,700
G-3	1410	28 March	3	1,015
G-4	1420	28 March	2.0	—
	1232	26 March	4.0	680.
G-5	1500	25 March	1.7	187
G-6	1400	25 March	0.800	86
G-7	1330	25 March	0.360	39
G-8	1300	25 March	0.044	4.6
G-9	1230	25 March	0.027	2.8
G-10	1200	25 March	0.016	1.6
G-11	1345	26 March	0.012	2.1
G-12	1400	26 March	0.008	1.4
G-13	1415	26 March	0.001	0.21
H-1	1320	26 March	24	4,160
	1413	28 March	12	3,810
H-2	1430	28 March	12	3,810
H-3	1450	28 March	5	1,580
H-4	1455	28 March	2	634
H-5	1215	25 March	1.25	128
H-6	1200	25 March	0.300	—
H-7	1155	25 March	0.100	10.2
H-8	1335	26 March	0.140	24.3
H-9	1345	26 March	0.130	22.7
H-10	1130	25 March	0.034	3.4
H-11	1115	28 March	0.006	1.9
H-12	1140	28 March	0.005	1.6
H-13	1154	28 March	0.012	3.8
I-1	1415	28 March	10.	—
I-2	1410	28 March	39.	—
	1317	26 March	10.	1,730
I-3	1415	28 March	1.650	—
	1315	26 March	4.	692
I-4	1247	25 March	2.	210
I-5	1240	25 March	1.7	179
I-6	1230	25 March	0.16	16.6
I-7	1330	26 March	0.024	4.2
I-8	1315	26 March	0.017	2.9
I-9	1300	26 March	0.01	1.7
I-10	1230	26 March	0.003	0.49
I-11	1115	26 March	—	—
I-12	1130	26 March	0.002	0.25
I-13	1200	26 March	0.0008	0.13
J-1	1411	28 March	6.	—
	1305	26 March	9.	1,550
J-2	1409	28 March	1.45	—
	1303	26 March	3.2	550
J-3	1407	28 March	0.5	157
	1300	26 March	—	—
J-4	1255	26 March	0.4	69.
J-5	1250	26 March	0.16	27.4
J-6	1242	26 March	0.08	13.7
K-1	1240	26 March	8.	1,368

TABLE D.3 NRDL SURVEY DATA CONTINUED

Station Location	Time of Survey		Radiation Intensity	Corrected to H + 1 Hour
	hour	date	r/hr	r/hr
K-2	1240	26 March	2.3	393
K-3	1230	26 March	1.1	185
K-4	1230	26 March	0.45	85.
K-5	1347	24 March	0.375	18.4
K-6	1351	24 March	0.023	1.1
L-1	1220	28 March	3.4	1,080
L-2	1215	28 March	1.4	444
L-3	1345	30 March	0.170	—
L-4	1336	24 March	2.1	101
L-5	1327	24 March	0.006	0.29
L-6	1400	24 March	0.003	0.15
M-1	1220	28 March	3.4	1,080
M-2	1203	26 March	2.6	437
M-3	1447	24 March	3.8	194
M-4	1440	24 March	0.080	4.1
M-5	1443	24 March	0.004	0.2
M-6	1423	24 March	0.004	0.2
N-1	1230	28 March	6.0	1,900
N-2	1207	26 March	4.	671
N-3	1502	24 March	2.3	195
N-4	1456	24 March	0.035	1.8
N-5	1513	24 March	0.008	0.42
N-6	1521	24 March	0.008	0.42
O-1	1230	28 March	2.1	666
O-2	1205	25 March	2.5	255
O-3	1530	24 March	2.	108
O-4	1551	24 March	0.016	0.91
O-5	1539	24 March	0.008	0.43
O-6	1532	24 March	0.008	0.43
P-1	1240	28 March	2.7	856
P-2	1225	25 March	3.6	375
P-3	1220	25 March	0.046	4.8
P-4	1345	24 March	0.008	0.39
P-5	1335	24 March	0	0
P-6	1320	24 March	0	0
Q-1	1245	28 March	1.9	602
Q-2	1240	25 March	1.3	136
Q-3	1230	25 March	0.060	6.2
Q-4	1350	24 March	0.009	0.44
Q-5	1355	24 March	0.0002	0.0092
Q-6	1410	24 March	0	0
R-1	1240	28 March	1.7	539
R-2	1220	26 March	0.800	136
R-3	1320	28 March	0.019	3.8
	1245	25 March	0.060	6.3
R-4	1425	24 March	0.010	1.1
R-5	1430	24 March	0.0002	0.022
R-6	1420	24 March	0	0
L-7	1314	24 March	0.0006	0.28
L-8	1203	24 March	0	0

[redacted]

TABLE D.4 RAD-SAFE SURVEY DATA

Station Location	Time of Survey		Time after Shot	Radiation Intensity	Corrected to H + 1 Hour
	hour	date	hour and minute	mr/hr	r/hr
109	0710	24 March	18:40	4,500	150
	1530	25 March	51:00	2,000	230
108	0710	24 March	18:40	4,500	150
	1530	25 March	51:00	1,700	195
107	0710	24 March	18:40	5,000	170
	1530	25 March	51:00	2,300	265
106	0715	24 March	18:45	6,000	200
105	0715	24 March	18:45	10,000	340
	1530	25 March	51:00	8,000	930
104	1530	25 March	51:00	10,000	1,150
102.4	0711	26 March	66:41	10,000	1,160
114	1357	23 March	1:27	450	0.73
	0710	24 March	18:50	30	1.02
	1530	25 March	51:00	8.6	0.98
	0708	26 March	66:38	10	1.57
113	1358	23 March	1:28	1,000	1.62
	0710	24 March	18:50	60	2.05
	1530	25 March	51:00	19.5	2.25
112	1359	23 March	1:29	2,000	3.25
	0710	24 March	18:50	100	3.40
	1530	25 March	51:00	46	5.20
112.5	0709	26 March	66:39	100	15.70
111	1400	23 March	1:30	10,000	16.20
	0710	24 March	18:50	2,000	69
	1530	25 March	51:00	1,000	113
110	0710	24 March	18:50	4,000	137
	1530	25 March	51:00	1,800	205
110.8	0710	26 March	66:40	1,000	160
122	1351	23 March	1:21	10	0.014
121	1352	23 March	1:22	15	0.021
120	1353	23 March	1:23	22	0.031
119	1353	23 March	1:23	45	0.064
	0710	24 March	18:50	10	0.34
	1530	25 March	51:00	0.6	0.068
118	1354	23 March	1:24	100	0.155
	0710	24 March	18:50	20	0.68
	1530	25 March	51:00	0.9	0.105
117	1355	23 March	1:25	120	0.19
	0710	24 March	18:50	22	0.76
	1530	25 March	51:00	1.4	0.16
116	1356	23 March	1:26	150	0.24
	0710	24 March	18:50	23	0.79
	1530	25 March	51:00	2.3	0.262
115	1357	23 March	1:27	250	0.40
	0710	24 March	18:50	25	0.86
	1530	25 March	51:00	4.3	0.49
215	1330	25 March	49:00	1,350	145
214	1330	25 March	49:00	1,400	150
213	1330	25 March	49:00	1,550	166

TABLE D.4 RAD-SAFE SURVEY DATA - CONTINUED

Station Location	Time of Survey		Time after Shot	Radiation Intensity	Corrected to H + 1 Hour
	hour	date	hour and minute	mr/hr	r/hr
212	1330	25 March	49:00	1,700	182
211	1330	25 March	49:00	—	—
210	1330	25 March	49:00	2,000	216
209	1330	25 March	49:00	2,650	285
208	1330	25 March	49:00	2,850	305
207	0814	24 March	19:46	10,000	360
	1330	25 March	49:00	3,900	420
206	1330	25 March	49:00	11,000	1,200
206 + 0.5 (mile)	0753	26 March	67:23	10,000	—
205	1330	25 March	49:00	13,000	1,400
227	1500	23 March	2:30	7,000	21
	1330	25 March	49:00	300	33
226	1500	23 March	2:30	8,000	24
	1330	25 March	49:00	300	33
225	1501	23 March	2:31	9,000	27.5
	1330	25 March	49:00	310	33.5
224	1502	23 March	2:32	10,000	31
	1330	25 March	49:00	330	35.5
223	1330	25 March	49:00	300	33
222	0805	24 March	19:53	1,000	36.5
	1330	25 March	49:00	330	35.5
221	1330	25 March	49:00	390	42.5
220	1330	25 March	49:00	—	—
219	1330	25 March	49:00	485	53
218	1330	25 March	49:00	600	65
217	1330	25 March	49:00	217	23.5
216	1330	25 March	49:00	216	23.4
236	1455	23 March	2:25	10	0.030
235	1455	23 March	2:25	15	0.045
234	1455	23 March	2:25	25	0.075
233	1455	23 March	2:25	45	0.135
232	1457	23 March	2:27	100	0.300
	1330	25 March	49:00	75	8.0
231	1457	23 March	2:27	200	6.0
	1330	25 March	49:00	80	8.7
231.5	0802	24 March	19:32	10	—
230	1458	23 March	2:28	1,000	3.0
	1330	25 March	49:00	110	12
230.5	0742	26 March	67:12	10	1.6
299	1458	23 March	2:28	3,500	10.5
	1330	25 March	49:00	160	17.2
229.5	0803	24 March	19:33	100	3.55
228	1459	23 March	2:29	6,000	18.2
	1330	25 March	49:00	250	27.5
	0744	26 March	67:14	100	13

TABLE D.4 RAD-SAFE SURVEY DATA, CONTINUED

Station Location	Time of Survey		Time after Shot	Radiation Intensity	Corrected to H + 1 Hour
	hour	date	hour and minute	mr/hr	r/hr
322	1330	25 March	49.00	1,100	117
321	1330	25 March	49:00	1,400	148
320	1330	25 March	49:00	1,700	18
319	1330	25 March	49:00	2,000	212
318	1330	25 March	49:00	2,000	212
	0716	26 March	66:46	1,000	160
317	1330	25 March	49:00	2,600	280
316	1330	25 March	49:00	3,500	370
315	0734	24 March	19:04	10,000	350
	1330	25 March	49:00	4,000	430
314	1330	25 March	49:00	4,800	510
313	1330	25 March	49:00	9,000	950
312	1330	25 March	49:00	10,000	1,070
307	0721	26 March	66:51	10,000	1,600
413	1338	25 March	49:08	4,000	425
	0734	26 March	67:04	1,000	160
412	1339	25 March	49:09	5,000	530
411	1340	25 March	49:10	5,000	530
410	1341	25 March	49:10	7,000	740
409	0701	24 March	18:31	10,000	330
	1342	25 March	49:12	9,000	950
408	1343	25 March	49:13	11,000	1,170
406	0731	26 March	67:01	10,000	1,580
331	0711	26 March	66:41	600	93
330	0713	26 March	66:43	400	62
329	1330	25 March	49:00	800	85
328	1330	25 March	49:00	750	80
327	1330	25 March	49:00	900	95
326	1330	25 March	49:00	950	101
325	1330	25 March	49:00	950	101
324	1330	25 March	49:00	950	101
323	1330	25 March	49:00	1,000	107
426	1355	23 March	1:25	5,500	8.4
	1348	25 March	49:18	80	8.5
425	1356	23 March	1:26	7,000	10.7
	1347	25 March	49:17	140	14.8
424	1357	23 March	1:27	10,000	15.6
	1346	25 March	49:16	150	16.0
423	1345	25 March	49:15	220	23
	0738	26 March	67:08	100	16
422	1344	25 March	49:14	250	26.5
421	1330	25 March	49:00	320	34
420	1331	25 March	49:01	450	47
419	1332	25 March	49:02	1,600	170

[redacted]

TABLE D.4 RAD-SAFE SURVEY DATA CONTINUED

Station Location	Time of Survey		Time after shot	Radiation intensity	Corrected to H + 1 Hour
	hour	date	hour and minute	mr/hr	r/hr
418	0701	24 March	18:31	1,000	33
	1333	25 March	49:03	2,000	210
417	1334	25 March	49:04	2,400	260
416	1335	25 March	49:05	3,000	320
415	1336	25 March	49:06	3,200	340
414	1337	25 March	49:07	3,400	360
431	1353	23 March	1:23	2,400	3.5
	0704	24 March	18:34	10	0.330
	1353	25 March	49:23	50	5.3
	0741	26 March	67:11	20	3.2
528	1330	25 March	49:00	80	8.5
527	1330	25 March	49:00	75	7.9
526	1330	25 March	49:00	70	7.4
525	1330	25 March	49:00	90	9.6
524	1330	25 March	49:00	90	9.6
523	1330	25 March	49:00	110	116
522	1330	25 March	49:00	120	12.7
521	1330	25 March	49:00	130	13.8
520	1330	25 March	49:00	140	14.8
519	1330	25 March	49:00	160	17.0
518	1330	25 March	49:00	190	20.0
607	0700	24 March	18:30	7,000	230
	1530	25 March	51:00	2,000	229
606	0700	24 March	18:30	7,500	250
	1530	25 March	51:00	2,000	229
605	0700	24 March	18:30	8,000	270
	1530	25 March	51:00	2,800	320
604	0700	24 March	18:30	10,000	330
	1530	25 March	51:00	9,000	1,030
603	1530	25 March	51:00	5,000	570
536	1330	25 March	49:00	14	1.480
535	0700	24 March	18:30	38	1.26
	1330	25 March	49:00	18	1.91
	0645	26 March	66:15	10	1.55
534	1330	25 March	49:00	20	2.1
613	1346	23 March	1:16	1,000	1.3
	0700	24 March	18:30	30	1.0
	1530	25 March	51:00	10.2	1.21
	0735	26 March	67:05	10	1.6
612	1348	23 March	1:18	1,900	2.6
	0700	24 March	18:30	60	2.0
	1530	25 March	51:00	23	2.6
611	1350	23 March	1:20	10,000	14
	0700	24 March	18:30	400	13
	1530	25 March	51:00	180	20.5
	0738	26 March	67:08	100	16.5
610	0700	24 March	18:30	3,020	101
	1530	25 March	51:00	4,200	136

[redacted]

TABLE D.4 RAD-SAFE SURVEY DATA CONTINUED

Station Location	Time of Survey		Time after Shot	Radiation Intensity	Corrected to H + 1 Hour
	hour	date	hour and minute	mr/hr	r/hr
609	0700	24 March	18:30	4,000	134
	1530	25 March	51:00	1,500	170
608	0700	24 March	18:30	6,000	200
	1530	25 March	51:00	1,800	202
620	1335	23 March	1:05	28	0.031
	1530	25 March	51:00	1.8	0.203
619	1337	23 March	1:07	44	0.050
	1530	25 March	51:00	1.8	0.203
618	1338	23 March	1:08	80	0.093
	1530	25 March	51:00	2.0	0.230
617	1340	23 March	1:10	120	0.144
	1530	25 March	51:00	2.1	0.240
430	1353	23 March	1:23	3,200	4.7
	0703	24 March	18:33	10	0.330
	1352	25 March	49:22	60	6.4
429	1354	23 March	1:24	4,400	6.6
	0703	24 March	18:33	100	3.3
	1351	25 March	49:21	60	6.4
428	1354	23 March	1:24	5,000	7.5
	0702	24 March	18:32	100	3.3
	1350	25 March	49:20	80	8.5
427	1355	23 March	1:25	3,500	5.3
	0702	24 March	18:32	100	3.3
	1349	25 March	49:19	80	8.5
436	1350	23 March	1:20	1,000	1.42
	0706	24 March	18:36	50	1.66
	1330	25 March	49:00	80	8.55
	0744	26 March	67:14	66	10.5
435	1350	23 March	1:20	1,200	1.7
	0706	24 March	18:36	45	1.5
	1356	25 March	49:26	60	6.4
434	1351	23 March	1:21	1,300	1.87
	0705	24 March	18:35	45	1.5
	1356	25 March	49:26	40	4.3
	0742	26 March	67:12	30	4.7
433	1351	23 March	1:21	2,000	2.9
	0705	24 March	18:35	40	1.3
	1355	25 March	49:25	50	5.3
432	1352	23 March	1:22	2,200	3.2
	0704	24 March	18:34	50	1.7
	1354	25 March	49:24	50	5.4
517	1330	25 March	49:00	240	26
	0652	26 March	66:22	100	15.5
516	1330	25 March	49:00	270	29
515	1330	25 March	49:00	310	33
514	1500	23 March	2:30	10,000	30
	1330	25 March	49:00	340	36
513	0700	24 March	18:30	1,000	33
	1330	25 March	49:00	380	40
512	1330	25 March	49:00	470	50

[redacted]

TABLE D.4 RAD-SAFE SURVEY DATA CONTINUED

Station Location	Time of Survey		Time after Shot	Radiation Intensity	Corrected to H + 1 Hour
	hour	date	hour and minute	mr/hr	r/hr
511	1330	25 March	49:00	500	53
510	1330	25 March	49:00	800	85
507	0655	26 March	66:25	1,000	155
505	0700	24 March	18:30	10,000	330
504	0700	26 March	66:30	10,000	1,550
533	1450	23 March	1:20	1,000	1.42
	1330	25 March	49:00	27	2.90
532	0700	24 March	18:30	100	3.30
	1330	25 March	49:00	32	3.40
531	1330	25 March	49:00	37	3.90
530	1330	23 March	1:00	10,000	10
	1330	25 March	49:00	45	4.8
529	1330	25 March	49:00	80	8.5
616	1342	23 March	1:12	200	0.250
	1530	25 March	51:00	28	0.320
615	1343	23 March	1:13	320	0.400
	1530	25 March	51:00	3.1	0.352
614	1344	23 March	1:14	600	0.770
	0700	24 March	18:30	10	0.330
	1530	25 March	51:00	5	0.570
636	1530	25 March	51:00	2.9	0.330
635	1530	25 March	51:00	2.9	0.330
634	1530	25 March	51:00	2.4	0.270
633	1530	25 March	51:00	2.4	0.270
632	1530	25 March	51:00	1.9	0.220
631	1530	25 March	51:00	1.0	0.114
630	1530	25 March	51:00	1.4	0.158
629	1530	25 March	51:00	1.6	0.180
628	1530	25 March	51:00	1.5	0.170
627	1530	25 March	51:00	1.6	0.180
626	1530	25 March	51:00	1.8	0.202
625	1530	25 March	51:00	2.0	0.228
624	1530	25 March	51:00	1.9	0.220
623	1330	23 March	1:00	10	0.010
	1530	25 March	51:00	2	0.228
622	1331	23 March	—	12	—
	1530	25 March	51:00	1.8	0.202
621	1333	23 March	—	20	—
	1530	25 March	51:00	2	0.228
708	1340	23 March	1:10	4,200	5.06
	0713	24 March	18:43	190	6.4
707	1342	23 March	1:12	10,000	12.5
	0714	24 March	18:44	390	13.2
	0656	26 March	66:24	100	15.5
706	0715	24 March	18:45	3,900	130

[redacted]

TABLE D.4 RAD-SAFE SURVEY DATA CONTINUED

Station Location	Time of Survey		Time after Shot	Radiation Intensity	Corrected to H + 1 Hour
	hour	date	hour and minute	mr/hr	r/hr
705	0720	24 March	18:50	10,000	333
	1520	25 March	51:00	5,000	570
	0659	26 March	66:27	100	165
704	1522	25 March	51:00	6,000	690
703	1524	25 March	51:00	8,000	920
702	1526	25 March	51:00	9,000	1,030
	0703	26 March	66:30	10,000	1,650
701	1528	25 March	51:00	20,000	2,300
717	1331	23 March	1:01	25	—
	1400	25 March	50:00	4.4	0.049
716	1332	23 March	1:02	40	—
715	1333	23 March	1:03	50	—
714	1334	23 March	1:04	120	0.130
713	1335	23 March	1:05	190	0.210
712	1336	23 March	1:06	330	0.370
	0709	24 March	18:39	10	0.330
711	1337	23 March	1:07	600	0.690
	0710	24 March	18:40	16	0.530
710	1338	23 March	1:08	1,200	1.4
	0711	24 March	18:41	29	0.980
709	1339	23 March	1:09	2,100	2.5
	0712	24 March	18:42	100	3.4
	0655	26 March	66:30	10	1.6
734	1600	25 March	51:30	3	0.340
733	1558	25 March	51:28	3	0.340
732	1556	25 March	51:26	2	0.230
731	1554	25 March	51:24	2	0.230
730	1552	25 March	51:22	4	0.460
729	1550	25 March	51:20	3	0.340
728	1548	25 March	51:18	4	0.460
727	1546	25 March	51:16	4	0.460
726	1544	25 March	51:14	2	0.230
725	1542	25 March	51:12	2	0.230
724	1540	25 March	51:10	2	0.230
723	1538	25 March	51:08	8	0.910
722	1536	25 March	51:06	6	0.680
721	1534	25 March	51:04	4	0.460
720	1532	25 March	51:02	4	0.460
719	1329	23 March	0:59	10	0.460
	1530	25 March	51:00	4	0.460
718	1330	23 March	1:00	15	—
	1400	25 March	49:30	3.8	0.430
809	1333	23 March	1:03	2,000	2.1
	0708	24 March	18:38	80	2.7
	1400	25 March	49:30	17	1.8

[redacted]

TABLE D.4 RAD-SAFE SURVEY DATA CONTINUED

Station Location	Time of Survey		Time after Shot	Radiation Intensity	Corrected to H + 1 Hour
	hour	date	hour and minute	mr/hr	h/hr
808	1334	23 March	1:04	3,600	3.9
	1400	25 March	49:30	33	3.5
808.5	0718	26 March	66:48	10	1.6
807	1335	23 March	1:05	10,000	11
	0710	24 March	18:40	300	10
	1400	25 March	49:30	100	10.7
	0720	26 March	66:50	100	16.5
806	0712	24 March	18:42	4,000	135
	1400	25 March	49:30	1,400	149
806.5	0721	26 March	66:51	1,000	164
805	0714	24 March	18:44	6,000	202
	1400	25 March	49:30	10,000	1,070
804	0715	24 March	18:45	10,000	340
801	0723	26 March	66:52	10,000	1,650
816	1326	23 March	—	36	—
	1400	25 March	51:00	2	0.230
815	1327	23 March	—	60	—
	1400	25 March	51:00	2	0.230
814	1328	23 March	—	85	—
	1400	25 March	51:00	2	0.230
813	1329	23 March	—	110	—
	1400	25 March	51:00	2	0.230
812	1330	23 March	—	270	—
	0702	24 March	18:30	12	0.400
	1400	25 March	51:00	2.5	0.280
811	1331	23 March	—	470	—
	0704	24 March	18:30	18	0.600
	1400	25 March	51:00	3.5	0.400
810	1332	23 March	—	900	—
	0706	24 March	18:30	34	1.14
	1400	25 March	51:00	4	0.460
906	1420	23 March	1:50	10,000	208
	0739	24 March	18:30	8,000	270
	1554	25 March	51:00	3,200	360
905	0740	24 March	18:30	8,000	270
	1556	25 March	51:00	4,600	520
904	0740	25 March	18:30	10,000	333
	1600	26 March	51:00	11,000	1,250
903 + 1 mile to ground zero					
	0655	26 March	66:25	10,000	1,650
820	1322	23 March	—	10	—
819	1323	23 March	—	11	—
818	1324	23 March	—	15	—
	0700	24 March	18:30	12	0.400
	1400	25 March	51:00	2	0.230
817	1325	23 March	—	24	—
	1400	25 March	51:00	1.5	0.170
912	1404	23 March	1:34	180	0.310
	0733	24 March	18:30	35	1.18
	1542	25 March	51:00	7	0.8

[redacted]

TABLE D.4 RAD-SAFE SURVEY DATA CONTINUED

Station Location	Time of Survey		Time after Shot	Radiation Intensity	Corrected to H + 1 Hour
	hour	date	hour and minute	mr/hr	h/hr
911	1407	23 March	1:37	360	0.650
	0734	24 March	18:30	60	2.0
	1544	25 March	51:00	11	1.25
910	1410	23 March	1:40	700	1.3
	0735	24 March	18:30	80	2.7
	1546	25 March	51:00	20	2.25
910.7	0652	26 March	57:00	10	1.65
909	1412	23 March	1:42	1,400	2.64
	0736	24 March	18:30	220	7.3
	1548	25 March	51:00	80	9.2
908.8	0653	26 March	67:00	1,000	165
908	1415	23 March	1:45	2,400	4.7
	0737	24 March	18:30	1,000	33
	1550	25 March	51:00	375	42
	0653	26 March	67:00	100	16.5
907	1417	23 March	1:47	8,000	16
	0738	24 March	18:30	8,000	270
	1552	25 March	51:00	3,000	340
918	1346	23 March 24 March	1:16	10	0.013
	1530	25 March 26 March	51:00	2.5	0.280
917	1349	23 March 24 March	1:19	15	0.021
	1532	25 March 26 March	51:00	2.5	0.280
916	1352	23 March 24 March	1:22	22	0.032
	1534	25 March 26 March	51:00	2.5	0.280
915	1355	23 March	1:25	36	0.055
	0731	24 March	18:30	10	0.330
	1538	25 March	51:00	2.8	0.320
914	1358	23 March	1:28	60	0.095
	0732	24 March	18:30	40	1.34
	1540	25 March	51:00	3.2	0.360
913	1401	23 March	1:31	100	0.165
	0733	24 March	18:30	50	1.67
	1542	25 March	51:00	3.9	0.440

TABLE D.5 CORPS OF ENGINEERS "PATHFINDER" SURVEY DATA, MERCURY, NEVADA

Time		Grid Coordinates		Radiation Intensity r/hr		
Day	After Shot	N Meters	E Meters	TIB	Victoreen	Average Corrected to H + 1 Hour
hour	hour - minute					
24 March 1955						
1111		00000	00000			
1133		843N	00031E			
1142		1504N	00167W			
1152		2112N	00111W			
1205		3008N	00464W			
1300		—	—			
1320		4092N	00460W			
1323		4252N	00455W			
1327		4432N	00458W			
			Reset Counters to Approximate Map Grids			
—		10230N	08430E			
1355		11403N	08367E			
1432		11658N	08890E			
1505		11041N	10111E			
1530	27:00	10834	10173	2	2	0.106
1531	27:01	10784	10175	3	3	0.157
1532	27:02	10702	10186	4	4	0.210
1533	27:03	10617	10196	2	1.8	0.100
1534	27:04	10590	10200	1.3	1.3	0.068
1540	27:10	10611	10170	—	5	0.262
1541	27:11	10610	10170	2.5	2.3	0.126
1542	27:12	10605	10147	2	2	0.107
1550	27:20	10573	9932	2	2	0.107
1600	27:30	10547	9825	8	5	0.350
—	—	10541	9815	—	—	—
1601	27:31	10528	9802	10	8	0.480
1604	27:34	10490	9745	14	10	0.640
1650	28:20	10488	9745	12	12	0.670
1710	28:40	10435	9741	80	60	3.900
1715	28:45	10351	9765	100	80	5.100
1718	28:48	10284	9783	58	58	3.300
1735	29:05	10010	9751	80	50	3.700
1750	29:20	9755	9641	3	3	0.175
1810	29:40	9800	9430	No mr readings		
26 March 1955			New Odometer Cable obtained and installed.			
Latitude 36 degrees; Grid Sec. 0.6 degrees west						
1520	74:50	00000	00000			
1543	75:13	00834	00019W			
1551	75:25	01495	00150W			
1557	75:31	02105	00095W			
1609	75:43	03002	00465W			
1626	76:00	—	—			
1638	76:12	04424	00452W			
			Reset Counter to Approximate Grid Coordinates			
—	—	10230N	08430E			
1649	—	10923	8545			
1651	76:21	10988	8563			
1652	76:22	11020	8558	20	20	3.7
1653	76:23	11038	8552	14	15	2.7
1655	76:25	11054	8546	20	20	3.7
1657	76:27	11092	8539	26	28	5.0
1658	76:28	11099	8523	42	40	7.5
1659	76:29	11104	8523	42	45	8.0
1700	76:30	11103	8511	18	22	3.7
1701	76:31	11098	8481	10	12	2.1
1702	76:32	11080	8478	4	5	0.82
1704	76:34	11047	8498	7	8	1.38
1706	76:36	11027	8510	—	7.5	1.38
1707	76:37	11012	8521	11	11	2.1
1707.5	76:37.5	11007	8526	22	20	3.9

[redacted]

TABLE D.5 CORPS OF ENGINEERS "PATHFINDER" SURVEY DATA, MERCURY, NEVADA

Time		Grid Coordinates		Radiation Intensity r/hr		
Day	After Shot	N Meters	E Meters	T1B	Victoreen Average	Corrected to H + 1 Hour
hour	hour - minute					
1708	76:38	10998	8531	32	30	5.7
1709	76:39	10986	8536	42	40	7.5
1710	76:40	10976	8543	150	150	27.5
1711	76:41	10967	8527	100	—	18.5
1712	76:42	10967	8500	40	—	7.3
1712.5	76:42.5	10967	8476	10	10	1.85
1713	76:43	10968	8460	2	2	0.370
1714	76:44	10982	8434	1	1	0.185
1716	76:46	11020	8416	1.7	1.5	0.29
1717	76:47	11059	8415	1.5	1	0.23
1719	76:49	11103	8418	1.4	1.8	0.29
1721	76:51	11158	8430	2.1	2.5	0.58
1722	76:52	11170	8444	4	5.5	0.87
1722.5	76:52.5	11185	8451	12	10	2.1
1723	76:53	11197	8455	20	22	3.9
1724	76:54	11205	8451	28	25	4.9
1724.5	76:54.5	11213	8449	36	33	6.3
1725	76:55	11217	8444	52	50	9.3
1725.5	76:55.5	11217	8440	50	60	10.1
1726	76:56	11218	8435	10	12	2.1
1726.5	76:56.5	11225	8430	7	7	1.3
1730	77:00	11257	8415	5.5	5.5	1.02
1745	77:15	11264	8424	8	8	1.48
1745.5	77:15.5	11268	8427	10	10	1.85
1746	77:16	11276	8433	21	20	3.80
1748	77:18	11273	8426	10	10	1.85
1746.5	77:16.5	11280	8436	30	30	5.6
1749	77:19	11266	8412	4	5	8.4
1751	77:21	11250	8392	2.5	2.5	0.46
1752.5	77:22.5	11212	8356	2.0	1.8	0.35
1753	77:23	11181	8328			
1754	77:24	11140	8340			
1803	77:33	10228	8467			
1823	77:53	7926	8908			
1832	78:02	7314	8868			
1839	78:07	6655	9010			
1855	78:25	5812	9032			
			Total Mileage 78.2 Miles = 125,900 Meters			
27 March 1955						
Latitude 36 degrees; Grid Dec. 0.6 degrees; Scale Adj = 0						
1030	—	5812	9032			
1045	—	6656	8991			
1112	—	8818	8510			
1155	—	10242	8541			
			Reset Counters to Approximate Grid Coordinates			
—	—	10230	8430			
1214	95:44	11258	8432	4.5	4	1.07
—	—	11290	8436	—	—	—
1216	95:46	11296	8443	10	11	2.56
1219	95:49	11326	8436	6	6	1.46
1220	95:50	11356	8443	6	6	1.46
1222	95:52	11367	8455	10	10	2.45
1224	95:54	11379	8476	34	32	8.
1225	95:55	11384	8486	50	50	12.2
1226	95:56	11382	8501	500	500	122.
1227	95:57	11381	8510	1	1.5	0.31
—	—	11386	8497	—	—	—
1228	95:58	11392	8496	62	60	14.8
1230	96:00	11413	8503	16	16	3.9
1231	96:01	11400	8518	100	100	24.5
1232	96:02	11394	8524	500	—	122.
1233	96:03	11391	8528	1,000	1,000	245

[redacted]

TABLE D.5 CORPS OF ENGINEERS "PATHFINDER" SURVEY DATA, MERCURY, NEVADA

Time		Grid Coordinates		Radiation Intensity r/hr		
Day	After Shot	N Meters	E Meters	T1B	Victoreen	Average Corrected to H + 1 Hour
hour	hour - minute					
1234	96:04	11385	8531	—	1,800	440
1236	96:06	11421	8525	26	26	6.4
1238	96:08	11421	8547	550	550	133.
1239	96:09	11413	8548	1,000	1,200	270.
1240	96:10	11414	8559	1,000	1,000	245.
1241	96:11	11424	8560	1,000	900	230.
1242	96:12	11432	8558	300	300	76.
1243	96:13	11447	8560	15	20	4.3
1244	96:14	11464	8563	3	4	0.88
1248	96:18	11468	8576	3.5	3	0.79
1250	96:20	11456	8587	10	10	2.45
1252	96:22	11447	8622	18	20	4.6
1255	96:25	11448	8640	15	13	3.4
1303	96:33	11444	8645	20	20	4.9
1305	96:35	11433	8655	300	300	73.
1306	96:36	11424	8673	350	350	85.
1307	96:37	11418	8685	200	200	49.
1308	96:38	11412	8697	75	80	19.
1309	96:39	11400	8707	45	50	11.5
1310	96:40	11391	8731	30	30	7.3
1311	96:41	11378	8748	100	100	24.5
1312	96:42	11370	8771	80	80	19.5
1313	96:43	11366	8796	30	30	7.3
1314	96:44	11366	8808	8	10	2.2
1315	96:45	11356	8820	5	4.5	1.15
1316	96:46	11339	8823	12	10	2.7
1317	96:47	11306	8819	50	40	10.9
1318	96:48	11269	8814	30	30	7.3
1320	96:50	11243	8832	32	28	7.3
1322	96:52	11209	8856	24	23	5.7
1324	96:54	11273	8888	27	28	6.7
1325	96:55	11249	8904	30	30	7.3
1326	96:56	11111	8921	48	45	11.3
1329	96:59	11066	8948	42	40	10
1330	97:00	11008	8954	13	13	3.15
1335	97:05	10919	8918	30	30	7.3
1340	97:10	10844	8928	34	32	8.0
1343	97:13	10803	8929	60	60	14.5
1345	97:15	10768	8893	30	30	7.3
1347	97:17	10771	8845	20	20	4.9
1350	97:20	10767	8791	14	12	3.2
1553	97:23	10783	8757	20	20	4.9
1355	97:23	10833	8687	20	20	4.9
1400	97:30	10854	8582	8	7	1.82
1401	97:31	10854	8509	60	55	14.
1402	97:32	10879	8512	120	100	27.
1403	97:33	10914	8517	30	40	8.5
1404	97:34	11032	8532	30	30	7.3
1405	97:35	11070	8539	50	50	12.2
1406	97:36	11104	8544	100	100	24.5
1407	97:37	11137	8548	—	300	73.
1408	97:38	11154	8550	900	800	209
1409	97:39	11142	8541	220	250	58.
1410	97:40	11125	8590	200	250	55.
1411	97:41	11114	8464	100	100	24.
1412	97:42	11137	8461	200	200	49.
1413	97:43	11163	8458	300	300	73.
1414	97:44	11180	8456	0.500	500	122.
1415	97:45	11193	8455	1.050	900	254
1420	97:50	10758	8491			
1429	97:59	10106	8490			

[redacted]

TABLE D.5 CORPS OF ENGINEERS "PATHFINDER" SURVEY DATA, MERCURY, NEVADA

Time		Grid Coordinates			Radiation Intensity r/hr	
Day	After Shot	N Meters	E Meters	T1S	Victoreen Average Corrected to H + 1 Hour	
hour	hour - minute					
1513	98:13	8685	8618			
1613	99:13	6530	9098			
1629	99:29	5688	9135			
28 March 1955 Test No. 4 Nevada Proving Ground						
Latitude 36 degrees; Grid Dec. 6 degrees; Scale Adj = 0						
Purpose: to locate 10 r/hr line						
1015		5688	9135			
1030		6523	9087			
1048		8670	8575			
1200		10091	8561			
			Reset Counters to Approximate Grid Coordinates			
1200		10230	8430			
1203		11305	8548	1.0		0.322
—		11315	8543	1.6		0.510
—		11319	8450	1.8		0.582
—		11331	8533	3.0		0.96
—		11348	8528	5.0		1.6
1205		11352	8527	6.0		1.9
—		11365	8520	6.0		1.9
—		11362	8513	8.0		2.53
1205		11360	8504	10.		3.2
—		No change	—	12		3.8
1206		11356	8504	10		3.2
—		11351	8502	8		2.53
—		11350	8496	6		1.9
—		11333	8487	4		1.27
—		11333	8484	2		0.64
1212		11331	8481	1		0.32
—		11339	8467	0.8		0.253
—		11356	8468	1.5		0.48
—		11361	8472	2.5		0.8
—		11367	8476	5		1.6
—		11377	8478	6		1.9
—		11377	8480	8		2.53
—		11390	8488	6		1.9
—		11396	8495	4		1.27
—		11399	8500	4		1.27
1220		11413	8486	2		0.14
—		11389	8442	—		—
—		11389	8466	1		0.32
—		11383	8476	4		1.27
1225		11382	8477	8		2.53
—		11390	8459	3		0.96
1228		11389	8452	2		0.64
1233		11367	8312	—		—
1235		11152	8317	—		—
1238		10897	8378	—		—
1240		10740	8458	—		—
1241		10670	8478	—		—
1245		10230	8449	—		—
1301		8811	8499	—		—
1353		6668	9022	—		—
1410		5823	9070	—		—
			Coordinates of Ground Zero for Shot 7:			
			East 584,893.59			
			North 4,113,775.52			

TABLE D.6 PROJECT 3.1.2 SURVEY DATA (U.S.A.)

Station Location				Radiation Intensity at H + 1 Hours mr/hr
Papoose Valley Road				
5 miles south of junction,	37° 15.4' N Latitude			3.56
	115° 51.5' W Longitude			
6 miles south of junction	"	"	"	3.56
7 miles south of junction	"	"	"	3.56
8 miles south of junction	"	"	"	24.49
9 miles south of junction	"	"	"	4.94
10 miles south of junction	"	"	"	5.73
11 miles south of junction	"	"	"	38.12
11.5 miles south of junction	"	"	"	103.49
12.0 miles south of junction	"	"	"	173.60
12.5 miles south of junction	"	"	"	704.29
13.0 miles south of junction	"	"	"	854.58
13.5 miles south of junction	"	"	"	1,078.75
14.0 miles south of junction	"	"	"	868.21
14.5 miles south of junction	"	"	"	584.40
14.7 miles south of junction	"	"	"	442.99
Indian Springs Road				
9 miles south of Groom Lake,	37° 17.5' N Latitude			8.89
	115° 47.2' W Longitude			
12.1 miles south of Groom Lake	"	"	"	104.68
16.2 miles south of Groom Lake	"	"	"	Bkg.
23.0 miles south of Groom Lake	"	"	"	198.09
25.0 miles south of Groom Lake	"	"	"	542.73
27.0 miles south of Groom Lake	"	"	"	451.09
29.0 miles south of Groom Lake	"	"	"	217.05
34.0 miles south of Groom Lake	"	"	"	11.65
Sheep Canyon Road				
50.3 miles north of Highway No. 95,	36° 26.8' N Latitude			
	115° 26.3' W Longitude			
				2.37
45.4 miles north of Highway No. 95	"	"	"	11.85
43.3 miles north of Highway No. 95	"	"	"	25.48
41.1 miles north of Highway No. 95	"	"	"	22.91
39.3 miles north of Highway No. 95	"	"	"	23.90
37.3 miles north of Highway No. 95	"	"	"	38.51
37.1 miles north of Highway No. 95	"	"	"	185.85
34.1 miles north of Highway No. 95	"	"	"	168.27
33.6 miles north of Highway No. 95	"	"	"	93.02
28.4 miles north of Highway No. 95	"	"	"	109.91
23.5 miles north of Highway No. 95	"	"	"	16.99

D.7 PROJECT 2.5.1 SURVEY ON D + 99 DAYS

Station Location	Radiation Intensity	Station Location	Radiation Intensity	Station Location	Radiation Intensity
	mr/hr*		mr/hr*		mr/hr*
A-1	60	G-1	220	L-1	70
A-2	27	G-2	150	L-2	30
A-3	11	G-3	90	M-1	40
B-1	55	G-4	37	M-2	28
B-2	39	G-5	12	M-3	12
B-3	16	H-1	190	N-1	44
C-1	80	H-2	240	N-2	36
C-2	46	H-3	90	N-3	12
C-3	9	H-4	38	O-1	34
D-1	90	H-5	5	O-2	12
D-2	32	I-1	170	P-1	70
D-3	15	I-2	150	P-2	13
E-1	90	I-3	43	Q-1	37
E-2	60	I-4	11	Q-2	16
E-3	22	J-1	100	R-1	30
E-4	10	J-2	50	R-2	9
F-1	150	J-3	10		
F-2	90	K-1	90		
F-3	46	K-2	22		
F-4	9	K-3	7		

* All readings taken in the afternoon on 30 June 1955. Where reading was less than 5 mr/hr, it was not recorded.

[redacted]

Appendix E

METEOROLOGICAL DATA

TABLE E.1 METEOROLOGICAL DATA, YUCCA LAKE

Sky condition: $^3/_{10}$ thin cirrus; visibility unrestricted. 23 March 1955, 1245 PST

Height	Wind	Pressure	Temperature	Dew Point	Relative Humidity
Thousands of ft, MSL	deg/knots	mb	°C	°C	pct
SFC	310/10	883	18.0	−4.8	21
4	310/10	878	17.9	−5.8	21
4.951	—	850	14.0	−6.1	23
5	310/13	848	13.8	−7.0	23
6	310/15	820	10.2	−7.0	28
7	320/15	790	6.7	−10.0	29
7.874	—	765	3.4	−12.1	31
8	320/16	759	3.0	−12.0	32
9	330/20	732	0.8	−12.4	36
9.219	—	726	0.4	−12.7	36
9.810	—	709	0.3	−15.5	28
10	340/26	704	0.1	−15.8	29
10.148	—	700	0.0	−16.0	28
10.466	—	691	−0.5	−16.0	29
11	350/23	675	−1.7	−17.5	29
11.614	—	662	−2.7	−19.2	26
12	360/21	653	−3.6	−19.2	28
13	340/23	628	−6.2	−18.8	31
14	330/25	604	−9.0	−20.2	38
15	330/31	581	−11.9	−22.6	40
16	310/34	559	−14.4	−23.2	46
17	300/35	536	−16.3	−26.5	40
18	290/36	514	−18.1	−28.6	38
18.655	—	500	−19.5	−30.0	37
19	290/35	492	−20.2	−30.4	38
20	290/37	474	−22.9	−32.5	39
21	290/37	453	−25.2	−34.8	40
22	290/40	434	−28.0	−37.0	42
22.679	—	420	−29.8	−38.0	43
23	290/43	416	−30.0	−39.2	41
23.261	—	412	−30.4	−40.0	39
23.950	—	400	−32.1		
24	290/48	398	−32.5		
25	290/47	381	−34.5		
30	290/56	306	−36.5		
30.380	—	300	−48.2		
34.245	—	250	−57.4		
35	300/51	245	−58.6		
38.756	—	200	−66.5		
40	300/58	189	−65.6		
44.527	—	150	−61.4		
45	280/47	146	−62.0		
50	270/48	115	−59.0		
52.812	—	100	−59.9		
55	270/53	90	−60.0		
60	280/48	72	−60.1		
63.123	—	60	−59.7		

[redacted]

TABLE E.2 WINDS ALOFT, YUCCA LAKE

22 March 1955	23 March 1955								
	1900	0100	0600	0920	1040	1110	1245	1500	1830
SFC	230/13	Calm	270/10	350/06	300/02	300/09	310/10	280/15	300/04
4	230/14	270/02	280/10	350/06	300/03	300/08	310/10	280/14	300/05
5	260/19	270/06	330/12	350/08	300/05	290/11	310/13	310/15	300/11
6	290/16	280/08	330/18	340/10	300/07	290/11	310/15	320/13	300/11
7	300/15	300/10	320/23	330/16	300/08	290/13	320/15	330/17	300/12
8	310/17	310/13	320/26	320/22	310/10	300/15	320/16	330/19	300/14
9	320/18	310/18	310/25	320/25	330/14	310/17	330/20	330/19	300/17
10	320/18	300/25	300/28	320/28	330/20	320/18	340/26	320/20	300/21
12	320/28	300/31	310/32	320/31	320/27	310/28	360/21	320/22	300/27
14	320/48	310/35	310/35	320/31	330/25	320/28	330/25	310/33	300/28
16	330/58	320/37	310/36	330/26	330/27	320/29	310/34	310/38	300/26

TABLE E.3 WINDS ALOFT, YUCCA FLAT

	Station 353,* Yucca Flat, 23 March 1955					
	0600	0630	0700	0730	0800	0830
SFC	320/09	330/08	330/07	350/08	Calm	340/05
5	330/23	330/20	330/12	330/13	340/05	340/07
6	310/25	320/27	330/18	330/16	340/09	340/09
7	310/22	320/27	330/20	330/19	340/12	320/11
8	320/21	320/25	330/22	330/23	320/16	320/15
9	310/22	320/26	320/24	330/35	330/25	320/21
10	310/27	320/30	320/30	330/42	330/35	330/34
12	310/40	320/48	320/44	330/56	320/42	330/45
14	320/50	320/56	320/43	330/77	310/44	320/41
16	320/45	320/39	320/33	320/57	320/33	330/22
	0900	0930	1000	1030	1100	1130
SFC	330/09	350/09	340/10	Calm	300/06	330/08
5	340/11	350/09	330/09	330/07	330/11	330/08
6	350/13	330/12	330/09	330/12	300/13	330/10
7	340/13	320/17	340/14	340/10	300/10	310/09
8	320/16	320/22	320/19	340/10	320/07	290/10
9	330/19	320/27	310/23	330/11	330/05	300/11
10	320/20	320/29	320/31	320/15	350/06	300/13
12	—	310/34	320/47	320/34	320/32	320/33
14	—	310/22	310/35	320/42	320/49	320/48
16	—	340/19	340/17	330/37	320/40	330/35

* Station 353 is approximately 2½ miles southwest of ground zero. A pibal team was temporarily located at this site to obtain morning wind runs. The surface winds are estimated.

Appendix F

DISCUSSION OF SHOT 7 FALLOUT

Assume that at H + 1 hour there existed an actual relation between the intensity (I) of an isodose line and the area within this line (A), which is the area having an intensity of I or greater, whether this area is within one isodose line or not. (That is, the distribution may be spotty or have holes in it.) Let this function be f, which gives:

$$I = f(A) \tag{F.1}$$

The total radioactivity (R) resulting from this fallout will then be given by:

$$R = K \int_0^\infty I dA = K \int_0^\infty f(A)\, dA \tag{F.2}$$

Where K = a constant to be determined.

The problem of evaluating R then can be broken into two parts, evaluation of the constant K and evaluation of the integral.

The evaluation of the constant K will not be considered further here, except to note that an accurate evaluation of it may be quite different because of the unknown amount of covering of the radioactive dust by shielding dust, because of the uneven nature of the terrain which has a similar effect especially in the crater hole, and because of the difficulty of extrapolating back to H + 1 hour accurately.

Measurements were made to determine the function, f. The areas measured were only those within the outside isodose line enclosing them. If the intensity in the crater dropped off from the rim value, then these areas will be too high correspondingly. This fact will not effect the integral given in equation F.1, however, if integration is restricted to the region of known values of the intensity. These data are given in Table F.1 in columns 1 and 2. A numerical evaluation of the integral can be made by plotting dose rate versus area and determining the area under the curve. However, because of the large range of values, this direct method is impractical. To overcome this difficulty, consider the following mathematical transformation:

$$\int_{A_1}^{A_2} I dA = \int_{A_1}^{A_2} \frac{(AI)\,(dA)}{A} = \int_{\ln A_1}^{\ln A_2} (IA)\, d(\ln A) \tag{F.3}$$

The values of IA and lnA are given in Table F.1 in columns 3 and 4. From the development shown in Equation F.3, it can be seen that the integral may also be evaluated by plotting IA versus lnA and measuring the area under this curve. The plot of IA versus lnA is shown in Figure F.1. A smooth curve has been drawn through the points. The area under the solid curve is 1,150 r · mi^2/hr. Dividing by 4, one gets 287 mc.

The preceding calculation is subject to the following uncertainties:

1. The entrapolation of dose rates to H + 1 hour was carried out on the assumption of a uniform $t^{-1.2}$ decay. This is probably somewhat in error because of such factors as fractionation and the presence of capture products.
2. Data were not available to extend the integration to zero area, so that the result is too small.
3. The factor for conversion of activity per unit area to dose rate 3 feet above an infinite plane is not known accurately and in the presence of fractionation may vary with range.

An overall error of ± 50 percent is not unreasonable.

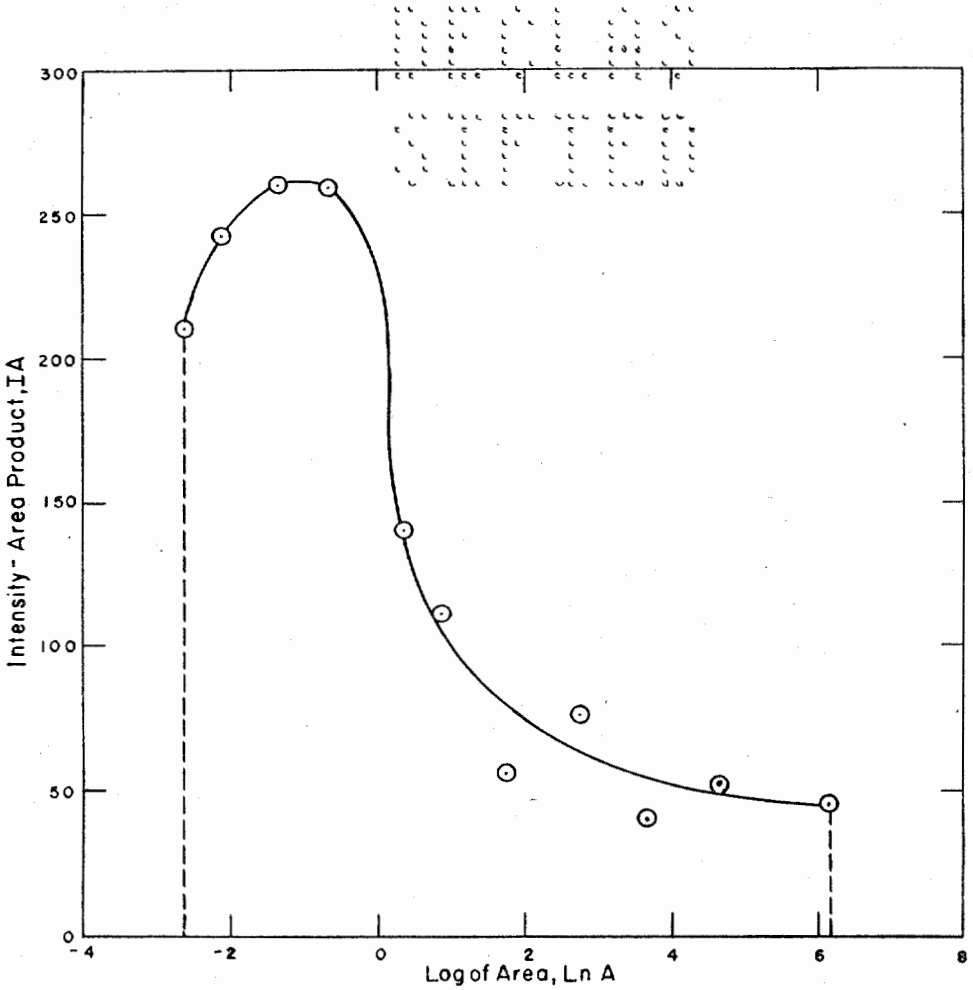

Figure F.1 Area activity inclosed by dose-rate contours at H + 1 hour.

TABLE F.1 AREA ACTIVITY OF FALLOUT

1 Intensity (1)	2 Area (A)	3 IA	4 ln A
r/hr	mi^2		
3,000	0.070	210	−2.64
2,000	0.121	242	−2.11
1,000	0.261	261	−1.34
500	0.518	259	−0.66
100	1.41	141	0.34
50	2.42	121	0.88
10	5.55	55.5	1.71
5	15.20	76	2.72
1	39.20	39.2	3.67
0.5	102.9	51.3	4.63
0.1	450.9	45.1	6.11

Appendix G

CORE SAMPLER, EVALUATION AND SAMPLING DATA

Two basically different types of core samplers were investigated. The first consisted of a straight 2-inch pipe with a diaphragm closure on the lower end. The second consisted of one slotted tube within another slotted tube which could be inserted in the ground in the closed position, rotated to an open position for sampling, closed, and withdrawn. The slotted-tube core sampler was selected for production after a competitive test of the two prototype models. Twenty core samplers were fabricated by the Chemical Corps.

To insure that no cross-contamination from one level to the next occurred, the core samplers were tested at the NTS as follows: hot dirt containing Tesla fallout was sprinkled on the ground surface of the Jangle underground lip; then the core sampler was driven in with a sledge hammer, using a wood or leather buffer, opened, rotated to pick up a sizeable sample, closed, withdrawn and the samples from each slot analyzed for radioactivity. It was discovered that the core sampler (No. 1) carried a great deal of radioactive material to all depths (see Table G.1). It appeared that the sharp edges on the outer slots might be causing this carry-down so all such edges were beveled. Resultant samples (No. 2, Table G.1) showed little improvement. Attempts to use a copper shield over the length of the core sampler and a shield at ground level only were unsuccessful. To reduce vibration caused by sledge hammering, one core sampler was pushed into the ground with an hydraulic jack. The results from this trial indicated no carry-down; however, the use of hydraulic methods did not appear feasible, but it did suggest that some method of reducing the vibration of the sampler, and subsequent enlarging of the hold, was needed.

Soil stabilization, using a freshly prepared polystyrene resin, was next tested. A beveled core sampler was driven in with a sledge hammer through the resin wetted area. The desired effect of keeping the hole small was obtained. The results (No. 3, Table G.1) indicated essentially no carrydown. The sampling technique adopted was: (1) premix polysterene resin, (2) pour on selected site, (3) drive core sampler in with sledge hammer, (4) open the core sampler, (5) rotate the entire sampler several times, and (6) close and withdraw.

All the core samplers were beveled and each was steam cleaned to remove any traces of oil, just prior to use.

It was recognized that the core sampler would not define the radioactivity in the top three inches of soil. Therefore, surface samples were taken with glass jars at each core sampling area.

The polystyrene resin formulation used consisted of the following: 300 ml polystyrene resin, 75 ml methyl ethyl butane, 45 ml styrene, 12 ml lupersol, and 15 ml Nuodex (cobalt napthenate).

The methyl ethyl butane and styrene were added to reduce the viscosity of the resin sufficiently to penetrate into the soil. The first four components were mixed together in the laboratory and the Nuodex was added in the field just prior to use.

Lip samples for Shot 7 were taken in the following manner: after obtaining intensity levels around the crater lip from Rad-Safe and project aerial survey missions, 4 men (2 in each of two $^3/_4$-ton trucks) drove to the starting point which was the 100 mr/hr line away from the crater-lip area and on the first leg that core samples were taken. At this point the sampling team checked its equipment and procedures. Each member received a numbered core sampler and sample jar, sledge hammer and a bottle of polystyrene resin formulation. The resin was freshly mixed at the starting point as described above. The lead man carried a rope, 120 feet long, with knots at 30-foot intervals to mark sampling positions. When ready to take samples, the sampling team drove in as close as possible to the crater. Getting out of the vehicle, the lead man dragged the knotted rope to the top edge of the lip near the crater and took samples at that position. The other men proceeded to the located sampling positions, poured the resin on the ground, picked up a surface sample and took a core sample. Intensity readings were taken at each sampling position before returning to the vehicles. This procedure was repeated at other locations with the team members rotating positions.

Crater samples were taken in essentially the same manner as described above except that the men and equipment were lowered into the crater with the aid of ropes and more time was available since the activity had decayed down appreciably when this phase of the operation was carried out (D + 97 days).

TABLE G.1 "CARRY-DOWN" BY CORE SAMPLERS

Slot Number	Depth in Inches	Specific Activity (cpm/gm)		
		No. 1 Plain Core Sampler	No 2 Beveled Core Sampler	No 3 Beveled with Surface Stabilized
1	2-4	5,600	1,090	0
2	5-7	9,400	900	125
3	10-14	6,900	740	0
4	16-20	1,700	860	24
5	22-26	4,100	860	0
6	28-32	1,930	820	0
7	34-38	74	910	0
Surface Reading		100 mr/hr	30 mr/hr	

TABLE G.2 CORE SAMPLER ACTIVITY DATA (D + 97—99 Days)

Samples taken at NL, NM, NN, NO, SM, EM, WL, EL, SA, and SL indicated background only.

Depth Below Surface in Feet	Activity, cpm per 3 grams	Percent of Total Activity	Cumulative Percent	Activity, cpm per 3 grams	Percent Total Activity	Cumulative Percent
	Location NA			Location NB		
0	7.0×10^3	26.94	26.94	1.0×10^4	13.37	13.37
0.5	1.2×10^4	46.19	73.13	1.5×10^4	20.05	33.42
1.0	0.5×10^4	19.25	92.38	2.2×10^4	29.41	62.83
1.5	1.0×10^3	3.85	96.23	1.9×10^4	25.40	88.23
2.0	3.0×10^2	1.15	97.38	7.0×10^3	9.36	97.59
2.5	2.1×10^2	0.81	98.19	1.2×10^3	1.60	99.19
3.0	2.5×10^2	0.96	99.15	3.7×10^2	0.49	99.68
3.5	2.2×10^2	0.85	100.00	2.3×10^2	0.31	100.00
	Location NC			Location ND		
0	1.6×10^4	14.50	14.50	2.1×10^4	31.29	31.29
0.5	3.0×10^4	27.19	41.69	1.5×10^4	22.35	53.64
1.0	2.8×10^4	25.37	67.06	1.4×10^4	20.86	74.50
1.5	2.3×10^4	20.84	87.90	1.3×10^4	19.37	93.87
2.0	1.0×10^4	9.06	96.96	2.6×10^3	3.87	97.74
2.5	2.0×10^3	1.81	98.77	1.0×10^3	1.49	99.23
3.0	7.5×10^2	0.68	99.45	3.3×10^2	0.49	99.72
3.5	6.0×10^2	0.54	100.00	1.8×10^2	0.27	100.00
	Location NE			Location NF		
0	1.1×10^4	19.40	19.40	2.1×10^4	26.53	26.53
0.5	1.5×10^4	26.45	45.85	1.8×10^4	22.74	49.27
1.0	1.5×10^4	26.45	72.30	1.9×10^4	24.01	73.28
1.5	1.0×10^4	17.63	89.93	1.2×10^4	15.16	88.44
2.0	3.2×10^3	5.64	95.57	3.8×10^3	4.80	93.24
2.5	1.1×10^3	1.94	97.51	8.5×10^2	1.07	94.31
3.0	1.2×10^3	2.12	99.63	2.5×10^3	3.16	97.47
3.5	2.1×10^2	0.37	100.00	2.0×10^3	2.53	100.00
	Location NP			Location EA		
0	3.0×10^3	2.80	2.80	1.8×10^4	24.53	24.53
0.5	2.1×10^4	19.63	22.43	2.5×10^4	34.07	58.60
1.0	1.7×10^4	15.89	38.32	2.3×10^4	31.34	89.94
1.5	1.8×10^4	16.82	55.14	4.0×10^3	5.45	95.39
2.0	1.4×10^4	13.08	68.22	1.7×10^3	2.32	97.71
2.5	1.5×10^4	14.02	82.24	6.8×10^2	0.93	98.64
3.0	7.0×10^3	6.54	88.78	4.0×10^2	0.55	99.19
3.5	1.2×10^4	11.21	100.00	6.0×10^2	0.82	100.00

[redacted]

TABLE G.2 CONTINUED

Samples taken at NL, NM, NN, NO, SM, EM, WL, EL, SA, and SL indicated background only.

Depth Below Surface in Feet	Activity, cpm per 3 grams	Percent of Total Activity	Cumulative Percent	Activity, cpm per 3 grams	Percent Total Activity	Cumulative Percent
	Location EB			Location EC		
0	3.0×10^4	24.39	24.39	4.2×10^4	30.32	30.32
0.5	2.8×10^4	22.76	47.15	6.0×10^3	4.33	34.65
1.0	2.8×10^4	22.76	69.91	2.9×10^4	20.94	55.59
1.5	2.4×10^4	19.51	89.42	2.0×10^4	14.44	70.03
2.0	8.0×10^3	6.50	95.92	1.7×10^4	12.27	82.30
2.5	1.9×10^3	1.54	97.46	5.0×10^3	3.61	85.91
3.0	2.1×10^3	1.71	99.17	4.5×10^3	3.25	89.16
3.5	1.0×10^3	0.81	100.00	1.5×10^4	10.83	100.00
	Location ED			Location EE		
0	5.0×10^3	4.50	4.50	—	—	—
0.5	6.0×10^3	5.40	9.90	—	—	—
1.0	1.6×10^4	14.48	24.30	1.0×10^4	8.45	8.45
1.5	1.7×10^4	15.30	39.60	2.2×10^4	18.58	27.03
2.0	3.3×10^4	29.70	69.30	1.7×10^4	14.36	41.39
2.5	2.7×10^4	24.30	93.60	6.6×10^4	55.74	97.13
3.0	5.0×10^3	4.50	98.10	2.5×10^3	2.11	99.24
3.5	2.1×10^3	1.89	100.00	9.0×10^2	0.76	100.00
	Location EF			Location WA		
0	2.0×10^4	18.52	18.52	2.1×10^4	21.91	21.91
0.5	—	—	—	2.5×10^4	26.08	47.99
1.0	2.4×10^4	22.22	40.74	2.3×10^4	24.00	71.99
1.5	2.4×10^4	22.22	62.96	2.3×10^4	24.00	95.99
2.0	2.1×10^4	19.44	82.40	2.6×10^3	2.71	98.70
2.5	1.2×10^4	11.11	93.51	6.0×10^2	0.63	99.33
3.0	6.0×10^3	5.56	99.07	2.9×10^2	0.30	99.63
3.5	1.0×10^3	0.93	100.00	3.6×10^2	0.38	100.00
	Location WB			Location WC		
0	2.1×10^4	33.31	33.31	2.4×10^4	36.31	36.31
0.5	2.3×10^4	36.48	69.79	—	—	—
1.0	1.2×10^4	19.03	88.82	—	—	—
1.5	2.5×10^3	3.97	92.79	1.2×10^4	18.15	54.46
2.0	3.0×10^3	4.76	97.55	1.5×10^4	22.69	77.15
2.5	7.5×10^2	1.19	98.74	1.1×10^4	16.64	93.79
3.0	4.0×10^2	0.63	99.37	2.0×10^3	3.03	96.82
3.5	4.0×10^2	0.63	100.00	2.1×10^3	3.18	100.00
	Location WD			Location WE		
0	2.0×10^4	16.33	16.33	5.0×10^4	33.33	33.33
0.5	2.2×10^4	17.96	34.29	—	—	—
1.0	2.1×10^4	17.14	51.43	—	—	—
1.5	2.0×10^4	16.33	67.76	—	—	—
2.0	1.2×10^4	9.80	77.15	—	—	—
2.5	1.0×10^4	16.64	93.79	—	—	—
3.0	1.0×10^4	3.03	96.82	5.0×10^4	33.33	66.66
3.5	7.5×10^3	3.18	100.00	5.0×10^4	33.33	100.00
	Location WF			Location WM		
0	6.0×10^4	41.38	41.38	6.0×10^2	8.82	8.82
0.5	—	—	—	7.5×10^2	11.03	19.85
1.0	—	—	—	8.5×10^2	12.50	32.35
1.5	—	—	—	2.0×10^3	29.41	61.76
2.0	—	—	—	6.5×10^2	9.56	71.32
2.5	—	—	—	8.0×10^2	11.76	83.08
3.0	3.5×10^4	24.14	65.52	1.0×10^3	14.71	97.79
3.5	5.0×10^4	34.48	100.00	1.5×10^2	2.21	100.00

[redacted]

TABLE G.2 CONTINUED

Samples taken at NL, NM, NN, NO, SM, EM, WL, EL, SA, and SL indicated background only.

Depth Below Surface in Feet	Activity, cpm per 3 grams	Percent of Total Activity	Cumulative Percent	Activity, cpm per 3 grams	Percent Total Activity	Cumulative Percent
	Location WP			Location WN		
0	4.0×10^3	4.76	4.76	2.3×10^2	1.38	1.38
0.5	4.0×10^3	4.76	9.52	9.0×10^3	54.02	55.40
1.0	4.0×10^3	4.76	14.28	2.5×10^3	15.01	70.41
1.5	1.0×10^4	11.90	26.18	2.0×10^3	12.00	82.41
2.0	1.7×10^4	20.24	46.42	1.3×10^3	7.80	90.21
2.5	1.7×10^4	20.24	66.66	9.0×10^2	5.40	95.61
3.0	1.3×10^4	15.48	82.14	3.7×10^2	2.22	97.83
3.5	1.5×10^4	17.86	100.00	3.6×10^2	2.16	100.00
	Location SB			Location SC		
0	1.7×10^4	31.40	31.40	3.6×10^3	4.24	4.24
0.5	1.4×10^4	25.86	57.26	2.2×10^4	25.92	30.16
1.0	1.5×10^4	27.71	84.97	2.1×10^4	24.74	54.90
1.5	6.0×10^3	11.08	96.05	1.9×10^4	22.38	77.28
2.0	9.7×10^2	1.79	97.84	1.1×10^4	12.96	90.24
2.5	5.0×10^2	0.92	98.76	6.0×10^3	7.07	97.31
3.0	4.1×10^2	0.76	99.52	1.7×10^3	2.00	99.31
3.5	2.6×10^2	0.48	100.00	5.8×10^2	0.68	100.00
	Location SD			Location SE		
0	1.1×10^4	9.92	9.92	2.2×10^4	20.40	20.40
0.5	1.3×10^4	11.72	21.64	2.1×10^4	19.48	39.88
1.0	1.6×10^4	14.43	36.07	1.8×10^4	16.69	56.57
1.5	4.0×10^4	36.08	72.15	2.0×10^4	18.55	75.12
2.0	3.0×10^4	27.06	99.21	1.4×10^4	12.98	88.10
2.5	4.5×10^2	0.41	99.62	9.0×10^3	8.35	96.45
3.0	2.3×10^2	0.21	99.83	3.5×10^3	3.25	99.70
3.5	2.0×10^2	0.18	100.00	3.2×10^2	0.30	100.00
	Location SF			Location SN		
0	5.0×10^4	20.75	20.75	1.7×10^2	4.31	4.31
0.5	—	—	—	1.8×10^2	4.57	8.88
1.0	—	—	—	2.7×10^2	6.85	15.73
1.5	—	—	—	3.0×10^2	7.61	23.34
2.0	5.0×10^4	20.75	41.50	4.8×10^2	12.18	35.52
2.5	4.3×10^4	17.84	59.34	4.4×10^2	11.17	46.69
3.0	3.8×10^4	15.77	75.11	1.2×10^3	30.46	77.15
3.5	6.0×10^4	24.90	100.00	9.0×10^2	22.84	100.00
	Location SO					
0	2.3×10^2	3.87	3.87			
0.5	2.0×10^2	3.37	7.24			
1.0	2.6×10^2	4.38	11.62			
1.5	9.5×10^2	15.99	27.61			
2.0	9.0×10^2	15.15	42.76			
2.5	7.0×10^2	11.78	54.54			
3.0	2.5×10^3	42.09	96.63			
3.5	2.0×10^2	3.37	100.00			

Core sampler activity data obtained on D+ 97 to 99 days are presented in Table G.2.

Descriptions of the sampling stations where core samples were taken are as follows (letters refer to locations around the crater-lip area as indicated in Figure 2.14):

L, surrounded by eroded cliffs; west, south, and north, taken between existing cliffs in soft, loose ground composed of fines and small pebbles, east taken on a cliff which was of moderate hardness and composed of fines, small pebbles and rocks.

M, just below cliffs; ground soft and loose, composed of fines and medium sized pebbles.

N, on open slope; soil sandy to pebbly.

O, on open slope just above the flat bottom; definite vertical stratifications varying from gravel to small rock; ground was loose.

P, flat bottom covered with rocks and small boulders which in turn covered a firm packed sand bottom into which the sampler could be easily driven.

A, juncture of the lip and crater; west and east broken down and flat; north and south were sharp; soil was composed of fines and pebbles.

B, at the edge of the high portion of the lip; fines and pebbles.

C, on shallow portion of the lip with occasional dunes; fines and pebbles.

D, on shallow portion of the lip with occasional dunes; fines and pebbles.

E, on flat portion of the lip; fines and pebbles; west, south, and east core samplers apparently hit ground about 2–3 feet down.

F, on flat portion of the lip; fines and pebbles; core sampler apparently hit hard ground at about 1 foot on the west, south, and east radii.

[redacted]

Appendix H

FOUR-PI COUNTING

A four-pi flow counter was constructed similar to one shown in Figure H.1 and Reference 48, except that a cylindrical counting chamber with a 5-inch diameter window was used. The counters were operated in the Geiger region. The corrections that were made were essentially those described in Reference 49.

A dissolved sample was evaporated on the surface of the window and then placed between the counters. This was kept as small as possible, taking into consideration the activity necessary for a long term decay sample. It was hoped to compare this with a solid portion of the same sample in the standard radiophysics defined geometry counting setup as shown in Figure H.2 and described in detail in Reference 29.

In the dissolution of the sample certain nuclides were known to be lost. It was intended to correct for this loss when the comparison was made with the solid sample. However, it appears that other nuclides

TABLE H.1 COMPARISON OF COUNTING TECHNIQUES

Time	Defined Geometry	Four Pi	Percent Difference
hour	cpm	cpm	
316	73,900	72,000	3
1008	36,600	34,000	7
1194	29,300	28,300	5
1368	25,600	23,900	6

are partially or totally lost and no correction could be made for these. It was therefore necessary to compare the four-pi count with a count of an evaporated dissolved sample in the defined geometry system. A sample with mass comparable to the mass of dry samples, used in the test, was made. The comparison was made at various times. The values are tabulated in Table H.1.

The difference between the two values is not necessarily an indication that the defined geometry system is this much in error. In the correction that was made, the rubber hydrochloride film[1] (Section 2.3.2) was assumed to be thin enough to make the backscattering negligible in comparison to the film absorption. Because time limitations in procurement made it necessary to use a rather thick Mylar film (2.2 mg/cm^2) in the four-pi counting, this assumption may be in error. However, the closeness of the two values does indicate that, within reasonable error, the values given are absolute measurements.

[1] Rubber hydrochloride film is available from the Reed Laboratories, Akron, Ohio.

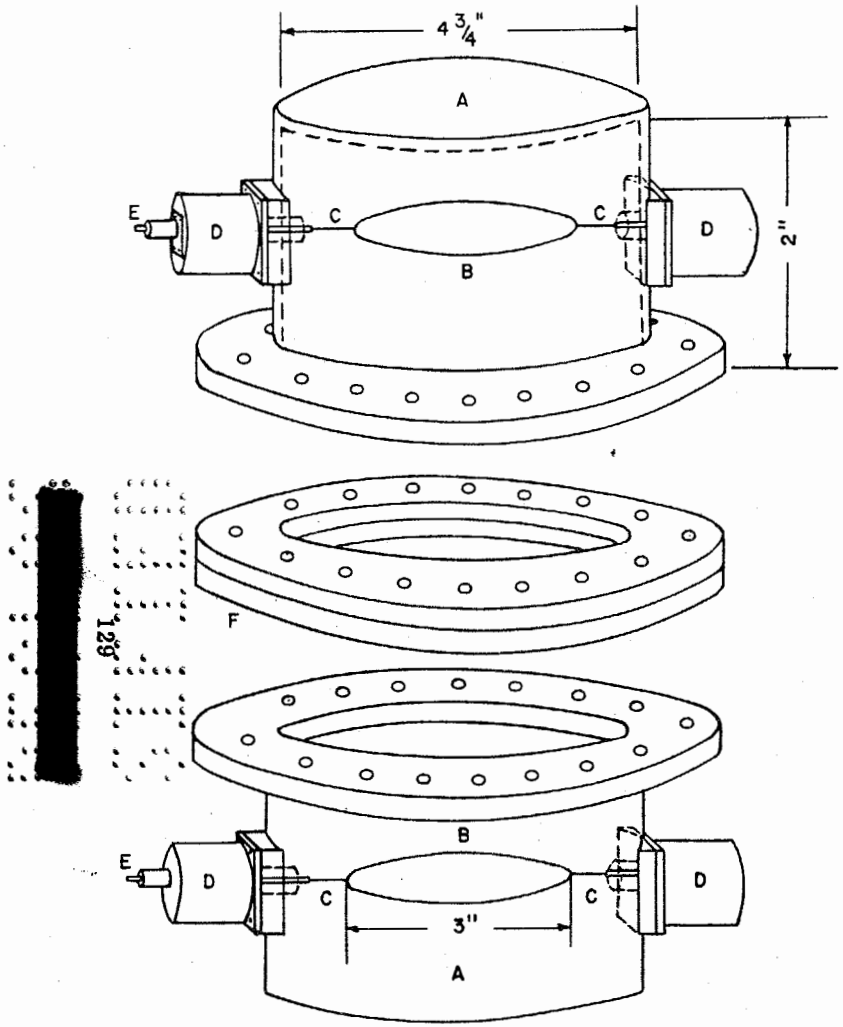

A. Cylindrical counter tube, brass
B. Anode, 3 mil nichrome wire
C. Hypodermic needle, #20 guage
D. Anode safety caps, steel
E. Connector, amphenol
F. Window, Mylar, 2 mg/cm²; between brass rings

Figure H.1 Four-pi flow counter.

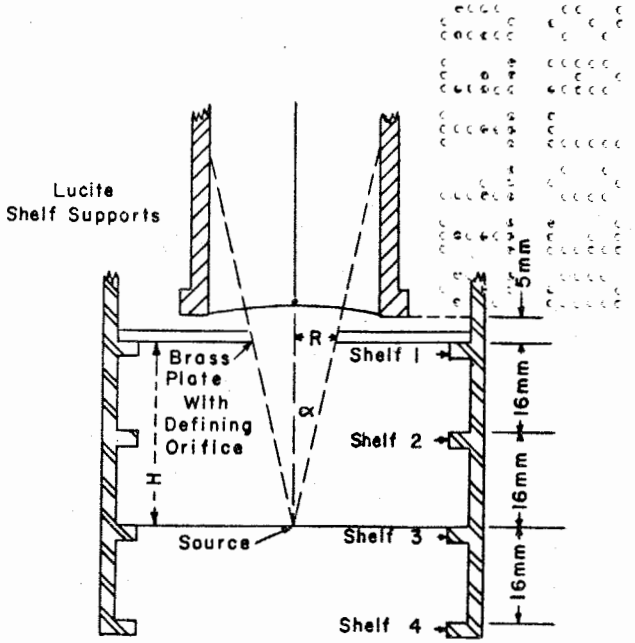

Figure H.2 Defined geometry counting setup.

Appendix I

TREATMENT OF DECAY CURVES FOR THE EXTRAPOLATION OF ACTIVITIES

A statistical analysis was made of all decay curves to determine if there were any significant variation in the decay curves of the different samples under consideration. The most desirable method of test for this variance in the samples is the analysis of slopes. Using the 99 percent confidence level, it was found that no significant variance was observed.

The assumption that so many samples from different time periods after shot and different geographic locations fractionated the same way is not probable; therefore, it was assumed that no fractionation existed. The Hunter and Ballou curve, a mathematical determination of slow-fission-product activity, was a reasonable representation of the sample fission activity. The validity of this was further indicated by the close fit of the theoretical curve to the experimental data (top curve in Figure 3.37 which is the Hunter-Ballou curve plus capture activities).

It will be noted that the assumption of no fractionation is in apparent disagreement with the work done by the Radiochemistry Section of these laboratories. It must be remembered that the degree of sensitivity of the two techniques for the measurement of fractionation of certain nuclides may be entirely different. For a statistically significant variation of gross activity in the decay curves, the variation must be of the order of magnitude of 3 percent. It can be seen that nuclides contributing little to the activity can vary considerably without the detection of the variation by this method. Variation of several nuclides may tend to cancel, thus adding to the insensitivity of the method.

Although no significant variation was found in the region where decay curves were measured, 48 to 3,000 hours, this is not an indication that no variation exists in other portions of the curve. The assumption of no variation over the entire curve is made only because no other information is available. It appears, however, that for the extrapolation to one hour no significant error is encountered.

As in previous tests, it has been determined that a large amount of uranium-neutron capture activity is present in the samples along with the fission-yield activity. It would have been desirable to estimate this capture activity by the same manner as that used in Operation Castle, Reference 16, but sufficient yield data were not available for the type weapons used in this test. U^{237}, U^{239}, U^{240}, Np^{238}, Np^{240}, are found to be significant contributors to the neutron capture activity. It was decided to determine the contribution of each by best fit to the experimentally determined decay curve. This was done in the following manner:

$$A_t = \alpha \left[A_{U^{239}} + A_{Np^{239}} + (A_{U^{240}} + A_{Np^{240}}) \right] + \beta A_{U^{237}} + \gamma A_F \qquad (I.1)$$

Where: A_t = total activity
A_F = fission product activity (The time dependence of A_F is taken to be the standard Hunter-Ballou curve for fission product decay.)

It will be indicated that: $A_{Np^{239}} = 0.00699\ A_{U^{239}}$

$A_{Np^{240}} = 1.01\ A_{U^{240}}$

$A_{U^{240}} = 0.00725\ A_{U^{239}}$

The following equation was solved by simultaneous equations for the constants α, β, and γ using experimental points from the decay curve:

$$A_t = \alpha \left[e^{-1.77t} + 0.00699e^{-0.0124t} + 0.0147e^{-0.0495t} \right] + \beta e^{-0.00431t} + \gamma A_F \qquad (I.2)$$

The relative amounts of Np^{239} and Np^{240} are known from parent-daughter relationship. Since Np^{240} is a daughter of U^{240} an equilibrium situation exists after a short time. This gives an apparent decay of the

U^{240} half-life for the parent-daughter equilibrium. The contributions of U^{237} and U^{239} are determined by solution of simultaneous equations. The relative amount of U^{240} could not be determined by the simultaneous equation solution because of the insensitivity of the curve to variations of this constituent. Therefore, the Castle Shot Bravo value was used. The value is not critical because at time "one" the activity amounts to less than 5 percent of the total. The resulting values are $\alpha = 21{,}900$, $\beta = 18.5$ and $\gamma = 37.0$. The final equation is:

$$A_t = 21{,}900 \left[e^{-1.77t} + 0.00699e^{-0.0124t} + 0.0147e^{-0.0495t} \right] + 18.5e^{-0.00431t} + 37.0\, A_F \qquad \text{(I.3)}$$

The activities calculated from Equation I.3 are found in Table I.1 along with experimental values. Both sets of values are in close agreement with each other and a plot of the experimental points indicates the close fit to the theoretical curve.

TABLE I.1 FISSION SAMPLE ACTIVITY VERSUS TIME

Time	Calculated Activity	Experimental Activity
hour		
1	6490	—
48	156	155
84	85.5	86.0
187	30.0	37.0
244	19.0	18.4
507	4.81	4.51
716	2.52	2.55
887	1.70	1.83
1055	1.25	1.45
1559	0.687	0.778
2064	0.488	0.484

Appendix J

CALCULATION OF THEORETICAL CAPTURE EFFICIENCIES FOR PARTICLE DIAMETERS BETWEEN 0.1 AND 100 MICRONS

Let A denote the cross-sectional area of the port or opening of a horizontal sampling tube. A particle having a horizontal velocity component equal to V_w and a settling velocity equal to V_s moves toward the sampling port along a line with a slope equal to $\tan(V_s/V_w)$. The particle "sees" a sampling port with cross-sectional area given by $A \cos \theta$, where $\theta = \arctan (V_s/V_w)$. Thus, the effective cross-sectional area of the sampling tube is reduced. The capture efficiency of the sampling port may be defined as the ratio of the effective sampling area to the true sampling area. Thus,

$$e = \frac{A \cos \theta}{A} = \cos \theta = \sqrt{\frac{1}{1 + (V_s/V_w)^2}} \qquad (J.1)$$

and it follows that maximum capture efficiency is obtained for particles having small settling velocities compared with the wind velocity.

To determine the particle sizes which correspond to a given capture efficiency, the above equation is solved for V_s in terms of V_w and e. This yields

$$V_s = \left(\sqrt{(1/e)^2 - 1}\right) V_w \qquad (J.2)$$

Thus, if the capture efficiency and wind velocity are prescribed, the preceding equation yields a unique settling velocity. From a corrected form of Stoke's law, the particle size corresponding to the resulting settling velocity may be determined. This yields a critical diameter, d*, having the property that all particles having diameters less than d* are captured by the sampling port with an efficiency greater than e.

Table J.1 shows the calculated settling velocities of particles with diameters ranging between 0.1 and 100 microns. These velocities were calculated using Davies equation (Reference 50) which corrects Stoke's law for slip. The particles having a density of 2.6 were assumed to be dispersed in air at 20 C, 760 mm pressure.

Table J.2 shows the expected sampling results based on a capture efficiency of 0.99 and wind velocities between 1 and 10 mph. The table shows, for example, that the capture efficiency is greater than 99 percent for all particles having a diameter less than 25 microns when a horizontal wind velocity of 1 mile per hour prevails. Increased wind velocity increases the range of particle sizes captured.

Figure J.1 shows a plot of capture efficiency as a function of particle diameter for horizontal wind velocities of 1 and 5 mph. With a horizontal wind velocity of 5 mph, the capture efficiency exceeds 0.97 for all particles in the range of 0.1 to 100 microns.

The results of this limited study indicate that, for velocities above 5 mph, the particle settling velocity will have almost no effect on the collection efficiency of particles in the size range of 0.1 to 100 microns.

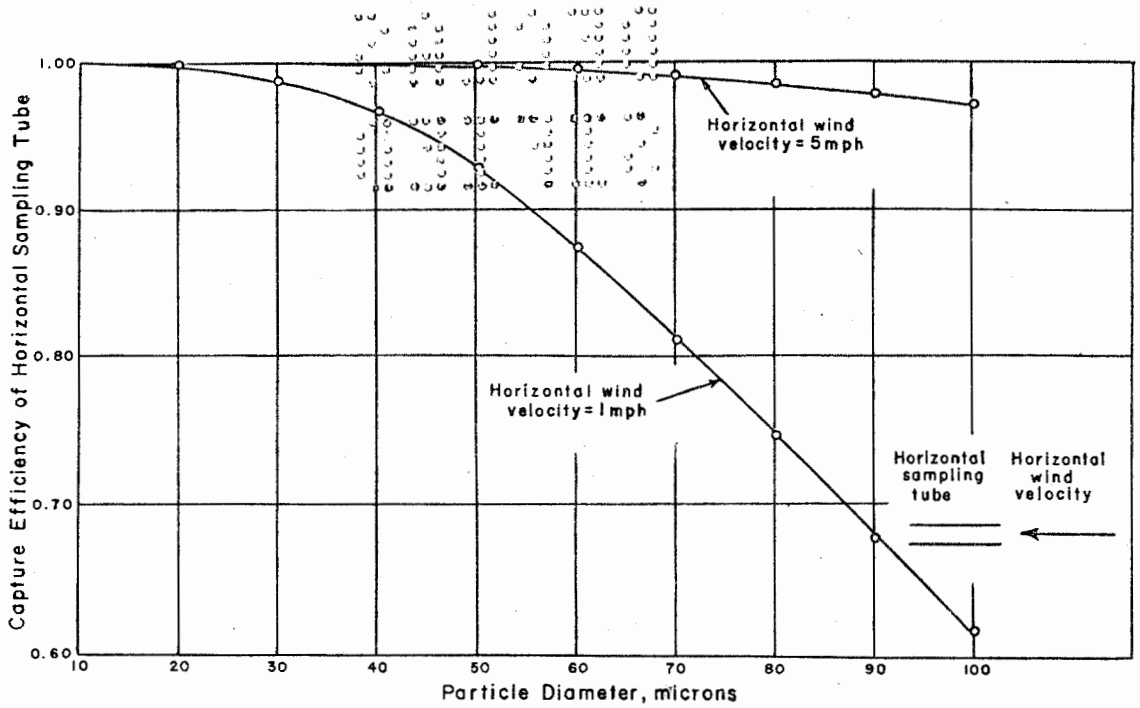

Figure J.1 Capture efficiency as a function of particle diameter.

TABLE J.1 SETTLING VELOCITIES OF PARTICLES IN AIR WITH DENSITY OF 2.6 gm/cm^3 IN AIR AT 20 DEGREES CENTIGRADE AND 760 mm PRESSURE

Particle diameter, d	Settling Velocity, V_s
microns	mph
0.1	5.047×10^{-6}
0.5	6.009×10^{-5}
1.0	2.029×10^{-4}
5.0	4.523×10^{-3}
10.0	1.771×10^{-2}
15.0	3.960×10^{-2}
20.0	6.988×10^{-2}
25.0	1.078×10^{-1}
30.0	1.539×10^{-1}
40.0	2.664×10^{-1}
50.0	4.027×10^{-1}
60.0	5.530×10^{-1}
70.0	7.143×10^{-1}
80.0	8.888×10^{-1}
90.0	1.081
100.0	1.276

TABLE J.2 RANGE OF PARTICLE SIZE CAPTURED WITH MORE THAN 99 PERCENT EFFICIENCY

Wind Velocity	Range of Particle Diameters
mph	microns
1	0-25
5	0-70
10	0-100

REFERENCES

1. S. Glasstone; "The Effects of Nuclear Weapons"; June 1957, Page 46; U.S. Government Printing Office, Washington, D.C.; Unclassified.

2. M.G. Schorr and E.S. Gilfillan; "Predicted Scaling of Radiological Effects to Operational Weapons"; Project 2.0, Operation Jangle, WT-391, June 1952, Page 29; Technical Operations Inc., Arlington, Massachusetts; Secret Restricted Data.

3. G.A. Young; "Base Surge Analysis – HE Tests"; Project 1 (9)-4, Operation Jangle, WT-339, May 1952; U.S. Naval Ordnance Laboratory, White Oak, Maryland; Confidential.

4. G.A. Young and M.L. Milligan; "Base Surge Analysis for Nuclear Tests"; Project 1 (9)b, Operation Jangle, WT-390, June 1952; U.S. Naval Ordnance Laboratory, White Oak, Maryland; Secret Restricted Data.

5. R.C. Tompkins and P.W. Krey; "Radiochemical Analysis of Fallout"; Project 2.6b, Operation Castle, WT-918, February 1956; Chemical and Radiological Laboratories, Army Chemical Center, Maryland; Secret Restricted Data.

6. R.D. Cadle; "Final Report on the Effects of Soil, Yield, and Scaled Depth on Contamination from Atomic Bombs"; SRI Project CU-641, June 1953, Contract No. DA 18-108-CML-3842; Stanford Research Institute, Stanford, California; Secret Restricted Data.

7. R.L. Willey and others; "Base Surge Measurements by Photography"; Project 1.1c, Operation Castle, WT-903, September 1955; U.S. Naval Ordnance Laboratory, White Oak, Maryland; Secret Restricted Data.

8. S. Glasstone; "The Effects of Atomic Weapons"; June 1950, Pages 33 to 35 and 271 to 275; U.S. Government Printing Office, Washington, D.C.; Unclassified.

9. S. Glasstone; "The Effects of Atomic Weapons"; June 1950, Pages 279 to 285; U.S. Government Printing Office, Washington, D.C.; Unclassified.

10. C.E. Adams and others; "Fallout Phenomenology"; Annex 6.4, Operation Greenhouse, WT-4, August 1951; U.S. Naval Radiological Defense Laboratory, San Francisco, California; Secret Restricted Data.

11. C. Robbins and others; "Particle Studies"; Operation Jangle, WT-371, July 1952; Armed Forces Special Weapons Project, Washington, D.C.; Secret Restricted Data.

12. R.K. Laurino and I.G. Poppoff; "Contamination Patterns at Operation Jangle"; USNRDL-399, April 1953; U.S. Naval Radiological Defense Laboratory, San Francisco, California; Secret Restricted Data.

13. N.M. Lulejian; "Radioactive Fallout from Atomic Bombs"; November 1953; Air Research and Development Command, Baltimore, Maryland; Secret Restricted Data.

14. E.H. Bouton and others; "Fallout and Cloud-Particle Studies"; Project 5.4b, Operation Ivy, WT-617, November 1952; Chemical and Radiological Laboratories, Army Chemical Center, Maryland; Secret Restricted Data.

15. W.B. Heidt, Jr. and others; "Nature, Intensity, and Distribution of Fallout from Mike Shot"; Project 5.4a, Operation Ivy, WT-615, April 1953; U.S. Naval Radiological Defense Laboratory, San Francisco, California; Secret Restricted Data.

16. E.F. Wilsey and others; "Fallout Studies"; Project 2.5b, Operation Castle, WT-916, February 1956; Chemical Warfare Laboratories, Army Chemical Center, Maryland; Secret Restricted Data.

17. R.L. Stetson and others; "Distribution and Intensity of Fallout"; Project 2.5a, Operation Castle, WT-915, January 1956; U.S. Radiological Defense Laboratory, San Francisco, California; Secret Restricted Data.

18. D.C. Borg and others; "Radioactive Fallout Hazards from Surface Bursts of very high Yield Nuclear Weapons"; AFSWP No. 507, May 1954; Armed Forces Special Weapons Project, Washington, D.C.; Secret Restricted Data.

19. "Summary Report, Weapon Effects Tests", Operation Jangle, WT-414, November 1952; Armed Forces Special Weapons Project, Washington, D.C.; Secret Restricted Data.

20. D.C. Campbell; "Some HE Tests and Observations on Craters and Base Surges"; Project 1 (9)-3, Operation Jangle, WT-410, 1952; Armed Forces Special Weapons Project, Washington, D.C.; Secret Restricted Data.

21. "Analysis of Atomic Weapons Effects Programs"; AFSWP-807, July 1954; Armed Forces Special Weapons Project, Washington, D.C.; Secret Restricted Data.

22. M.B. Forbes and others; "Remotely Controlled Sampling Techniques"; Project 2.6a, Operation Jangle, WT-334, February 1952; Signal Corps Engineering Laboratories, Fort Monmouth, New Jersey; Secret.

23. Letter Report, USNRDL File 3-901-756 from E.P. Cooper to Dr. T.G. Walsh, Engineer Research and Development Laboratories, Fort Belvoir, Virginia, dated 29 July 1954; U.S. Naval Radiological Defense Laboratory, San Francisco, California; Confidential.

24. "Capabilities of Atomic Weapons"; TM 23-200, December 1954; Armed Forces Special Weapons Project, Washington D.C.; Secret Restricted Data.

25. W.A. Spraker and others; "Final Report on Development of a Radioactive-Dust Collector"; Contract No. DA 18-108-CML-5095, September 1954; Battelle Memorial Institute, Columbus, Ohio; Unclassified.

26. R.H. Sugarman and E.C. Ellstrom; "Helicopter to Ground Radiological Survey Equipment"; Technical Memorandum No. M-1541, October 1953; Evans Signal Laboratory, Belmar, New Jersey; Unclassified.

27. J.P. Johnson and others; "Description and Operation of Chemical Corps Helicopter to Ground Aerial Instrument"; CWLR to be published; Chemical Warfare Laboratories, Army Chemical Center, Maryland; Unclassified.

28. "Instruction Manual Mobile Land Survey Radiation Recorder"; Contract No. DA 18-108-CML-759, February 1954; Tracerlab Inc., Boston, Massachusetts; Unclassified.

29. G.I. Gleason and others; "Absolute Beta Counting at Defined Geometries"; Nucleonics Vol. 8, No. 5, May 1951, Pages 12 to 21; McGraw-Hill Publishing Company, New York; Unclassified.

30. T.P. Kohman; "A General Method for Determining Coincidence Corrections of Counting Instruments"; Bulletin MDDC-905, June 1945; U.S. Atomic Energy Commission, Oak Ridge, Tennessee; Unclassified.

31. B.P. Burtt, "Absolute Beta Counting"; Nucleonics Vol. 5. No. 2, August 1949, Pages 28 to 43; McGraw-Hill Publishing Company, New York, N. Y.; Unclassified.

32. G.I. Gleason and others; "Absolute Beta Counting at Defined Geometries"; Nucleonics Vol. 8, No. 5, May 1951, Pages 15 to 18; McGraw-Hill Publishing Company, New York, N. Y.; Unclassified.

33. C.D. Coryell and N. Sugarman; "Radiochemical Studies: The Fission Products"; Book I, 1951; McGraw-Hill Publishing Company, New York, N.Y.; Unclassified.

34. H.F. Hunter and N.E. Ballou; "Simultaneous Slow Neutron Fission of U^{235} Atoms. I. Individual and Total Rates of Decay of the Fission Products"; ADC-65, April 1949; U.S. Naval Radiological Defense Laboratory, San Francisco, California; Unclassified.

35. F. Gabbard and others; "Absolute Beta Measurement of Mixed Nuclides"; CRLR 561, March 1956; Chemical and Radiological Laboratories, Army Chemical Center, Maryland; Unclassified.

36. "Tentative Method for Subsieve Analysis of Granular Metal-Powders by Air Classification"; M.P.A. Standard 12-51T, January 1951; Metal Powder Association, New York, N.Y.; Unclassified.

37. J.B. Graham and G. Carp; "Gamma Dose Rate versus Time and Distance"; Project 2.4, Operation Teapot, ITR-1118, May 1955; Evans Signal Laboratory, Belman, New Jersey; Confidential Restricted Data.

38. R.G. Larrick and others; "Gamma Exposure versus Distance"; Project 2.1, Operation Teapot, ITR-1115, May 1955; Evans Signal Laboratory, Belmar, New Jersey; Secret Restricted Data.

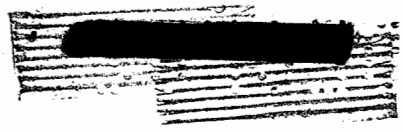

39. B.H. Grossman and L. Machta. "Atomic Cloud Growth Study"; Project 9.4, Operation Teapot, ITR-1152; Air Force Cambridge Research Center, Cambridge, Massachusetts; Secret Restricted Data.

40. G.S. Layne and P.W. Krey; "Radiochemical Analyses and their Interpretation of Base Surge and Crater Lip Samples"; Operation Teapot, CWLR to be published; Chemical Warfare Laboratories, Army Chemical Center, Maryland; Secret

41. P.V. Barrans and R.E. Brueckmann; "Test of Two Jordan Electronic Mfg. Co. Model AGB-10-SR Survey Meters"; NBS Report 4653, April 1956; National Bureau of Standards, Washington, D.C.; Official Use Only.

42. J.P. Johnson and M. Morgenthau; "Description of Aerial Radiological Survey Methods"; CWLR 2174 to be published; Chemical Warfare Laboratories, Army Chemical Center, Maryland; Unclassified.

43. "Capabilities of Atomic Weapons"; TM 23-200, June 1955, including Changes 1 and 2; Armed Forces Special Weapons Project, Washington, D.C.; Confidential.

44. C.F. Ksanda and others; "Scaling of Contamination Patterns, Surface and Underground Detonations"; USNRDL-TR-1, September 1953; U.S. Naval Radiological Defense Laboratory, San Francisco, California; Secret Restricted Data.

45. M. Ehrlich; "Photographic Dosimetry of X- and Gamma Rays"; Handbook 57, August 1954, Page 10; National Bureau of Standards, U.S. Department of Commerce, Washington, D.C.; Unclassified.

46. R.G. Evans and W.H. Van Horn; "Land Reclamation of a Crater Lip Area Using Earth Moving Equipment"; Project 8-12-75-001, November 1956; Engineer Research and Development Laboratories, Fort Belvoir, Virginia; Confidential.

47. C.E. Adams and others; "The Nature of Individual Radioactive Particles. I. Surface and Underground ABD Particles from Operation Jangle"; USNRDL-374, November 1952; U.S. Naval Radiological Defense Laboratory, San Francisco, California; Secret.

48. E.H. Wakefield and C.R. Memhardt; "A Superior Flow Counter, The RCL Counter"; Vol. 2, No. 2, March 1955; Radiation Counter Laboratories, Skokie, Illinois; Unclassified.

49. H.H. Seliger and L. Cavallo; "The Absolute Standardization of Radioisotopes by 4π Counting"; Research Paper 2226, Journal of Research of the Bureau of Standards, Vol. 47, No. 1, July 1951; Pages 41 to 44; U.S. Government Printing Office, Washington, D.C.; Unclassified.

50. C.N. Davies; "The Sedimentation of Small Suspended Particles"; Symposium of Particle Size Analysis, February 1947; Institution of Structural Engineers, London, England; Unclassified.

Distribution

Military Distribution Categories 5-40, 5-45, and 5-70

ARMY ACTIVITIES

1 Asst. Dep. Chief of Staff for Military Operations, D/A, Washington 25, D.C. ATTN: Asst. Executive (R&SW)
2 Chief of Research and Development, D/A, Washington 25, D.C. ATTN: Atomic Division
3- 4 Chief of Ordnance, D/A, Washington 25, D.C. ATTN: ORDTX-AR
5 Chief Signal Officer, D/A, P&O Division, Washington 25, D.C. ATTN: SIGRD-8
6- 7 The Surgeon General, D/A, Washington 25, D.C. ATTN: MEDNE
8- 9 Chief Chemical Officer, D/A, Washington 25, D.C.
10- 11 The Quartermaster General, D/A, Washington 25, D.C. ATTN: Research and Development
12- 14 Chief of Engineers, D/A, Washington 25, D.C. ATTN: ENGNB
15- 16 Chief of Transportation, Military Planning and Intelligence Div., Washington 25, D.C.
17- 19 Commanding General, Headquarters, U. S. Continental Army Command, Ft. Monroe, Va.
20 President, Board #1, Headquarters, Continental Army Command, Ft. Sill, Okla.
21 President, Board #2, Headquarters, Continental Army Command, Ft. Knox, Ky.
22 President, Board #3, Headquarters, Continental Army Command, Ft. Benning, Ga.
23 President, Board #4, Headquarters, Continental Army Command, Ft. Bliss, Tex.
24 Commanding General, Headquarters, First U. S. Army, Governor's Island, New York 4, N.Y.
25 Commanding General, Headquarters, Second U. S. Army, Ft. George G. Meade, Md.
26 Commanding General, Headquarters, Third U. S. Army, Ft. McPherson, Ga. ATTN: ACofS, G-3
27 Commanding General, Headquarters, Fourth U. S. Army, Ft. Sam Houston, Tex. ATTN: G-3 Section
28 Commanding General, Headquarters, Fifth U. S. Army, 1660 E. Hyde Park Blvd., Chicago 15, Ill.
29 Commanding General, Headquarters, Sixth U. S. Army, Presidio of San Francisco, San Francisco, Calif. ATTN: AMGCT-4
30 Commanding General, U.S. Army Caribbean, Ft. Amador, C.Z. ATTN: Cml. Off.
31 Commanding General, USARFANT & MDPR, Ft. Brooke, Puerto Rico
32 Commanding General, Southern European Task Force, APO 168, New York, N.Y. ATTN: ACofS, G-3
33 Commanding General, Eighth U.S. Army, APO 301, San Francisco, Calif. ATTN: ACofS, G-3
34- 35 Commanding General, U.S. Army Alaska, APO 942, Seattle, Wash.
36- 37 Commanding General, U.S. Army Europe, APO 403, New York, N.Y. ATTN: OPOT Div., Combat Dev. Br.
38- 39 Commanding General, U.S. Army Pacific, APO 958, San Francisco, Calif. ATTN: Cml. Off.
40- 41 Commandant, Command and General Staff College, Ft. Leavenworth, Kan. ATTN: ALLLS(AS)
42 Commandant, Army War College, Carlisle Barracks, Pa. ATTN: Library
43 Commandant, The Artillery and Missile School, Ft. Sill, Okla.
44 Secretary, The U.S. Army Air Defense School, Ft. Bliss, Texas. ATTN: Maj. Ergan V. Roth, Dept. of Tactics and Combined Arms
45 Commanding General, Army Medical Service School, Brooke Army Medical Center, Ft. Sam Houston, Tex.
46 Director, Special Weapons Development Office, Headquarters, CONARC, Ft. Bliss, Tex. ATTN: Capt. T. E. Skinner
47 Commandant, Walter Reed Army Institute of Research, Walter Reed Army Medical Center, Washington 25, D. C.
48 Superintendent, U.S. Military Academy, West Point, N. Y. ATTN: Prof. of Ordnance
49 Commandant, Chemical Corps School, Chemical Corps Training Command, Ft. McClellan, Ala.
50- 51 Commanding General, U.S. Army Chemical Corps, Research and Development Command, Washington, D.C.
52- 53 Commanding General, Aberdeen Proving Grounds, Md. ATTN: Director, Ballistics Research Laboratory
54 Commanding General, The Engineer Center, Ft. Belvoir, Va. ATTN: Asst. Commandant, Engineer School
55 Commanding Officer, Engineer Research and Development Laboratory, Ft. Belvoir, Va. ATTN: Chief, Technical Intelligence Branch
56 Commanding Officer, Picatinny Arsenal, Dover, N.J. ATTN: ORDBB-TK
57 Commanding Officer, Frankford Arsenal, Philadelphia 37, Pa. ATTN: Col. Tewes Kundel
58 Commanding Officer, Army Medical Research Laboratory, Ft. Knox, Ky.
59- 60 Commanding Officer, Chemical Warfare Laboratories, Army Chemical Center, Md. ATTN: Tech. Library
61 Commanding Officer, Transportation R&D Station, Ft. Eustis, Va.
62 Commandant, The Transportation School, Ft. Eustis, Va. ATTN: Security and Information Officer
63 Director, Technical Documents Center, Evans Signal Laboratory, Belmar, N.J.
64 Director, Waterways Experiment Station, PO Box 631, Vicksburg, Miss. ATTN: Library
65 Director, Armed Forces Institute of Pathology, Walter Reed Army Medical Center, 6825 16th Street, N.W., Washington 25, D.C.
66 Operations Research Office, Johns Hopkins University, 6935 Arlington Rd., Bethesda 14, Md.
67- 68 Commanding General, Quartermaster Research and Development, Command, Quartermaster Research and Development Center, Natick, Mass. ATTN: CBR Liaison Officer
69 Commandant, U.S. Army Aviation School, Fort Rucker, Ala.
70 President, U.S. Army Aviation Board, CONARC, Fort Rucker, Ala.
71 Commanding Officer, Diamond Ordnance Fuze Laboratories, Washington 25, D.C., ATTN: Coordinator, Atomic Weapons Effects Tests
72- 73 Commanding General, Quartermaster Research and Engineering Command U.S. Army, Natick, Mass.
74- 78 Technical Information Service Extension, Oak Ridge, Tenn.

NAVY ACTIVITIES

79- 80 Chief of Naval Operations, D/N, Washington 25, D. C. ATTN: OP-36
81 Chief of Naval Operations, D/N, Washington 25, D.C. ATTN: OP-03EG
82- 83 Chief, Bureau of Medicine and Surgery, D/N, Washington 25, D.C. ATTN: Special Weapons Defense Div.
84 Chief, Bureau of Ordnance, D/N, Washington 25, D.C.
85 Chief of Naval Personnel, D/N, Washington 25, D.C.
86- 87 Chief, Bureau of Ships, D/N, Washington 25, D.C. ATTN: Code 348
88 Chief, Bureau of Yards and Docks, D/N, Washington 25, D.C. ATTN: D-440
89 Chief, Bureau of Supplies and Accounts, D/N, Washington 25, D.C.
90- 91 Chief, Bureau of Aeronautics, D/N, Washington 25, D.C.
92 Chief of Naval Research, Department of the Navy Washington 25, D.C. ATTN: Code 811
93 Commander-in-Chief, U.S. Atlantic Fleet, U.S. Naval Base, Norfolk 11, Va.

[redacted]

94- 97 Commandant, U.S. Marine Corps, Washington 25, D.C. ATTN: Code A03H
98 President, U.S. Naval War College, Newport, R.I.
99 Superintendent, U.S. Naval Postgraduate School, Monterey, Calif.
100 Commander, Joint Task Force Seven, Arlington Hall Station, Arlington 12, Va., ATTN: TS and RD
101 Commanding Officer, U.S. Naval Schools Command, U.S. Naval Station, Treasure Island, San Francisco, Calif.
102 Commanding Officer, U.S. Fleet Training Center, Naval Base, Norfolk 11, Va. ATTN: Special Weapons School
103-104 Special Weapons Unit, Pacific, U.S. Naval Air Station, North Island, San Diego 35, Calif.
105 Commanding Officer, Air Development Squadron 5, VX-5, China Lake, Calif.
106 Commanding Officer, U.S. Naval Damage Control Training Center, Naval Base, Philadelphia, Pa. ATTN: ABC Defense Course
107 Commander, U.S. Naval Ordnance Laboratory, Silver Spring 19, Md. ATTN: EH
108 Commander, U.S. Naval Ordnance Laboratory, Silver Spring 19, Md. ATTN: R
109 Commander, U.S. Naval Ordnance Test Station, Inyokern, China Lake, Calif.
110 Officer-in-Charge, U.S. Naval Civil Engineering Res. and Evaluation Lab., U.S. Naval Construction Battalion Center, Port Hueneme, Calif. ATTN: Code 753
111 Commanding Officer, U.S. Naval Medical Research Inst., National Naval Medical Center, Bethesda 14, Md.
112 Director, U.S. Naval Research Laboratory, Washington 25, D.C. ATTN: Mrs. Katherine H. Cass
113 Director, The Material Laboratory, New York Naval Shipyard, Brooklyn, N. Y.
114 Commanding Officer and Director, U.S. Navy Electronics Laboratory, San Diego 52, Calif. ATTN: Code 4223
115-118 Commanding Officer, U.S. Naval Radiological Defense Laboratory, San Francisco, Calif. ATTN: Technical Information Division
119 Commanding Officer and Director, David W. Taylor Model Basin, Washington 7, D.C. ATTN: Library
120 Commander, U.S. Naval Air Development Center, Johnsville, Pa.
121 Commanding Officer, Clothing Supply Office, Code 1D-0, 3rd Avenue and 29th St., Brooklyn, N.Y.
122 Commandant, U.S. Coast Guard, 1300 E. St. N.W., Washington 25, D.C. ATTN: Capt. O. C. B. Wey, USCG
123 Commander-in-Chief Pacific, Pearl Harbor, TH
124 Commander, Norfolk Naval Shipyard, Portsmouth 8, Va. ATTN: Code 270
125 Officer-in-Charge, U.S. Naval Civil Engineering Research & Evaluation Lab., Construction Battalion Center, Port Hueneme, Calif. ATTN: Atomic Energy Div.
126-130 Technical Information Service Extension, Oak Ridge, Tenn. (Surplus)

AIR FORCE ACTIVITIES

131 Asst. for Atomic Energy Headquarters, USAF, Washington 25, D.C. ATTN: DCS/O
132 Director of Operations, Headquarters, USAF, Washington 25, D.C. ATTN: Operations Analysis
133 Director of Plans, Headquarters, USAF, Washington 25, D.C. ATTN: War Plans Div.
134 Director of Research and Development, DCS/D, Headquarters, USAF, Washington 25, D.C. ATTN: Combat Components Div.
135-136 Director of Intelligence, Headquarters, USAF, Washington 25, D.C. ATTN: AFOIN-IB2
137 The Surgeon General, Headquarters, USAF, Washington 25, D.C. ATTN: Bio. Def. Br., Pre. Med. Div.
138 Asst. Chief of Staff, Intelligence, Headquarters, U.S. Air Forces-Europe, APO 633, New York, N.Y. ATTN: Directorate of Air Targets
139 Commander, 497th Reconnaissance Technical Squadron (Augmented), APO 633, New York, N.Y.
140 Commander-in-Chief, Pacific Air Forces, APO 953, San Francisco, Calif. ATTN: PFCIE-MB, Base Recovery
141 Commander-in-Chief, Strategic Air Command, Offutt AFB, Omaha, Nebraska. ATTN: OAWS
142 Commander, Tactical Air Command, Langley AFB, Va. ATTN: Documents Security Branch
143 Commander, Air Defense Command, Ent AFB, Colo.
144-145 Research Directorate, Headquarters, Air Force Special Weapons Center, Kirtland AFB, New Mexico. ATTN: Blast Effects Res.
146 Director of Installations, DCS/O, Headquarters, USAF, Washington 25, D.C. ATTN: AFOIE-E
147 Commander, Air Research and Development Command, Andrews AFB, Washington 25, D.C. ATTN: RDDN
148 Commander, Air Proving Ground Command, Eglin AFB, Fla. ATTN: Adj./Tech. Report Branch
149-150 Director, Air University Library, Maxwell AFB, Ala.
151-156 Commander, Air Training Command, Randolph AFB, Tex.
157-158 Commandant, Air Force School of Aviation Medicine, Randolph AFB, Tex.
159-161 Commander, Wright Air Development Center, Wright-Patterson AFB, Dayton, Ohio. ATTN: WCOSI
162-163 Commander, Air Force Cambridge Research Center, LG Hanscom Field, Bedford, Mass. ATTN: CRQST-2
164-166 Commander, Air Force Special Weapons Command, Kirtland AFB, N. Mex. ATTN: Tech. Infor. Office
167 Commander, Lowry AFB, Denver, Colo. ATTN: Department of Special Weapons Training
168 Commander, 1009th Special Weapons Squadron, Headquarters, USAF, Washington 25, D.C.
169-170 The RAND Corporation, 1700 Main Street, Santa Monica, Calif. ATTN: Nuclear Energy Division
171 Commander, Second Air Force, Barksdale AFB, La. ATTN: Operations Analysis Office
172 Commander, Eighth Air Force, Westover AFB, Mass. ATTN: Operations Analysis Office
173 Commander, Fifteenth Air Force, March AFB, Calif. ATTN: Operations Analysis Office
174 Commander, Western Development Div. (ARDC), PO Box 262, Inglewood, Calif. ATTN: WDSIT, R. G. Weitz
175-179 Technical Information Service Extension, Oak Ridge, Tenn. (Surplus)

OTHER DEPARTMENT OF DEFENSE ACTIVITIES

180 Asst. Secretary of Defense, Research and Engineering, D/D, Washington 25, D.C. ATTN: Tech. Library
181 U.S. Documents Officer, Office of the U.S. National Military Representative, SHAPE, APO 55, New York, N.Y.
182 Director, Weapons Systems Evaluation Group, OSD, Rm 2E1006, Pentagon, Washington 25, D.C.
183 Chairman, Armed Services Explosives Safety Board, D/D, Building T-7, Gravelly Point, Washington 25, D.C.
184 Commandant, Armed Forces Staff College, Norfolk 11, Va. ATTN: Secretary
185 Commander, Field Command, Armed Forces Special Weapons Project, PO Box 5100, Albuquerque, N. Mex.
186 Commander, Field Command, Armed Forces Special Weapons Project, PO Box 5100, Albuquerque, N. Mex. ATTN: Technical Training Group
187-191 Commander, Field Command, Armed Forces Special Weapons Project, P.O. Box 5100, Albuquerque, N. Mex. ATTN: Deputy Chief of Staff, Weapons Effects Test
192-202 Chief, Armed Forces Special Weapons Project, Washington 25, D.C. ATTN: Documents Library Branch
203 Commanding General, Military District of Washington, Room 1543, Building T-7, Gravelly Point, Va.
204-208 Technical Information Service Extension, Oak Ridge, Tenn. (Surplus)

ATOMIC ENERGY COMMISSION ACTIVITIES

209-211 U.S. Atomic Energy Commission, Classified Technical Library, Washington 25, D.C. ATTN: Mrs. J. M. O'Leary (For DMA)
212-213 Los Alamos Scientific Laboratory, Report Library, PO Box 1663, Los Alamos, N. Mex. ATTN: Helen Redman
214-218 Sandia Corporation, Classified Document Division, Sandia Base, Albuquerque, N. Mex. ATTN: H. J. Smyth, Jr.
219-221 University of California Radiation Laboratory, PO Box 808, Livermore, Calif. ATTN: Clovis G. Craig
222 Weapon Data Section, Technical Information Service Extension, Oak Ridge, Tenn.
223-230 Technical Information Service Extension, Oak Ridge, Tenn. (Surplus)

[redacted]